

University of Southampton Research Repository ePrints Soton

Copyright © and Moral Rights for this thesis are retained by the author and/or other copyright owners. A copy can be downloaded for personal non-commercial research or study, without prior permission or charge. This thesis cannot be reproduced or quoted extensively from without first obtaining permission in writing from the copyright holder/s. The content must not be changed in any way or sold commercially in any format or medium without the formal permission of the copyright holders.

When referring to this work, full bibliographic details including the author, title, awarding institution and date of the thesis must be given e.g.

AUTHOR (year of submission) "Full thesis title", University of Southampton, name of the University School or Department, PhD Thesis, pagination

Development and interaction of segmented fault systems

Paul Graham Kelly

submission for the degree of Doctor of Philosophy

School of Ocean and Earth Science

Faculty of Science

October 1998



UNIVERSITY OF SOUTHAMPTON
ABSTRACT
FACULTY OF SCIENCE
SCHOOL OF OCEAN AND EARTH SCIENCE

Doctor of Philosophy

DEVELOPMENT AND INTERACTION OF SEGMENTED FAULT SYSTEMS

by Paul Graham Kelly

Faults in contractional and extensional settings have been studied, both during fieldwork and from interpretation of 2D and 3D seismic sections. Detailed analysis of the geometries of faults, with displacements of a few mm to 100's m, has provided insights into the development of fault networks. Faults evolve from the amalgamation of initially isolated fault segments, and deformation is eventually localised onto 'master' faults. A model for the development of conjugate strike-slip fault zones at Beadnell, Northumbria, and Kilve, Somerset, involves (1) random development of vein arrays, to (2) isolated development of several unconnected conjugate faults, through (3) intersection of a conjugate set of master faults and linkage with minor antithetic faults, and formation of new vein arrays, to (4) breaching of intersection points by dominant faults, and finally (5) propagation towards oversteps that are breached to form a through-going fault. The geometry of the active structures simplifies, as strain is localised along master faults. The conjugate strike-slip faults at Kilve are associated with reverse-reactivated normal faults, and are related to Alpine-related contraction. Selective reactivation is attributed to: (1) low fault plane frictions, (2) domino block rotation, (3) displacement magnitude, and (4) a percolation model. The style of displacement transfer between the reverse-reactivated normal faults is dependent on the original fault network geometry. Conjugate strike-slip faults accommodated the shortening between two overlapping reverse-reactivated normal faults. Obliquely orientated reverse-faults perform a similar role in an underlapping fault zone.

The segmented geometries of normal faults, in cross-section and map view, in the Wytch Farm Oilfield are described. The deformation is dominated by recurrent normal fault reactivation, onto which the extension is localised. The localisation is more intense in the Triassic, with a more homogenous strain distribution in the Jurassic. The reactivated faults are identified from multiple growth sequences. Displacement profiles do not show a simple upward decrease in displacement, but have one displacement maxima in the Triassic, and one in the Middle Jurassic. The throws in the Jurassic are often greater than those in the Trias, but the heaves are less due to steeper faults. The geometries are attributed to thin-skinned extension of the Jurassic sequence above a postulated detachment in the Upper Triassic or Lower Jurassic. The existence of a detachment questions the practice of locating the poorly-imaged Sherwood Sandstone reservoir unit on 2D seismic sections from an isopach from the White Lias horizon. Uncertainty in the structure of the Sherwood Sandstone exists due to the quality of a 2D seismic data set, and a gap that exists between two 3D seismic surveys. Fault analysis methods have been applied to the re-interpretation of the Sherwood Sandstone structure, and new maps are presented that represent the uncertainties. These illustrate that the 2D seismic data can be interpreted in several ways, based on variation of throw, geometry and position of the fault system. A comparison of the geometries of the normal fault systems exposed at Kilve with those in Wytch Farm reveals that there are many geometrical similarities. There is, however, no evidence for strike-slip faults, or reverse-reactivated normal faults at Wytch Farm.

Contents

List of figures	v
List of tables	xvii
List of enclosures	xix
Acknowledgements	xx
1. Introduction	1
1.1 OBJECTIVES	1
1.2 STUDY AREAS	1
1.2.1 <i>Kilve, north Somerset</i>	2
1.2.2 <i>Beadnell, Northumbria</i>	3
1.2.3 <i>Wytch Farm, Dorset</i>	3
1.3 THESIS LAYOUT	4
2. Linkage and evolution of conjugate strike-slip fault zones in limestones of Somerset and Northumbria	5
2.1 SUMMARY	5
2.2 INTRODUCTION	6
2.3 STRIKE-SLIP FAULTS AT BEADNELL, NORTHUMBRIA, UK	10
2.3.1 <i>Kinematic analysis</i>	13
2.4 STRIKE-SLIP FAULTS AT KILVE, SOMERSET, UK	16
2.4.1 <i>Metre-scale examples</i>	16
2.4.2 <i>Exposure-scale strike-slip fault network</i>	18
2.5 STRAIN ANALYSIS	21
2.5.1 <i>Results</i>	23
2.6 FAULT ZONE EVOLUTION	23
2.6.1 <i>Stage 1 - Extensional vein development</i>	24
2.6.2 <i>Stage 2 - Formation of conjugate strike-slip faults</i>	24
2.6.3 <i>Stage 3 - Fault linkage and renewed extensional vein opening</i>	25
2.6.4 <i>Stage 4 - Breaching of the intersection points</i>	26
2.6.5 <i>Stage 5 - Linkage with other fault systems</i>	27
2.7 CONCLUSIONS	27
3. Selective reverse-reactivation of normal faults and hanging-wall indentation in north Somerset	28
3.1 SUMMARY	28
3.2 INTRODUCTION	29
3.3 GEOLOGICAL SETTING	30
3.4 SELECTIVE REVERSE-REACTIVATION	33
1.1.1 <i>Fault-plane friction</i>	35
1.1.2 <i>Domino block rotation</i>	36
1.1.3 <i>Fault size</i>	37

3.4.4 <i>Percolating network of connected faults</i>	39
3.5 GEOMETRIES OF OVERLAPPING AND UNDERLAPPING ZONES	40
3.5.1 <i>Strike-slip network</i>	41
3.5.1a <i>Interaction of strike-slip and dip-slip faults</i>	41
3.5.2 <i>Obliquely-oriented high-angle reverse faults</i>	44
3.6 DEFORMATION MODEL	46
3.7 CONCLUSIONS	47
4. Normal fault segment interaction in the Wytch Farm Oilfield, Wessex Basin	50
4.1 SUMMARY	50
4.2 INTRODUCTION	51
4.2.1 <i>Geological setting</i>	52
4.2.2 <i>Exploration history</i>	52
4.2.3 <i>Seismic data</i>	54
4.3 METHODS	56
4.3.1 <i>Seismic interpretation</i>	56
4.3.2 <i>Displacement-distance analysis</i>	57
4.3.3 <i>Timing of movement</i>	57
4.3.4 <i>Extension analysis</i>	58
4.4 FAULT GEOMETRIES	61
4.4.1 <i>Cross-section interpretations</i>	61
4.4.2 <i>Fault interpretations</i>	66
4.4.3 <i>Branches, intersections and oversteps</i>	72
4.4.4 <i>Fault orientations</i>	72
4.4.5 <i>Timing of movement</i>	77
4.5 NORMAL REACTIVATION	78
4.5.1 <i>Mechanics of individual faults</i>	81
4.5.1a <i>Reverse reactivation</i>	84
4.5.1b <i>Extensional detachment</i>	84
4.5.2 <i>Preferential normal reactivation</i>	86
4.6 DEFORMATION HISTORY	86
4.6.1 <i>Comparison with the regional structure of the Wessex Basin</i>	87
4.7 CONCLUSIONS	88
5. New interpretations of the structure of the Sherwood Reservoir, Wytch Farm Oilfield, Dorset, UK	90
5.1 SUMMARY	90
5.2 INTRODUCTION	91
5.2.1 <i>Geological setting</i>	91
5.2.2 <i>Structural uncertainties</i>	93
5.3 METHODS	95

5.3.1	<i>Horizon interpretation</i>	95
5.3.2	<i>Calibration of the seismic data</i>	95
5.3.3	<i>Timing of movement</i>	99
5.3.4	<i>Displacement-distance and displacement-length analysis</i>	100
5.3.5	<i>Pre-Triassic structural geometry</i>	103
5.3.6	<i>Arne Fault map construction</i>	104
5.4	INTERPRETATION OF THE ARNE FAULT	105
5.4.1	<i>Fault plane map</i>	105
5.4.1a	Zone A	108
5.4.1b	Zone B	108
5.4.1c	Zone C	109
5.4.1d	Zone D	109
5.4.2	<i>Seismic calibration with well data</i>	109
5.4.3	<i>Timing of movement</i>	109
5.4.4	<i>New maps</i>	111
5.4.4a	Map 1	117
5.4.4b	Map 2	117
5.4.4c	Map 3	118
5.4.4d	Map 4	119
5.4.5	<i>Volumetrics</i>	119
5.5	EEC 3D SURVEY AREA RESULTS	120
5.5.1	<i>Interpretation based on TWL pick</i>	120
5.5.2	<i>Alternative interpretation</i>	121
5.5.2a	Fault geometries	124
5.5.3	<i>Continuation of the Wytch Farm Fault and other faults into the EEC survey area</i>	126
5.6	CONCLUSIONS	129
5.6.1	<i>Arne Fault</i>	129
5.6.2	<i>EEC survey area</i>	129
6.	A comparison of the structure of Kilve, Somerset, and the Wytch Farm Oilfield, Dorset	130
6.1	SUMMARY	130
	INTRODUCTION	131
6.2.1	<i>Map construction</i>	132
6.3	FAULT GEOMETRIES	137
6.3.1	<i>Overview of the structures on the north Somerset coast</i>	138
6.3.1a	Normal faults	138
6.3.1b	Reverse-reactivated normal faults	139
6.3.1c	Strike-slip faults	141
	<i>Structure of the Wytch Farm Oilfield</i>	146
6.3.2a	Normal faults	146

6.3.2b Strike-slip and reverse-reactivated normal faults	147
6.4 APPLICABILITY OF FIELD STUDY TO SEISMIC INTERPRETATION	148
6.5 CONCLUSIONS	150
7. Conclusions	151
7.1 EXTENSIONAL DEFORMATION	151
7.2 CONTRACTIONAL DEFORMATION	152
7.3 STRAIN DISTRIBUTION	153
7.4 RECOMMENDATIONS FOR FURTHER WORK	153
References	154

List of figures

- Fig. 1.1. Map of part of the British Isles that shows the three study areas: Kilve, north Somerset, Beadnell, Northumberland, and Wytch Farm, Dorset. _____ 2
- Fig. 2.1. The location of a zone of effective tension at the tip of a right-propagating sinistral fault containing tensile microcracks (Reches and Lockner, 1994). The process zone moves with the propagating fault, and coalescence of the microcracks influences the position of the damage zone (Scholz *et al.*, 1993). _____ 6
- Fig. 2.2. (a) Map of part of the British Isles showing the locations of (b) Beadnell, Northumbria, and (c) Kilve, Somerset. The locations of the strike-slip fault zones described in the text are also shown. MHW = mean high water, and MLW = mean low water. _____ 7
- Fig. 2.3. Field examples from Beadnell and Kilve of (a) and (b) vein arrays, (c) a pull-apart array, and (d) a strike-slip fault with adjacent sheared calcite-filled pull-aparts. _____ 9
- Fig. 2.4. Schematic diagrams of convergent (Type 1) vein arrays, and bisector parallel veins (Type 2) (after Beach, 1975). _____ 9
- Fig. 2.5. Data from the mapped fault zones at Beadnell, Northumbria. (a) Equal-area stereogram of poles to planes of sinistral ($n = 15$) and dextral ($n = 11$) strike-slip faults, and of thrusts ($n = 4$). Lineation data and synoptic great circles for the faults are also shown. (b) Rose diagram of the vein array orientations within these fault zones ($n = 100$). The data can be divided into three groups based on orientations: (i) NW-SE, (ii) ENE-WSW and (iii) \approx E-W. The first two form a conjugate set of arrays, with a sinistral NW-SE group and a dextral ENE-WSW group. _____ 11
- Fig. 2.6. (overleaf) Conjugate strike-slip fault zones mapped at Beadnell at a scale of 1:25. Displacements are in mm. The circled letters are referred to in the text. For location see Fig. 2.1(b). (a) Fault zone showing a conjugate arrangement of strike-slip faults that have not linked to form a network. (b) Network of linked strike-slip faults. _____ 11
- Fig. 2.7. (a) Graphs of zone boundary orientation and vein orientation to show the distribution of vein array geometries from Fig. 2.6. When the infinitesimal wallrock displacement direction (A) is equal to the angle between the vein array and zone boundary (w), the vein array has an extensional geometry. A difference of 90° signifies contraction, and one of 45° indicates that the array has a simple-shear geometry. The lines of extension and contraction separate zones of dextral and sinistral displacement sense. The shaded areas indicate sinistral sense. TT = transtension; TP = transpression. (i) Data from Fig. 2.6(a), $n = 56$. The two distinct clusters of data indicate conjugate vein arrays that have predominantly simple-shear geometries. (ii) Data from Fig. 2.6(b), $n = 60$. The single data cluster, centred on the extensional zone of the graph, demonstrates that the vein arrays in this fault zone have transtensional geometries, but are dominated by extension. (b) Schematic diagram of vein arrays with simple-shear, transtensional and extensional geometries. (c) The construction of McCoss (1986) for each of vein arrays in Fig. 2.7(b). This method treats each vein array as a transtensional or transpressional zone (Sanderson and Marchini, 1984), to determine the infinitesimal displacement direction (A) of the wall-rocks from the zone boundary and the vein angle. A line parallel to the veins is drawn from point y to the circumference of a circle, z , that

- touches the zone boundary. A second line is drawn from z that passes through the centre of the circle, to find A. _____ 14
- Fig. 2.8. Maps of the wallrock displacement directions from vein systems (double-headed arrows). Extension (long axis of cross) and contraction (short axis) orientations are superimposed on maps of the master faults from Fig. 2.6 (a) the unconnected network which is dominated by co-linear vein arrays with simple-shear geometries, and (b) the connected network, where transtensional vein arrays have predominantly extensional geometries. _____ 15
- Fig. 2.9. Block-diagram of the strike-slip faults in the cliff at Kilve which exhibit a wide range of geometries. Measured orientations of the strike-slip faults have been used to construct the plan (dashed lines) of the strike-slip faults on top of the cliff. The lateral displacements have been calculated using the trigonometric relationship between the slickenside lineation pitch and the vertical separation of beds. The shaded horizons represent individual limestone beds. _____ 17
- Fig. 2.10. (above) Equal-area stereogram of poles to planes of dextral ($n = 19$) and sinistral ($n = 66$) strike-slip faults, normal faults ($n = 53$), and of thrusts and reverse reactivated normal faults ($n = 18$) at Kilve, Somerset. Lineation data and great circles are shown to represent the fault planes. _____ 18
- Fig. 2.11. (right) Conjugate strike-slip fault zone developed in the wallrock of a 3.5 m maximum displacement dextral strike-slip fault, from Kilve, Somerset (originally mapped at 1:25). Displacements are in mm. See Fig. 2.6 for key. The circled letters are referred to in the text. _____ 18
- Fig. 2.12. Map of the strike-slip fault network mapped from aerial photographs at a scale of 1:500. The shaded areas represent individual limestone units. Displacements are in metres. Note the location of Fig. 2.11. _____ 20
- Fig. 2.13. Cumulative displacement-distance graphs for the two traverses indicated by the dashed lines in Fig. 2.12. (a) Y-Y', and (b) Z-Z'. The fault that corresponds to the point at which the gradient of the graph in (a) shallows considerably is marked as 'C' in Fig. 2.12. _____ 22
- Fig. 2.14. Model for the development of strike-slip fault zones to include conjugate fault development and overstepping zones. The arrowed faults indicate those parts active at that particular stage. (a)-(c) Models based on observations at Beadnell. (d)-(e) Expansion of the model to include the observations of fault network development at Kilve. The model is discussed in full in the text. (f) Idealised graph of vein strike and zone boundary orientation for (a)-(c) (c.f. Fig. 2.7). Veins in (a) are parallel to each other, but there is the potential for the zone boundaries to have the whole range of orientations. The data from (b) plot in two distinct clusters that represent Type 1 veins within arrays with predominantly simple-shear geometries. The data from the natural examples (Fig. 2.6) show some overlap in vein strike of the two clusters. The veins in (c) are sub-parallel within the transtensional-extensional arrays, and the spread of zone boundary orientations is limited, so the data plot in a single cluster. Veins with transtensional-extensional geometries were not observed within the fault zones at Kilve. _____ 25
- Fig. 3.1. Map of the foreshore of part of the north Somerset Coast to show the location of Fig. 3.2, and (inset) map of Great Britain to show the location of Kilve. _____ 29
- Fig. 3.2. (overleaf) (a) Map of the faulting between East Quantoxhead and St. Audrie's Bay. The bold lines refer to the reverse and reverse-reactivated normal faults, and the ticks are on the hanging-walls of

- the faults. The Blue Lias and Quantock's Beds have been further divided into approximately equal thickness units of 10m. The lettered locations are referred to in the text. (b) Fault data and copy of part of the map in (a) with unreactivated normal and strike-slip faults removed for clarity. _____ 30
- Fig. 3.3(a). (previous page) Map of the strike-slip fault network between the two major reverse-reactivated faults (see Fig. 3.2 for location). The strike-slip faults form a linked network within the overlapping faults to the west of the map, and are far more segmented on the periphery, to the east. (b) (right) Stereographic projection of dextral and sinistral faults, and slickenside lineations. _____ 33
- Fig. 3.4. Comparison of the properties of normal and reverse-reactivated faults. Stereographic projection of fault plane and slickenside lineation orientations for (a) normal faults and (b) reverse and reverse-reactivated normal faults. (c) Graph of displacements plotted against dip angle for normal, reverse and reverse-reactivated faults (negative values indicate reverse displacements). Reverse and reverse-reactivated normal faults are considered together, as it was impossible to distinguish the nature of the fault on the wave-cut platform. _____ 34
- Fig. 3.5. (a) Schematic diagram to show how steep faults initiate in the more brittle layers (white), but have shallower profiles in the more ductile layers (shaded) (Peacock and Sanderson, 1992; Peacock and Zhang, 1994). (b) The faults assume a shallower, smoother profile during movement of brittle layers past ductile layers. (c) Block diagram to illustrate how fault gouge can occur along faults that have large enough displacements to juxtapose limestones against the shale-dominated units. Smaller displacement faults wholly within the Blue Lias are less likely to contain gouge material. _____ 36
- Fig. 3.6. Rotation of the fault blocks occurs during extension (a), which can be reversed during contraction (b). The master faults undergo the largest rotations to shallower dips, and smaller antithetic faults will be rotated to steeper dips during extension, and therefore make greater angles with σ_1 during the contraction. The filled arrow heads indicate the displacement sense of the active faults in each diagram; the unfilled arrow heads indicate inactive faults. The latest sense of movement is indicated by the filled arrows on the double-headed symbols. _____ 37
- Fig. 3.7. Model for basement-involved reverse-reactivation (modified from a model for faulting at Flamborough Head, Peacock and Sanderson, 1994b; Peacock, 1996). The orientations of the maximum (σ_1), intermediate (σ_2) and minimum (σ_3) principal compressive stresses are shown. (a) E-W striking 'basement' faults occur, and the Jurassic is a 'cover' sequence. (b) The basement faults were normally-reactivated after Jurassic deposition and have the largest normal displacements. A network of small normal faults developed throughout the sequence. (c) The basement faults show reverse-reactivation, but the smaller faults (represented using finer lines) were not reactivated. _____ 38
- Fig. 3.8. Cross-section of the Quantock's Head region (see Fig. 3.2 for line location). Fault dimensions were determined from the juxtaposed units, and fault displacements. Maximum displacements were assumed at the surface, and the radial fault growth model (e.g. Walsh and Watterson, 1988) was applied to determine the fault lengths. All the faults have been extended above the present-day surface with a length equal to that estimated at depth. Deformation (and fluid flow) is concentrated on a network of large displacement, connected faults that extend through the sequence. The smaller, poorly-connected or impermeable faults are not reactivated. _____ 39

- Fig. 3.9. (a) Line drawing of a relay ramp in a reverse-reactivated normal fault system. (b) Model to illustrate the style of faults at transfer zones between reverse-reactivated fault segments (c.f. Peacock and Sanderson, 1991). _____ 41
- Fig. 3.10. Maps of strike-slip faults at intersections with earlier E-W striking dip-slip faults at Kilve, Somerset; the shading represents shale beds. (a) Intersection of a sinistral strike-slip relay ramp and a reactivated normal fault zone. The antithetic right-lateral faults within the relay ramp are truncated at the normal fault and the main segment has propagated through, but ends shortly after intersection in the Kilve Shales. (b) Right-lateral strike-slip faults terminate at reverse faults, and bend into the normal faults. (c) The right-lateral strike-slip faults cross-cut an unreactivated normal fault zone. _____ 42
- Fig. 3.11. Schematic diagram to illustrate a mechanism for the formation of the strike-slip network in the overlap between the Quantock's Head and Kilve Pill Faults. Dextral transpression causes the formation of sinistral faults and block rotation. The shortening is accommodated by the formation of thrusts at the foot of the block, that are oblique to the Quantock's Head Fault. Unfilled arrows = local stress axes, filled arrows = 'regional' stress axes. _____ 45
- Fig. 3.12. Block diagram of the interpretation of the formation of the obliquely-oriented high-angle reverse faults east of the Blue Ben Headland. A NE-SW trending anticline forms initially, due to loading of the corner of the underlap zone by the hanging-wall of the Quantock's Head Fault. The beds in the south of the fold hinge dip towards the loaded corner of the underlap zone to the ESE, whilst those in the footwall dip WNW. Continued shortening, driven by the northwards movement of the Quantock's Head Fault hanging-wall causes failure along the anticline hinge, and new NE-striking reverse faults develop. Open arrows = local stress axes, closed arrows = 'regional' stress axes. _____ 46
- Fig. 3.13. Block diagrams to illustrate the contractional deformation at Kilve as one single on-going event controlled by the reverse-reactivation of the Quantock's Head Fault. (a) The Kilve Pill Fault is offset and rotated clockwise by sinistral faults that form in response to dextral transpression along the Quantock's Head Fault. The northwards movement of the hanging-wall of the Quantock's Head Fault indents its footwall, and the local principal stress axes and existing structures are rotated anti-clockwise to the west of the fault, and clockwise to the east. (b) Further indentation of the Quantock's Head Fault and σ_1 is further perturbed such that reverse faults oblique to existing faults form in an underlap to the west of the fault. To the east of the fault, a network of conjugate strike-slip faults develops, that suggests a NNE σ_1 orientation. _____ 49
- Fig. 4.1. Map of part of the south Dorset Coast to show the location of the Wytch Farm Oilfield and the extent of the seismic data (see inset for location of main map in Great Britain). The inlines run from N-S, and the crosslines from E-W in both 3D surveys. _____ 51
- Fig. 4.2. (a) Map of the Wessex Basin to show the fault trends and the location of the main sub-basins (after Karner *et al.*, 1987). (b) Satellite photo of Dorset with the location of Wytch Farm and the Purbeck-Isle of Wight Disturbance highlighted. © Dorset County Council, used with permission. _____ 53
- Fig. 4.3. Synoptic cross-section of the Wytch Farm Oilfield horst. The sequence within the central horst consists of Upper Triassic to Middle Jurassic sediments. Upper Jurassic sediments occur in the _____

- hanging-walls of the horst-bounding faults. The Cretaceous lies unconformably above the Jurassic sequence. _____ 54
- Fig. 4.4. Stratigraphy of the Wytch Farm Oilfield, based on A6SP well log. The reservoir units are shaded. _____ 55
- Fig. 4.5. Interpretation of inline 9350 with shading to denote the thickened hanging-wall sedimentary sequences adjacent to the Wytch Farm, Northern and Arne Faults. The hanging-wall and footwall sequence thicknesses were measured parallel to the fault planes. _____ 58
- Fig. 4.6. The timing of growth faulting derived from the ratio of the hanging-wall unit thickness to the footwall unit thickness measured parallel and adjacent to the fault plane. A value of > 1 indicates a thicker hanging-wall sequence. An overestimation of the hanging-wall thickness would result from a vertical measure of rotated beds and hence overstate the extent of growth faulting. The interval thicknesses were calculated for only the interpreted horizons and not individual reflectors (inline interval = 50). A grey scale is used to indicate the size of the ratio. ND = No Data. _____ 59
- Fig. 4.7. (a) Summary of fault timing data from identification of growth sequences. The results show the range of activity across the entire faults, so not every part of the fault moved at the same time. (b) Approximate orientations of the faults at the listed horizons (c.f. Fig. 4.14). _____ 60
- Fig. 4.8. (overleaf) Seismic cross-sections taken from the 2D survey area. The horizontal scale refers to the National Grid, and the vertical depth is in TWTT (ms). The sections (top to bottom = west to east) show how the fault system changes from one dominated by parallel, south-dipping faults to one dominated by a central conjugate fault structure. The numbers in the top left corners refer to the name of the seismic line. The seismic lines are located onto a combined 2D and 3D area map of the Top White Lias faults. _____ 61
- Fig. 4.9. Cross-sections through the 3D survey, and map of the Top White Lias. The numbers in the bottom right corners represent the seismic inline numbers (see map for location), the horizontal scale numbers are cross-line numbers, and the vertical depth is in TWTT (ms). The cross-sections are regularly spaced every 625 metres (50 inlines) and show how the structure changes from west to east across the survey. _____ 63
- Fig. 4.10. Vertical d - x profiles for the 2D seismic interpretations illustrated in Fig. 4.8. The throw minima for the Top White Lias and the IntraLias are an interpretation artefact, as these horizons were not identifiable in every section. Additionally, survey resolution decreases with depth, so there is less confidence in the results for the Triassic units. _____ 64
- Fig. 4.11. Vertical d - x profiles for each of the inlines in Fig. 4.9. There is an overall increase in throw from the deepest to the shallowest units, which reflects the greater fault densities in the Jurassic sequence. _____ 65
- Fig. 4.12. (following three pages) Heave and throw diagrams for (a) the Wytch Farm Fault, (b) the Northern Fault and (c) the Arne Fault. The hanging-wall and footwall cut-offs are shown for each of the horizons illustrated in the cross-sections (Fig. 4.8 and 4.9), with the exception of the Corallian, due to insufficient data, and the Chalk, which is mostly unfaulted. _____ 66
- Fig. 4.13. (overleaf) Fault plane maps with throw contours to illustrate the distribution of displacement maxima and minima in the 3D survey area, for (a) the Wytch Farm Fault, (b) the Northern Fault and

(c) the Arne Fault. Fault throw in ms. A 50 m (horizontal) by 5 ms (vertical) grid was derived from the data which was contoured using *Surfer32* (Golden Software Inc., Golden, Colorado). A contour interval of 20 ms was chosen for the Wytch Farm Fault, and 10 ms for the other two faults. The outer boundary for each map reflects the mapped extent of the fault plane itself, and the inner boundary represents the limit of the throw data. The crosses on the maps indicate the location of an intersecting fault plane. The data used in the maps' construction was found by calculating the fault throw (in ms) for the mapped horizons between, and including, the Top Sherwood and the Cornbrash from every tenth inline in the 3D survey (9100 to 9800). The contour maps cover only the 3D area due to variable quality of the 2D seismic data, its poorer resolution and greater spacing.

- _____ 70
- Fig. 4.14. (following three pages) Structural interpretations for (a) Top Sherwood, (b) the Top White Lias, and (c) the Bridport Sands. The reactivated faults are unfilled; Jurassic and Triassic faults are filled. The arrows indicate fault dip direction, and displacements (in italics) are in ms. _____ 72
- Fig. 4.15. Rose diagrams of fault strike for the (a) Top Sherwood, (b) Top White Lias and (c) Bridport Sands. The fault strike was measured in the interval between every tenth inline. The faults in the Top Sherwood have the greatest range of strikes, and those in the Bridport Sands have a tighter distribution centred on E-W. _____ 77
- Fig. 4.16. Idealised throw contours on a fault plane for four scenarios (dashed lines represent former tip-lines): (a) Normal reactivation of an existing single, isolated fault. (b) Normal reactivation of the lower segment and interaction with the upper segment. (c) Overprinting of the lower fault by a larger upper fault. (d) Upper and lower faults abut, with or without reactivation of the lower fault. The elliptical contours in each diagram are based on radial propagation of a fault where $D \propto L^2$ (Walsh and Watterson, 1988; D = displacement and L = fault length). _____ 79
- Fig. 4.17. (a) Normal fault with pre-, syn- and post-rift sediments. (b) Reactivation of the fault and upward expansion into newly deposited segments and (c) idealised vertical $d-x$ of the reactivated fault that suggests that a displacement minimum occurs at the top of the original syn-rift unit. The largest displacements are associated with the deepest parts of the fault, under a simple model of reactivation. _____ 81
- Fig. 4.18. (a) Idealised fault geometry to illustrate that an individual fault can have a smaller throw at depth, and a constant downthrow across the whole fault zone. The heave at depth is half of the combined heave of the upper two faults in this example. (b) Modification of the fault plane geometry so the heave is constant. The throw on the lower section is the same as in (a), but the heave is doubled. Any decrease in the fault dip at depth would lead to an increase in the heave, assuming that the throw remains constant. h = heave, t = throw and the numbers represent the number of units of each. _____ 82
- Fig. 4.19. Three synoptic vertical profiles of (a) fault heave and (b) fault throw, and (c) the fault plane of the Wytch Farm Fault. The data have been converted to depths from TWTT, with interval velocities calculated from mapped horizons depths in an exploration well (98/6-7) and the 3D seismic data. The fault has a shallower dip at depth in all three examples. _____ 83

- Fig. 4.20. Two methods to explain the fault geometries: (a) modification of the normally-reactivated fault plane by reverse-reactivation of the deeper parts of the fault, and (b) fault development with the presence of a detachment horizon. Stage 1 is identical for both models, and simply illustrates the presence of an early fault (c.f. Fig. 4.17a). In the reverse-reactivation model, the Triassic fault is initially normally-reactivated and propagates up-section (Stage 2). The lower parts of the fault are reverse-reactivated, and the upper parts remain unaffected (Stage 3). Shortening in-between is accommodated by ductile compaction of the Mercia Mudstone. In the detachment model, the Triassic fault reactivation and Jurassic fault initiation above a detachment horizon (Zone D Anhydrite) are contemporaneous (Stage 2). Continued expansion of the deeper fault into the upper sections occurs after faulting of the detachment layer. The upper fault acquires a larger displacement through thin-skinned extension above the detachment. 85
- Fig. 4.21. Block diagram to illustrate the changes in active fault orientation and the alteration in the principal stress axes orientation through time. 87
- Fig. 5.1. Map of part of the south Dorset Coast to show the extent of the seismic data. The inlines run N-S, and the crosslines E-W in both 3D surveys. 91
- Fig. 5.2. Existing structural interpretation of the Sherwood Sandstone reservoir (mapped by Giles Watts, BP Exploration and Production, Wytch Farm), and location of the Arne Fault picks used in this study on the 2D seismic lines (black diamonds) within Poole Harbour. The map is based on the interpretation of 2D and 3D seismic data, and the horizon depths are calibrated to available well data. 94
- Fig. 5.3. Illustration of the extent of fault throw and position uncertainties (after Martin *et al.* 1993). The throw uncertainty was set at ± 15 ms, and the fault positions are accurate to ± 200 m to reflect the 2D seismic data resolution. 96
- Fig. 5.4. Graphs of (a) unit thickness and (b) depth to the units taken from the wells that intersect the Arne Fault and the exploration wells in the EEC area, arranged in geographical order from west to east. The unit thickness graph is centred on the Mercia Mudstone/Sherwood Sandstone boundary to illustrate the thickness change in the Sherwood Sandstone. A curved line at the column bases indicates those wells which terminated above the base of the Sherwood Sandstone. A hanging-wall (HW) or footwall (FW) position for the well in the Sherwood Sandstone is indicated in (a), and the intersection of the Arne Fault with the well is represented by a cross on (b). 98
- Fig. 5.5. Detail of the 2D seismic data area to show the position of the seismic lines within Poole Harbour (c.f. Fig. 5.1). The seismic lines that fall within the grey box were used in the reinterpretation of the Arne Fault. 99
- Fig. 5.6. Line drawing of the interpretation of seismic line BP85-02 (Fig. 5.5) with two phases of identified growth faulting: (1) above the Cornbrash pick and (2) in the Mercia Mudstone, below the Zone D Anhydrite. 100
- Fig. 5.7. (overleaf) Relationships between (a) horizontal displacement-distance graphs, (b) fault plane geometry in map view and (c) cross-section, (d) vertical displacement-distance graphs and (e) fault throw diagrams, for (i) simple planar faults, (ii) conjugate faults and (iii) relay ramps. 100

Fig. 5.8. (a) Graph of total trace length against maximum displacement for 14 faults in the Sherwood reservoir (filled squares), and segment trace length against displacement for those faults which have segmented profiles (open squares). Every tenth seismic line was included, equalling a spacing of 125m, so trace length error bars are shown when the symbol width < 250 m. Lines with slopes of 1 and 2 have been drawn on for reference only, as there is no clear linear relationship for this restricted data set. (b) and (c) Throw contours on fault planes of two methods of fault growth, to illustrate how *D-L* relationships vary with the mode of fault growth (Cartwright et al., 1995). 103

Fig. 5.9. Illustration of possible fault orientations associated with NW-SE extension over basement structures oriented E-W and NW-SE, based on Chadwick (1986). (a) The underlying structure influenced the position of the faults but not their orientation. The new faults have an en echelon arrangement that is oriented NW-SE. (b) The E-W orientation was reactivated during extension and continued to grow upwards. Further displacement was accommodated by a relay ramp or a new NE-SW fault segment, that is a reflection of the extension direction. (c) All of the pre-existing faults were reactivated and propagated upward into the Top Sherwood. (d) This example shows how an E-W oriented en echelon zone of NE-SW faults might develop above an E-W fault (Chadwick, 1986). 104

Fig. 5.10. Fault throw diagram incorporating the existing interpretation of the 3D survey area (Ellis 1997), showing the hanging-wall (downthrown) and footwall (upthrown) separations and depths for the Arne Fault system for each of the horizons in Table 5.1. The fault plane has been divided into several vertical and horizontal zones on the basis of fault segmentation (see text for explanation). The Lower Arne Fault has maximum throws close to the Top Sherwood level. The Upper Arne Fault terminates at the unconformity below the Base Chalk, whilst retaining some throw. This indicates that the upper tip-line of the fault propagated further up through the stratigraphy, but was eroded away prior to Chalk deposition. The irregular profiles of the footwalls and hanging-walls within the 2D area may be a function of the lower quality of seismic data on the older surveys. 106

Fig. 5.11. Two maps to illustrate how displacement is transferred from one normal fault to another at an overstep. In both examples it would be possible to follow a route through the relay ramp that does not intersect a fault and, therefore, never encounter a fault-imposed permeability barrier. (a) Map of a relay ramp in the Lower Permian of East Greenland, after Larsen (1988). Displacement is transferred between the fault segments via a zone of rotated bedding. The NW-SE oriented fault in the north of the map may represent a linking fault that has breached a relay ramp. (b) Map of an antithetic relay ramp from Kolve, Somerset (mapped by D.J. Sanderson). Oblique (WNW-ESE) antithetic faults formed to accommodate displacement in the overstep between two E-W trending normal faults. At an antithetic/synthetic fault intersection point, the dip direction of the bounding fault changes polarity, and the strike of the new fault is similar to that of the original bounding fault. The displacement from the bounding faults is taken up by several en echelon antithetic faults. 107

Fig. 5.12. Map of the Arne Fault within the BP 3D area with arrows superimposed to represent the direction of maximum throw for each location. 111

Fig. 5.13. (Following four pages) Four interpretations of the Arne Fault within the 2D area at the Top Sherwood level. The contours represent the depth in TWTT (ms). (a) Map of an interpretation of the Arne Fault system within the 2D seismic studies area with dominant ENE-WSW and NW-SE trends.

The two distinct trends are a reflection of the influence of the basement structures suggesting that the heterogeneity of the basement rock influenced the orientation of the NW-SE structures, and the position of the later ENE-WSW faults. (b) Map of an interpretation of the Arne Fault system to include only E-W trending fault segments. The short nature of the many fault segments indicates that there are many places along the fault system where the displacement is at a minimum and would imply that the reservoir is juxtaposed quite irregularly along the fault zone. Linkage between interacting segments, below the resolution of this survey, may indicate that there are several parallel faults on some parts of the system. The existence of linked fault segments would depend on the maturity of the fault system. (c) Interpretation showing an en echelon arrangement of ENE-WSW trending fault segments. This arrangement may reflect an NW-SE extension direction, and the location of an underlying structural trend. The faults are less segmented than in (b), but segment linkage would follow a similar style. (d) Interpretation of the geometry of the Arne Fault that corresponds most closely to the acquired timing data (Table 5.4), the fault orientations and the direction of maximum displacement within the 3D survey area. 112

Fig. 5.14. (a) Graph to illustrate the STOOIP (Stock Tank Oil Originally In Place) for each of the four new fault geometries (Fig. 5.13). Most of the changes are confined to the lower zones. The difference between the two extremes is approximately 27 mb. (b) Graph to show the amount of change from the original interpretation (Fig. 5.2) in total volume for each of the models. 120

Fig. 5.15. Interpretation of seismic line 300 to which illustrates the depth to the Top Sherwood when based on the assumption that the prominent reflector represents the Top White Lias across the entire survey. The Top Sherwood is too shallow in the extreme south of the section to tie in with the BP survey, and the well data. 121

Fig. 5.16. Map of the Top Sherwood horizon pick based on an isopach down from the consistent Top White Lias (Top White Lias) pick in the EEC Survey area. The reservoir horizon is too shallow when compared with well data south of the Wytch Farm Fault, but that there is no structure to account for the depth difference between the two surveys. In this interpretation there is no obvious continuation of the Wytch Farm Fault into the EEC survey area. 122

Fig. 5.17. (a) A new interpretation of the Top Sherwood horizon based on the new horizon pick (Fig. 5.18). The horizon is now calibrated to the 98/11-1 well data, and there is also a much tighter correlation with the depth to the Top Sherwood picked on the BP 3D data. (b) Synoptic cross-section through the EEC 3D survey to illustrate the division of the area into four distinct fault-bounded zones. 123

Fig. 5.18. A re-interpretation of seismic line 300 (Fig. 5.15) to show the new pick for the Top Sherwood, south of the new southern fault (Fault D), based on the data from well 98/11-1. The reflector formally considered to represent the Top White Lias south of the fault must in fact relate to a boundary higher in the Liassic stratigraphy, such as the Blue Lias (c.f. Fig. 4.4). 124

Fig. 5.19. Fault plane maps showing the vertical hanging-wall/footwall separations at the Top Sherwood level for the block-bounding fault zones (vertical scale = ms), and their location on a map of the interpreted faults in the EEC survey area (the arrows indicate fault dip direction). The fault plane

- maps show an amalgamation of the displacement at sites of segment overlap where it was not possible to determine accurately the throw of each segment. placement is conserved. The 125
- Fig. 5.20. (Following two pages) Interpretations of the fault geometries in the gap between the two 3D surveys (Fig. 5.1). In the three suggestions, the displacement of the Wytch Farm Fault diminishes eastwards, and the throw is accommodated by several faults with lesser displacements. (a) The continuation of the Wytch Farm Fault with a NW-SE strike that links with Fault D (c.f. Fig. 5.19). The western end of Fault E continues beyond the EEC survey boundary and connects to a fault to the immediate north of the Wytch Farm Fault. (b) Interpretation of the faults based on E-W orientations, without any linkage between the faults. synthetic normal faults in the cliffs 25 m east of (b) 126
- Fig. 6.1. Map of SW Great Britain (after Lake and Karner, 1987) to show the location of the Wytch Farm Oilfield, Dorset, and Kilve, Somerset, in the Wessex Basin. The Wytch Farm Oilfield lies to the immediate north of the Channel Basin (Karner *et al.*, 1987), and the Lower Lias at Kilve is the onshore exposure of the Bristol Channel Basin, both sub-basins of the Wessex Basin. Both the Wytch Farm Oilfield and Kilve are adjacent to the eastern side of dextral NW-SE strike-slip faults that traverse SW England. at least 20 m of reverse throw in the Blue Lias Headland. The fault 131
- Fig. 6.2. Stratigraphic logs of (a) the Lower Liassic exposure at Kilve, compared to published accounts, and (b) the Jurassic and Triassic of the Dorset coast (after House, 1993) with a log from Well A6SP, Wytch Farm (from BP Well Completion Report). The logs are shown side-by-side, and centred on the Triassic/Jurassic boundary, for comparison. All thicknesses are in metres to allow a direct comparison. ment under the fault at Kilve and Wytch Farm. The normal faults on the foreshore 133
- Fig. 6.3. overleaf. (Reproduced at a larger scale as Enclosure 1). Two time-slice maps and cross-sections of the Wytch Farm Oilfield. The time-slices are at 900 and 925 ms, which represents an approximate depth difference of 45 m. The two levels were chosen as they contain the greatest areas of Blue Lias sediments, and therefore allow a direct comparison with the map of the foreshore at Kilve (Fig. 6.4). The diagrams include data from the BP 2D and 3D seismic surveys, that are calibrated with well data. The 3D survey extends eastwards from 401250, and its greater resolution and tighter spacing is evident in the detail of the fault geometries. The cross-section A-A' was produced from the projection of the two closest 2D seismic lines onto the line of the section; B-B' and C-C' were directly constructed from 3D lines. ed by an E-W synthetic-reactivated cleavage adjacent to the 134
- Fig. 6.4. overleaf. (Reproduced at a larger scale as Enclosure 2). Map of the exposure at Kilve (mapped by P.G. Kelly and D.J. Sanderson, drawn by D.C.P. Peacock and P.G. Kelly), and a composite cross-section. The stratigraphic divisions of Palmer (1972) are preferred for descriptive reasons. Normal and reverse-reactivated normal faults have approximately E-W strikes, dextral strike-slip faults strike NNW-SSE and sinistral strike-slip faults have NE-SW strikes. The cross-section construction is discussed in the text. and dextral faults are separated from one fault to another at 10° strikes 135
- Fig. 6.5. Graph of fault height and throw for 301 fault measurements in the Wytch Farm data set. The faults were measured from seismic sections, and the throws and heights were depth converted. 137
- Fig. 6.6. Rose diagrams of fault orientations at Kilve. (a) Normal faults have approximately E-W strikes, whilst (b) the reverse-reactivated fault strikes have a greater range. (c) Sinistral faults strike NE-SW, and (d) dextral faults have strikes between NNE-SSW and NNW-SSE. 138

- Fig. 6.7. Map of a relay ramp at Kilve (from Peacock and Sanderson, 1995a). The displacement on the two overstepping faults decreases into the ramp, but the total displacement is conserved. The contours indicate that the bedding is rotated from the 'regional' orientation to be almost perpendicular in the ramp, and also steeper. _____ 139
- Fig. 6.8. Line drawings, from photographs, of normal faults at Kilve. (a) Conjugate normal faults in the cliff to the immediate west of the steps at East Quantock's Head. The displacement is marked as > 11 m when it was not possible to match the beds on either side of the fault planes (*i.e.* the displacement $>$ cliff height). (b) Fault with synthetic branches in the cliffs to the east of Kilve Pill. (c) Line-drawing of a network of antithetic and synthetic normal faults in the cliffs, 25 m east of (b). The faults are steeper in the limestone units, and shallower in the interbedded shales. _____ 140
- Fig. 6.9. Three types of reverse-reactivated normal faults exposed in the cliffs. (a) Quantock's Head Fault. The fault has a finite normal displacement *c.* 45 m, but the over-tightened roll-over in the hanging-wall contains thrusts (Peacock and Sanderson, 1992). The hanging-wall exposure on the foreshore is characterised by highly disrupted bedding and a complicated network of strike-slip, reverse and normal faults (Fig. 6.4). (b) Fault with 8 m finite reverse throw in the Blue Ben Headland. The fault continues eastwards along the foreshore and oversteps with the Quantock's Head Fault (Fig. 6.4). (c) Fault zone in the cliffs to the east of Kilve Pill, with a net normal displacement of 5 m. The fault zone is composed of two sub-parallel faults, one of which has a finite reverse displacement, whilst the other has normal displacement. _____ 141
- Fig. 6.10. Displacement ranges for faults at Kilve and Wytch Farm. The normal faults on the foreshore at Kilve are bounded to the south by the 200 m displacement Blue Ben Fault (Fig. 6.4), but the largest fault on the foreshore has a displacement of 33.8 m. The average displacements for the normal fault from both areas is indicated by the dotted lines. Negative values = finite reverse displacements. Displacements on the dip-slip faults were measured as throws, and parallel to the strike of strike-slip faults. _____ 142
- Fig. 6.11. (Above and next two pages) The geometry of strike-slip faults. (a) Map of a mm-scale fault zone to the immediate west of the Blue Ben Headland (Fig. 6.4), The faults have highly irregular planes, and through-going faults are not fully developed from pull-apart arrays (Kelly *et al.*, in press). The acute conjugate angles are dominated by an E-W pressure-solution cleavage adjacent to the intersections. Anti-clockwise rotated blocks are delimited by the pressure-solution cleavage between two sub-parallel sinistral faults. (b) Map of a network of conjugate strike-slip faults between two overlapping reverse-reactivated normal faults (Kelly *et al.*, in press; in review). (c) Map of a m-scale conjugate fault zone at East Quantoxhead (Kelly *et al.*, in press). There are rare occurrences of pull-apart arrays between master faults, and sheared pull-aparts adjacent to the master faults. The strike-slip faults often overstep and displacement is transferred from one fault to another at (d) a strike-slip relay ramp (after Peacock and Sanderson, 1995a). (e) Strike-slip fault zone exposed in the cliff at East Quantoxhead. The strike-slip fault has a minor component of normal displacement, and resembles a normal fault in cross-section. Fault plane dip and dip direction are shown with lineation pitches in brackets. _____ 143

Fig. 6.12. Rose diagram of the normal faults at Wytch Farm. The strikes are calculated for each interpreted inline, by assuming a straight line between the location on the two adjacent inlines. The faults strike between NE-SW to NW-SE. _____ 146

Fig. 6.13. Normal fault geometries in the Wytch Farm Oilfield. The faults are segmented in cross-section, and overlap at either extensional or contractional oversteps. The reflectors are often chaotic in oversteps, so it is not always possible to interpret the displacements on the individual segments. The deformation style across the seismic survey is dominated by conjugate normal faults. _____ 147

Fig. 6.14. Three cross-sections through the conjugate Faults E and F. The sections are truncated seismic inline interpretations, whose numbers are indicated in the bottom left corners, and arranged from west to east (left to right). The circled numbers represent the relative timing of the faults on each section (1 = oldest movements, 3 = most recent). Growth sequences in the hanging-walls were used to identify fault activity. Fault E experienced the most recent movements, in all three cases. A breakdown of fault zone evolution is detailed in the text. _____ 148

Table 4.1. Comparison of the displacements and dips of the south-dipping and north-dipping normal and conjugate faults. Faults are included that have no directions. All other values refer to reverse displacements, and positive values refer to normal displacements. _____ 32

Table 4.2. Comparison of the two wells west of the interpretation. A comparison of well and seismic data indicates that the fault zone is a major boundary, located at the base of the Permian. In A and B, the fault is _____ 56

Table 4.3. Evolution of the fault zone in the _____ with the extension of the Acre Chalk, the Corallian and the Permian. The faults have been analysed at several stages of their evolution. The amount of extension is shown in the far seaward, and the amount of contraction is shown in the landward and onshore. The faults are shown with their original position. The faults are with growth in the landward and may be with contraction in the seaward. The faults are with growth in the landward and may be with contraction in the seaward. _____ 80

The faults are shown with their original position. The faults are with growth in the landward and may be with contraction in the seaward. The faults are with growth in the landward and may be with contraction in the seaward. _____ 86

Table 4.4. History of the fault zone at the _____ the Acre Chalk from BP Well _____ 92

Table 4.5. Evolution of the fault zone in the _____ the Acre Chalk from BP Well _____ 98

Table 4.6. Evolution of the fault zone in the _____ the Acre Chalk from BP Well _____ 110

List of tables

- Table 2.1. Summary of field observations for Figs. 2.6, 2.11 and 2.12. The vein type refers to the classification of Beach (1975): Type 1 = convergent, and Type 2 = bisector parallel. TT = transtension, SS = simple-shear and Ext. = extensional. The vein arrays strikes for Fig. 2.6(a) have been subdivided into dextral (D) and sinistral (S). The dextral and sinistral vein arrays in Fig. 2.6(b) have similar orientations, so have not been sub-divided. _____ 19
- Table 2.2. Results of the strain analysis for sample lines from each of the maps (X-X' and Y-Y': Figs. 2.6, 2.11 and 2.12). Data along two sample lines were collected for each map, with the exception of Fig. 2.6(b) due to insufficient displacement data. e_1 = extension axis, e_3 = shortening axis, and e_2 = intermediate axis (negative = contractional, positive = extensional). The number of faults for each sample line refers to the number of faults with measurable displacement that were included in the analysis, and not the actual number. The extensional and contractional axes orientations (eigenvectors) are indicated by the arrows in the final column (north is at the top of the page). ____ 22
- Table 3.1. Comparison of the displacements and dips of the south-dipping and north-dipping normal and reverse/reverse-reactivated normal faults. Faults are included that have dip directions 30° either side of north and south. Negative displacement values refer to reverse displacements, and positive values to normal displacements. _____ 33
- Table 4.1. Description of the horizons used in the interpretation. A comparison of well and seismic data indicates that the IntraLias pick represents the Middle Lias/Upper Lias boundary, located at the base of the Junction Bed (e.g. House, 1993). _____ 56
- Table 4.2. % Extension for the horizons in Table 4.1, with the exception of the Base Chalk, the Corallian and the IntraSherwood (due to a lack of meaningful data). The faults have been analysed at heave cut-offs of 100, 10, and 1 m. The greatest amount of extension occurred in the Top Sherwood, and the lower extensions are related to the Zone D Anhydrite and IntraLias horizons. Triassic faults are defined as those entirely within the Trias; Jurassic faults are with growth in the Jurassic, and may or may not extend into the Trias. The reactivated faults have growth in the Triassic units, but extend upwards into the Jurassic. _____ 80
- Table 5.1. List of the horizons used for this study (c.f. Fig. 5.6). Existing BP picks within the 3D survey area (mapped by Giles Watts and Peter Ellis, BP Exploration and Production) were extrapolated west to the 2D survey lines and east to the EEC study area. In the 2D data, all horizons below the Base White Lias are low-confidence picks, due to poor data quality. _____ 96
- Table 5.2. Details of the wells that are reported as having intersected the Arne Fault (from BP Well Completion Reports, and Knight, 1994). _____ 97
- Table 5.3. Summary of the zonation applied by Ellis (1997) to the Arne Fault in the BP 3D survey area. _____ 108
- Table 5.4. Details of the segment orientation, and pre-, syn- and post-rift sequences where identified for the Arne Fault. The post-rift deposits identified here relate to the first parallel reflectors above the syn-rift sediments. In some cases the post-rift is also faulted, and forms the pre-rift to shallower package of syn-rift sediments. The blanks in the table represent unidentifiable sedimentary sequences, but do not imply their presence/absence. _____ 110

Table 5.5. Criteria for the construction of the four new maps of the Arne Fault within the 2D survey area that reflect position, fault throw, orientation and segmentation uncertainties. The rationale behind the formulation of each map is discussed in the text. 112

chosen as they contain the greatest areas of Blue Hill sediments, and they also allow a direct comparison with a map of the structure of Kive (Fig. 6.4). The diagrams include data from the BP 3D and 4D seismic surveys that are calibrated with well data. The 3D survey extends eastwards from MW 301, and its greater resolution and tighter spacing is evident in the detail of the fault geometries. The cross-sections A-A' are produced from the projection of the two closest 2D seismic lines onto the line of the tertiary B-B' and C-C' were directly constructed from 3D lines.

Enclosure 2. Map of the exposure of Kive (mapped by P.C. Kelly and G.J. Sanderson, drawn by D.C.P. C. Wood and P.C. Kelly), and 4 cross-sections. The stratigraphic divisions of Palmer (1972) are preferred to those of other authors. Normal and reverse-sense normal faults have approximately 1 MW strike, oblique strike-slip faults strike NNW-SSE and sinistral strike-slip faults have 40-50° strike. The cross-sections are described in the text.

List of Appendices

- A1. 1. Photograph of the intersection between the conjugate strike-slip faults illustrated in Fig. 2.4;
- A1. 2. Photograph of example of strike-slip fault exposed in the cliff to the east of Quainock's Head (Fig. 2.9);
- A1. 3. The track of a conjugate strike-slip fault zone with associated pull apart basins (Fig. 3.3 and Fig. 3.11);
- A1. 4. Photograph of oversteepened normal faults exposed in the Ark of Kive (Fig. 6.9);
- A1. 5. Diagrams of the relationship between conjugate strike-slip faults and the reverse-sense normal Kive Hill Fault Zone (Fig. 3.10);
- A2. 1. Map of the strike-slip fault zone in Fig. 2.4 (a);
- A2. 2. Map of the strike-slip fault zone in Fig. 2.4 (b);
- A2. 3. Map of the strike-slip fault zone in Fig. 2.4 (c);
- A2. 4. Map with colour contour lines used to show the variation in fault dip for the normal and reverse-sense normal faults on the Kive structure. There is no interfingered relationship between dip direction and dip amount.

List of enclosures

Enclosure 1. Two time-slice maps and cross-sections of the Wytch Farm Oilfield. The time-slices are at 900 and 925 ms, which represents an approximate depth difference of 45 m. The two levels were chosen as they contain the greatest areas of Blue Lias sediments, and therefore allow a direct comparison with the map of the foreshore at Kilve (Fig. 6.4). The diagrams include data from the BP 2D and 3D seismic surveys, that are calibrated with well data. The 3D survey extends eastwards from 401250, and its greater resolution and tighter spacing is evident in the detail of the fault geometries. The cross-section A-A' was produced from the projection of the two closest 2D seismic lines onto the line of the section; B-B' and C-C' were directly constructed from 3D lines.

Enclosure 2. Map of the exposure at Kilve (mapped by P.G. Kelly and D.J. Sanderson, drawn by D.C.P. Peacock and P.G. Kelly), and a composite cross-section. The stratigraphic divisions of Palmer (1972) are preferred for descriptive reasons. Normal and reverse-reactivated normal faults have approximately E-W strikes, dextral strike-slip faults strike NNW-SSE and sinistral strike-slip faults have NE-SW strikes. The cross-section construction is discussed in the text.

List of Appendices

- A1. 1. Photograph of the intersection between the conjugate strike-slip faults illustrated in Fig. 2.6.
- A1. 2. Photographs of example of strike-slip fault exposed in the cliff to the east of Quantock's Head (Fig. 2.9).
- A1. 3. Photograph of a conjugate strike-slip fault zone with associated pull-apart arrays (Fig. 2.3 and Fig. 6.11).
- A1. 4. Photograph of reverse-reactivated normal faults exposed in the cliffs at Kilve (Fig. 6.9).
- A1. 5. Photograph of an intersection zone between strike-slip faults and the reverse-reactivated Kilve Pill Fault Zone (Fig. 3.10).

- A2. 1. Map of the strike-slip fault zone in Fig. 2.6 (a)
- A2. 2. Map of the strike-slip fault zone in Fig. 2.6(b)
- A2. 3. Map of the strike-slip fault zone in Fig. 2.11(b)
- A2. 4. Map with colour-coded fault traces to show the variation in fault dip for the normal and reverse-reactivated normal faults on the Kilve foreshore. There is no unambiguous relationship between dip direction and dip amount.

Acknowledgements

There are so many people to acknowledge, but most importantly I thank my two supervisors: David Sanderson and David Peacock. Completion of the project would not have been possible without the supervision and excellent advice that I received, both during preliminary field work and subsequent discussions and suggestions that improved the papers and thesis. I am particularly grateful to David Peacock for recommending me for the project in the first place, to Dave Sanderson for timely encouragement, and also to Mark Anderson (Plymouth) for pre-Southampton structural geology supervision. Thank you to the University of Southampton for funding, much of which has been heavily re-invested in the city's leisure industry. Field work in Northumbria and Somerset was partly funded by Elf Aquitaine, and arranged by Keith Rawnsley. Part of the work contained in this thesis was carried out during a summer project at BP Wytch Farm. I am extremely grateful for all of the help, advice and support from the Reservoir Development group: Andy Bowler, Tony Drayton, Alison Hardy, Peter Harrison, Tor Meling, Paddy Parsons, Alfonso Rodriguez, Steve Thompson, Mike Tothill, Alison Wildgoose, and, in particular, Giles Watts, Andrew Hogg, Jonathan Evans and Ian Lonsdale, and Peter Ellis at the Subsurface team, Sunbury. Half of the thesis was made possible from the generous access that BP Wytch Farm allowed to their seismic data sets. Joe Cartwright at Imperial College, London, provided the use of a seismic workstation, and Dustin Lister is thanked for the crash course in the software.

Members of the Geomechanics Research Group, past and present, provided much advice, humour and an amazing collection of laughs: Gavin Day, Steve Dee, Cat Greenfield, Rob Hunsdale, Danny Hyam, Richard Jolly, Young-Seog Kim, Joe Lenham, Rory Quinn, Dominic Riley, George Tuckwell, Rakesh Walia and Xing Zhang. Jim Andrews, Andy Barker and Norman Hamilton are thanked for their advice and guidance throughout the project. All of the support staff in the department have been amazing, even under constant badgering. Seven years at university would not have passed so quickly and happily without all the friends that shared the waves, haze, rocks and shocks of student life at both Plymouth and Southampton; Al Alexander, Katie Allen, Tim Cane, Ian Harding, Mike Reeder and Russell Wynn all had the dubious pleasure of sharing houses in Southampton. There's so many other people to mention, but you know who you are.

Finally, where would we all be without our families? I'm particularly fortunate to have Rosalind as a sister, and am thankful for her support, especially during the last couple of years (I'm glad we stopped fighting!). Thanks, mum and dad, for not being too hard on me when giving up school, when leaving a secure job, and when wanting to return to, and then to continue, studying; I hope you appreciate that it was all worth it.

1. Introduction

The segmentation, linkage and displacement geometries of normal faults are well-documented from studies in map view (e.g. Peacock and Sanderson, 1991; 1994a; Schlische, 1993; Anders and Schlische, 1994; Cartwright et al., 1995; Childs et al., 1995) and in cross-section (Muraoka and Kamata, 1983; Peacock and Sanderson, 1994b, Childs et al., 1996, Mansfield and Cartwright, 1996). Peacock and Zhang (1994) and Willemse (1997) compared the geometries of normal faults in the field with numerical analogues. The above-mentioned studies address linkage between faults that formed during single deformation events. Normal fault reactivation and propagation during polyphase extension has been recognised in, for example, the Wessex Basin (Chadwick, 1986), the North Sea (Færseth, 1996; Thomas and Coward, 1995), and the East African Rift (Bosworth, 1992). These studies provide basin-scale viewpoints on structural reactivation, but do not discuss geometries of individual normally-reactivated faults.

Post-extensional compression (or *inversion*) is a common feature of the hydrocarbon basins around the British Isles (e.g. Wessex Basin, Stoneley, 1982; Karner et al., 1987; southern North Sea, Badley et al., 1989; East Shetland Basin, Thomas and Coward, 1995), but the selective reverse-reactivation of normal faults is not fully understood. Reverse-reactivated faults are exposed on the north Somerset coast (McLachlan, 1986; Dart et al., 1995; Nemcok et al., 1995), that are an expression of Tertiary basin inversion (McLachlan, 1986; Peacock and Sanderson, 1992). Strike-slip faults, which are thought to have formed at a similar time (Dart et al., 1995; Peacock and Sanderson, 1995a) are also present. However, the significance of the conjugate strike-slip faults in the contraction, and the geometries of displacement transfer zones between reverse-reactivated faults, have not been discussed.

1.1 OBJECTIVES

The objective of this thesis is two-fold: to propose models that describe the development of segmented normal, strike-slip and reverse-reactivated normal faults and, secondly, to apply fault analysis methods to problematic areas in the seismic interpretation of normal faults in the Wessex Basin.

1.2 STUDY AREAS

The two field areas for the study (Fig. 1.1) were chosen because of the quality of the exposure. Kilve, on the north Somerset coast, has normal, reverse-reactivated normal and strike-slip faults exposed in the cliffs and on the gently-dipping beds of the wave-cut platform. The deformation at Beadnell, on the Northumbrian coast, consists largely of strike-slip faults that are associated with mm-scale thrusts. 2D and 3D seismic data, supplied by BP Wytch Farm, that cover the onshore – offshore transition zone of the Dorset coast in Poole Harbour, were used for the analysis of normal fault geometries.

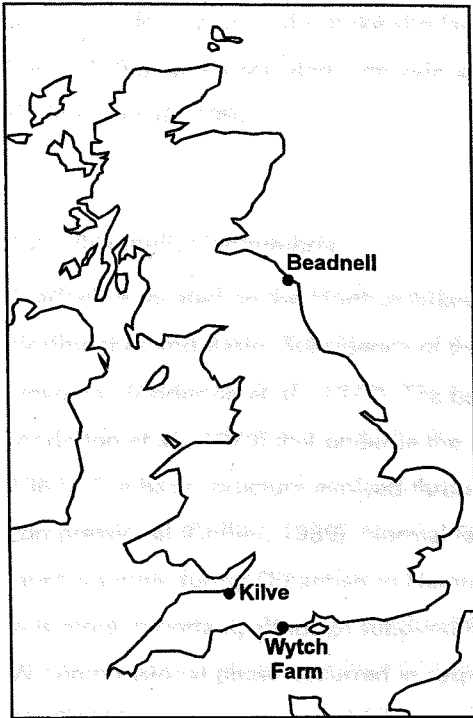


Fig. 1.1. Map of part of the British Isles that shows the three study areas: Kilve, north Somerset, Beadnell, Northumberland, and Wytch Farm, Dorset.

1.2.1 Kilve, north Somerset

The foreshore at Kilve is the onshore continuation of the Bristol Channel Basin (e.g. McGrath and Davison, 1995; Peacock and Sanderson, 1995a), which is a sub-basin in the north-west extreme of the Wessex Basin (Kent, 1949). The E-W striking, gently dipping rocks exposed on the wave-cut platform and in the cliffs are of Lower Liassic age (Lower Jurassic), and consist of an interbedded sequence of predominantly limestones and shales (Whittaker and Green, 1983). The strata are truncated by normal faults related to the Mesozoic formation of the Bristol Channel (Brooks *et al.*, 1988), reverse-reactivated normal faults (McLachlan, 1986; Dart *et al.*, 1995; Nemcok *et al.*, 1995) and strike-slip faults that formed during Alpine-associated contraction (Van Hoorn, 1987; Peacock and Sanderson, 1992; 1995a; McGrath and Davison, 1995). The normal faults strike approximately E-W, and are associated with veins with similar strikes and geometries (Bowyer and Kelly, 1995). The segmentation of the normal faults in map view has been described by Peacock and Sanderson (1991; 1994a), and the deformation at fault tips has been discussed by McGrath and Davison (1995). The normal faults exposed in the cliffs often have irregular planes that are steeper in the limestones than in the shales (Peacock and Sanderson, 1991).

There are examples of reverse-reactivated faults exposed in the cliffs, that are recognised from thrusts in the hanging-walls, tight rollover anticlines and kink bands (Peacock and Sanderson, 1992), sub-horizontal veins with vertical fibres (Sibson, 1995) and multiple sets of slickenside lineations. Strike-slip faults on the wave-cut platform, and in the cliffs, are conjugate about approximately N-S (Peacock and Sanderson, 1995a). Dextral faults strike NW-SE and sinistral faults strike NE-SW (Peacock and Sanderson, 1995a). The strike-slip faults have sub-horizontal slickenside lineations, although occasional gently-inclined lineations indicate either reverse or normal displacement components. The strike-slip faults are

also segmented, at strike-slip relay ramps in map view (Peacock and Sanderson, 1995a), and in cross-section. Deformation in the strike-slip fault zones at the mm-scale is achieved through block rotations (Kelly, 1996), and associated with vein arrays and pressure solution (Peacock and Sanderson, 1995b; Willemse et al., 1997).

1.2.2 Beadnell, Northumbria

Beadnell is located on the Northumbrian coast of north-east England (Fig. 1.1) and lies within the Northumberland Basin. Subsidence of the basin, above the Iapetus collision zone, was initiated in the Devonian (Anderton et al., 1979). The basin-fill consists of fluvial Upper Old Red Sandstone sediments (Anderton et al., 1979) that underlie the Lower Carboniferous limestones exposed at Beadnell (Shiells, 1964). The basin structure evolved through three tectonic episodes, two extensional and one compressional (Collier, 1989). Normal faults were formed in response to extensional reactivation of the Iapetus suture during Dinantian to Namurian N-S extension (Kimbell et al., 1989). Thermal subsidence was more important, although subdued fault activity continued, in the Westphalian (Collier, 1989). An E-W compressional phase occurred in response to movements in the Carboniferous (Shiells, 1964; Collier, 1989). N-S striking thrusts and folds are found adjacent to strike-slip faults, and vertical shear zones, that are conjugate about E-W (Shiells, 1964). The strike-slip fault zones were mapped by Shiells (1964) at several localities along the Northumbrian coast, between Beadnell and Berwick-upon-Tweed, and on Holy Island. Shear zones dominated the deformation during the closing compressional movements (Shiells, 1964). Mafic dykes and sills, including the Whin Dykes and the Great Whin Sill, were intruded and some of the ENE-WSW normal faults were reactivated during renewed extension in the Permian (Robson, 1977; Collier, 1989).

1.2.3 Wytch Farm, Dorset

The Wytch Farm Oilfield (Fig. 1.1) on the Dorset coast, lies on the southern margin of the onshore extent of the Wessex Basin. The basin was initiated in the Permian as a series of mainly down-to-the-south asymmetric E-W half-graben (Chadwick, 1986; Lake and Karner, 1987). The Triassic basin-fill consists of the Sherwood Sandstone, which lies unconformably on Permian sediments, and the Mercia Mudstone and Penarth Groups (Hogg et al., in press). The Permo-Triassic normal faults were reactivated in response to Jurassic to Cretaceous extension (Chadwick, 1986; Lake and Karner, 1987), during which listric growth faults developed (Stoneley, 1982). The Jurassic to Cretaceous fill consists of Lower – Middle Jurassic sediments, below an unconformity at the base of the Chalk. The extensional development of the basin was followed by Alpine-related basin inversion (Stoneley, 1982; Lake and Karner, 1987; Chadwick, 1993). Normal faults in the Wytch Farm Oilfield are segmented in both map view and cross-section, and therefore provide ideal subjects for a study of dip-linkage (Mansfield and Cartwright, 1996) between normal faults of different ages.

1.3 THESIS LAYOUT

Models that describe the development of segmented faults in both extensional and compressional settings are formulated in Chapters 2-4. Chapter 2 describes the geometries and proposes a model for the formation of conjugate strike-slip fault zones in limestones. The chapter has been accepted, in its present form, for publication with the *Journal of Structural Geology*. D.C.P. Peacock and D.J. Sanderson are included as co-authors on the paper, as they contributed through discussions of the structures, and by editing the paper. The reverse-reactivated normal faults at Kilve are discussed in Chapter 3. Selective reactivation of the normal faults is used as a basis to formulate a model for the contractional deformation on the north Somerset coast. The model includes the role in the contraction of the strike-slip faults described in Chapter 2. Chapter 3 is currently in review with the *Journal of Structural Geology*. D.C.P. Peacock, D.J. Sanderson and A.C. McGurk are co-authors, in recognition of their contribution to the mapping, and for editing the paper. Normal faults that developed during polyphase extension of the Wessex Basin, interpreted from the BP Wytch Farm seismic data sets, are illustrated in Chapter 4. The application of fault analysis methods to re-interpret the structure of the Sherwood Sandstone in selected areas of the Wytch Farm Oilfield in the Wessex Basin in Chapter 5. Chapter 6, is a comparison of the fault geometries mapped in the field at Kilve and from the Wytch Farm seismic data. The overall conclusions to Chapters 2-6 are made in Chapter 7.

A review of previous work at the localities, and on the subject matter, and the methods used are included within each chapter.

2. Linkage and evolution of conjugate strike-slip fault zones in limestones of Somerset and Northumbria

2.1 SUMMARY

Conjugate strike-slip fault zones that cover metre-scale areas at Beadnell, Northumbria, and Kilve, Somerset, were initiated as conjugate vein arrays. Early conjugate faults are linked by the propagation of one fault that eventually by-passes the other fault. A model for the development of strike-slip faults is presented, using fault and vein geometries and the position of damage zones with respect to the master faults as an indication of the propagation direction. This model includes the evolution of networks from (1) the initial random development of vein arrays, to (2) the isolated development of several unconnected conjugate fault segments that pass into vein arrays, through (3) the intersection of a conjugate set of master faults and linkage with minor antithetic faults, and the formation of new vein arrays with extensional geometries after a linked network of faults is established, to (4) breaching of intersection points by dominant faults, and finally (5) the propagation towards oversteps that are breached to form a through-going fault. The geometry of the active structures simplifies with time, as strain is localised along the master fault, but the complexities are preserved in the fault walls.

Process zone in effective tension

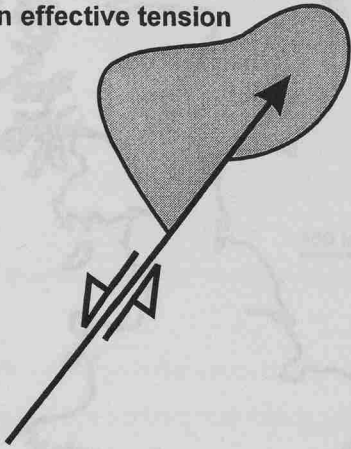


Fig. 2.1. The location of a zone of effective tension at the tip of a right-propagating sinistral fault containing tensile microcracks (Reches and Lockner, 1994). The process zone moves with the propagating fault, and coalescence of the microcracks influences the position of the damage zone (Scholz et al., 1993).

2.2 INTRODUCTION

Damage zones consist of small faults and veins (*subsidiary fractures*) in the vicinity of larger structures (*master faults*) (Chester and Logan, 1986). Such zones are often related to the propagation of the larger fault (Scholz et al., 1993; Reches and Lockner, 1994) and processes at fault-tips (McGrath and Davison, 1995). In particular, Reches and Lockner (1994) identify a process zone, during experimental fracture of Western Granite, consisting of an area of extensional (Mode 1) fracture at the fault-tip that enhances fault propagation (Fig. 2.1). The process zone moves with the fault-tip, leaving damaged rock in its wake (Scholz et al., 1993). The process zone is asymmetric about a Mode II tip, reflecting the propagation direction and sense, and controls the location and width of the damage zone. Zones of 'damaged' rock adjacent to faults may also arise from structures that form prior to the development of a through-going fault. Cowie and Scholz (1992) demonstrate how a planar fault develops from arrays of fractures that coalesce to form an irregular fault plane. The asperities are by-passed during displacement accumulation, leading to the formation of a smooth fault plane. On the metre-scale, strike-slip relay ramps (Peacock and Sanderson, 1995a) form in contractional zones in between overstepping strike-slip fault segments. In their model, a smooth fault plane with a contractional bend develops after the relay ramp has been breached, and the inactive parts of the structure are preserved adjacent to the fault.

The location and geometry of damage zones are important as they may contribute to the compartmentalisation a reservoir, or provide fracture-controlled fluid flow pathways in addition to the master fault (e.g. Knott et al., 1996). The development of strike-slip fault zones is of interest in permeability studies, as it will be demonstrated that these faults develop initially in isolation, and linkage of fractures may occur during later evolution.

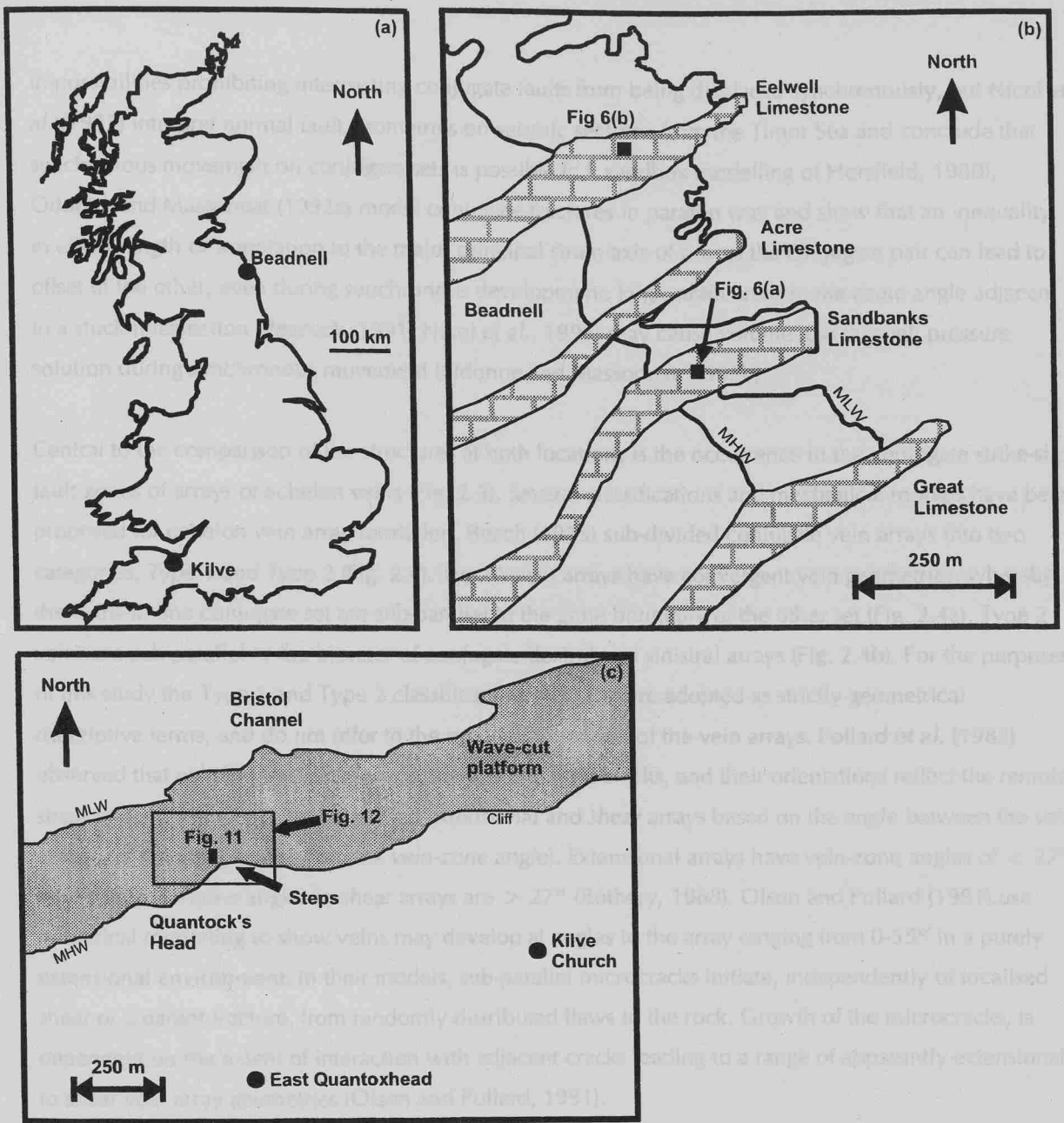


Fig. 2.2. (a) Map of part of the British Isles showing the locations of (b) Beadnell, Northumbria, and (c) Kilve, Somerset. The locations of the strike-slip fault zones described in the text are also shown. MHW – mean high water, and MLW – mean low water.

The aim of this chapter is to show how the development of conjugate strike-slip faults in limestones, over scales of millimetres to 10's metres, may be described with a common fault evolution model. The formulation of the model is based on field observations at two locations: Kilve, Somerset, and Beadnell, Northumbria (Fig. 2.2). The justification of using two locations and several examples, is based on the range of comparable structures in both areas. The mechanics of conjugate fault development have been the subject of much debate, with particular emphasis on the nature of the intersection or offset of the conjugate sets. For example, Freund (1974), using analogue modelling, identifies geometrical

impossibilities prohibiting intersecting conjugate faults from being displaced synchronously, but Nicol et al. (1995) interpret normal fault geometries on seismic sections from the Timor Sea and conclude that synchronous movement on conjugate sets is possible (c.f. sandbox modelling of Horsfield, 1980). Odonne and Massonnat (1992a) model conjugate fractures in paraffin wax and show that an inequality in either length or orientation to the major principal strain axis of one of the conjugate pair can lead to offset of the other, even during synchronous development. High strain areas in the acute angle adjacent to a stuck intersection (Peacock, 1991; Nicol et al., 1995) may cause volume loss through pressure solution during synchronous movement (Odonne and Massonnat, 1992b).

Central to the comparison of the structures at both locations is the occurrence in the conjugate strike-slip fault zones of arrays of echelon veins (Fig. 2.3). Several classifications and mechanical models have been proposed for echelon vein array formation. Beach (1975) sub-divided conjugate vein arrays into two categories, *Type 1* and *Type 2* (Fig. 2.4). *Type 1* vein arrays have convergent vein geometries, whereby the veins in one conjugate set are sub-parallel to the zone boundary of the other set (Fig. 2.4a). *Type 2* veins are sub-parallel to the bisector of conjugate dextral and sinistral arrays (Fig. 2.4b). For the purposes of this study the *Type 1* and *Type 2* classifications (Fig. 2.4) are adopted as strictly geometrical descriptive terms, and do not refer to the mode of formation of the vein arrays. Pollard et al. (1982) observed that echelon fractures form at the tips of parent cracks, and their orientations reflect the remote stress system. Rothery (1988) classified *extensional* and *shear* arrays based on the angle between the vein strike and the array orientation (the *vein-zone angle*). Extensional arrays have vein-zone angles of $< 27^\circ$, whilst the vein-zone angles in shear arrays are $> 27^\circ$ (Rothery, 1988). Olson and Pollard (1991) use numerical modelling to show veins may develop at angles to the array ranging from $0-55^\circ$ in a purely extensional environment. In their models, sub-parallel microcracks initiate, independently of localised shear or a parent fracture, from randomly distributed flaws in the rock. Growth of the microcracks, is dependent on the extent of interaction with adjacent cracks leading to a range of apparently extensional to shear vein array geometries (Olson and Pollard, 1991).

Gamond (1983) and Peacock and Sanderson (1995b) demonstrate how vein arrays evolve into pull-apart arrays through dilation of the veins between overstepping 'P'-shears (Fig. 2.3b) that may be eventually faulted (Fig. 2.3c) (Cowie and Scholz, 1992). Pull-aparts occur in dilational jogs between overstepping shear fractures (Sibson, 1989) over several orders of magnitude (Aydin and Nur, 1982), from the millimetre-scale (Peacock and Sanderson, 1995b), to sedimentary basins on the kilometre-scale (e.g. Hempton and Dunne, 1984). A dilational jog occurs between either right-stepping dextral faults or left-stepping sinistral faults (Segall and Pollard, 1980), and may also occur during movement at a releasing bend found at the intersection point of oblique fault segments (Mann et al., 1983; Sibson, 1989).

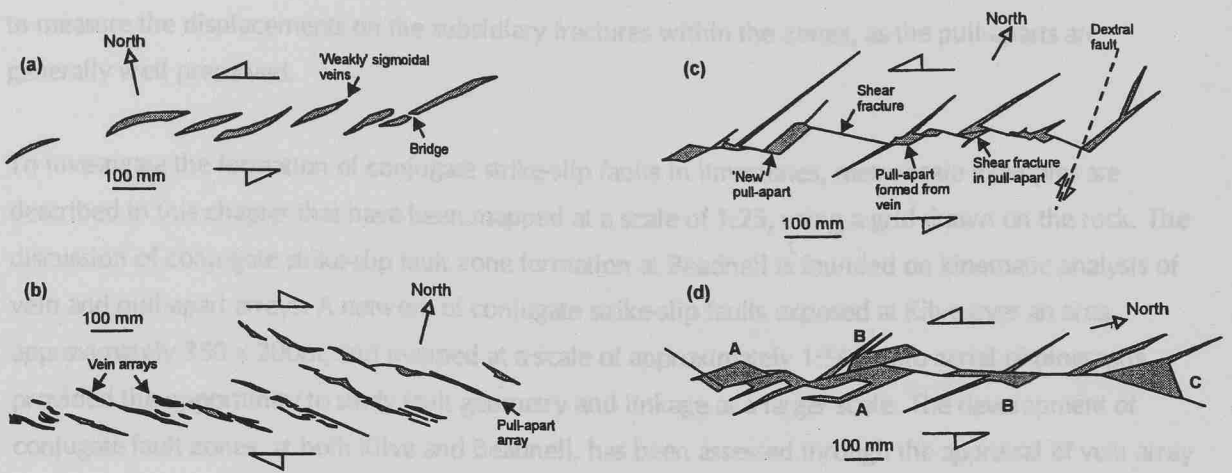


Fig. 2.3. Field examples from Beadnell [NU4237 6294] of (a) and (b) vein arrays, and from Kolve [ST3119 1438] (c) a pull-apart array, and (d) a strike-slip fault with adjacent sheared calcite-filled pull-aparts.

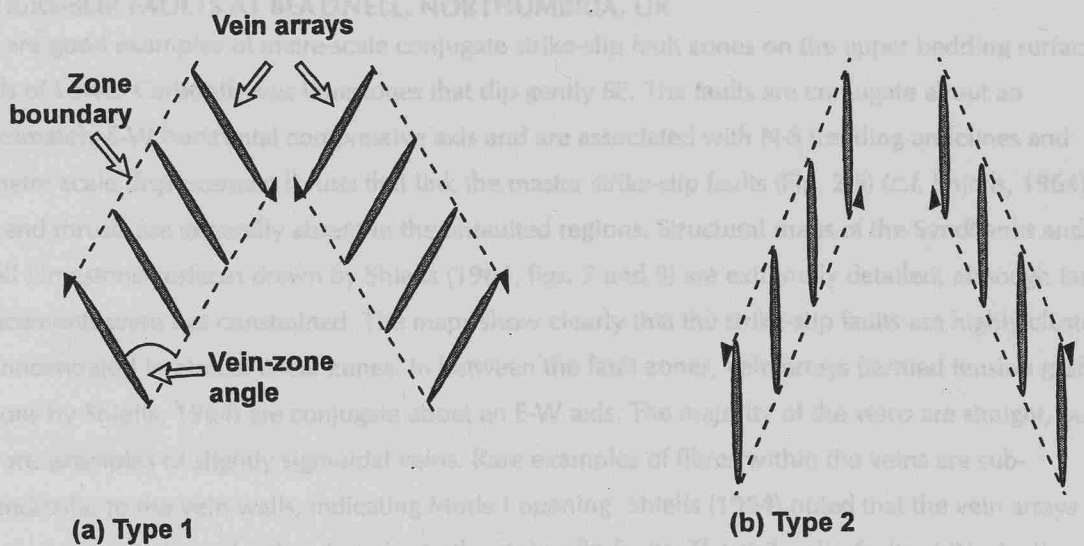


Fig. 2.4. Schematic diagrams of convergent (Type 1) vein arrays, and bisector parallel veins (Type 2) (after Beach, 1975).

For the purposes of the metre-scale maps, the *master faults* are those that define the triangles of the conjugate sets, are relatively through-going and have larger displacements (> 100 mm in the examples mapped). The *subsidiary fractures* are the smaller displacement faults and veins adjacent to the master faults. The offset of earlier faults and veins, the length of pull-aparts, and the strike-separation of faulted pull-aparts may all be used to estimate fault displacements (Peacock and Sanderson, 1995b). It is easier

to measure the displacements on the subsidiary fractures within the zones, as the pull-aparts are generally well preserved.

To investigate the formation of conjugate strike-slip faults in limestones, metre-scale examples are described in this chapter that have been mapped at a scale of 1:25, using a grid drawn on the rock. The discussion of conjugate strike-slip fault zone formation at Beadnell is founded on kinematic analysis of vein and pull-apart arrays. A network of conjugate strike-slip faults exposed at Kilve over an area approximately 350 x 200m, and mapped at a scale of approximately 1:500 onto aerial photographs, provided the opportunity to study fault geometry and linkage at a larger scale. The development of conjugate fault zones, at both Kilve and Beadnell, has been assessed through the appraisal of vein array geometries, fault propagation direction using the asymmetric distribution of fracture density adjacent to the faults (c.f. Scholz *et al.*, 1993; Reches and Lockner, 1994), and the modified displacement-gradient tensor method of fault-strain analysis (Jamison, 1989; Peacock and Sanderson, 1993). In conclusion, a conjugate strike-slip fault zone evolution model has been developed by combining the observations at both localities.

2.3 STRIKE-SLIP FAULTS AT BEADNELL, NORTHUMBRIA, UK

There are good examples of metre-scale conjugate strike-slip fault zones on the upper bedding surfaces of beds of Lower Carboniferous limestones that dip gently SE. The faults are conjugate about an approximately E-W horizontal compressive axis and are associated with N-S trending anticlines and millimetre-scale displacement thrusts that link the master strike-slip faults (Fig. 2.5) (c.f. Shiells, 1964). Folds and thrusts are generally absent in the unfaulted regions. Structural maps of the Sandbanks and Eelwell Limestone surfaces drawn by Shiells (1964, figs. 7 and 9) are extremely detailed, although fault displacements were not constrained. The maps show clearly that the strike-slip faults are highly clustered and concentrated in almost linear zones. In between the fault zones, vein arrays (termed tension gash echelons by Shiells, 1964) are conjugate about an E-W axis. The majority of the veins are straight, but there are examples of slightly sigmoidal veins. Rare examples of fibres within the veins are sub-perpendicular to the vein walls, indicating Mode I opening. Shiells (1964) noted that the vein arrays are not only conjugate to each other, but also to the strike-slip faults. The strike-slip faults at Beadnell occurred as a result of approximately E-W compression during the Variscan Orogeny (Shiells, 1964; Collier, 1989), that also caused N-S trending folds (Benard *et al.*, 1990). The compressional phase occurs between two extensional phases that affected NE England (Collier, 1989). ENE-WSW to NE-SW striking normal faults initiated in the Late Devonian (Shiells, 1964) and ceased during the Early Carboniferous (Collier, 1989). The Whin Dykes were intruded and some of the ENE-WSW normal faults were reactivated during post-compressional extension in the Permian (Robson, 1977; Collier, 1989). The fault traces are exposed on the surfaces of limestone units, but their three-dimensional geometries are more difficult to observe.

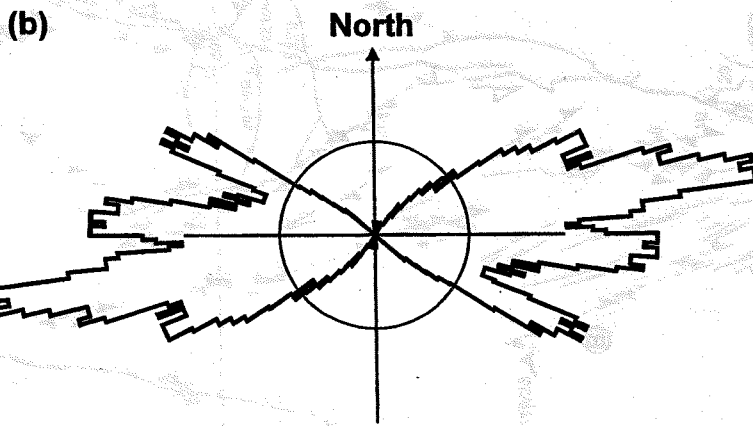
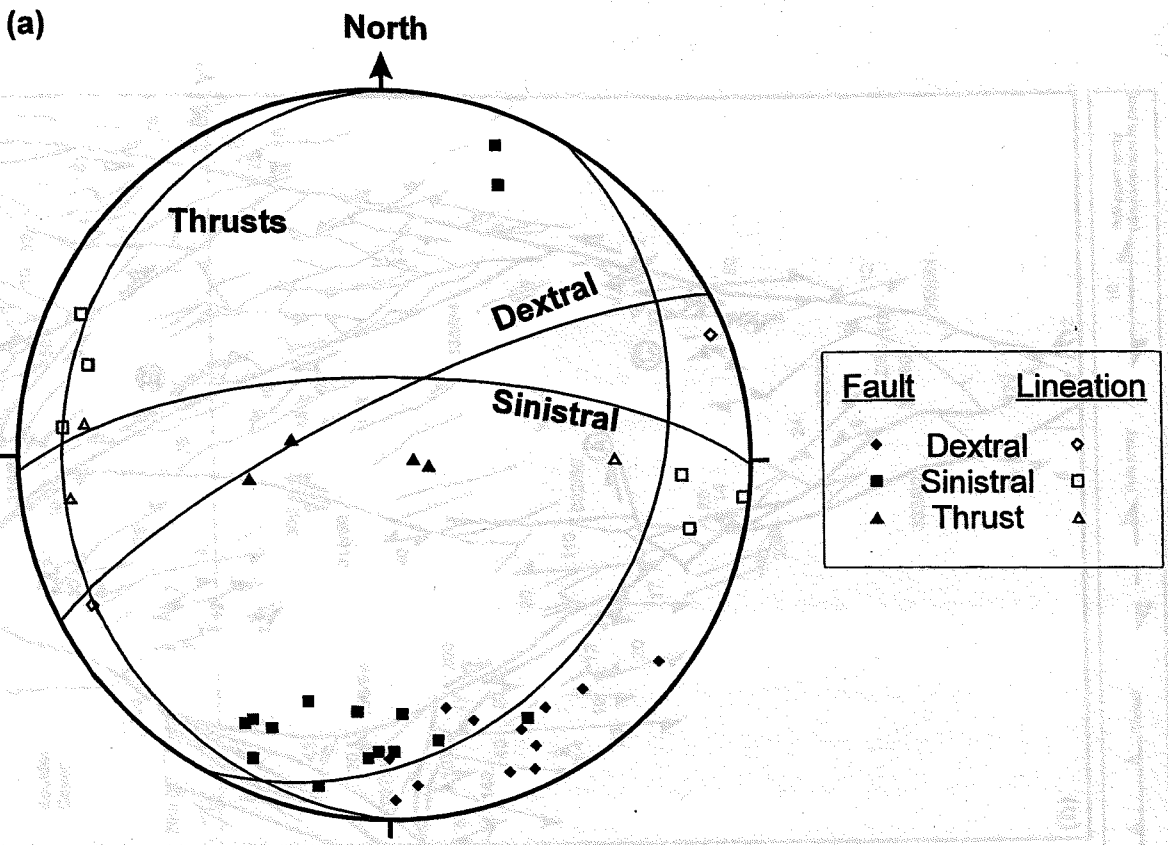


Fig. 2.5. Data from the mapped fault zones at Beadnell, Northumbria. (a) Equal-area stereogram of poles to planes of sinistral ($n = 15$) and dextral ($n = 11$) strike-slip faults, and of thrusts ($n = 4$). Lineation data and synoptic great circles for the faults are also shown. (b) Rose diagram of the vein array orientations within these fault zones ($n = 100$). The data can be divided into three groups based on orientations: (i) NW-SE, (ii) ENE-WSW and (iii) = E-W. The first two form a conjugate set of arrays, with a sinistral NW-SE group and a dextral ENE-WSW group.

Fig. 2.6 (overleaf) Conjugate strike-slip fault zones mapped at Beadnell at a scale of 1:25. Displacements are in mm. The circled letters are referred to in the text. For location see Fig. 2.1(b). (a) Fault zone showing a conjugate arrangement of strike-slip faults that have not linked to form a network [NU4238 6289]. (b) Network of linked strike-slip faults [NU4237 6294].

The fault zone shown in Fig. 2.6(a) contains strike-slip faults associated with veins and pull-apart arrays. Veins oblique to the strike of the faults are common, and usually terminate at the fault. The maximum fault displacement, measured parallel to a fault, is 225 mm. The faults have irregular planes, and fault segments often terminate or link at contractional or dilational oversteps. The master fault planes do not link to form a through-going network of faults (i.e. a percolating cluster, Stauffer and Aharony, 1992), but terminate in the rock and are co-linear with arrays of veins and pull-aparts. The majority of the arrays form conjugate sets and have convergent vein geometries (Type 1, Beach, 1975), where the veins in one conjugate set parallel the zone boundary of the other conjugate set. There are some examples of bisector-parallel veins close to the terminations of master faults (Type 2, Beach, 1975). Thrusts with millimetre-scale displacements link with the strike-slip faults, some of which are offset and matchable across the strike-slip faults. There are, however, rare examples of thrusts that terminate at strike-slip faults.

A second example from Beadnell is of a much more linked network (Fig. 2.6b). The maximum fault displacement is approximately 500 mm, and the master faults have much more continuous traces than in the first example (Fig. 2.6a). Sheared pull-apart structures (Fig. 2.3c) occur along-side some of the faults, and there are examples of fault segments that overstep at dilational jogs. The largest faults link mainly by fault-tips abutting fault walls (tip-wall linkage), and there are no vein arrays that are co-linear with the faults. Damage between the largest faults consists of networks of clustered vein arrays and subsidiary faults with millimetre-scale displacements. The majority of the veins are sub-parallel to the acute bisector angle of the conjugate master fault traces (Type 2, Beach, 1975), with few exceptions. A N-S striking dextral strike-slip fault offsets the northern conjugate set, indicating a later stage of deformation (at A, Fig. 2.6b).

2.3.1 Kinematic analysis

The kinematic evolution of the veins and pull-apart arrays in the fault zone maps can be determined using the construction of McCoss (1986), to find the relative infinitesimal wallrock displacement direction (Fig. 2.7). Graphs of zone boundary orientation plotted against the strike of the veins within the arrays show major differences in the vein-zone angle for each of these two maps (Fig. 2.7a). In the map of unconnected faults there is a greater proportion of simple-shear arrays (Fig. 2.6a) that plot in two clusters, one dextral and the other sinistral (Fig. 2.7a). The vein and pull-apart arrays from the connected network of strike-slip faults (Fig. 2.6b) plot in one cluster centred on the line of extension (Fig. 2.7a). In sharp contrast to the arrays in the unconnected strike-slip network (Fig. 2.6a), the majority of the transtensional arrays in the connected network (Fig. 2.6b) have a predominantly extensional component.

Figure 2.7 (a) and (b) show the construction of McCoss (1986) for each of vein arrays in Fig. 2.6(a). This method treats each vein array as a transtensional or transpressional zone (Sanderson and Marchant, 1994), to determine the infinitesimal displacement direction (A) of the wall-rock from the zone boundary and the vein angle. A line parallel to the vein is drawn from point y to the circumference of a circle, z, that touches the zone boundary. A second line is drawn from y that passes through the centre of the circle, to find A.

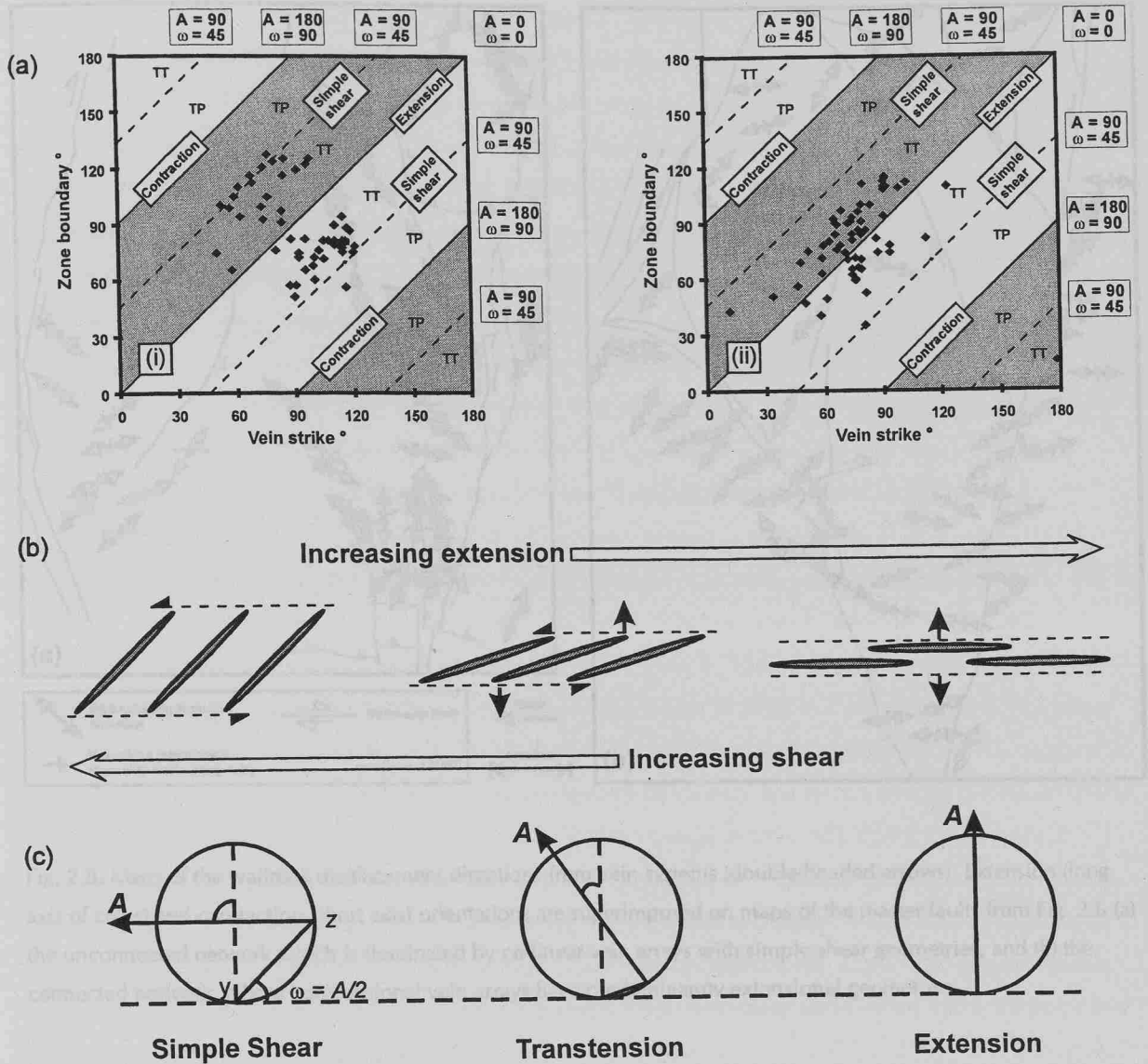


Fig. 2.7. (a) Graphs of zone boundary orientation and vein orientation to show the distribution of vein array geometries from Fig. 2.6. When the infinitesimal wallrock displacement direction (A) is equal to the angle between the vein array and zone boundary (w), the vein array has an extensional geometry. A difference of 90° signifies contraction, and one of 45° indicates that the array has a simple-shear geometry. The lines of extension and contraction separate zones of dextral and sinistral displacement sense. The shaded areas indicate sinistral sense. TT = transtension; TP = transpression. (i) Data from Fig. 2.6(a), $n = 56$. The two distinct clusters of data indicate conjugate vein arrays that have predominantly simple-shear geometries. (ii) Data from Fig. 2.6(b), $n = 60$. The single data cluster, centred on the extensional zone of the graph, demonstrates that the vein arrays in this fault zone have transtensional geometries, but are dominated by extension. (b) Schematic diagram of vein arrays with simple-shear, transtensional and extensional geometries. (c) The construction of McCoss (1986) for each of vein arrays in Fig. 2.7(b). This method treats each vein array as a transtensional or transpressional zone (Sanderson and Marchini, 1984), to determine the infinitesimal displacement direction (A) of the wall-rocks from the zone boundary and the vein angle. A line parallel to the veins is drawn from point y to the circumference of a circle, z , that touches the zone boundary. A second line is drawn from z that passes through the centre of the circle, to find A .

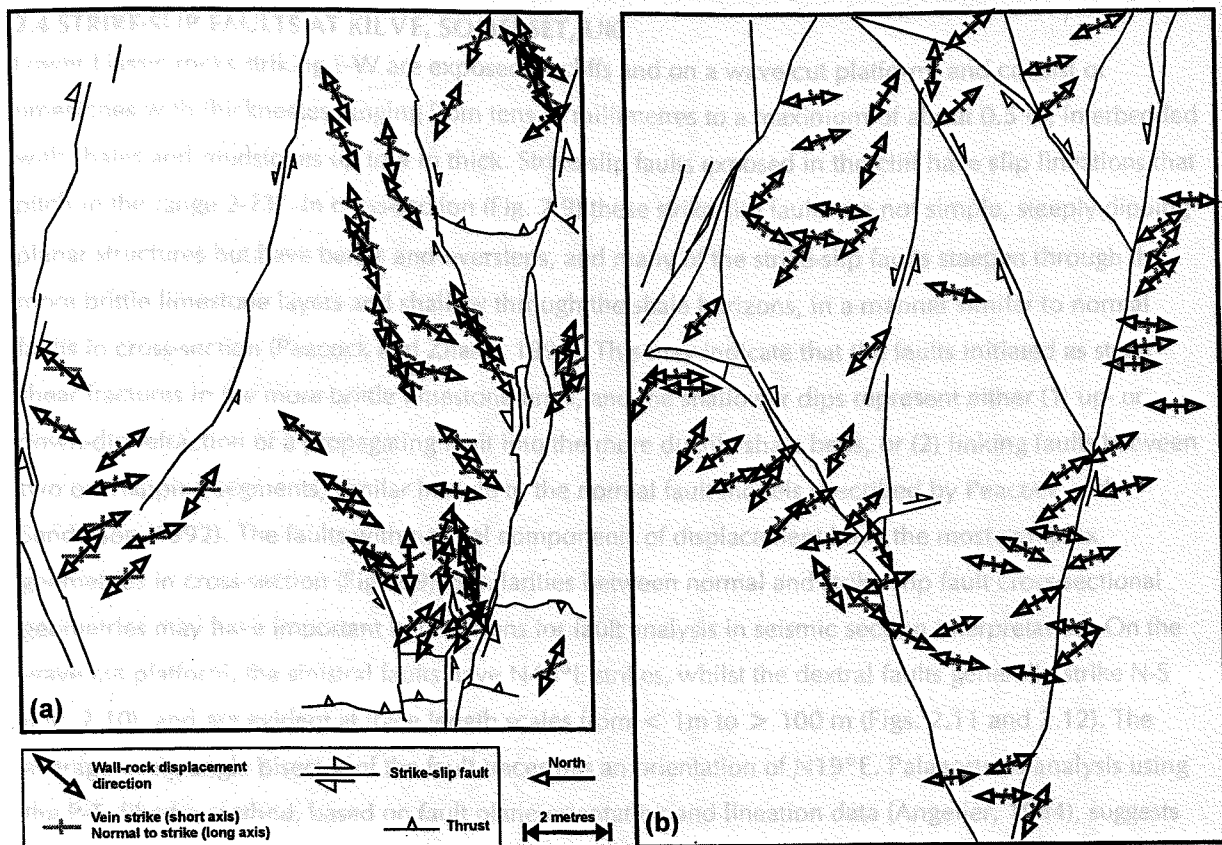


Fig. 2.8. Maps of the wallrock displacement directions from vein systems (double-headed arrows). Extension (long axis of cross) and contraction (short axis) orientations are superimposed on maps of the master faults from Fig. 2.6 (a) the unconnected network which is dominated by co-linear vein arrays with simple-shear geometries, and (b) the connected network, where transensional vein arrays have predominantly extensional geometries.

The displacement directions and extension and contraction axes are plotted onto maps of the master faults (Fig. 2.8). The vein arrays have simple-shear geometries in the unconnected example which implies that displacement directions are sub-parallel within linear zones, and reflects the displacement sense on co-linear strike-slip faults (Fig. 2.8a). The wall-rock displacement direction indicated by the vein arrays with transensional geometries in the connected network of strike-slip faults illustrated in Fig. 2.8(b) are sub-perpendicular to the conjugate dihedral angle bisector orientation for the master fault traces. Therefore there is a marked contrast in the nature of veining in the two fault zones, with linear arrangements of simple-shear arrays dominating the unconnected network, and clustered transensional arrays dominating the connected fault zone. The significance of these observations is discussed fully in the Fault Evolution section below.

2.4 STRIKE-SLIP FAULTS AT KILVE, SOMERSET, UK

Lower Liassic rocks striking E-W are exposed in cliffs and on a wave-cut platform, and consist of limestones with thicknesses ranging from tens of millimetres to a maximum of about 0.5 m, interbedded with shales and mudstones up to 4 m thick. Strike-slip faults exposed in the cliff have slip lineations that pitch in the range 2-23°. In cross-section (Fig. 2.9) these strike-slip faults are not simple, steeply dipping planar structures but have bends and oversteps, and many of the strike-slip faults steepen through the more brittle limestone layers and shallow through the shale horizons, in a manner similar to normal faults in cross-section (Peacock and Zhang, 1994). This may indicate that the faults initiated as steep shear fractures in the more brittle limestone units, and the shallower dips represent either (1) up- or down-dip refraction of a propagating fault into the more ductile shale beds, or (2) linking faults between two overlapping segments, similar in style to the normal fault models described by Peacock and Sanderson (1992). The faults with normal components of displacement have the most complex geometries in cross-section (Fig. 2.9). Similarities between normal and strike-slip fault cross-sectional geometries may have important implications for fault analysis in seismic section interpretation. On the wave-cut platform, the sinistral faults have N40°E strikes, whilst the dextral faults generally strike N-S (Fig. 2.10), and are evident at trace length scales from < 1m to > 100 m (Figs. 2.11 and 2.12). The average acute angle bisector of the fault traces has an orientation of N19°E. Palaeostress analysis using the P-T dihedral method, based on fault plane orientation and lineation data (Angelier, 1984), suggests that the maximum principal stress axis was approximately horizontal and NNE trending during strike-slip fault formation. The minimum principal stress axis was horizontal with an ESE trend. Cross-cutting relationships indicate that the strike-slip faults post-date Mesozoic E-W striking normal faults (Chadwick, 1986; Brooks *et al.*, 1988; Peacock and Sanderson, 1991, Bowyer and Kelly, 1995). The Cretaceous to Tertiary contraction responsible for the formation of the conjugate strike-slip faults, also caused reverse reactivation on the E-W normal faults (Lake and Karner, 1987; Whittaker and Green, 1983; Peacock and Sanderson, 1992; Bowyer and Kelly, 1995).

2.4.1 Metre-scale examples

The example in Fig. 2.11 shows a through-going dextral fault that is comparable in style to the master sinistral fault in the connected fault network at Beadnell (Fig. 2.6b). There are conjugate sets of faults with millimetre-scale displacement adjacent to both of these master faults along which strain is localised (Figs. 6b and 11). The breached intersection point in Fig. 2.11 is the major difference between these two examples. The intersection (at A, Fig. 2.11) of the master sinistral and dextral faults has been breached first by the sinistral fault, which in turn is displaced by a dextral fault that extends for approximately 50 m past the intersection point. The maximum strike-slip separation of a marker measured on the dextral fault is 3.5 m. A branch of the dextral fault bypasses the conjugate intersection, and linkage between the two branches is achieved through antithetic faults. Pull-apart arrays are rare, but do occur in these zones and faulted examples preserved along the length of the faults indicate their existence prior to through-fault development. On the inside of a bend on the main dextral fault, at the northern end of the map a network of conjugate subsidiary faults and pull-apart arrays occurs.

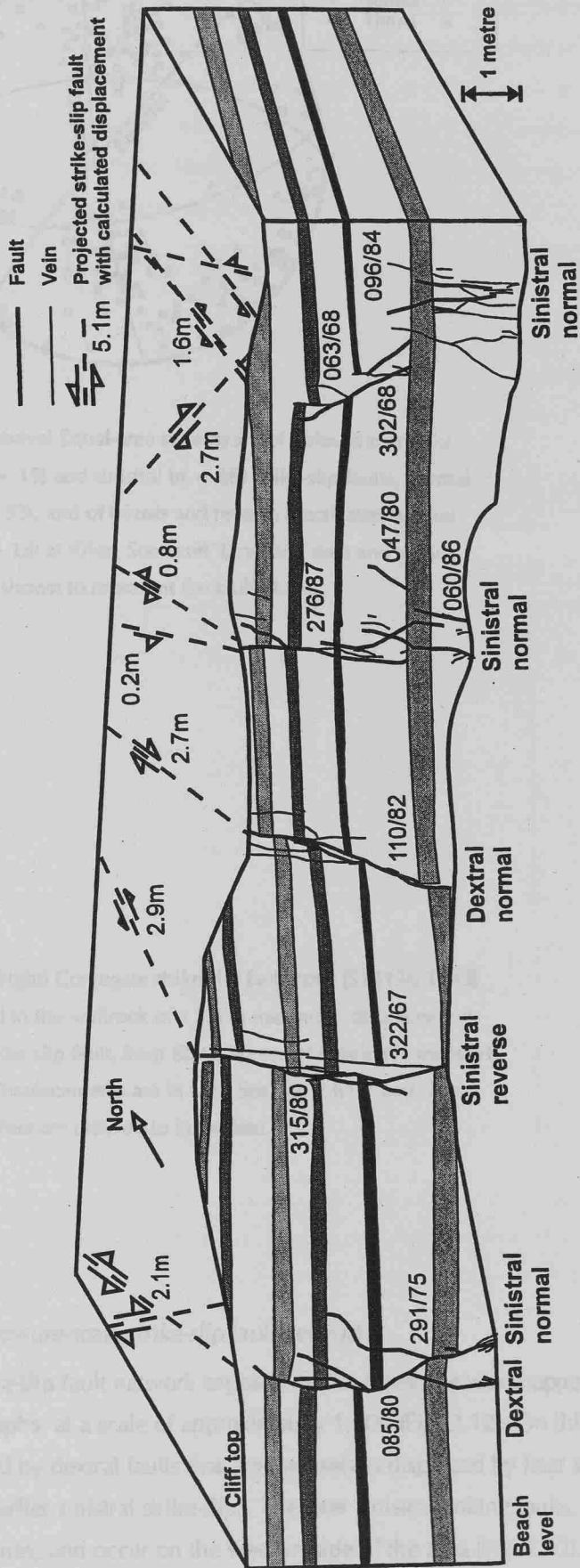


Fig. 2.9. Block-diagram of the strike-slip faults in the cliff at Kilve [ST 3137 1443] which exhibit a wide range of geometries. Measured orientations of the strike-slip faults have been used to construct the plan (dashed lines) of the strike-slip faults on top of the cliff. The lateral displacements have been calculated using the trigonometric relationship between the slickenside lineation pitch and the vertical separation of beds. The shaded horizons represent individual limestone beds.

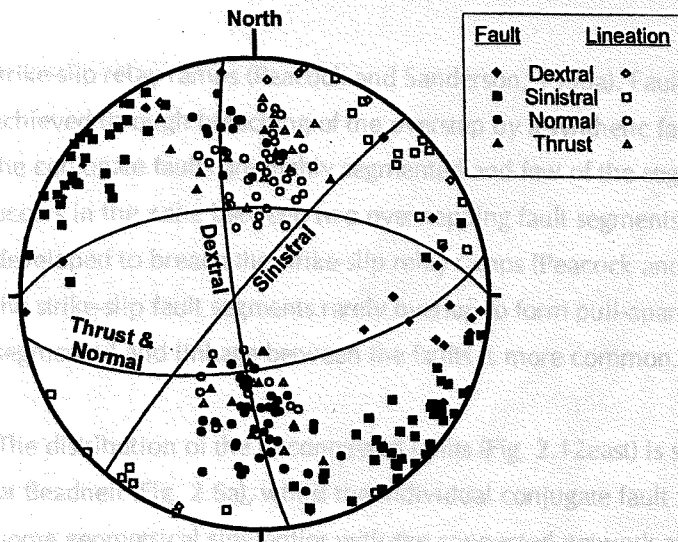


Fig. 2.10 (above) Equal-area stereogram of poles to planes of dextral ($n = 19$) and sinistral ($n = 66$) strike-slip faults, normal faults ($n = 53$), and of thrusts and reverse reactivated normal faults ($n = 18$) at Kolve, Somerset. Lineation data and great circles are shown to represent the fault planes.

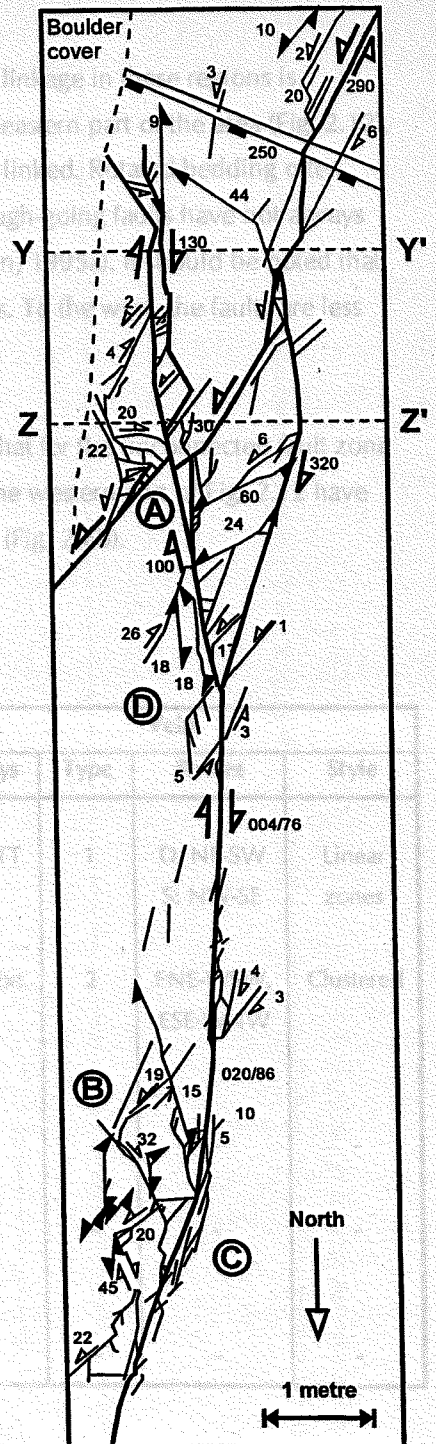


Fig. 2.11 (right) Conjugate strike-slip fault zone [ST3136 1443] developed in the wallrock of a 3.5 m maximum displacement dextral strike-slip fault, from Kolve, Somerset (originally mapped at 1:25). Displacements are in mm. See Fig. 2.6 for key. The circled letters are referred to in the text.

Table 2.1: Summary of field observations for Figs. 2.10, 2.11 and 2.12. The vein type refers to the classification of Wood (1975): Type 1 = convergent, and Type 2 = dextral parallel. TT = tensional, SS = simple shear and Ex = extensional. The vein group codes for Fig. 2.6(a) have been subdivided into dextral (D) and sinistral (S). The dextral and sinistral vein groups in Fig. 2.6(a) have similar orientations, so have not been subdivided.

2.4.2 Exposure-scale strike-slip fault network

The strike-slip fault network exposed on the foreshore was mapped onto a basemap composed of aerial photographs, at a scale of approximately 1:500 (Fig. 2.12). On this scale, early sinistral faults are displaced by dextral faults that are themselves displaced by later sinistral faults formed between the larger, earlier sinistral strike-slips. The later sinistral linking faults, have a more easterly strike than the earlier ones, and occur on the western side of the area (Fig. 2.12). Features present include oversteps and

strike-slip relay ramps (Peacock and Sanderson, 1995a). Fault segment linkage in these regions is achieved through breaching of the overstep by a synthetic fault. In the eastern part of the area (Fig. 2.12), the conjugate faults are highly segmented and few of the segments are linked. Rotated bedding often occurs in the zone between two overstepping fault segments, but through-going faults have not always developed to breach the strike-slip relay ramps (Peacock and Sanderson, 1995a). It should be noted that the strike-slip fault segments rarely overlap to form pull-apart structures. To the west, the faults are less segmented and linkage between the faults is more common.

The distribution of the unconnected faults (Fig. 2.12east) is similar to that for the unconnected fault zone at Beadnell (Fig. 2.6a), whilst the individual conjugate fault zones in the western part of Fig. 2.12 have some geometrical similarities with the connected network at Beadnell (Fig. 2.6b).

Table 2.1 summarises the field observations at both locations.

Figure	Network	Displacement range	Fault strikes		Vein			
			Dextral	Sinistral	Arrays	Type	Strikes	Style
<i>Beadnell</i> 6(a)	Unconnected	1 - 200 mm	ENE-WSW	WNW-ESE	SS - TT	1	D: NE-SW S: NW-SE	Linear zones
6(b)	Connected	1 - 500 mm	NE-SW	NW-SE	TT - Ext.	2	ENE-WSW, ESE-WNW	Clustered
<i>Kilve</i> 11	Connected	1 - 320 mm	N-S	NE-SW	-	-	-	-
12 W	Connected	0.08 - 3.6 m	N-S	NNE-SSW	-	-	-	-
12 E	Unconnected	0.5 - 1 m	N-S	NE-SW	-	-	-	-

Table 2.1. Summary of field observations for Figs. 2.6, 2.11 and 2.12. The vein type refers to the classification of Beach (1975): Type 1 = convergent, and Type 2 = bisector parallel. TT = transtension, SS = simple-shear and Ext. = extensional. The vein arrays strikes for Fig. 2.6(a) have been subdivided into dextral (D) and sinistral (S). The dextral and sinistral vein arrays in Fig. 2.6(b) have similar orientations, so have not been sub-divided.

2.5 STRAIN ANALYSIS

The method of Peacock and Sanderson (1993) is used to estimate the magnitudes and orientations of the principal strain axes for each of the described fault zones (Figs. 2.6, 2.11 and 2.12). Their approach is based on the displacement-gradient tensor method (Jamison, 1989), but modified to allow fault-strain calculation from a line sample that traverses faults with various orientations. The total fault-strain is derived from the following data for each fault: dip and dip direction, displacement sense, direction and magnitude. The displacement is weighted to account for the angle between the perpendicular to the fault and the sample line, so the estimation of the fault-strain is independent of the line orientation (Peacock and Sanderson, 1993). The weighted displacement-gradient tensor approach provides an ideal method to compare directly fault-strain magnitudes over the two scales of observation. In the analysis of strain for the networks of conjugate strike-slip faults, the sample lines have been drawn perpendicular to the acute angle bisector of the fault traces (X-X' and Y-Y': Figs. 2.6, 2.11 and 2.12), so that their orientations form similar angular relationships with the shortening and extension directions to those of the normal fault set examined by Peacock and Sanderson (1993). The results that are presented are, therefore, derived from an estimation of the summed extension across each fault zone.

The fault-strain analysis of the metre-scale fault zones from Beadnell (Fig. 2.6) and Kilve (Fig. 2.11) assumes that all the deformation occurred in the horizontal plane (*i.e.* plane strain); available slickenside lineation data support this assumption but were not obtainable for all faults. Slickenside lineation data were more widely available for the faults illustrated in Fig. 2.12, so three-dimensional strain analysis was possible. The displacement-gradient tensor method is an estimation, as the fault-related brittle deformation is approximated to ductile deformation of the strain ellipsoid (or ellipse for two-dimensional analysis) (Jamison, 1989). Moreover, the analysis was carried out for only the master faults on all of the maps. Vein and pull-apart arrays were not included in the analysis of the metre-scale examples, and faults < 1 m long were excluded from the survey of the strike-slip fault network illustrated by the larger-scale map (Fig. 2.12). A further assumption was made concerning the displacement of the fault at intersection with the sample line. A displacement value was estimated by interpolating between the nearest measured values on either side of the sample line. Unfortunately, this method assumes a linear displacement gradient between the two points, which represents an over-simplification when compared with displacement profiles for individual faults (*c.f.* Williams and Chapman, 1983; Peacock, 1991; Odonne and Massonnat, 1992a).

The deformation in an area must be statistically homogeneous to provide a rigorous strain estimation (Wojtal, 1989; Jamison, 1989), so the sample line should be sub-divided if there is considerable heterogeneity (Peacock and Sanderson, 1993). The measured faults in the three metre-scale maps (Figs. 2.6 and 2.11) are approximately homogeneous, but there is some variation across the larger-scale map (Fig. 2.12). Cumulative displacement-distance graphs of the faults intersected by the sample lines demonstrate the heterogeneity from east to west of fault spacing and displacement distribution (Fig. 2.13). The data from the sample line Y-Y' has been sub-divided into two sets, based on the marked shallowing of the slope at approximately 175 m (Fig. 2.13).

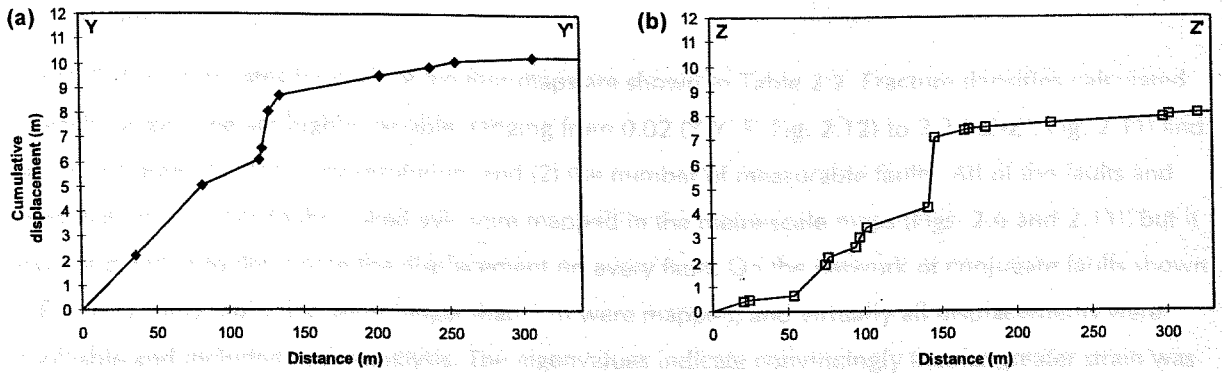


Fig. 2.13. Cumulative displacement-distance graphs for the two traverses indicated by the dashed lines in Fig. 2.12. (a) Y-Y', and (b) Z-Z'. The fault that corresponds to the point at which the gradient of the graph in (a) shallows considerably is marked as 'C' in Fig. 2.12.

Figure	Line	Length (m)	Number of faults	Density N.m ⁻¹	Eigenvalues (2sf)			Strain axes
					e ₁	e ₂	e ₃	
6(a)	Y-Y'	15.2	4	0.26	0.0089	-	-0.0089	
	Z-Z'	15.2	4	0.26	0.0099	-	-0.0099	
6(b)	Y-Y'	14.8	6	0.41	0.038	-	-0.038	
11	Y-Y'	2.63	4	1.52	0.043	-	-0.043	
	Z-Z'	2.63	6	2.28	0.063	-	-0.063	
12	Y-Y'	313.3	10	0.03	0.026	0.00062	-0.026	
	E	138.3	4	0.02	0.00063	-0.00007	-0.0062	
	W	175.0	6	0.04	0.047	-0.0017	-0.048	
	Z-Z'	338.7	17	0.05	0.020	0.00069	-0.024	
	E	163.7	4	0.03	0.0037	0	-0.0026	
W	175.0	13	0.06	0.031	0.0011	-0.038		

Table 2.2. Results of the strain analysis for sample lines from each of the maps (X-X' and Y-Y': Figs. 2.6, 2.11 and 2.12). Data along two sample lines were collected for each map, with the exception of Fig. 2.6(b) due to insufficient displacement data. e₁ = extension axis, e₃ = shortening axis, and e₂ = intermediate axis (negative = contractional, positive = extensional). The number of faults for each sample line refers to the number of faults with measurable displacement that were included in the analysis, and not the actual number. The extensional and contractional axes orientations (eigenvectors) are indicated by the arrows in the final column (north is at the top of the page).

2.5.1 Results

The fault-strain estimates for each of the four maps are shown in Table 2.2. Fracture densities calculated for each sample line are highly variable, ranging from 0.02 (Y-Y' E, Fig. 2.12) to 2.27 (Z-Z', Fig. 2.11) and can be attributed to (1) survey resolution, and (2) the number of measurable faults. All of the faults and veins that were visible to the naked eye were mapped in the metre-scale maps (Figs. 2.6 and 2.11), but it was not possible to determine the displacement on every fault. On the network of conjugate faults shown in Fig. 2.12, only faults that were longer than 1 m were mapped, and virtually all displacements were resolvable and included in the analysis. The eigenvalues indicate convincingly that far greater strain was accommodated by the connected networks of strike-slip faults and veins (Figs. 2.6b, 2.11 and 2.12 west), than the unconnected examples (Figs. 2.6a and 2.12 east), even when interpreted in the context of the assumptions.

2.6 Fault zone evolution

2.6 FAULT ZONE EVOLUTION

It is appropriate to consider the two examples illustrated in Fig. 2.6, as representing two stages in conjugate fault zone evolution through comparison of the strain analysis and the various structures. The results of the strain analysis (Table 2.2) indicate that the connected fault zone (Fig. 2.6b) accommodates far greater strain than the unconnected fault zone (Fig. 2.6a). It has also been demonstrated by various workers that early fault development occurs through fracture propagation, interaction and subsequent linkage (Gamond, 1983; Cowie and Scholz, 1992; Peacock and Sanderson, 1995b). Intact vein and pull-apart arrays occur in the unconnected fault zone (Fig. 2.6a), and relics of faulted pull-apart structures occur adjacent to the master faults in the connected fault network (Fig. 2.6b). The observations of the fault zones at Kilve (Figs. 2.11 and 2.12) are also incorporated into the model (Fig. 2.14a-e), on the basis of their geometrical similarities with the maps illustrated in Fig. 2.6.

The Type 1 vein geometries (Fig. 2.6a) indicate that simple-shear deformation was an important process. Faults and vein arrays in the unconnected fault zone illustrated in Fig. 2.6(a) are preserved in various stages of development, such that there are (1) en echelon vein and pull-apart arrays, (2) fault segments with irregular traces that are co-linear with vein arrays, (3) fault segments 'linked' by en echelon vein arrays, and (4) contractional and extensional oversteps along master faults, but there are no conjugate intersection points between faults. The presence of this range of structures suggests that different parts of the rock deformed at different rates, but a lack of cross-cutting structures implies that these processes occurred during a single progressive event.

Analysis of the fault locations demonstrates that they propagate towards intersection points, and never initiate at them (Fig. 2.6a).

The Type 1 veins depicted in Fig. 2.6(a) form densely populated linear zones at fault-tips, and also form shear zones that are antithetic to master faults. Type 1 veins commonly occur in existing shear zones (Beach, 1975; Rothery, 1988), and localisation into linear zones may form at the periphery of a parent fracture (Pollard *et al.*, 1982; Cruickshank *et al.*, 1991). Type 2 veins are more commonly associated with vein arrays in extensional regimes (e.g. Beach, 1975; Rothery, 1988), but the Type 2 veins in Fig. 2.6(a) have vein-zone angles that indicate extensional to simple-shear deformation. The model of Olson and Pollard (1991) may be applicable, whereby sub-parallel fractures are able to grow and interact

during a single episode of extension to produce arrays with geometries that range from extensional to transpressional. The arrays can then serve to localise subsequent shear (Beach, 1975; Pollard et al., 1982; Rothery, 1988; Olson and Pollard, 1991). An alternative explanation for the presence of the Type 2 veins at A (Fig. 2.6a) is that they occur in a tensional quadrant adjacent to the tip of a master fault (e.g. Cruickshank et al., 1991) and represent a fault-tip damage zone (McGrath and Davison, 1995). A similar mode of formation, however, is not applicable to the veins in the antithetic arrays adjacent to B (Fig. 2.6b).

A sub-division of the veins into separate deformation events can be based on their orientations and interpreted formation mechanism.

2.6.1 Stage 1 - Extensional vein development

The model of Olson and Pollard (1991) is appropriate to describe the initial formation of sub-parallel Type 2 veins in the rock mass that form into arbitrarily orientated arrays during effective extension (Fig. 2.14a and f). These veins are interpreted as the first-formed structures as they were able to grow as sub-parallel extension fractures, and their orientations or geometries were not modified significantly by interaction with other structures or in shear zones.

2.6.2 Stage 2 - Formation of conjugate strike-slip faults

Two possible mechanisms to describe the formation of conjugate faults at low angles (*i.e.* $< 60^\circ$) to each other (*c.f.* Hancock, 1985) (Fig. 2.6a) are (1) coalescence of the Stage 1 vein arrays during continued growth, followed by shear, or (2) shear deformation localised onto the pre-existing extensional veins. The Type 1 vein geometries (Fig. 2.6a) indicate that simple-shear deformation was an important process (Beach, 1975; Rothery, 1988), and occurrence of veins at high angles adjacent to the master faults provide evidence that the strike-slip faults formed from arrays with simple-shear geometries (Fig. 2.14b and f). A three-dimensional view of the strike-slip fault network was not possible, so conclusions cannot be drawn to explain the localisation into linear zones of the vein arrays with simple-shear geometries (*c.f.* Cruickshank et al., 1991). The interpretation of the deformation shown in Fig. 2.6(a) involves several conjugate systems (of faults and veins) being active at a similar time (*c.f.* Nicol et al., 1995) before linking to produce master faults (Fig. 2.14b). Analysis of the fault locations demonstrates that they propagate towards intersection points, and never initiate at them (Fig. 2.6a).

2.6.2.1 Stage 3 - Fault linkage and renewed extensional vein opening

Linking faults with similar displacement magnitudes lock at an intersection, and propagation continues away from the point (Fig. 2.14c) (*c.f.* Passcock, 1991). The propagation direction of faults is evident from the distributions along side the master faults, with micro-cracks forming asymmetrically about a fault tip (Ramos and Lockner, 1994) (Fig. 2.1). Extensional fractures initiate at flaws in the rock (Olson and Pollard, 1991), so new veins that initiated in the wake of a process zone would have an asymmetric distribution (e.g. at B and C, Fig. 2.6b). Smaller faults that propagate towards the master fault become

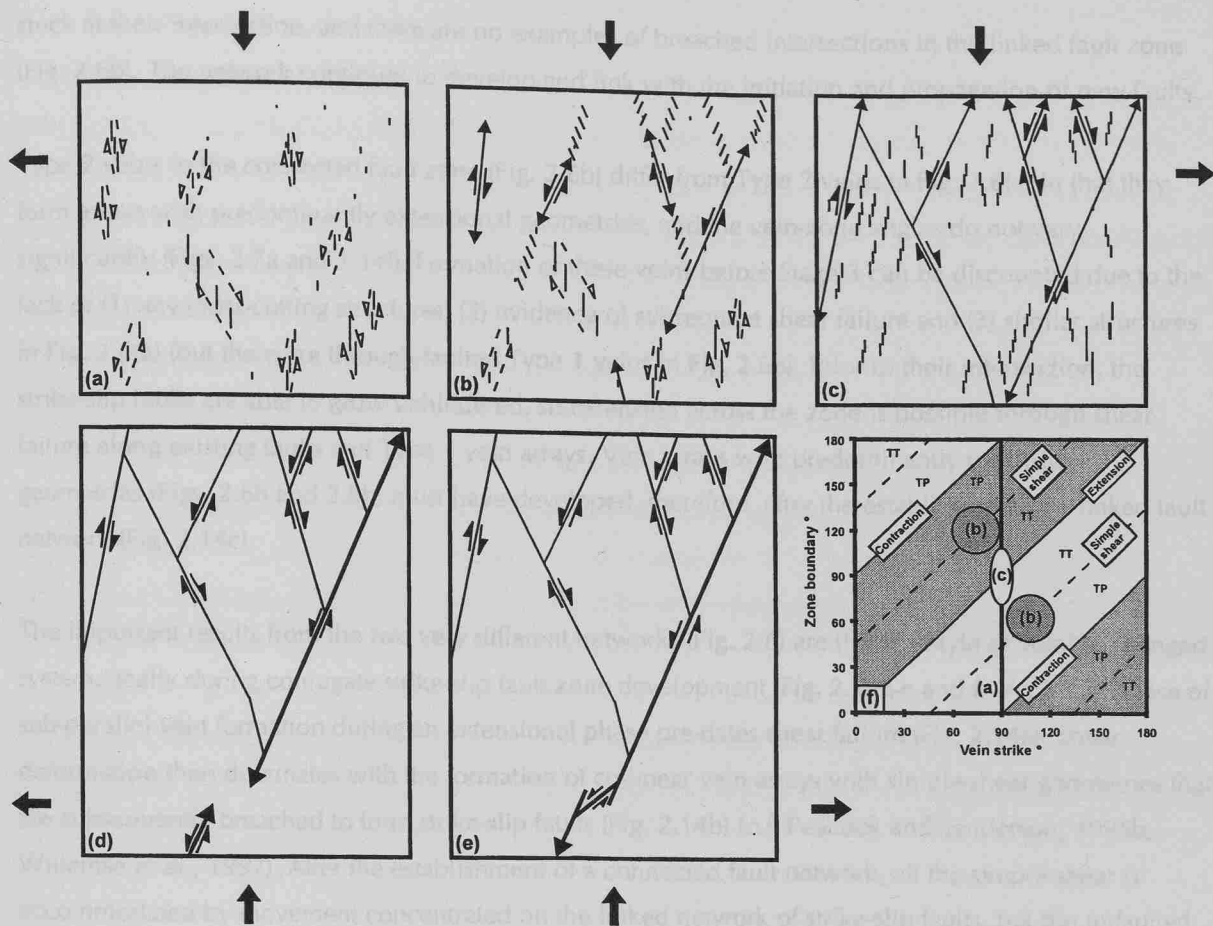


Fig. 2.14. Model for the development of strike-slip fault zones to include conjugate fault development and overstepping zones. The arrowed faults indicate those parts active at that particular stage. (a)-(c) Models based on observations at Beadnell. (d)-(e) Expansion of the model to include the observations of fault network development at Kilve. The model is discussed in full in the text. (f) Idealised graph of vein strike and zone boundary orientation for (a)-(c) (c.f. Fig. 2.7). Veins in (a) are parallel to each other, but there is the potential for the zone boundaries to have the whole range of orientations. The data from (b) plot in two distinct clusters that represent Type 1 veins within arrays with predominantly simple-shear geometries. The data from the natural examples (Fig. 2.6) show some overlap in vein strike of the two clusters. The veins in (c) are sub-parallel within the transtensional-extensional arrays, and the spread of zone boundary orientations is limited, so the data plot in a single cluster. Veins with transtensional-extensional geometries were not observed within the fault zones at Kilve.

2.6.3 Stage 3 - Fault linkage and renewed extensional vein opening

Conjugate faults with similar displacement magnitudes lock at an intersection, and propagation continues away from this point (Fig. 2.14c) (c.f. Peacock, 1991). The propagation direction of faults is evident from vein distributions along-side the master faults, with microcracks forming asymmetrically about a Mode II fracture tip (Reches and Lockner, 1994) (Fig. 2.1). Extensional fractures initiate at flaws in the rock (Olson and Pollard, 1991), so new veins that initiated in the wake of a process zone would have an asymmetric distribution (e.g. at B and C, Fig. 2.6b). Smaller faults that propagate towards the master fault become

stuck at their intersection, and there are no examples of breached intersections in the linked fault zone (Fig. 2.6b). The network continues to develop and link with the initiation and propagation of new faults.

Type 2 veins in the connected fault zone (Fig. 2.6b) differ from Type 2 veins in Fig. 2.6(a) in that they form arrays with predominantly extensional geometries, and the vein-zone angles do not vary significantly (Figs. 2.7a and 2.14f). Formation of these veins before Stage 3 can be discounted due to the lack of (1) any cross-cutting structures, (2) evidence of subsequent shear failure and (3) similar structures in Fig. 2.6(a) (but there are through-faulted Type 1 veins in Fig. 2.6b). Prior to their intersection, the strike-slip faults are able to grow unhindered, so extension across the zone is possible through shear failure along existing faults and Type 1 vein arrays. Vein arrays with predominantly extensional geometries (Figs. 2.6b and 2.8b) must have developed, therefore, after the establishment of a linked fault network (Fig. 2.14c).

The important results from the two very different networks (Fig. 2.6) are that the style of veining changed systematically during conjugate strike-slip fault zone development (Fig. 2.14a-c and f). An initial phase of sub-parallel vein formation during an extensional phase pre-dates shear failure (Fig. 2.14a). Shear deformation then dominates with the formation of co-linear vein arrays with simple-shear geometries that are subsequently breached to form strike-slip faults (Fig. 2.14b) (c.f. Peacock and Sanderson, 1995b, Willemse *et al.*, 1997). After the establishment of a connected fault network, all the simple-shear is accommodated by movement concentrated on the linked network of strike-slip faults, but the unfaulted rock mass is able to fail further through the development of extensional vein arrays (Fig. 2.14c). There is therefore a progression from (1) development of Type 2 veins from randomly distributed microcracks, through (2) Type 1 vein development (Mode I failure) within simple-shear vein arrays concentrated in linear zones (Fig. 2.6a), to (3) the formation of and shear across a linked network of strike-slip faults (Mode II), and finally (4) a renewed phase of Type 2 vein arrays with extensional geometries (Fig. 2.6b). The sole major difference between the examples in the two locations is that vein arrays with these geometries were not observed in the fault zones at Kilve (Figs. 2.11 and 2.12).

2.6.4 Stage 4 - Breaching of the intersection points

The next two stages of fault zone development are based on the geometries of the fault zones examined at Kilve, where intersection points are often breached (Figs. 2.11 and 2.12). In the metre-scale example (Fig. 2.11), the master sinistral fault first breached the sticking point, but is in turn offset by the dominant dextral fault that effectively by-passes the conjugate set. The offset of the sinistral fault by the dextral fault and a lack of evidence of pressure solution at the intersection point (Fig. 2.11) indicate sequential rather than synchronous fault activity (Odonne and Massonnat, 1992a), and the map shown in Fig. 2.11 implies that one fault became increasingly important during the later stages of development. In the model presented here, the sinistral fault breaches the overstep and continued to propagate in both directions (Fig. 2.14d).

2.6.5 Stage 5 - Linkage with other fault systems

In the final stage, the dominant fault continues to propagate in both directions, and eventually oversteps with another propagating fault segment. The overstep region is eventually broken through by a linking, synthetic fault at a strike-slip relay ramp (Fig. 2.14e) (Peacock and Sanderson, 1995a). Minor antithetic faults and relics of strike-slip relay ramps are often preserved along-side the through-going faults (Peacock and Sanderson, 1995a) (Fig. 2.14e). The occurrence of a conjugate network of strike-slip faults on the inside of the bend (at B, Fig. 2.11) can be attributed to two factors: (1) a contractional bend that would indicate that this part of the fault propagated southwards (Sibson, 1989), which is supported by subsidiary fractures on the opposite side of the fault (at C), or (2) a conjugate strike-slip fault zone that formed prior to the development of the master fault and was subsequently by-passed (see below). The damage at 'D' implies that this segment propagated northwards, and the probable linkage point between these two segments is at the branch-point of the fault adjacent to 'B'. A large fault network (Fig. 2.12) evolves from the continuing development, propagation and linkage of fault segments. The sinistral faults dominate the foreshore, and segment linkage has been observed on several trace-length scales from the millimetre-scale to the 100 metre-scale. Linkage between the larger faults, and compartmentalisation of the rock mass are rare during the early stages of development, but increase as faults breach the oversteps. The geometry of the active part of a fault zone simplifies with time as these heterogeneities are by-passed by single dominant faults (Figs. 2.11 and 2.12).

2.7 CONCLUSIONS

- (1) This paper describes the geometry and evolution of conjugate strike-slip fault zones in limestones, and shows that deformation becomes concentrated on the largest faults. Metre-scale examples are described in detail, that have similar geometries to larger fault networks.
- (2) Strain analysis indicates that far greater strains are accommodated by connected, rather than unconnected, networks of conjugate strike-slip faults.
- (3) The geometries of metre-scale strike-slip fault zones indicate the following stages of development (Fig. 2.14):
 - (a) Opening of dilational veins during extension.
 - (b) The subsequent processes that contribute to the formation of strike-slip networks (simple-shear vein array initiation and fault development) indicate strain accommodation at different rates in different areas of the fault zone. Conjugate sets of unlinked strike-slip faults develop in isolation and propagate towards intersection points.
 - (c) Once a linked network of faults is established, deformation is accommodated largely by slip on the master faults, with new vein arrays developing with predominantly extensional geometries.
 - (d) Intersection points are breached by dominant faults.
 - (e) The geometry of the active fault system simplifies after conjugate intersection points are breached and the complexities become inactive and are by-passed. By-passed portions remain preserved in the walls of the master faults.

3. Selective reverse-reactivation of normal faults, and deformation around reverse-reactivated faults in the Mesozoic of the Somerset coast

3.1 SUMMARY

Normal faults exposed in the Triassic-Jurassic limestones and shales of the Somerset coast were formed during the Mesozoic development of the Bristol Channel Basin. Reverse-reactivation of some of these normal faults occurred during Late Cretaceous to Early Tertiary N-S contraction. The contraction is also evident from thrusts and conjugate strike-slip faults. Preferential reactivation of the normal faults is attributed to: (1) decreased fault-plane friction, (2) domino block rotation, (3) displacement magnitude, and (4) fault connectivity.

The geometries of overlapping and underlapping zones in reactivated fault zones are dependent on the existing structural geometry. Two distinctive styles of displacement accommodation occur between reverse-reactivated normal faults: (1) formation of a network of strike-slip faults, conjugate about NNE-SSW, and (2) oblique steeply-dipping reverse faults. Interaction between strike-slip and an existing fault is dependent on whether the normal fault was reactivated.

The range of structures related to the N-S contraction have been incorporated into a single deformation model, controlled by the northwards movement of the hanging-wall of the Quantock's Head Fault. Pure dip-slip movement occurred in the centre of its curved fault trace, with a sinistral component at the western tip, and a dextral component of displacement and strike-slip block rotations occurred at the eastern tip. Shortening of these blocks was achieved through development of a strike-slip fault network and NW-striking thrusts. In an underlap zone, loading of the footwall by the hanging-wall block modified the local stress system to allow formation of oblique, steeply-dipping reverse faults.

Understanding of the processes of reactivation of normal faults in tectonic settings, e.g. in the Southern North Sea (Bradley et al., 1995), the East Shetland Basin (Thomas and Coward, 1995), and the East of Svalbard Basin (Lindbergh et al., 1995), has been improved by McArthur (1988), McArthur and Haxel (1992), Haxel et al. (1995) and Haxel et al. (1996), and by McArthur et al. (1997) and Haxel et al. (1998).

The high resolution aerial photographs used in this study were taken in 1987. The high resolution aerial photographs were taken in 1987. The high resolution aerial photographs were taken in 1987.

The geological map of the Somerset coast, followed by descriptions of the geological map of the Somerset coast, followed by descriptions of the geological map of the Somerset coast.

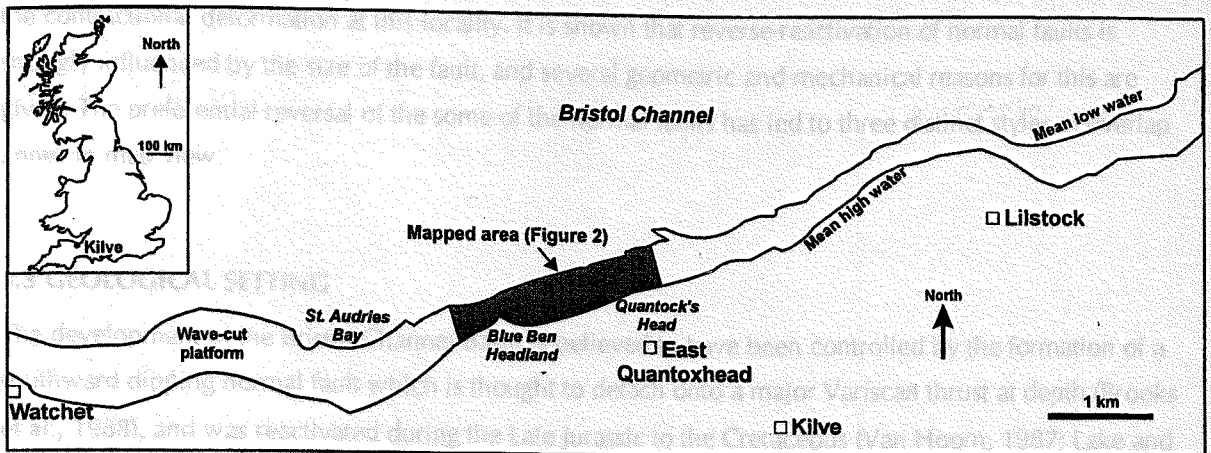


Fig. 3.1. Map of the foreshore of part of the north Somerset Coast to show the location of Fig. 3.2, and (inset) map of Great Britain to show the location of Kilve.

3.2 INTRODUCTION

Recent discussion of fault reactivation appears to have concentrated on the relationships between fault geometries (e.g. Cooper and Williams, 1989; Dart *et al.*, 1995), orientations of the fault plane to the stress axes (e.g. Sibson, 1985; Huyghe and Mugnier, 1992) and the role of pore fluids (e.g. Sibson, 1995). Gently-dipping normal faults, or steeply-dipping reverse faults may reflect a diverse fault history. For example, gently dipping normal faults have been shown to develop through normal reactivation of thrusts (Brewer and Smithe, 1984; Enfield and Coward, 1987), and reverse faults with steep dips may reflect a normal fault origin (e.g. Williams *et al.*, 1989).

This chapter is based on field observations of faults in the Mesozoic sediments of the Somerset coast in the East Quantoxhead area (Fig. 3.1). The foreshore and cliff exposures have provided an ideal opportunity to study reverse-reactivated normal faults (Fig. 3.2) and provide further understanding of similar structures that are often observed on seismic sections, e.g. in the Southern North Sea (Badley *et al.*, 1989), offshore of the British Isles (Roberts, 1989) and the East Shetland Basin (Thomas and Coward, 1995). Recent work on the Bristol Channel Basin has included field-based studies by McLachlan (1986), Peacock and Sanderson (1991; 1992; 1994a), Dart *et al.* (1995) and Nemcok *et al.* (1995), and seismic studies by Brooks *et al.* (1988) and Van Hoorn (1987).

Faults were mapped using a series of c. 1:500 scale aerial photographs as a basemap. The high resolution and quality of the aerial photographs enabled individual beds and fault offsets to be imaged. Cross-sections through individual fault zones were mapped onto photographs of the cliffs.

The chapter begins with an introduction to the geology of the Somerset coast, followed by descriptions of the fault properties. Four models for the preferential reverse-reactivation of the normal faults are discussed, and the geometries of underlapping and overlapping zones are used to develop a model for

the contractional deformation at this locality. It is shown that reverse-reactivation of normal faults is strongly influenced by the size of the fault, and several geometric and mechanical reasons for this are given. The preferential reversal of some of the normal faults has led to three distinct styles of overlap zones in map view.

3.3 GEOLOGICAL SETTING

The development of the Bristol Channel Basin is believed to have been controlled by the formation of a southward dipping normal fault which is thought to detach onto a major Variscan thrust at depth (Brooks *et al.*, 1988), and was reactivated during the Late Jurassic to the Cretaceous (Van Hoorn, 1987; Lake and Karner, 1987; Dart *et al.*, 1995; Nemcok *et al.*, 1995). The onshore sedimentary sequence consists of Triassic marls and Jurassic limestones, shales and marls (Fig. 3.2) (Whittaker and Green, 1983). The stratigraphy of the Upper Triassic and Lower Liassic sediments used in this study is based on the divisions of Palmer (1972) as the descriptive names are more applicable to this study. The Kilve Shales and St. Audrie's Shales consist of thin (< 0.15 m thickness) limestones interbedded with shales and mudstones of up to 3 m thickness. The Blue Lias and the Quantock's Beds are also limestone/shale interbeds, but the limestone units are up to 0.6 m thick, and the shales have thicknesses that are < 2 m. These Mesozoic sedimentary rocks contain E-W trending normal faults (e.g. Peacock & Sanderson, 1991; 1992; Bowyer and Kelly, 1995).

A phase of contraction in the Tertiary (Van Hoorn, 1987; Brooks *et al.*, 1988; Chadwick, 1993; Dart *et al.*, 1995; Nemcok *et al.*, 1995) is evident from a seismic study by Van Hoorn (1987) and field exposures of reverse-reactivated normal faults (McLachlan, 1986; Peacock and Sanderson, 1992) and thrusts. Strike-slip faults are conjugate about N20°E (Fig. 3.3) (Peacock and Sanderson, 1992). Field evidence for the reverse-reactivation of individual normal faults includes thrusts in their hanging-walls, kink bands and crenulation cleavage (Peacock and Sanderson, 1992), hanging-wall buttress anticlines (Dart *et al.*, 1995), multiple sets of slickenside lineations on a fault plane, and drag of beds. Within a fault zone, individual faults frequently retain finite normal displacements, but are associated with contractional features and strike-slip faults, and occasionally pass laterally into reverse faults. In the Triassic marls at Watchet (Fig. 3.1), moderately-dipping to sub-horizontal gypsum veins occur with sub-vertical mineral fibres, in the footwall of a reverse-reactivated normal fault. Sibson (1995) suggests the veins are filled with fluids that migrated into a footwall dilational area, created during reverse-reactivation.

Fig. 3.2. (overleaf) (a) Map of the faulting between East Quantoxhead and St. Audrie's Bay. The bold lines refer to the reverse and reverse-reactivated normal faults, and the ticks are on the hanging-walls of the faults. The Blue Lias and Quantock's Beds have been further divided into approximately equal thickness units of 10m. The lettered locations are referred to in the text. (b) Fault data and copy of part of the map in (a) with unreactivated normal and strike-slip faults removed for clarity.

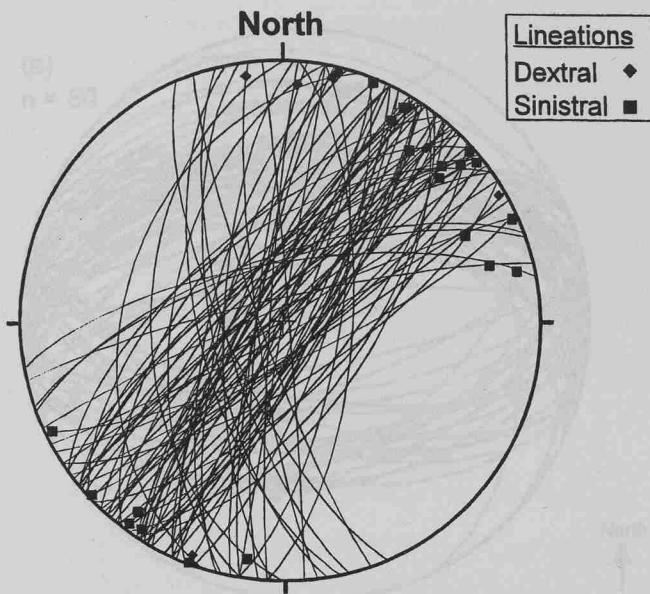


Fig. 3.3(a). (previous page) Map of the strike-slip fault network between the two major reverse-reactivated faults (see Fig. 3.2 for location). The strike-slip faults form a linked network within the overlapping faults to the west of the map, and are far more segmented on the periphery, to the east. (b) (left) Stereographic projection of dextral and sinistral faults, and slickenside lineations.

3.4 SELECTIVE REVERSE-REACTIVATION

To investigate the importance of fault geometries on the selective reverse-reactivation of the normal faults (Fig. 3.2), the properties of normal faults and reverse-reactivated normal faults are compared (Table 3.1 and Fig. 3.4).

	Dip direction	No	Dips °			Net Displacements (m)		
			Range	Mean	SD	Range	Mean	SD
Normal	North	58	24 - 86	51.41	14.74	0.1 to 20.0	3.23	4.66
	South	19	31 - 80	60.05	12.40	0.1 to 22.0	7.87	7.09
Reverse	North	23	20 - 82	44.83	17.35	-32.0 to +48.6	4.55	17.11
	South	12	41 - 72	59.67	8.65	-8.2 to +60.0	10.29	19.26

Table 3.1. Comparison of the displacements and dips of the south-dipping and north-dipping normal and reverse/reverse-reactivated normal faults. Faults are included that have dip directions 30° either side of north and south. Negative displacement values refer to reverse displacements, and positive values to normal displacements.

Fault dips and slickenside lineation orientations have similar distributions (Fig. 3.4a and b). All faults with finite normal displacements > 22 m show evidence of reverse-reactivation (Fig. 3.4c). Reverse-reactivated faults with lesser displacements occur, but it is not possible to calculate the pre-reactivated normal displacements. Note, however, that reverse-reactivation of the 200 m throw Blue Ben Fault (at A, Fig. 3.2) has not been directly proven, although it does have thrusts in its hanging-wall. The maximum observed reverse displacement is 32 m (49° dip) and is within the Blue Ben Fault damage zone (at A, Fig. 3.2).

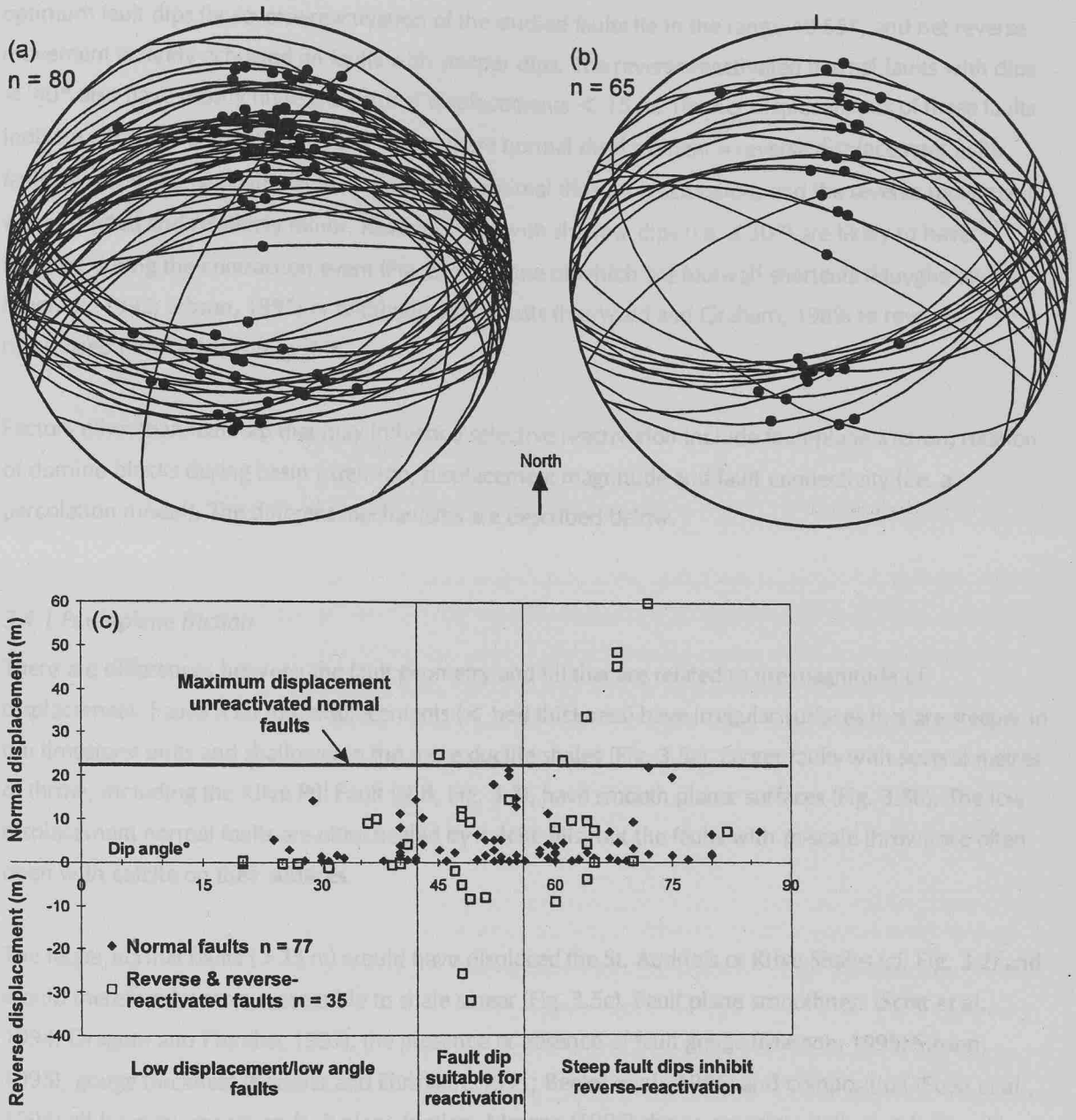


Fig. 3.4. Comparison of the properties of normal and reverse-reactivated faults. Stereographic projection of fault plane and slickenside lineation orientations for (a) normal faults and (b) reverse and reverse-reactivated normal faults. (c) Graph of displacements plotted against dip angle for normal, reverse and reverse-reactivated faults (negative values indicate reverse displacements). Reverse and reverse-reactivated normal faults are considered together, as it was impossible to distinguish the nature of the fault on the wave-cut platform.

The faults with the largest finite reverse displacements (up to 32 m) have dips in the range of 40-55 $^{\circ}$, and the faults with the largest finite normal displacements (23-60 m) have dips > 60 $^{\circ}$ (Fig. 3.4c). Sibson (1995) found an optimum angle between σ_1 and the fault plane for reactivation of normal faults of 25-30 $^{\circ}$. Further displacement is inhibited at twice this value (i.e. 50-60 $^{\circ}$) unless pore fluid pressures are sufficient (Sibson, 1985; 1995). The distribution of reverse displacements (Fig. 3.4c) indicates that the

optimum fault dips for reverse-reactivation of the studied faults lie in the range 40-55°, and net reverse movement is rarely achieved on faults with steeper dips. The reverse-reactivated normal faults with dips < 40° also have mostly finite extensional displacements < 15 m. The net displacements of these faults indicate either (1) optimally oriented faults where normal displacement = reverse displacement (with faults of any size), or (2) the faults did not have optimal dips for reactivation, and the reverse movement was restricted and relatively minor. Reverse faults with shallow dips (i.e. ≤ 30°) are likely to have initiated during the contraction event (Fig. 3.4c), some of which are footwall shortcuts (Huyghe and Mugnier, 1992; Sibson, 1995) or antithetic backthrusts (Hayward and Graham, 1989) to reverse-reactivated normal faults (Fig. 3.2).

Factors other than fault dip that may influence selective reactivation include fault-plane friction, rotation of domino blocks during basin extension, displacement magnitude and fault connectivity (i.e. a percolation model). The different mechanisms are described below.

3.4.1 Fault-plane friction

There are differences between the fault geometry and fill that are related to the magnitude of displacement. Faults with low displacements (< bed thickness) have irregular surfaces that are steeper in the limestone units and shallower in the more ductile shales (Fig. 3.5a). Larger faults with several metres of throw, including the Kilve Pill Fault (at B, Fig. 3.2), have smooth planar surfaces (Fig. 3.5b). The low displacement normal faults are often healed by calcite fills, but the faults with m-scale throws are often open with calcite on their surfaces.

The larger normal faults (> 25 m) would have displaced the St. Audrie's or Kilve Shales (cf. Fig. 3.2) and would therefore be most susceptible to shale smear (Fig. 3.5c). Fault plane smoothness (Scott *et al.*, 1994; Dragoni and Piombo, 1993), the presence or absence of fault gouge (Marone, 1995; Sibson, 1995), gouge thickness (Koestler and Ehrmann, 1991; Beeler *et al.*, 1996) and composition (Scott *et al.*, 1994) all have an impact on fault-plane friction. Marone (1995) shows experimentally that faults without gouge have higher frictional strengths and fail similarly to intact rock. In summary, the field evidence and studies of fault gouge indicate that it is the larger faults that have the lowest frictional strengths due to the likelihood of movement past a shale unit, and have smoother planes that formed from attrition during displacement accumulation. The fault-plane friction model permits the initiation of selective reverse-reactivation of gouge-filled, smooth faults and its subsequent cessation due to gouge thinning and extrusion (Scott *et al.*, 1994).

Reverse-rotation of the faults and hence steepening of their dip would occur during a late compressional stage (Sibson, 1994) (Fig. 3.5d).

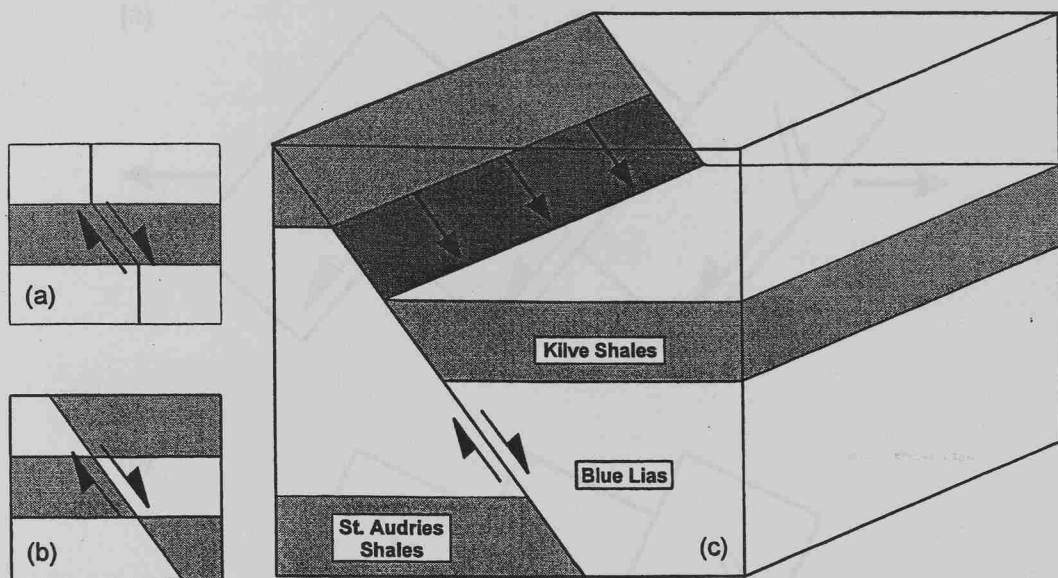


Fig. 3.5. (a) Schematic diagram to show how steep faults initiate in the more brittle layers (white), but have shallower profiles in the more ductile layers (shaded) (Peacock and Sanderson, 1992; Peacock and Zhang, 1994). (b) The faults assume a shallower, smoother profile during movement of brittle layers past ductile layers. (c) Block diagram to illustrate how fault gouge can occur along faults that have large enough displacements to juxtapose limestones against the shale-dominated units. Smaller displacement faults wholly within the Blue Lias are less likely to contain gouge material.

3.4.2 Domino block rotation

There is evidence for steepening of the larger south-dipping reverse-reactivated normal faults through reverse-rotation (e.g. the Quantock's Head Fault and the fault that passes through the Blue Ben Headland), as adjacent antithetic faults have considerably shallower dips (Fig. 3.2). In the areas where neighbouring faults have similar displacements, dips are similar for both north- and south-dipping faults. Faults that dip in the same direction as the beds may have been steepened during regional tilting, but this is not apparent in the gently south-dipping beds in the study area as many south-dipping faults dip at $< 50^\circ$, and there are numerous examples of steep north-dipping faults (Figs. 3.2 and 3.4). Normal faults can rotate to have dips of around $25\text{-}30^\circ$ (Sibson, 1995) during domino-style extension (e.g. Gibbs, 1987; Mandal and Chattopadhyay, 1995), with the greatest rotations occurring across the largest displacement faults (Fig. 3.6a). Faults antithetic to the large displacement faults would be rotated to higher dips which are unfavourable for reactivation (e.g. Sibson, 1985). Faults become locked when the angle between σ_1 and the fault plane exceeds the value determined by doubling the optimum reactivation angle (Sibson, 1995). Reverse-rotation of the faults and hence steepening of their dips would occur during a later contractional stage (Sibson, 1995) (Fig. 3.6b).

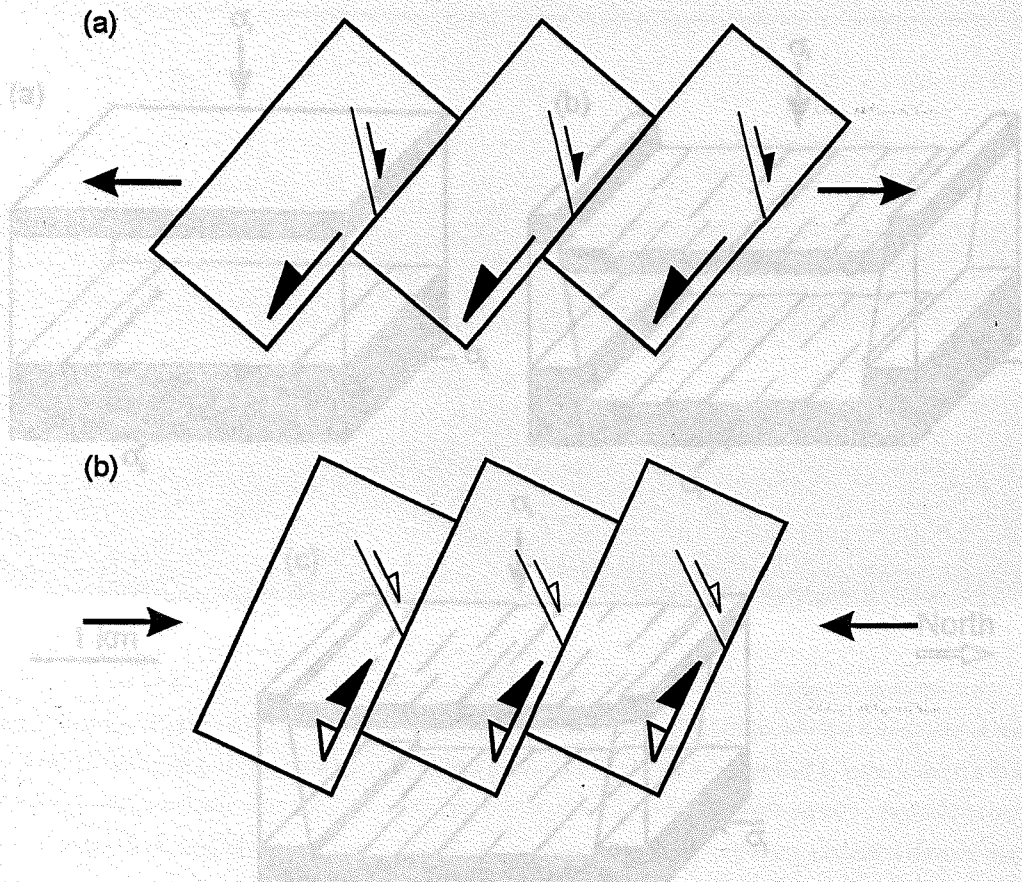


Fig. 3.6. (a) Domino-style fault blocks are defined by normal faults during extension. (b) Reverse-reactivation of the normal faults during contraction causes reverse-rotation of the fault blocks. The master faults undergo the largest rotations to shallower dips, and smaller antithetic faults will be rotated to steeper dips during extension, and therefore make greater angles with σ_1 during the contraction. The filled arrow heads indicate the displacement sense of the active faults in each diagram; the unfilled arrow heads indicate inactive faults. The latest sense of movement is indicated by the filled arrows on the double-headed symbols.

3.4.3 Fault size

Peacock and Sanderson (1991) show a fault with 0.4 m throw that has an 80m map length. A normal fault with 20 m throw would be expected, with the same displacement-length relationship, to be in the order of 4 km in map length, so could cut through the whole of the Jurassic sequence and into the deeper Triassic marls. A similar model to that for the faulting at Flamborough Head, East Yorkshire, may be appropriate, where reactivation may have been driven by stresses in the basement (Peacock and Sanderson, 1994b; Peacock, 1996) (Fig. 3.7). At Flamborough Head, E-W striking basement faults that developed during the Jurassic (Kirby and Swallow, 1987), and may extend back to the Carboniferous (Rawson and Wright, 1993), were reverse-reactivated (Peacock and Sanderson, 1994b; Peacock, 1996). Normal faults in the cover, initiated in the Cretaceous, have a wide range of orientations, and were not reverse-reactivated (Peacock, 1996). Faults in the Jurassic 'cover' in Somerset may have become detached from the Triassic 'basement', above one of the anhydrite units in the Mercia Mudstone (Warrington and Scrivener, 1980; House, 1993), and were not reactivated. The faults which extend from the 'basement' to the 'cover' are more likely to be reactivated than the faults that are small enough to be contained entirely within the 'cover', if the reactivation was driven by stresses in the basement.

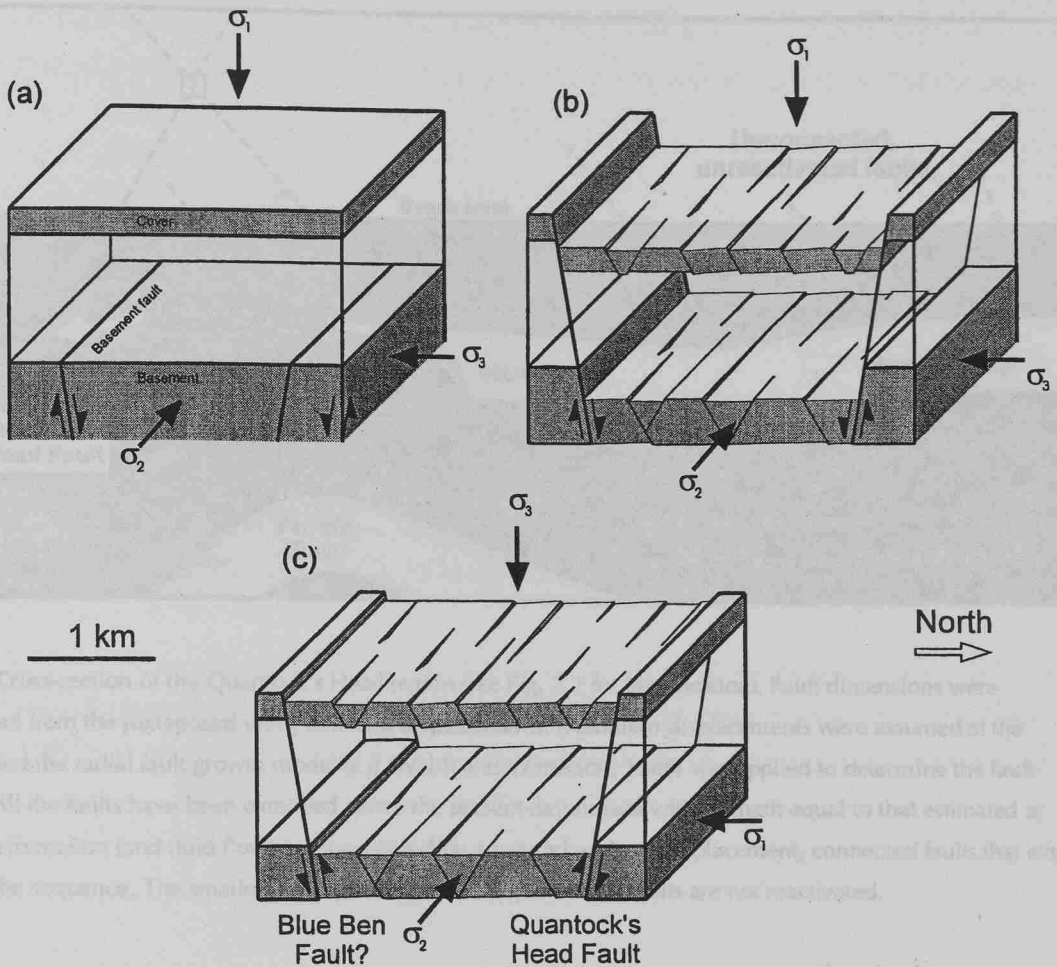


Fig. 3.7. Model for basement-involved reverse-reactivation (modified from a model for faulting at Flamborough Head, Peacock and Sanderson, 1994b; Peacock, 1996). The orientations of the maximum (σ_1), intermediate (σ_2) and minimum (σ_3) principal compressive stresses are shown. (a) E-W striking 'basement' faults occur, and the Jurassic is a 'cover' sequence. (b) The basement faults were normally-reactivated after Jurassic deposition and have the largest normal displacements. A network of small normal faults developed throughout the sequence. (c) The basement faults show reverse-reactivation, but the smaller faults (represented using finer lines) were not reactivated.

A detachment model was proposed by Roberts *et al.* (1990) to illustrate the reverse-reactivation of faults in the Central Graben, North Sea. In their model, an antithetic backthrust propagated from the reverse-reactivated fault, along a salt horizon which detached the Jurassic-Cretaceous sequence from the basement. The Jurassic-Cretaceous sequence was shortened independently by folds above the tip of the backthrust (Roberts *et al.*, 1990). Sibson (1995) proposed that a population of gypsum veins in the footwall of a reverse-reactivated normal fault within the Triassic marls exposed at Watchet (Fig. 3.1) indicates over-pressured fluid expulsion during fault-valve activity. Fluids accumulate in hydrofractures within impermeable strata adjacent to unsuitably oriented faults, and are expelled into the fault when the fluid pressure exceeds σ_1 and σ_3 (Sibson, 1995). A mechanism is thereby provided by which the reactivation could have affected only faults large enough to continue beyond the limestones into the deeper, less permeable Triassic marls.

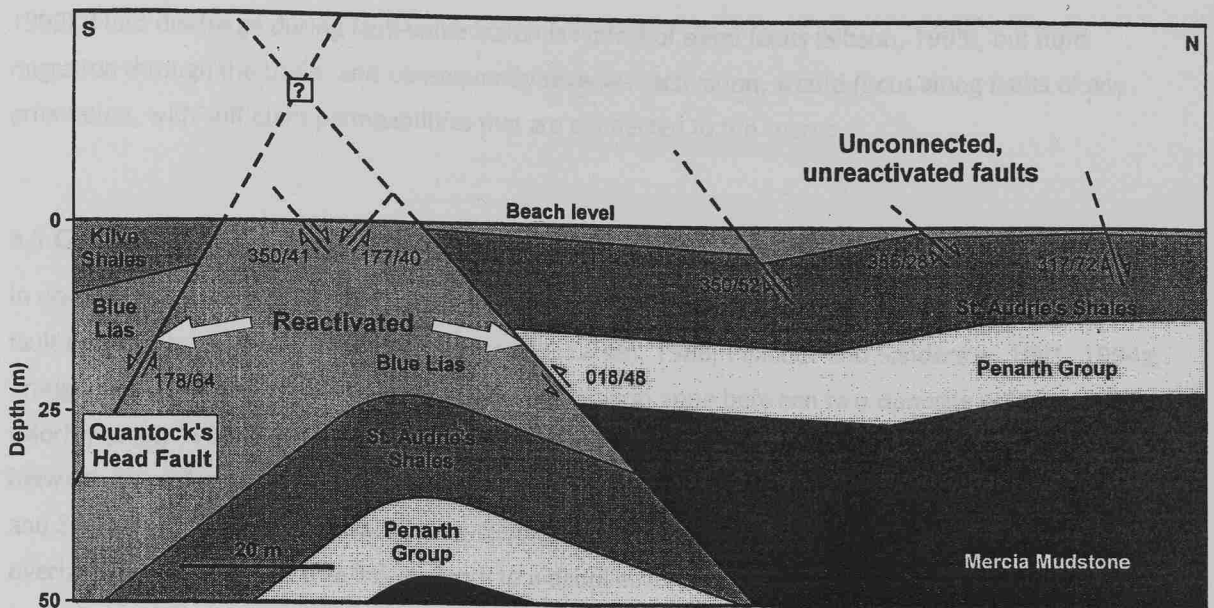


Fig. 3.8. Cross-section of the Quantock's Head region (see Fig. 3.2 for line location). Fault dimensions were determined from the juxtaposed units, and fault displacements. Maximum displacements were assumed at the surface, and the radial fault growth model (e.g. Walsh and Watterson, 1988) was applied to determine the fault lengths. All the faults have been extended above the present-day surface with a length equal to that estimated at depth. Deformation (and fluid flow) is concentrated on a network of large displacement, connected faults that extend through the sequence. The smaller, poorly-connected or impermeable faults are not reactivated.

3.4.4 Percolating network of connected faults

A cross-section of the Quantock's Head area (Fig. 3.8, line A-A' Fig. 3.2) illustrates the distribution of the reverse-reactivated faults. Projection above the present-day beach level of the Quantock's Head Fault and the 25 m displacement fault to the north, indicates that an intersection between the two would have occurred. These two faults are the only two reverse-reactivated faults on the section. Unreactivated faults have displacements of < 1 m, and appear isolated. One exception is an unreactivated fault inside the conjugate intersection of the reverse-reactivated faults, which links to the north-dipping fault.

The importance of fault connectivity in the selective reverse-reactivation of the normal faults can be demonstrated with a percolation model (e.g. Stark and Stark, 1991; Turcotte, 1995; Sahimi and Arbabi, 1996). A single percolation network on the Somerset coast would involve linkage of the reverse-reactivated Quantock's Head and Kilve Pill Faults (C and B, Fig. 3.2) which have opposing dips and are separated by a horst. Linkage of both the Quantock's Head and Kilve Pill Faults to an underlying fault (the Central Bristol Channel Fault Zone, Brooks *et al.*, 1988) would form a network of larger faults upon which the reverse-reactivation was concentrated. The passage of fluids through the basin would preferentially occur along the connected network of normal faults that form the backbone of the percolation cluster (e.g. Quantock's Head Fault, Fig. 3.8). Isolated, poorly connected or impermeable faults are not reactivated. Connectivity in itself does not guarantee that a fault will form part of the percolation backbone, as fluid flow through a network relies on fault permeability (Stauffer and Aharony,

1992). Fluid discharge during fault-valve action is typical of steep faults (Sibson, 1995), but fluid migration through the basin, and consequently reverse-reactivation, would focus along faults of any orientation, with sufficient permeabilities that are connected to the source.

3.5 GEOMETRIES OF OVERLAPPING AND UNDERLAPPING ZONES

In normal fault systems, displacement at an overlap zone in map view is transferred from one synthetic fault segment to another across a relay ramp (e.g. Larsen, 1988; Peacock and Sanderson, 1991, 1994a; Trudgill and Cartwright, 1994), or via an accommodation zone between two opposite polarity faults (Morley *et al.*, 1990; Gawthorpe and Hurst, 1993; McClay and White, 1995). Underlap zones occur between two offset synthetic fault segments, whose tips have not propagated past each other (Peacock and Sanderson, 1991). In contractional systems, a transfer zone is defined as the zone between two overlapping thrust planes that link at depth to a decollement (Dahlstrom, 1969; Boyer and Elliot, 1982). In map view, approximately uniform contraction is conserved across the transfer zone by the cumulative shortening of an echelon, sub-parallel faults and folds in the hanging-walls of thrusts (House and Gray, 1982), with displacement along the thrusts decreasing into the transfer zone. Alternatively, Lebel and Mountjoy (1995) use numerical modelling to show that displacement minima and maxima along a thrust, in map view, can occur through systematic shifting of the deformation from one thrust to another. Displacement on the most suitably oriented and positioned thrust occurs until movement is prevented, and the shortening is accommodated by another thrust (Lebel and Mountjoy, 1995).

In reverse-reactivated normal fault systems, the style of displacement accommodation is governed by the geometry of the pre-existing normal fault network, and by the selective reactivation of some of those normal faults. For example, relics of normal fault relay ramps (Larsen, 1988; Peacock and Sanderson, 1991; 1994a; Trudgill and Cartwright, 1994) that formed during the extension event (Fig. 3.9a) are often preserved adjacent to the reverse-reactivated normal fault. The through-going fault is reverse-reactivated, but the fault tips by-passed during breaching of the relay ramp are not reactivated (Fig. 3.9b). Several examples of breached relay ramps, between fault segments with spacings < 1 m, occur within the reverse-reactivated Kilve Pill Fault Zone (at B, Fig. 3.2).

Shortening between antithetic reverse-reactivated normal faults has been accommodated by (1) a strike-slip fault network within an overlap zone (at D, Figs. 3.2 and 3.3a), and (2) an array of obliquely oriented reverse faults at an underlap zone (at E, Fig. 3.2). Both of these occur between two steep ($\geq 60^\circ$) reverse-reactivated normal faults (Fig. 3.2). The traditional definition of a thrust transfer zone (Dahlstrom, 1969; Boyer and Elliot, 1982) does not apply to these examples, as they occur between faults with opposing dips, rather than between faults with similar dip directions that link at depth. The style of shortening accommodation is dependent on the structural heterogeneity inherited from the extensional phase of basin development, *i.e.* fault spacing and whether the faults overlap or underlap. For example, the strike-slip network (Fig. 3.3a) is between two reverse-reactivated normal faults that define a zone 500 m wide that contains relatively few normal faults.

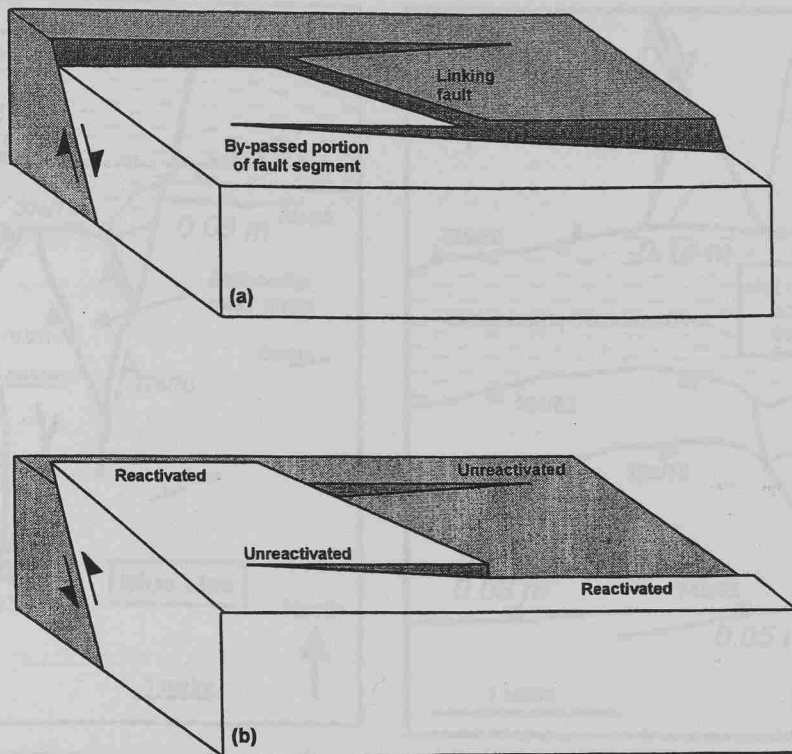


Fig. 3.9. (a) Line drawing of a relay ramp in a reverse-reactivated normal fault system. (b) Model to illustrate the style of faults at transfer zones between reverse-reactivated fault segments (c.f. Peacock and Sanderson, 1991).

3.5.1 Strike-slip network

A network of conjugate strike-slip faults occurs within a horst block, at an overlap between the south-dipping Quantock's Head Fault and the north-dipping Kilve Pill Fault (at D, Figs. 3.2 and 3.3a). The amount of overlap between the two reverse-reactivated normal fault zones is not known, as the tips of both faults are not exposed. The zone containing the strike-slip fault network is wholly within the interbedded Blue Lias limestones and shales. The Blue Lias is between the more ductile Kilve Shales and St. Audrie's Shales, and strike-slip faults in the shale units to the north of the Kilve Pill Fault are rare (Fig. 3.2). There is a marked change eastwards from a linked network of conjugate strike-slip faults in the overlap zone with displacements of a few metres, towards a highly segmented strike-slip fault system with displacements of < 1 m (Fig. 3.3a).

3.5.1a Interaction of strike-slip and dip-slip faults

There have been conflicting views on the relative timing of the strike-slip fault development and reverse-reactivation of the normal faults. To generate strike-slip faulting and reverse-reactivation of normal faults during one event, σ_3 and σ_2 must have been able to swap, at least locally. Dart *et al.* (1995) state that the strike-slip faults formed after the reverse-reactivation of the normal faults, but Nemcok *et al.* (1995) believe that the two modes of faulting were contemporaneous. A relative chronology is evident, however, from maps of cross-cutting strike-slip and dip-slip faults (Fig. 3.10).

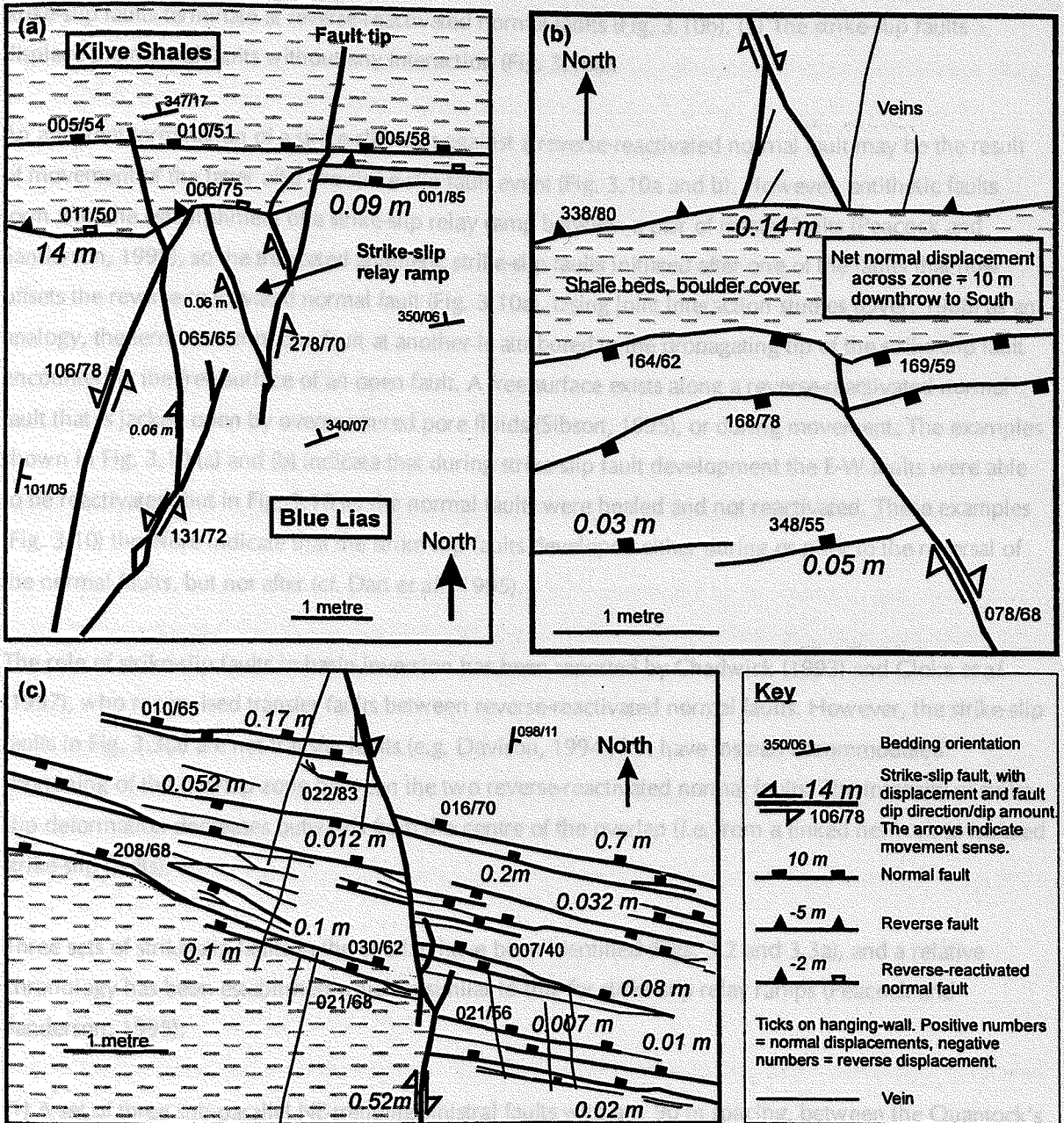


Fig. 3.10. Maps of strike-slip faults at intersections with earlier E-W striking dip-slip faults at Kilve, Somerset; the shading represents shale beds. (a) Intersection of a sinistral strike-slip relay ramp and a reactivated normal fault zone. The antithetic right-lateral faults within the relay ramp are truncated at the normal fault and the main segment has propagated through, but ends shortly after intersection in the Kilve Shales. (b) Right-lateral strike-slip faults terminate at reverse faults, and bend into the normal faults. (c) The right-lateral strike-slip faults cross-cut an unreactivated normal fault zone.

Three distinct styles of fault intersections occur where rare examples of strike-slip faults cross-cut normal and reverse-reactivated normal faults (Fig. 3.10). (1) In Fig. 3.10 (a), the main left-lateral fault crosses beyond the intersection point but terminates within a few metres of the dip-slip fault (Fig. 3.10a). Minor right-lateral faults abut both the main left-lateral fault and the reverse-reactivated normal fault. (2) All

strike-slip faults terminate at reverse-reactivated normal faults (Fig. 3.10b). (3) The strike-slip faults displace the normal faults without any interaction (Fig. 3.10c).

An apparent termination of a strike-slip fault against a reverse-reactivated normal fault may be the result of movement of the latter after the strike-slip fault event (Fig. 3.10a and b). However, antithetic faults form after the establishment of a strike-slip relay ramp between a pair of master faults (Peacock and Sanderson, 1995), so the truncated antithetic strike-slip faults initiated after one of the faults that now offsets the reverse-reactivated normal fault (Fig. 3.10a). Using joint interaction studies (Dyer, 1988) as an analogy, the termination of one fault at another is attributed to the propagating tip of the strike-slip fault encountering the free surface of an open fault. A free surface exists along a reverse-reactivated normal fault that is jacked open by overpressured pore fluids (Sibson, 1995), or during movement. The examples shown in Fig. 3.10 (a) and (b) indicate that during strike-slip fault development the E-W faults were able to be reactivated, but in Fig. 3.10 (c) the normal faults were healed and not reactivated. These examples (Fig. 3.10) therefore indicate that the strike-slip faults developed either during or prior to the reversal of the normal faults, but not after (*cf.* Dart *et al.*, 1995).

The role of strike-slip faults in basin inversion has been reported by Chadwick (1993) and Cloke *et al.* (1997), who recognised transfer faults between reverse-reactivated normal faults. However, the strike-slip faults in Fig. 3.3(a) are not transfer faults (e.g. Davison, 1994), but have instead accommodated shortening of the overlap zone between the two reverse-reactivated normal faults. The intensity of strike-slip deformation decreases outwards from the centre of the overlap (*i.e.* from a linked network to isolated strike-slip faults).

Three sets of strike-slip faults in the overlap have been identified (Figs. 3.2 and 3.3a), and a relative chronology has been established which is similar to that for strike-slip relay ramps (Peacock and Sanderson, 1995):

- (1) A set of three sub-parallel NE-trending sinistral faults with a c. 90 m spacing, between the Quantock's Head Fault and the Kilve Pill Fault that divide the overlap into blocks (*block-bounding faults*) (at F, G and H, Fig. 3.2). Block rotation between the strike-slip faults is evident from the clockwise rotation of the Kilve Pill Fault.
- (2) Dextral strike-slip faults with NNW strikes often offset the block-bounding sinistral faults, indicating that they are more recent.
- (3) Sinistral faults between the block-bounding faults which have more easterly strikes, and are generally shorter and often offset the dextral faults.

The last two sets are collectively termed *intra-block faults* in the following sections.

Antithetic faults that delimit rotating blocks commonly occur in overlaps between sub-parallel, synthetic strike-slip faults, e.g. on the km-scale between the San Andreas and San Jacinto Faults (Nicholson *et al.*,

1986), and on the mm-scale to the west of the Blue Ben Headland (at A, Fig. 3.2) (Kelly, 1996). The location of the sinistral block-bounding faults therefore suggests a component of dextral movement along one, or both, of the reverse-reactivated normal faults, prior to development of the intra-block faults. Block-bounding faults with sinistral displacements and sub-horizontal slickenside lineations could not have formed if either the Quantock's Head or Kilve Pill Faults had a sinistral component in this locality.

Immediately west of the western block-bounding fault (F, Fig. 3.2) there are two reverse faults that strike NW and are therefore oblique to the Quantock's Head Fault, but sub-parallel to the rotated Kilve Pill Fault. These faults strike obliquely to the majority of the normal faults on the foreshore, which they displace. The single set of slickenside lineations on the obliquely-oriented faults indicate reverse dip-slip movement, and therefore new thrusts that formed during the contraction. The strike of these two reverse faults and the acute dihedral angle bisector for the intra-block faults indicate that these faults formed with a local NE-trending σ orientation. The formation of the sinistral block-bounding faults, and the development of new oblique reverse faults can be combined into a dextral transpression model (Sanderson and Marchini, 1984); dextral movement is indicated by the block rotations, and contraction by reverse-reactivation (Fig. 3.11). In this model, the sinistral block-bounding faults form, and rotate the Kilve Pill Fault. The shortening direction within the overlap is modified by the new orientation of the Kilve Pill Fault, and the curved trace of the Quantock's Head Fault. Contraction of the overlap then dominates, and is accommodated by the formation of the conjugate intra-block faults, and reverse faults at the base of the western rotating block (Figs. 3.2 and 3.11). The transfer of movement between the reverse-reactivated normal faults, reverse faults and the strike-slip network is an example of systematic shifting from one structural style to another to accommodate the contraction through time (cf. Lebel and Mountjoy, 1995).

3.5.2 Obliquely-oriented high-angle reverse faults

In an underlap region between the western tip of the Quantock's Head Fault and a north-dipping reverse-reactivated normal fault to the NE of the Blue Ben Headland (at E, Fig. 3.2), there is an array of NE-striking reverse faults with $> 40^\circ$ dips which occur on the rim of a syncline. The beds dip gently towards the SE in the hanging-walls of the reverse faults, and are sub-horizontal in the footwalls (Fig. 3.2). The fault dips suggest that they originated as normal faults, but their strikes are inconsistent with N-S extension. If the faults formed during the extensional phase of basin development, and were reverse-reactivated during N-S shortening, there might be evidence of oblique-slip. The slickenside lineations however indicate that these faults are predominantly dip-slip, and are therefore probably reverse faults that developed during the contraction.

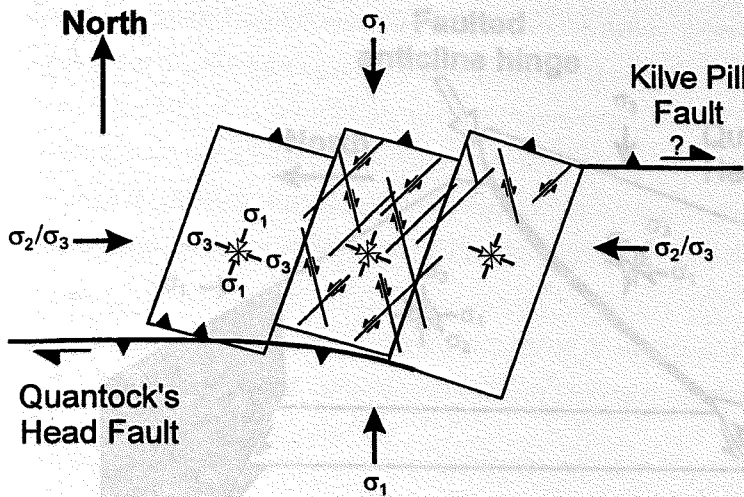


Fig. 3.11. Schematic diagram to illustrate a mechanism for the formation of the strike-slip network in the overlap between the Quantock's Head and Kilve Pill Faults. Dextral transpression causes the formation of sinistral faults and block rotation. The shortening is accommodated by the formation of thrusts at the foot of the block, that are oblique to the Quantock's Head Fault. Unfilled arrows = local stress axes, filled arrows = 'regional' stress axes.

Possible methods by which NE-striking reverse faults could have developed at this locality include: (1) a previously unrecognised phase of NW shortening, (2) sinistral transpression (Sanderson and Marchini, 1984), and (3) loading of the corner of the underlap zone. Regional NW directed shortening is rejected through lack of evidence, but the stress system could have been modified locally by other fault movements to form these structures.

Slickenside lineation orientations at the western end of the Quantock's Head Fault (Fig. 3.2b) are consistent with a component of sinistral strike-slip movement, although dip-slip dominates. The slickenside lineations on the northern fault indicate almost pure dip-slip movement, so sinistral movement of the Quantock's Head Fault would have been the dominant factor in a transpression model. The sinistral transpression model does not, however, account for the steepness of the reverse faults.

A third possibility is that the reverse faults formed during loading of the corner of the underlap zone by the hanging-wall of the Quantock's Head Fault (Fig. 3.2). In this model, an anticline with a NE-SW trending axis initially formed with a steeper SE limb, due to the applied load (Fig. 3.12). The beds in the south of the fold hinge dip towards the loaded corner of the underlap zone to the ESE, whilst those in the footwall dip WNW. Further shortening of the underlap, driven by sustained movement of the hanging-wall of the Quantock's Head Fault, caused the anticline to fail along the hinge, by means of NE-SW striking reverse faults.

It is commonly accepted that the deformation-related structures in the Wessex and Bristol Channel Basins are an expression of Alpine tectonism (Van Siborn, 1967; Brooks et al., 1986; Chadwick, 1993; Dani et al., 1995; Hancock et al., 1995), i.e. approximately N-S oriented shortening, and in the preceding sections the role of the Quantock's Head Fault has been analysed and discussed. For example, the obliquely-oriented reverse faults are unique to the underlap zone close to the termination of this fault (cf. Fig. 3.2), and suggest that movement of the Quantock's Head Fault was instrumental in their formation (Fig. 3.12). The dip-slip faults to the NE of the curved axis of the Quantock's Head Fault strike ESE, while those to the NW strike ENE (Fig. 3.2). The faults could have rotated to their present-day strikes during the deglaciation, if it is assumed that the orientations of the normal faults were originally vertical.

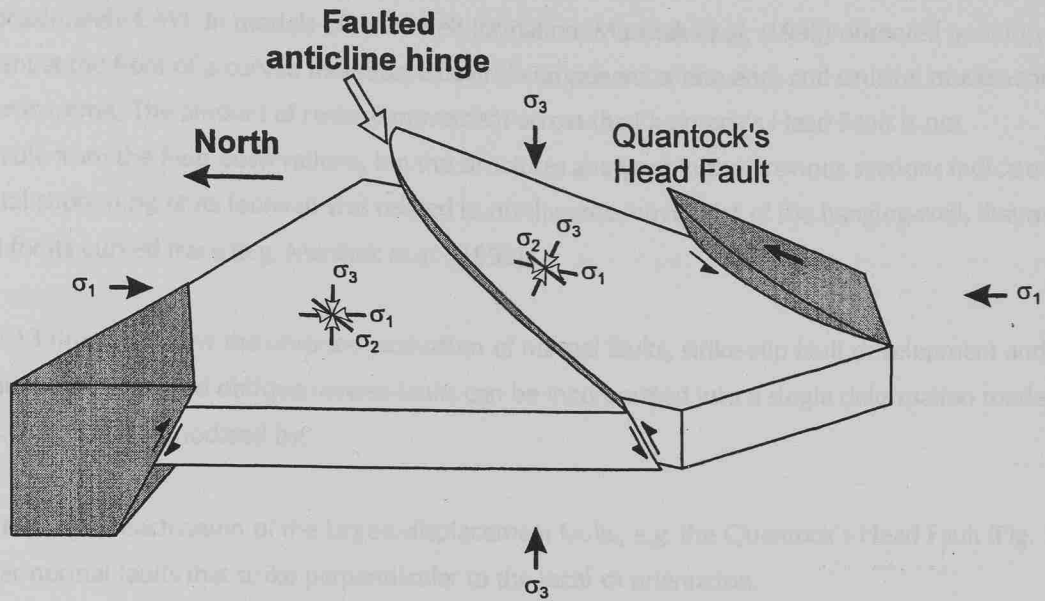


Fig. 3.12. Block diagram of the interpretation of the formation of the obliquely-oriented high-angle reverse faults east of the Blue Ben Headland. A NE-SW trending anticline forms initially, due to loading of the corner of the underlap zone by the hanging-wall of the Quantock's Head Fault. The beds in the south of the fold hinge dip towards the loaded corner of the underlap zone to the ESE, whilst those in the footwall dip WNW. Continued shortening, driven by the northwards movement of the Quantock's Head Fault hanging-wall causes failure along the anticline hinge, and new NE-striking reverse faults develop. Open arrows = local stress axes, closed arrows = 'regional' stress axes.

3.6 DEFORMATION MODEL

The geometries of the under- and overlap zones provide evidence to support a single progressive deformation event, during which the method by which shortening was accommodated switched between reverse-reactivation of normal faults, reverse faults and conjugate strike-slip faults. The sinistral movement identified at the western end of the Quantock's Head Fault (Fig. 3.2b), the dip-slip displacement at the centre and the postulated dextral motion at its eastern end (Fig. 3.11) imply that the footwall of the Quantock's Head Fault was deformed around its hanging-wall in map view. In addition, approximately N-S contraction of the hanging-wall is evident from thrusts (Peacock and Sanderson, 1992) and a hanging-wall buttress anticline (Dart *et al.*, 1995).

It is commonly accepted that the contraction-related structures in the Wessex and Bristol Channel Basins are an expression of Alpine tectonism (Van Hoorn, 1987; Brooks *et al.*, 1988; Chadwick, 1993; Dart *et al.*, 1995; Nemcok *et al.*, 1995), *i.e.* approximately N-S oriented shortening, and in the preceding sections the role of the Quantock's Head Fault has been analysed and discussed. For example, the obliquely-oriented reverse faults are unique to the underlap zone close to the termination of this fault (at E, Fig. 3.2), and suggest that movement of the Quantock's Head Fault was instrumental in their formation (Fig. 3.12). The dip-slip faults to the NE of the curved trace of the Quantock's Head Fault strike ESE, while those to the NW strike ENE (Fig. 3.2). The faults could have rotated to their present-day strikes during the contraction, if it is assumed that the orientations of the normal faults were originally similar

(i.e. approximately E-W). In models of thrust-belt formation, Marshak *et al.* (1992) observed pure dip-slip movement at the front of a curved indenter, a dextral component at one end, and sinistral movement at the other extreme. The amount of reverse movement across the Quantock's Head Fault is not quantifiable from the field observations, but the structures analysed in the previous sections indicate that horizontal shortening of its footwall was related to northwards movement of the hanging-wall, that may account for its curved trace (e.g. Marshak *et al.*, 1992).

Figure 3.13 illustrates how the reverse-reactivation of normal faults, strike-slip fault development and the development of steep and oblique reverse faults can be incorporated into a single deformation model. Deformation is accommodated by:

Selective reverse-reactivation of the largest-displacement faults, e.g. the Quantock's Head Fault (Fig. 3.2), and other normal faults that strike perpendicular to the local σ_1 orientation.

(a) Sinistral strike-slip faulting with clockwise block rotation during the reverse movement across the Quantock's Head Fault (Fig. 3.11). Shortening of the newly-formed blocks accommodated by the strike-slip fault network, that suggests a NNE σ_1 orientation (Figs. 3.3a and 3.11), and thrusts at the foot of the blocks. The strike-slip faults have the greatest displacements, and link to form a through-going network in the central block, and are more isolated with smaller displacements outside of the overlap to the east. The offset of the Quantock's Head Fault by one of the sinistral block-bounding faults (F, Fig. 3.2) accounts for the more intense strike-slip deformation within the central block, i.e. the hanging-wall is pushed further north at this point than in the western block. (b) σ_1 is locally perturbed such that reverse faults oblique to existing faults form to the west of the fault, at an underlap with other reverse-reactivated normal faults (Fig. 3.12).

3.7 CONCLUSIONS

1. Mapped examples of normal faults and reverse-reactivated normal faults suggest that all normal faults with > 22 m displacement were reactivated during basin contraction. Some faults with smaller displacements were also reverse-reactivated, and new thrusts propagated, some with displacements of > 1 m. Reverse-reactivation of the normal faults in Somerset appears to be independent of fault dip.

2. The field observations summarised in Fig. 4(c) suggest that both fault dip and size play major roles in selective reactivation. Possible reasons for the preferential reverse-reactivation of larger normal faults include:

(a) Decreased fault-plane friction due to smooth fault profiles and thicker gouges.

(b) Domino-style reverse-rotation.

(c) Contraction may have been driven from the basement, affecting only the basement-involved larger faults. Smaller faults within the cover sequence remained unreactivated.

(d) Deformation and fluid flow was concentrated onto a connected network of larger faults.

3. Fault geometries at overlapping and underlapping zones are controlled by the selective reactivation of normal faults, and in particular the width of the zone. Two styles are recognised: (a) A strike-slip network

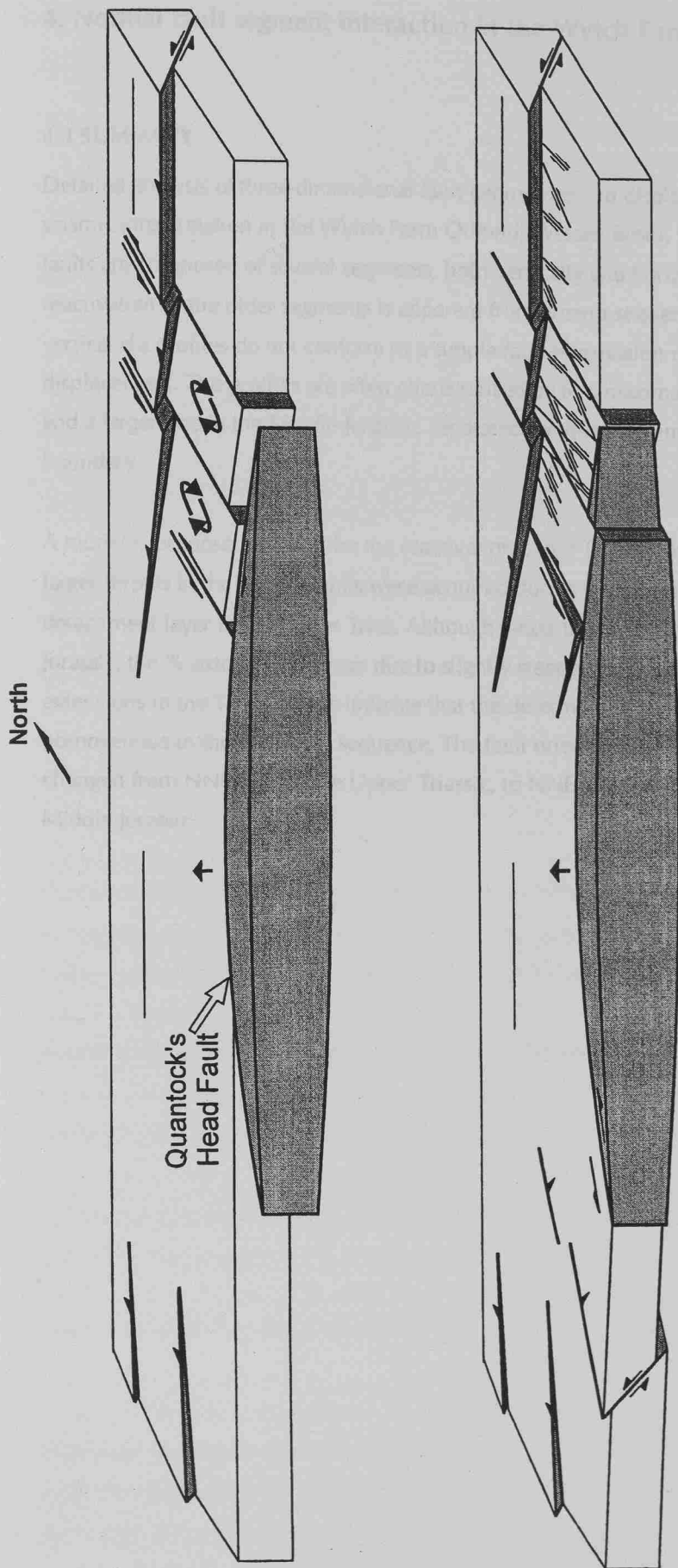


Fig. 3.13. Block diagrams to illustrate the contractional deformation at Kilve as one single on-going event controlled by the reverse-reactivation of the Quantock's Head Fault. (a) The Kilve Pill Fault is offset and rotated clockwise by sinistral faults that form in response to dextral transpression along the Quantock's Head Fault. The northwards movement of the hanging-wall of the Quantock's Head Fault indents its footwall, and the local principal stress axes and existing structures are rotated anti-clockwise to the west of the fault, and clockwise to the east. (b) Further indentation of the Quantock's Head Fault and σ_1 is further perturbed such that reverse faults oblique to existing faults form in an underlap to the west of the fault. To the east of the fault, a network of conjugate strike-slip faults develops, that suggests a NNE σ_1 orientation.

4. Normal fault segment interaction in the Wytch Farm Oilfield, Wessex Basin

4.1 SUMMARY

Detailed analysis of three-dimensional fault geometries and displacement-distance ($d-x$) profiles from 3D seismic interpretation in the Wytch Farm Oilfield, Wessex Basin, Dorset, UK has revealed that normal faults are composed of several segments, both vertically and horizontally, of various ages. Normal reactivation of the older segments is apparent from growth sequences at various stratigraphic levels, but vertical $d-x$ profiles do not conform to a simple fault reactivation model with upward decreases in displacement. The profiles are often characterised by two maxima, one centred on the Upper Triassic and a larger one in the Middle Jurassic, separated by throw minima in proximity to the Triassic-Jurassic boundary.

A model is proposed to describe the reactivation of the Triassic faults and their upward growth. The larger throws in the Jurassic units were acquired during thin-skinned extension above a postulated detachment layer in the Upper Trias. Although larger throws on the dominant faults are apparent in the Jurassic, the % extension is lower due to slightly steeper faults. Lower fault densities, but greater extensions in the Triassic units indicate that the deformation was localised in the deeper units, and more homogenous in the shallower sequence. The fault orientations suggest that the extension direction changed from NNW-SSE in the Upper Triassic, to NNE-SSW during the Lower Jurassic, and to N-S in the Middle Jurassic.

4.2 INTRODUCTION

Recent interest in the kinematics of normal faults has concentrated mainly on field studies of fault geometries in map view and their displacement characteristics (e.g. Furlong and Jamieson, 1971; 1984; Scholze, 1981; Andewé and Scholze, 1984; Chubb *et al.*, 1985), although 3D numerical modelling has also been used for similar purposes (Williams *et al.*, 1984; Williams, 1987). Studies of dip-slip behaviour of normal faults in seismic sections (Woodward and Cartwright, 1979) and in cross-sections (Murakami and Koyama, 1983; Peacock and Zhang, 1994; Chubb *et al.*, 1996) have been restricted to faults that were active during a single deformation phase. Normal faults in the Wytch Farm Oilfield, Dorset (Fig. 4.1), developed during polyphase extension on the foreland of the Late Permian and culminated in the Cretaceous (Andewé, 1984). The aim of this study is, (1) to provide a detailed description of the normal fault geometries in the Wytch Farm Oilfield, Dorset, UK, and (2) to propose a model for the evolution of individual faults, and their interaction during polyphase extension. The description includes analysis of the timing of movement of the faults, and interpretation of their linkage.

A description of the methods used is followed by analysis of the fault geometries in cross-section and map view. Fault-slip analysis (Andewé, 1984) has been carried out on each cross-section, a model has been developed to describe the evolution of individual faults in the study area, and the faults are then related to the regional extension.

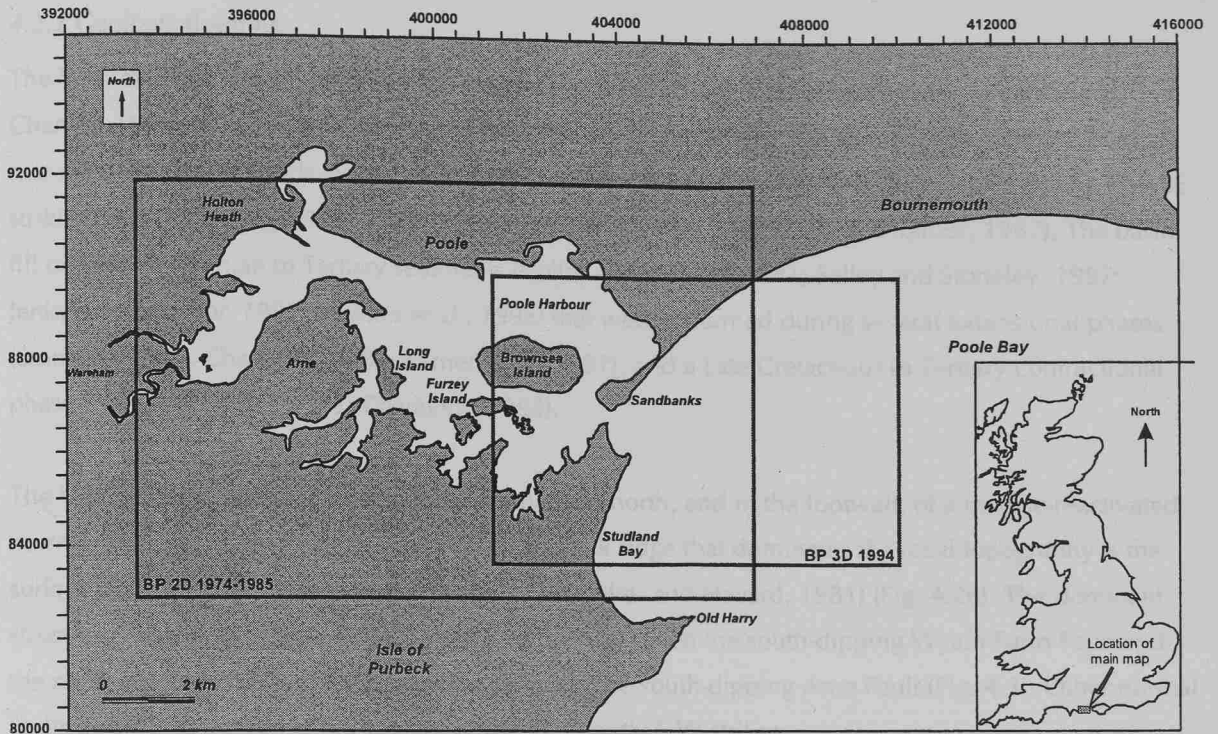


Fig. 4.1. Map of part of the south Dorset Coast to show the location of the Wytch Farm Oilfield and the extent of the seismic data (see inset for location of main map in Great Britain). The inlines run from N-S, and the crosslines from E-W in both 3D surveys.

4.2 INTRODUCTION

Recent interest in the linkage of normal faults has concentrated mainly on field studies of fault geometries in map view and their displacement characteristics (e.g. Peacock and Sanderson, 1991; 1994a; Schlische, 1993; Anders and Schlische, 1994; Childs *et al.*, 1995), although 3D numerical modelling has also been used for similar purposes (Willemsse *et al.*, 1996; Willemsse, 1997). Models of dip-linkage between normal faults on seismic sections (Mansfield and Cartwright, 1996) and in cliff-sections (Muraoka and Kamata, 1983; Peacock and Zhang, 1994; Childs *et al.*, 1996) have been restricted to faults that were active during a single deformation phase. Normal faults in the Wytch Farm Oilfield, Dorset (Fig. 4.1), developed during polyphase extension that initiated in the Late Permian and culminated in the Cretaceous (Chadwick, 1986). The aims of this study are, (1) to provide a detailed description of the normal fault geometries in the Wytch Farm Oilfield, Dorset, UK, and (2) to propose a model for the evolution of individual faults, and their interaction during pulsed extension. The description includes analysis of the timing of movement of the faults, and interpretations of their linkage.

A description of the methods used is followed by analysis of the fault geometries in cross-section and map view. Fault-strain analysis (Jamison, 1989) has been carried out on each cross-section, a model has been developed to describe the evolution of individual faults in the study area, and the faults are compared to the regional structure.

4.2.1 Geological setting

The Wessex Basin (Kent, 1949) comprises several sub-basins, including the Channel, Weald, Bristol Channel, Western Approaches and the Vale of Pewsey Basins (Fig. 4.2a) (Karner *et al.*, 1987). There are two major structural trends in the basin: normal faults trend approximately E-W and are offset by NW-SE striking faults (Stoneley, 1982; Chadwick, 1986; Karner *et al.*, 1987; Lake and Karner, 1987). The basin fill consists of Permian to Tertiary sediments (Colter and Havard, 1981; Selley and Stoneley, 1987; Jenkyns and Senior, 1991; Hawkes *et al.*, 1998) that were deformed during several extensional phases (Stoneley, 1982; Chadwick, 1986; Karner *et al.*, 1987), and a Late Cretaceous to Tertiary contractional phase (Lake and Karner, 1987; Chadwick, 1993).

The Wytch Farm Oilfield is located to the immediate north, and in the footwall, of a reverse-reactivated normal fault, the Purbeck-Isle of Wight Fault. A Chalk ridge that dominates the local topography is the surface expression of the reverse-reactivated fault (Colter and Havard, 1981) (Fig. 4.2b). The dominant structure of the Wytch Farm Oilfield is an E-W horst between the south-dipping Wytch Farm Fault and the north-dipping Northern Fault, between which is the south-dipping Arne Fault (Fig. 4.3). Other normal faults inside and outside of the horst have predominantly E-W strikes.

4.2.2 Exploration history

The Wytch Farm Oilfield is composed of three principal reservoirs: the Triassic Sherwood Sandstone; the Jurassic Bridport Sands and the limestone member of the Jurassic Frome Clay (Fig. 4.4). Other minor reservoirs occur within the basin: the fractured Cornbrash Limestone and Oxford Clay reservoirs were the first commercial discoveries in the late 1950's to early 1960's (Colter and Havard, 1981); the Kimmeridge Field is still producing at a rate of 100 barrels/day (Evans *et al.*, 1998). The Cornbrash reservoir was the only significant discovery in the hanging-wall anticline of the Purbeck Disturbance (Evans *et al.*, 1998), and it is thought that other accumulations were remobilised and expelled during basin inversion (Selley and Stoneley, 1986). Hydrocarbon generation in the Lower Jurassic rocks on the downthrown side of the Purbeck - Isle of Wight Fault began in the Early Cretaceous (Colter and Havard, 1981). The Bridport Sands and the Sherwood Sandstone were both structurally higher than the Liassic source during hydrocarbon mobilisation, and the Purbeck - Isle of Wight Fault probably served as the major migration pathway (Colter and Havard, 1981).

Fig. 4.2. (a) Map of the Wessex Basin to show the fault trends and the location of the main sub-basins (after Karner *et al.*, 1987). (b) Satellite photo of Dorset with the location of Wytch Farm and the Purbeck-Isle of Wight Disturbance highlighted. © Dorset County Council, used with permission.

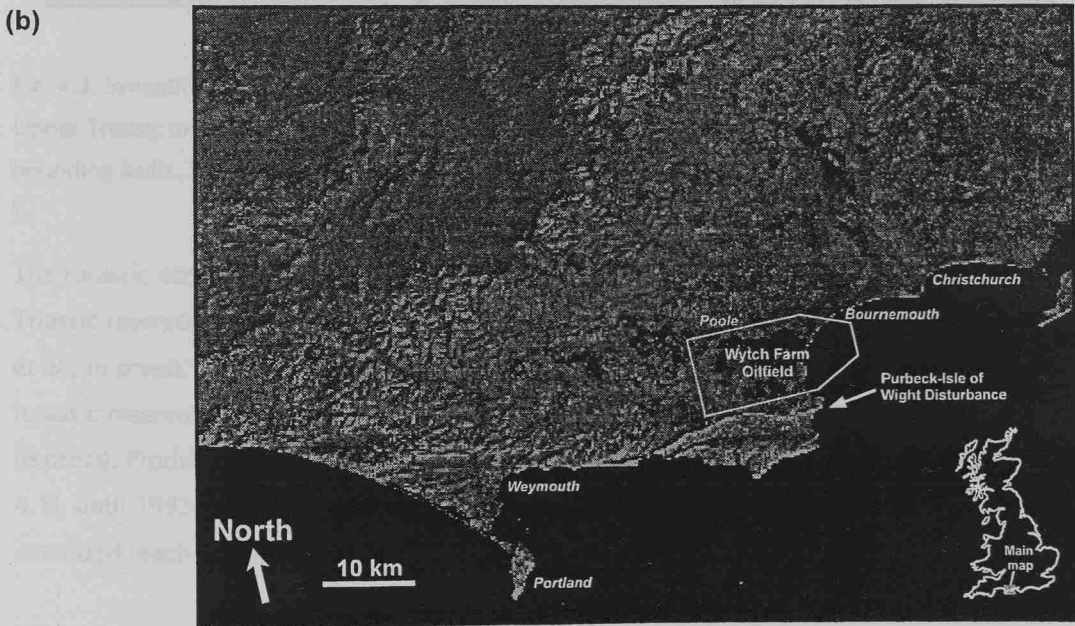
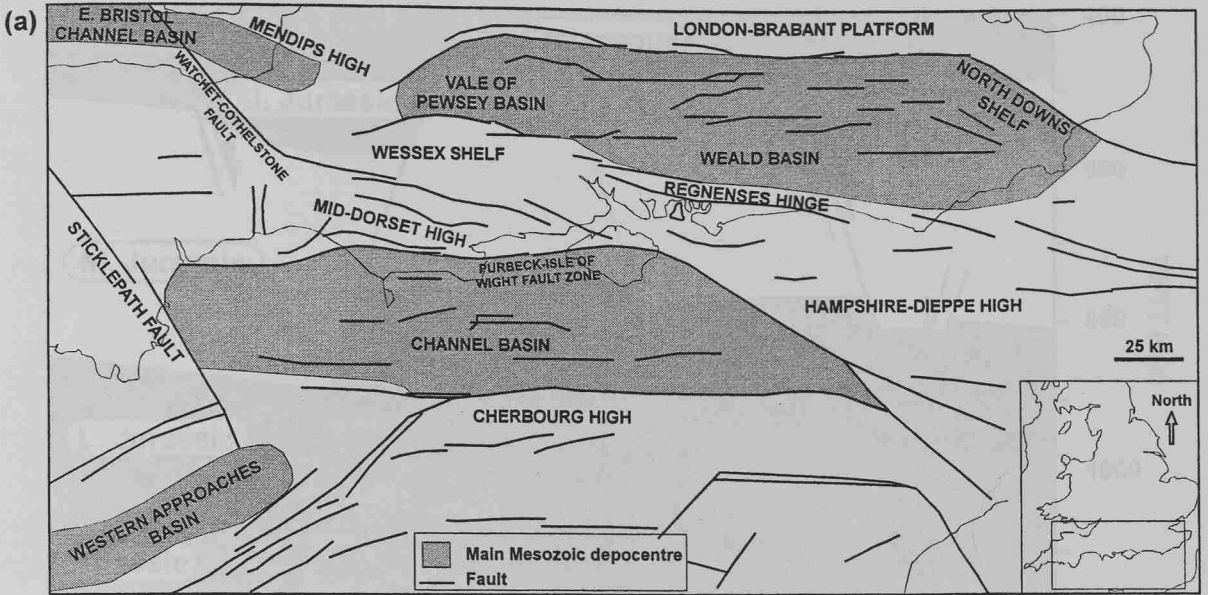


Fig. 4.2. (a) Map of the Wessex Basin to show the fault trends and the location of the main sub-basins (after Karner et al., 1987). (b) Satellite photo of Dorset with the location of Wytch Farm and the Purbeck-Isle of Wight Disturbance highlighted. © Dorset County Council, used with permission.

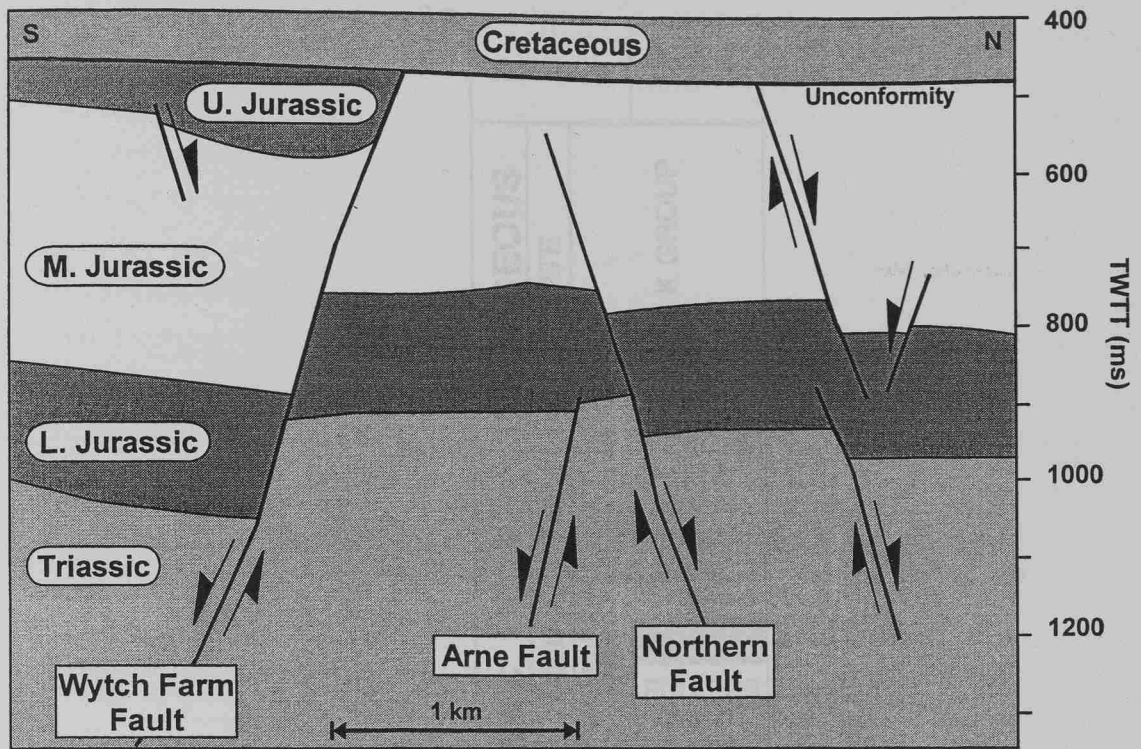


Fig. 4.3. Synoptic cross-section of the Wytch Farm Oilfield horst. The sequence within the central horst consists of Upper Triassic to Middle Jurassic sediments. Upper Jurassic sediments occur in the hanging-walls of the horst-bounding faults. The Cretaceous lies unconformably above the Jurassic sequence.

The Jurassic accumulations were discovered at the end of 1973, and in 1977, oil was found in the Triassic reservoir. The Sherwood Reservoir contained an estimated 450×10^6 barrels oil equivalent (Hogg *et al.*, in press), over half of which has been recovered (250×10^6 barrels, January 1998), whilst the two Jurassic reservoirs contained an estimated 31×10^6 barrels and 4×10^6 barrels respectively (Hogg *et al.*, in press). Production from the reservoirs was confined to the onshore area, within Poole Harbour (Fig. 4.1), until 1993 when the offshore part of the field (Bournemouth Bay) was exploited through a series of extended reach drilling (ERD) wells drilled from onshore (Hogg *et al.*, in press).

4.2.3 Seismic data

Acquisition of seismic data by BP at Wytch Farm began in 1974 and continued until 1995 (Fig. 4.1). A range of 2D surveys was undertaken to cover both onshore and offshore areas of the Oilfield, between 1974 and 1985. A 3D seismic data set was acquired in 1994, that straddles the transition zone between onshore Poole Harbour and offshore Bournemouth Bay (Fig. 4.1), and provided a consistent image of the Top Sherwood reflector. The 3D seismic lines were spaced at 12.5 m, with N-S inlines and E-W cross-lines.

4.2 METHODS

4.2.1 Seismic interpretation

The interpretation was undertaken using the software package *Seismic Interpretation* (Schlumberger GeoQuest, 1998) using a series of steps that are described in Table 4.1. The first step was to create a series of horizons from the seismic data. This was done by identifying key horizons and then using a series of filters to extract the data. The horizons were then correlated and a series of tie points were used to ensure consistency. The final step was to create a stratigraphic column from the horizons. This was done by identifying the units and their relative positions. The units are listed in Table 4.2 and are shaded to indicate reservoir units.

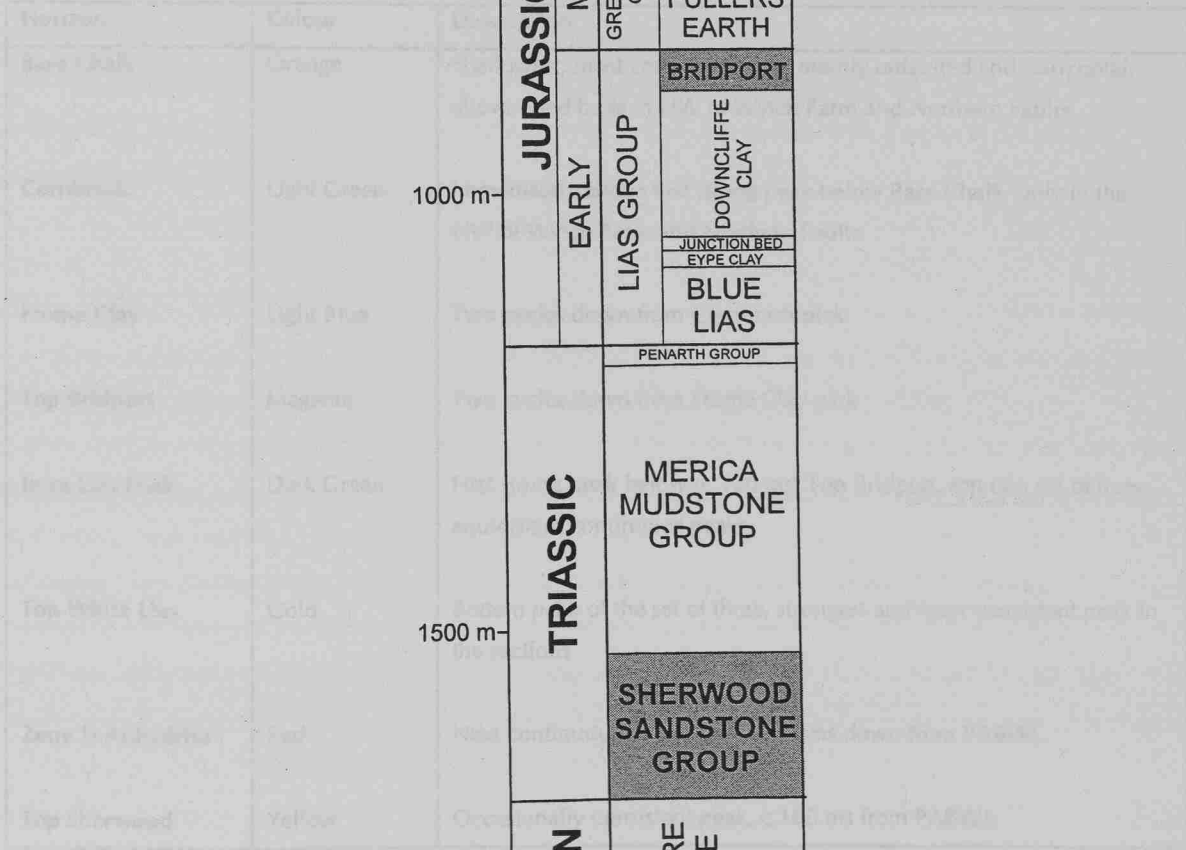


Fig. 4.4. Stratigraphy of the Wyitch Farm Oilfield, based on A6SP well log. The reservoir units are shaded.

4.3 METHODS

4.3.1 Seismic interpretation

The interpretation was undertaken on UNIX workstations using both *Schlumberger GeoQuest Charisma* and *Schlumberger GeoQuest IESX* software. The interpretation was based on the existing BP in-house picks (Table 4.1) that are tied to well data, and was extended where necessary. An initial re-interpretation of every tenth cross-line was carried out, and the cross-referenced points were used to position the horizons on every tenth inline to provide a 125 x 125 m grid within the survey boundaries. The seismic resolution is sufficient for fault positions to be accurate to ± 50 m (significantly < interpretation spacing) and throws to ± 5 m (Hogg *et al.*, in press). Faults were not imaged directly, so fault contacts (*i.e.* fault/horizon intersections) were interpreted at reflector terminations. Fault contacts were assigned automatically in *Charisma*, but were edited manually. Fault contact data form the basis of subsequent automated displacement and geometry analysis. The completed interpretation, composed of horizon, fault and contact data, was imported into a program developed with *Microsoft Visual Basic* to view cross-section and map interpretations, fault plane maps, and output fault-strain and fault data (2D/3D).

Horizon	Colour	Description
Base Chalk	Orange	Shallowest, most consistent peak, mainly unfaulted and horizontal, above tilted beds in HW of Wytch Farm and Northern Faults
Cornbrash	Light Green	Immediately above first strong peak below Base Chalk, only in the HW of Wytch Farm and Northern Faults
Frome Clay	Light Blue	Two cycles down from Cornbrash pick
Top Bridport	Magenta	Two cycles down from Frome Clay pick
Intra Lias Peak	Dark Green	First strong peak below (c.120 ms) Top Bridport, top of a set of three equidistant continuous peaks
Top White Lias	Gold	Bottom peak of the set of three, strongest and most consistent peak in the sections
Zone D Anhydrite	Red	Next continuous strong peak, c.80 ms down from PABWL
Top Sherwood	Yellow	Occasionally consistent peak, c.160 ms from PABWL

Table 4.1. Description of the horizons used in the interpretation. A comparison of well and seismic data indicates that the IntraLias pick represents the Middle Lias/Upper Lias boundary, located at the base of the Junction Bed (*e.g.* House, 1993).

4.3.2 Displacement-distance analysis

Vertical and horizontal d - x profiles are used throughout this study as a tool to identify the mode of fault growth, linkage development and displacement accommodation. A d - x profile is a graph of fault displacement plotted against the distance from the fault tip. Displacement-distance (d - x) plots have been used to study normal faults (Muraoka and Kamata, 1983), thrust geometries (Williams and Chapman, 1983), strike-slip faults (Peacock, 1991), and segmented normal faults (Peacock and Sanderson, 1991; Willemse *et al.*, 1996). Displacements along isolated normal faults in homogeneous media form approximately symmetrical d - x profiles either side of a central maximum (Muraoka and Kamata, 1983; Walsh and Watterson, 1987; Peacock and Sanderson, 1991). d - x profiles that are symmetrical about a central plateau of maximum displacement are common to faulting within heterogeneous materials (Muraoka and Kamata, 1983). Displacement maxima approximate to fault nucleation points, and displacement minima may represent linkage points between fault segments (Ellis and Dunlap, 1988; Peacock and Sanderson, 1991). Asymmetrical d - x profiles are indicative of fault interaction and linkage zones, and their shape is related to the relative size of the interacting faults and their initiation proximity (Peacock and Sanderson, 1991), and whether the faults over- or underlap (Willemse *et al.*, 1996). Combined displacements for segmented faults have d - x profiles that are similar to those for a single fault (Peacock and Sanderson, 1991), *i.e.* the maximum displacement usually occurs on the central segment (Willemse, 1997). Dip-linkage occurs when a fault propagating up-dip encounters and links with another propagating down-dip, and is recognisable from a displacement minimum on a vertical d - x profile (Mansfield and Cartwright, 1996).

4.3.3 Timing of movement

To constrain the ages for the Wytch Farm, Northern and Arne Faults, the ratio of hanging-wall thickness to footwall thickness (HW:FW) has been obtained for each stratigraphic interval (Fig. 4.5); syn-sedimentary faulting was indicated when HW:FW > 1 (Fig. 4.5). The ratios were plotted onto diagrams that represent maps of the fault planes, with a grey-scale to indicate ratio size (Fig. 4.6). The other faults in the basin were analysed using the same procedure, and the range of ages along the entire length of the faults has been plotted (Fig. 4.7). The ratio does not take into account the affect of differential compaction of the hanging-wall and footwall (*c.f.* Mansfield and Cartwright, 1996). The method, therefore, underestimates the extent and magnitude of growth faulting if, due to deeper burial, the hanging-wall compacted further. However, a comparison of individual unit thicknesses is valid as there is no reason to suspect heterogeneous compaction within the study area.

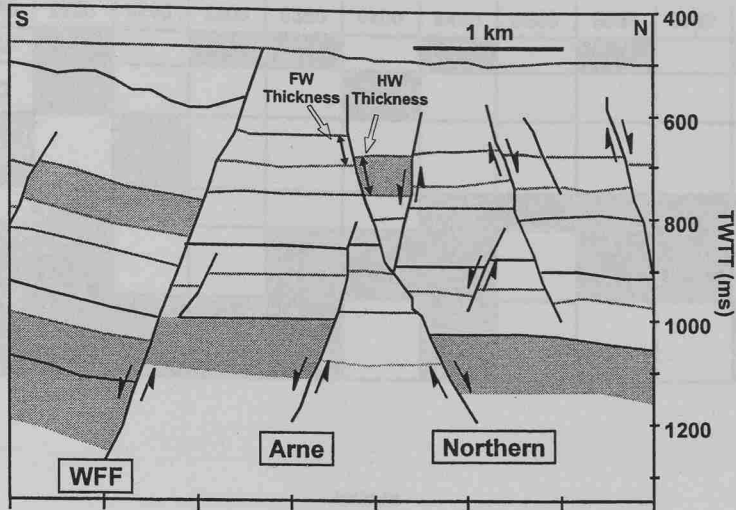


Fig. 4.5. Interpretation of inline 9350 with shading to denote the thickened hanging-wall sedimentary sequences adjacent to the Wyitch Farm, Northern and Arne Faults. The hanging-wall and footwall sequence thicknesses were measured parallel to the fault planes.

4.3.4 Extension analysis

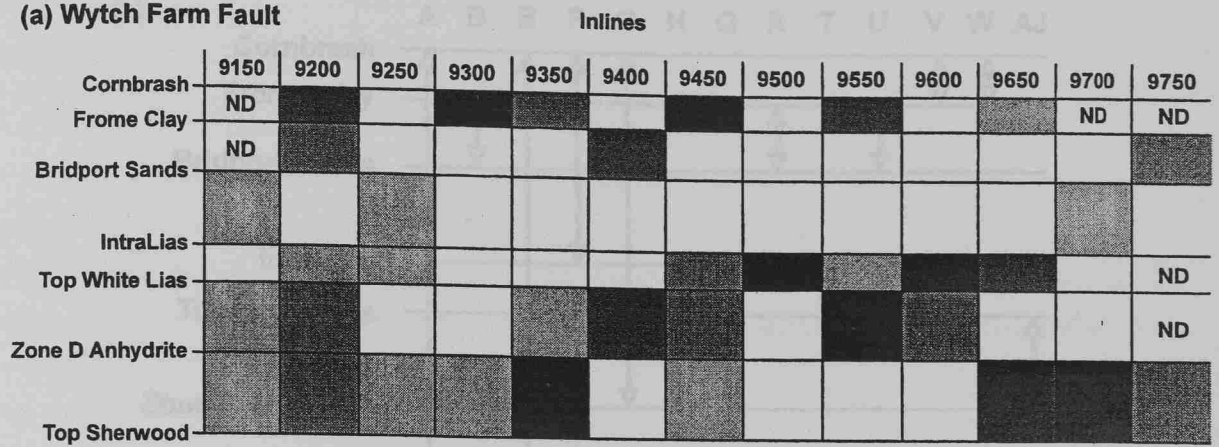
The % extension has been determined for the horizons listed in Table 4.1, with the exception of the Corallian, the IntraSherwood and the unfaulted Base Chalk. The Corallian is only exposed in the hanging-walls of the horst-bounding faults. Consequently, displacements are unresolvable and would anyway be a misrepresentation of the strain, due to a lack of information regarding faults within the horst. The IntraSherwood horizon has not been included in the analysis, as it was not possible to identify confidently the surface on all of the inlines.

The fault-strain (Jamison, 1989) was computed for each inline by summing the heaves for all faults ($\sum h$), and the length of the interpreted portion of the inline (l_f) within $2D/3D$ (Equation 3.1):

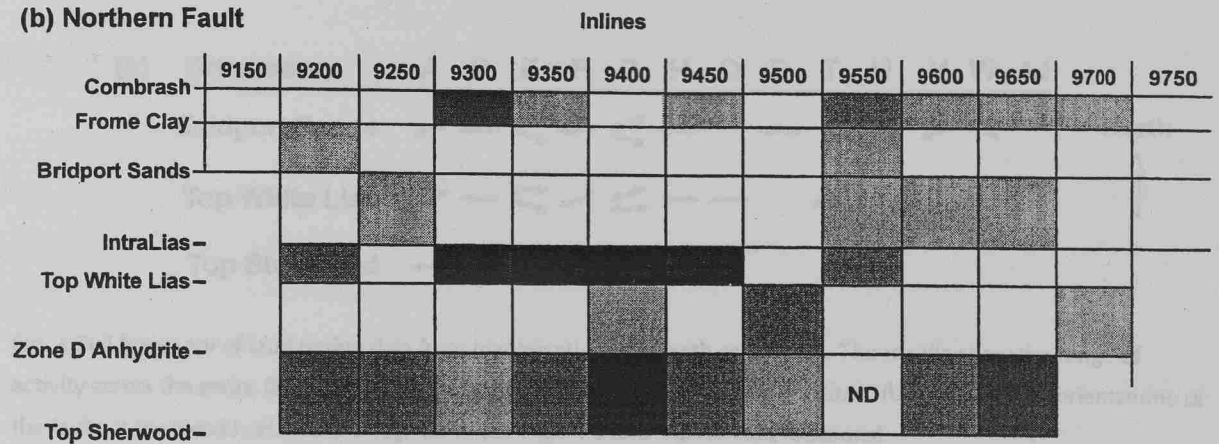
$$\%Extension = \frac{\sum h}{l_f - \sum h} \quad \text{Equation 3.1}$$

To investigate the contribution of a range of displacement magnitudes to the overall extension, strain was calculated separately for faults with heaves \geq cut-offs of 100, 10 and 1 m for each horizon. The strain was also calculated for the faults divided into groups based on the identification of growth faulting. All faults with > 5 m displacement (*i.e.* seismic resolution) were included in the analysis, and heaves were accurate to ± 5 m. The method assumes that the horizons are horizontal.

(a) Wytch Farm Fault



(b) Northern Fault



(c) Arne Fault

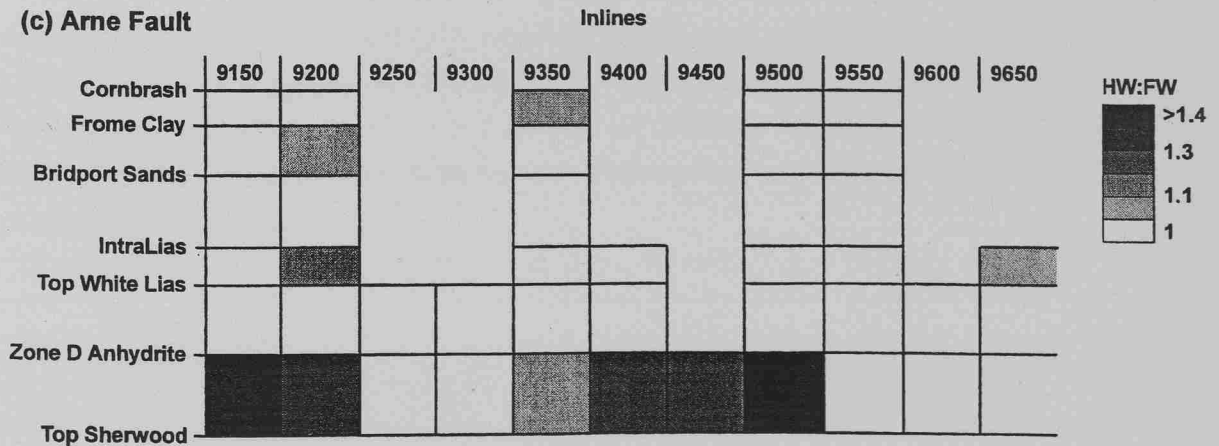


Fig. 4.6. The timing of growth faulting derived from the ratio of the hanging-wall unit thickness to the footwall unit thickness measured parallel and adjacent to the fault plane. A value of > 1 indicates a thicker hanging-wall sequence. An overestimation of the hanging-wall thickness would result from a vertical measure of rotated beds and hence overstate the extent of growth faulting. The interval thicknesses were calculated for only the interpreted horizons and not individual reflectors (inline interval = 50). A grey scale is used to indicate the size of the ratio. ND = No Data. (cf. Figs. 4.9 and 5.2 for fault locations).

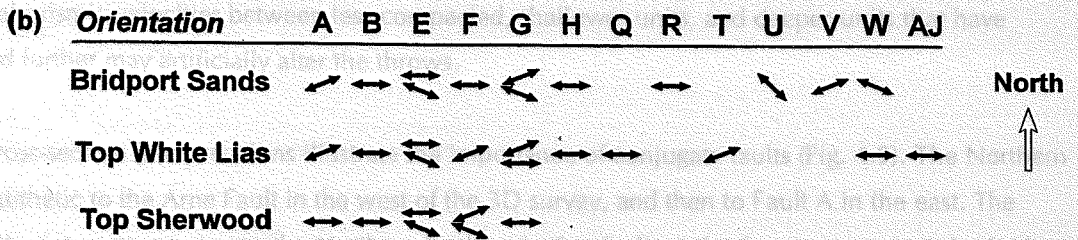
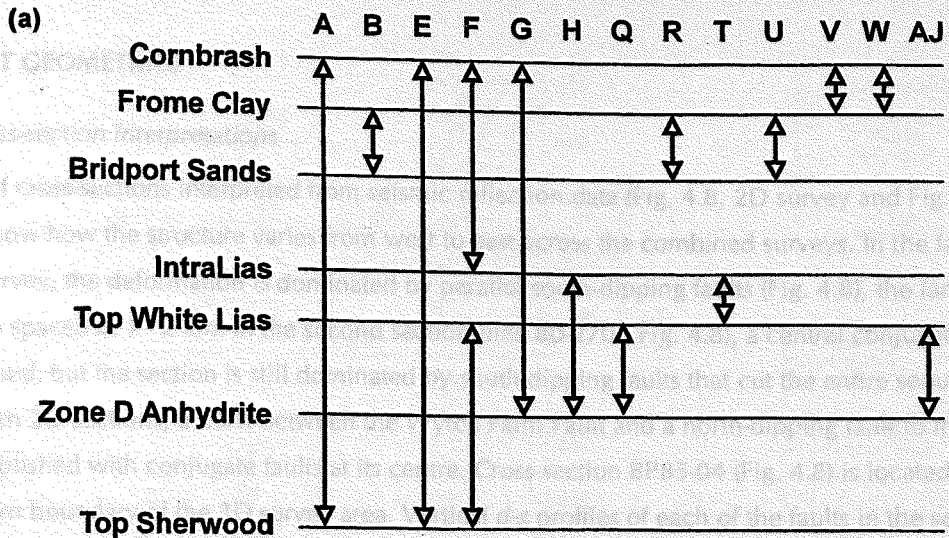


Fig. 4.7(a) Summary of fault timing data from identification of growth sequences. The results show the range of activity across the entire faults, so not every part of the fault moved at the same time. (b) Approximate orientations of the faults at the listed horizons (c.f. Fig. 4.14). (cf. Figs. 4.9 and 5.2 for fault locations).

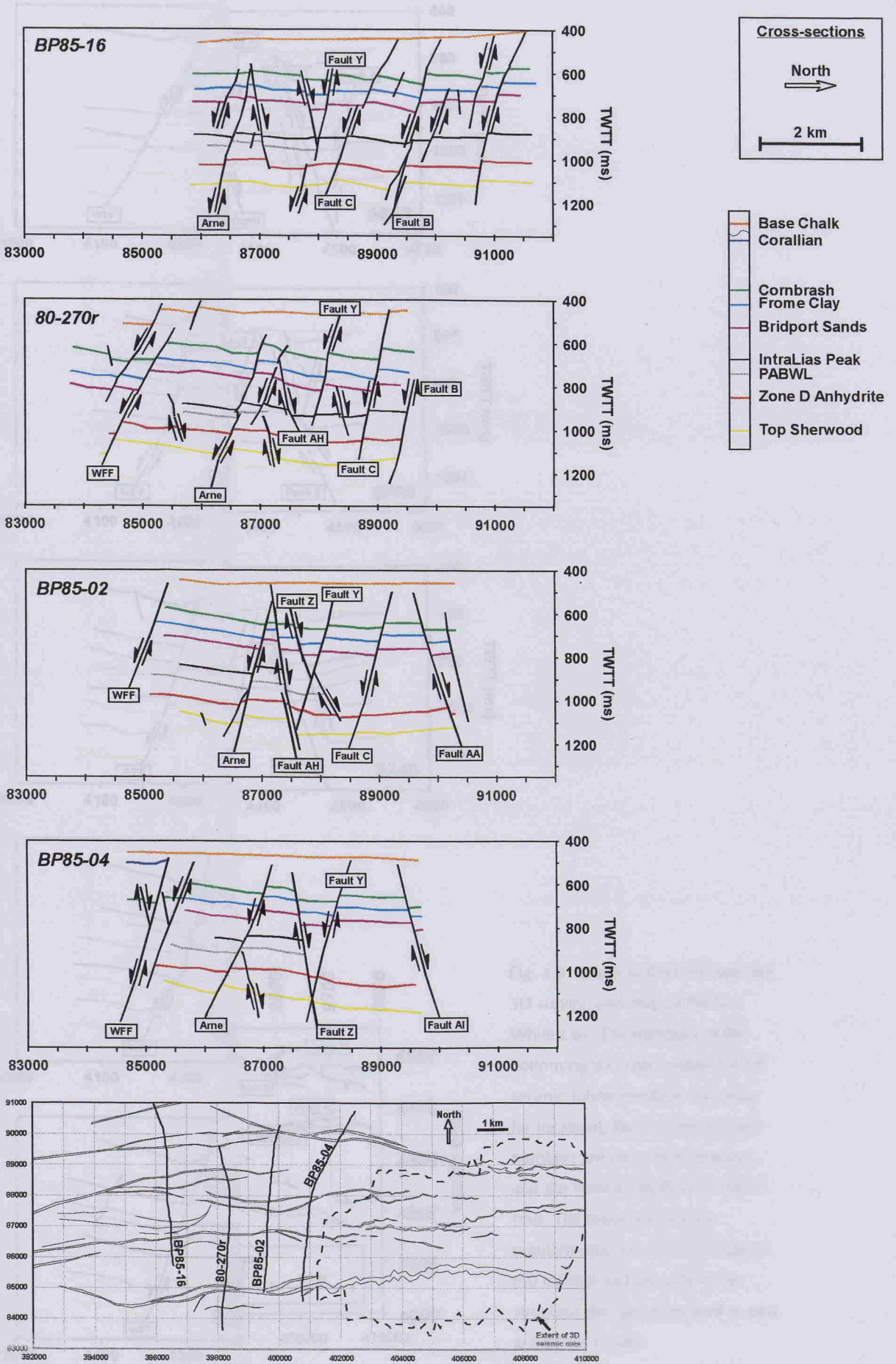
4.4 FAULT GEOMETRIES

4.4.1 Cross-section interpretations

A series of cross-sections interpreted from seismic reflection data (Fig. 4.8, 2D survey and Fig. 4.9, 3D survey) show how the structure varies from west to east across the combined surveys. In the far west of the 2D survey, the deformation is dominated by parallel south-dipping faults (Fig. 4.8), the largest of which are spaced at 1 - 2 km. In the second section (line 80-270r, Fig. 4.8), a central conjugate structure is developed, but the section is still dominated by south-dipping faults that cut the entire sequence. In the two eastern 2D sections, a horst between the Wytch Farm Fault and a north-dipping fault to the north has been established with conjugate faults at its centre. Cross-section BP85-04 (Fig. 4.8) is located adjacent to the western boundary of the 3D survey area. Vertical *d-x* profiles of each of the faults in the seismic interpretations show that the greatest combined throws occur in the shallower horizons (Fig. 4.10). Differential seismic velocities between less compacted, shallower units, and deeper units that have compacted further may artificially alter the throws.

The 3D cross-section interpretations illustrate the importance of conjugate faults (Fig. 4.9). The Northern Fault is antithetic to the Arne Fault in the west of the 3D survey, and then to Fault A in the east. The nature of the interaction between the Northern Fault and other faults varies from west to east. In the far west (inline 9150), the Northern Fault is a relatively minor antithetic fault to the more dominant Arne Fault, but increases in height and displacement eastwards at the expense of the Arne Fault (inlines 9250 to 9400). Although segmented, the two faults have similar heights and displacement magnitudes in the centre of the survey (inlines 9450 to 9550), and intersect with a geometry complicated by oversteps (inline 9500, Fig. 4.9). The fault geometries are simplest when one of the pair dominates the other (e.g. inline 9350, Fig. 4.9). The Northern Fault continues eastwards with a similar height and displacement, but the Arne Fault is restricted to the Triassic (inline 9600). In the final sections (inlines 9650 to 9750, Fig. 4.9) the Northern Fault is antithetic to Fault A, which dominates the conjugate set, and is in turn antithetic to Fault E (inlines 9700 to 9750, Fig. 4.9). There is, therefore, a shift northwards of a central pair of conjugate faults from west to east.

Fig. 4.8. (overleaf) Seismic cross-sections taken from the 2D survey area. The horizontal scale refers to the National Grid, and the vertical depth is in TWTT (ms). The sections (top to bottom = west to east) show how the fault system changes from one dominated by parallel, south-dipping faults to one dominated by a central conjugate fault structure. The numbers in the top left corners refer to the name of the seismic line. The seismic lines are located onto a combined 2D and 3D area map of the Top White Lias faults.



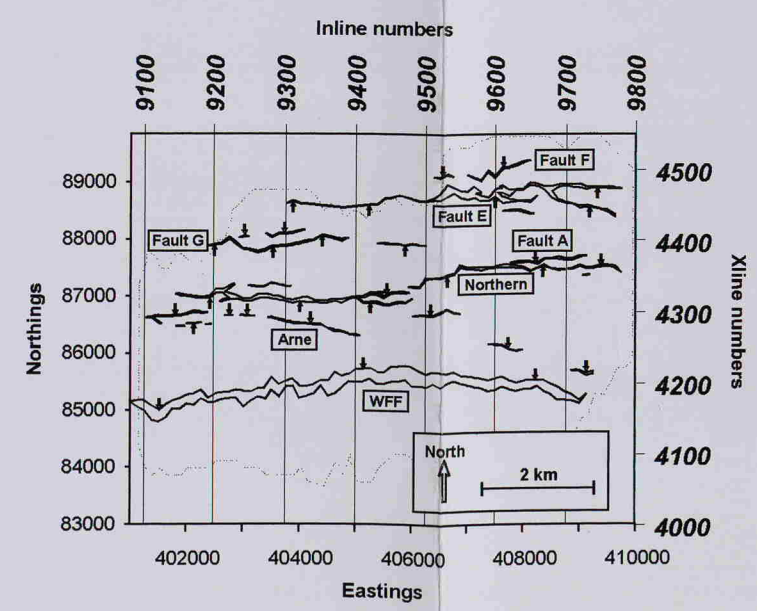
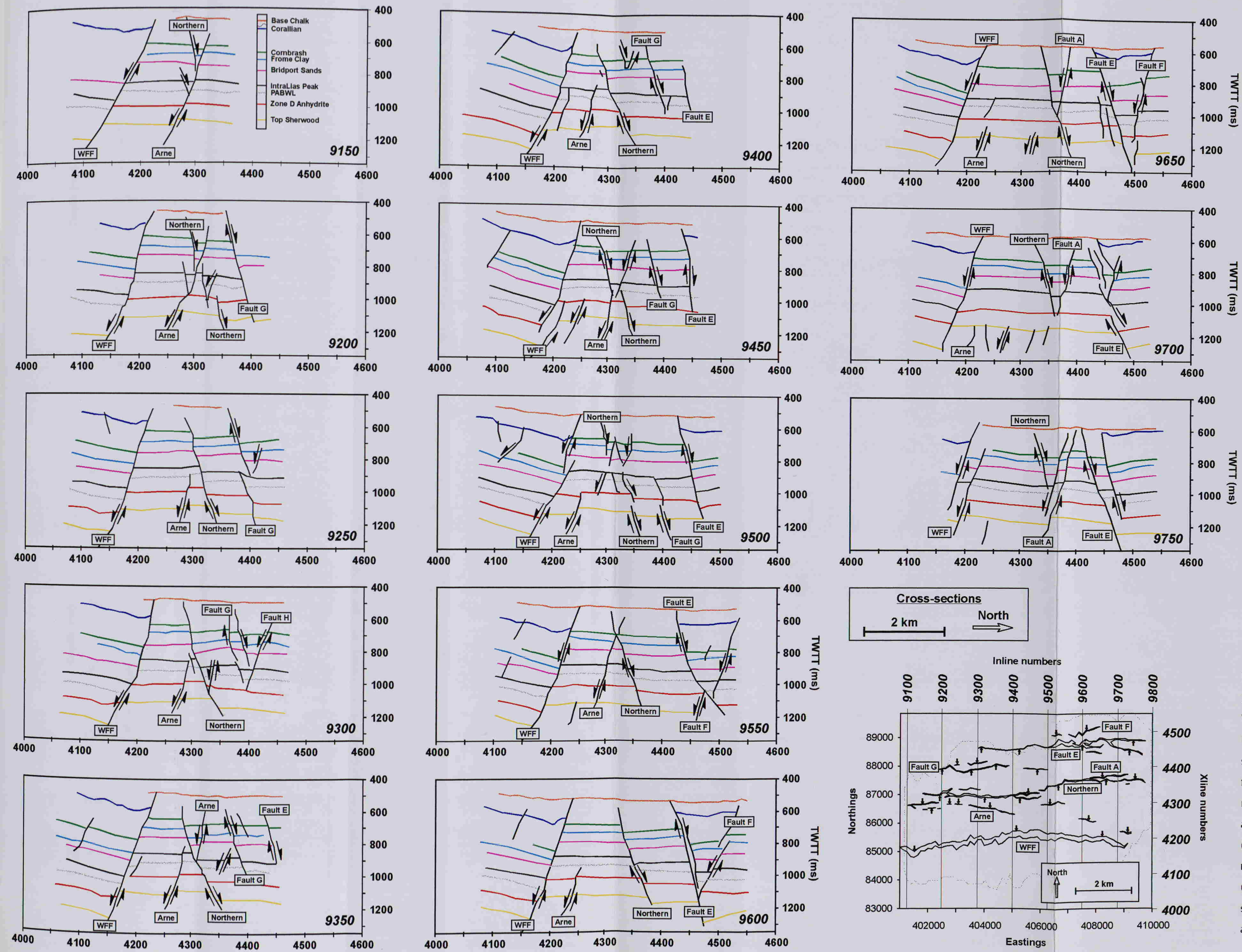


Fig. 4.9. Cross-sections through the 3D survey, and map of the Top White Lias. The numbers in the bottom right corners represent the seismic inline numbers (see map for location), the horizontal scale numbers are cross-line numbers, and the vertical depth is in TWTT (ms). The cross-sections are regularly spaced every 625 metres (50 inlines) and show how the structure changes from west to east across the survey.

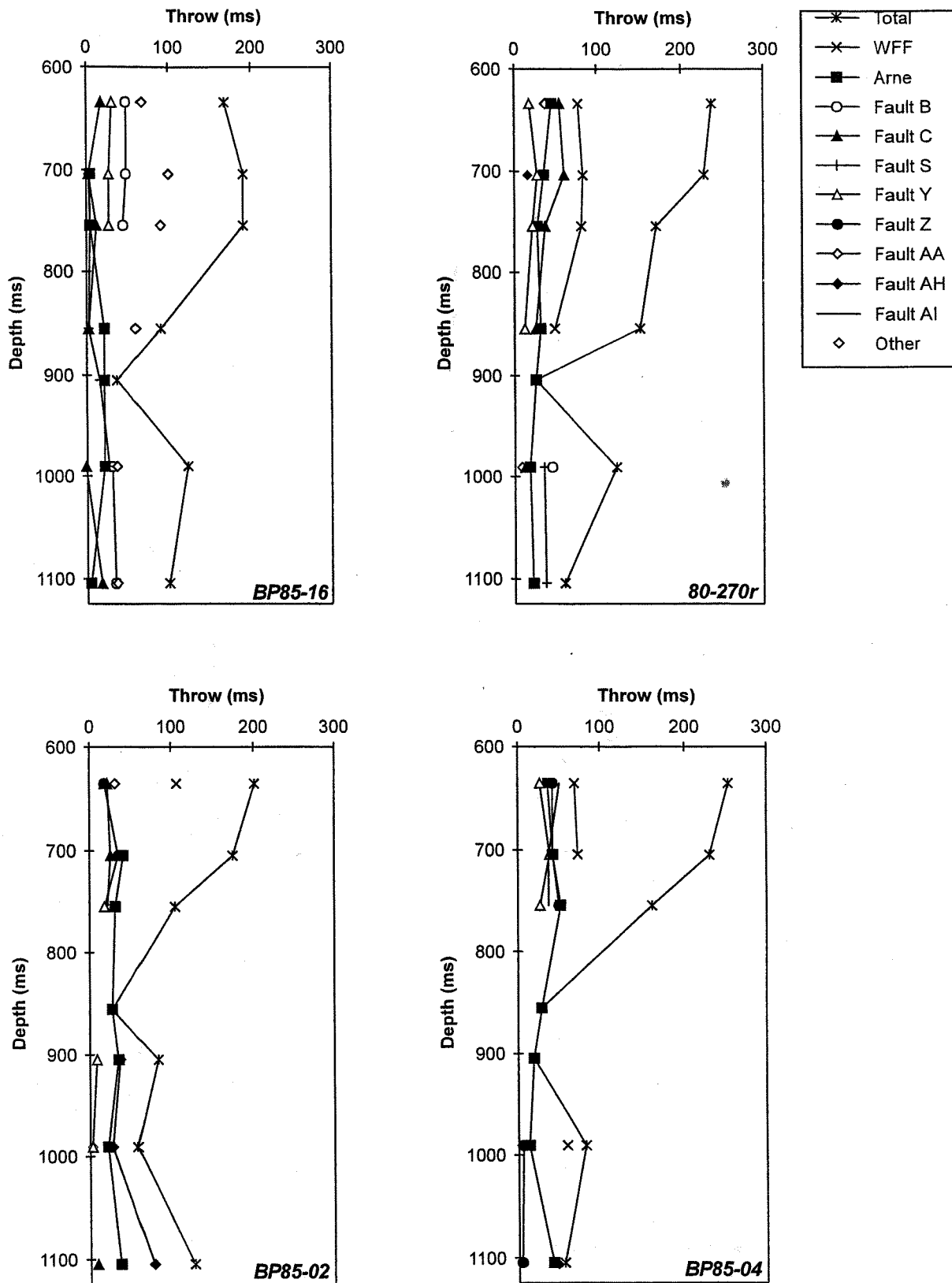
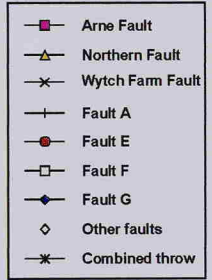
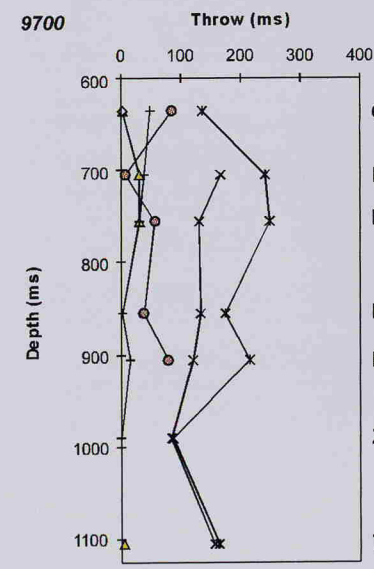
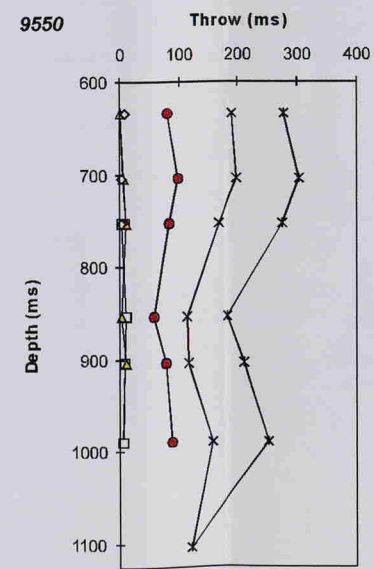
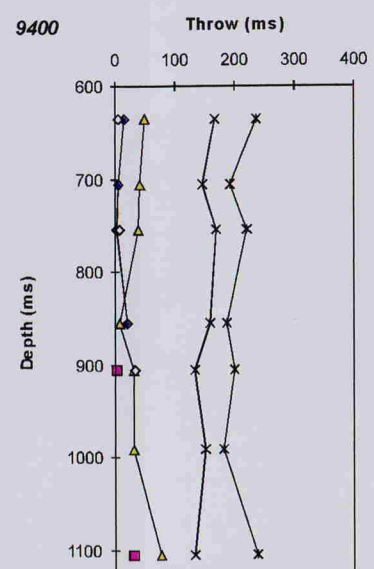
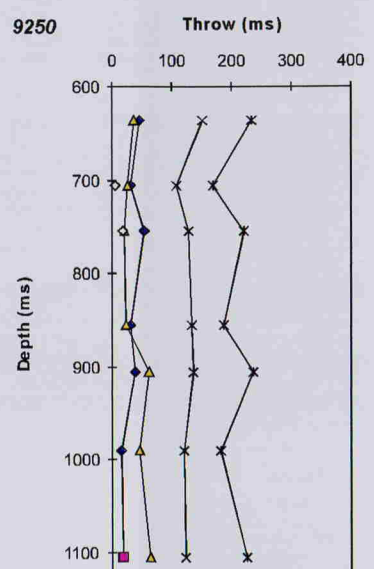
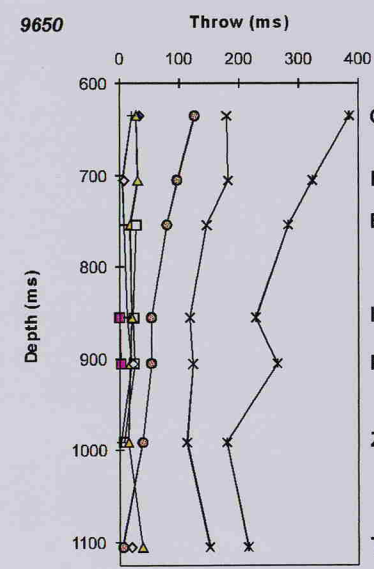
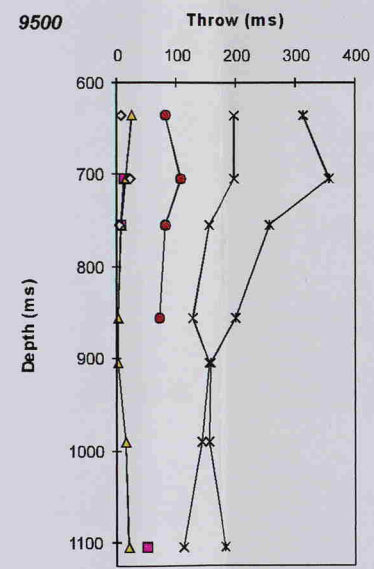
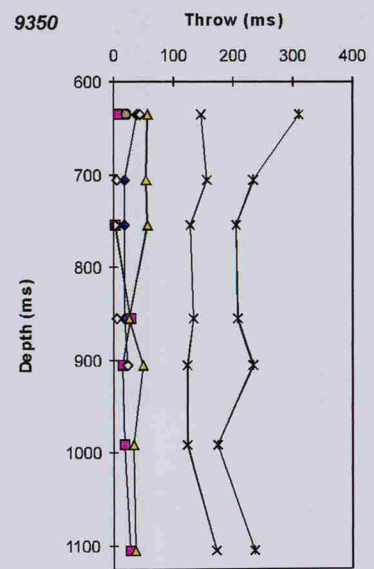
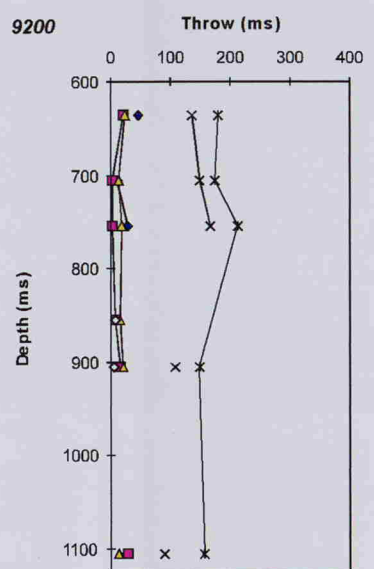
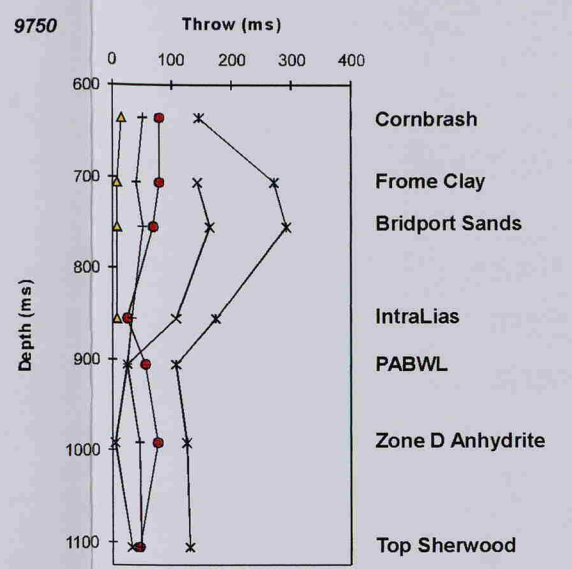
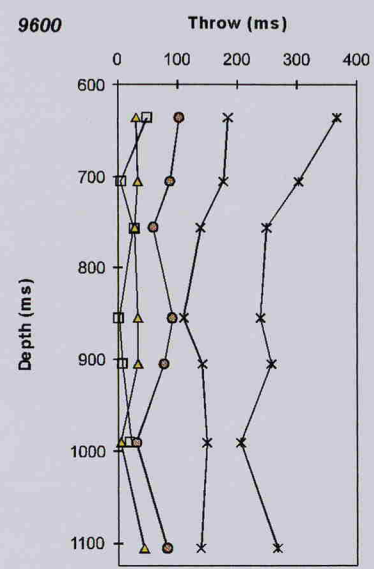
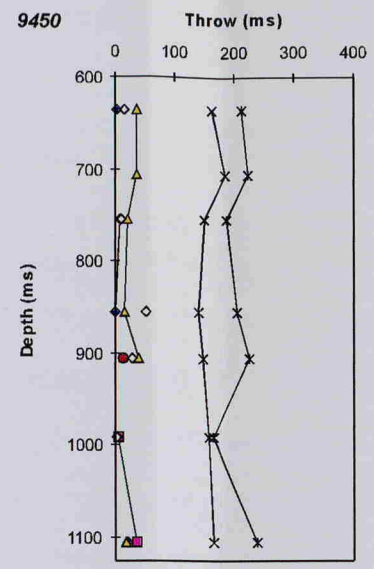
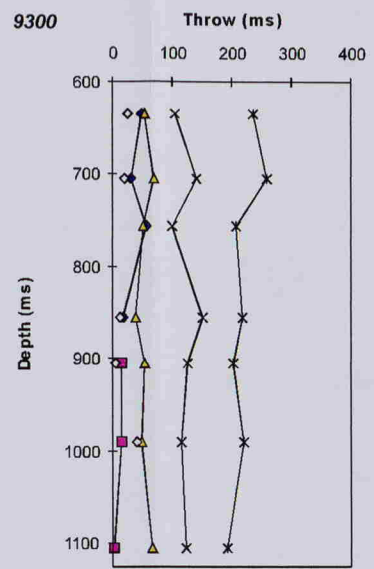
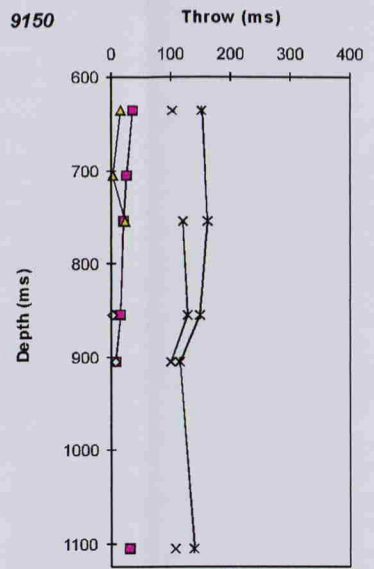


Fig. 4.10. Vertical $d-x$ profiles for the 2D seismic interpretations illustrated in Fig. 4.8. The throw minima for the Top White Lias and the IntraLias are an interpretation artefact, as these horizons were not identifiable in every section. Additionally, survey resolution decreases with depth, so there is less confidence in the results for the Triassic units.



Cornbrash
Frome Clay
Bridport Sands
IntraLias
PABWL
Zone D Anhydrite
Top Sherwood

Cornbrash
Frome Clay
Bridport Sands
IntraLias
PABWL
Zone D Anhydrite
Top Sherwood

Cornbrash
Frome Clay
Bridport Sands
IntraLias
PABWL
Zone D Anhydrite
Top Sherwood

Fig. 4.11. Vertical d-x profiles for each of the inlines in Fig. 4.9. There is an overall increase in throw from the deepest to the shallowest units, which reflects the greater fault densities in the Jurassic sequence.

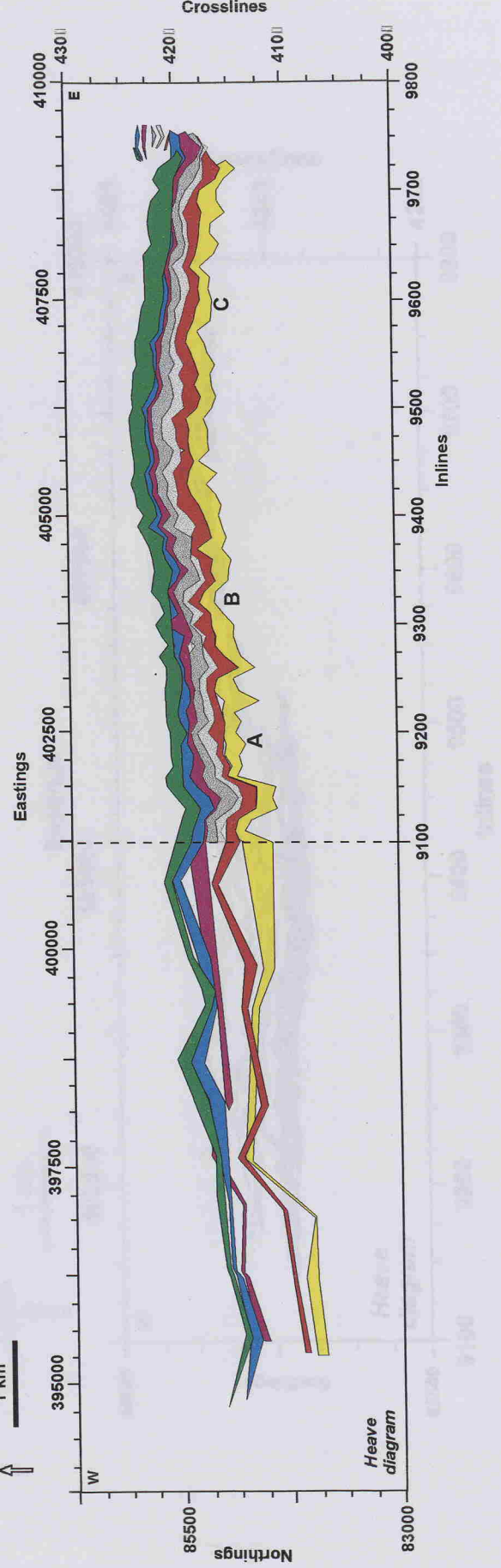
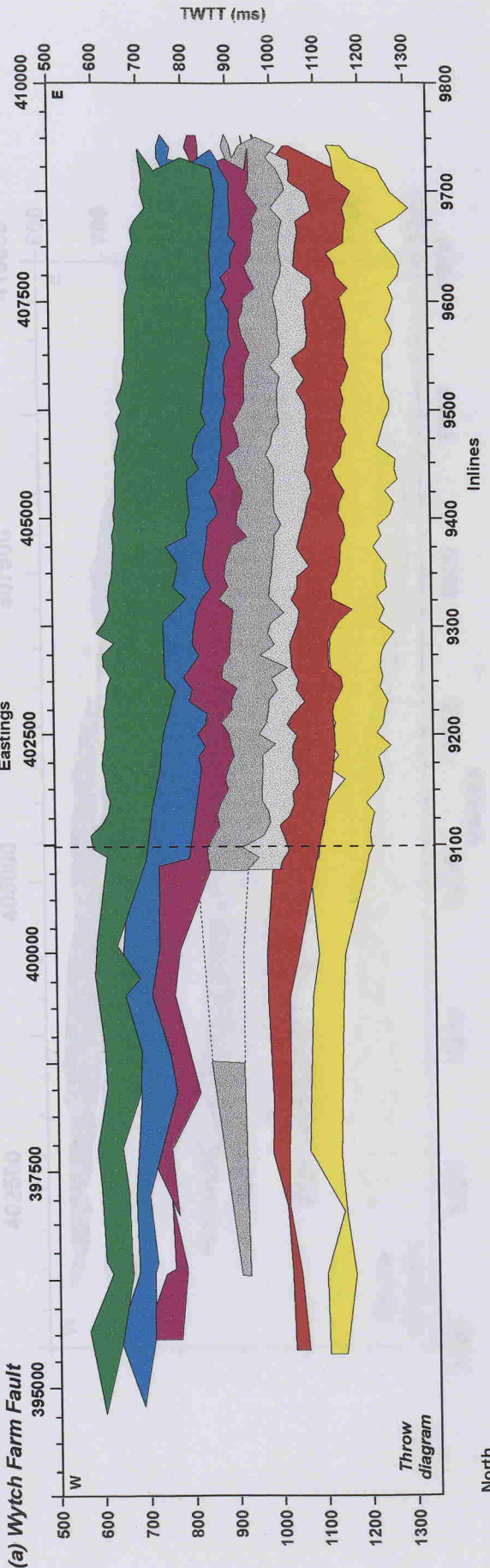
Vertical d - x profiles have been used to illustrate the variation in fault throw across the survey area (Fig. 4.11); fault throws are often lowest at the Zone D Anhydrite and IntraLias units. Zig-zag d - x profiles are symptomatic of interpretation errors, or faults within sediments that have experienced differential compaction, particularly post-deposition of syn-rift sequences (Wang, 1995). Fault planes shallow during compaction (Davison, 1987), so faults in the most compacted layers, that pre-date the compaction, would have the shallowest dips (Wang, 1995). Faults in this study are mainly sub-planar, and the displacement minima do not occur at obvious bends (Fig. 4.9). Either the faults must post-date the compaction, or the sediments compacted uniformly to form sub-planar faults.

There is little variation in total throw from the Cornbrash to the Top Sherwood for the inlines 9150 to 9450 (with the exception of 9350), but throws increase dramatically up-section for inlines 9500 to 9750. Although some of the throw increase may be attributed to the inclusion of Fault E, other faults do have increased displacements in the shallower units, e.g. Fault A, the Northern Fault and the Wytch Farm Fault (Fig. 4.11).

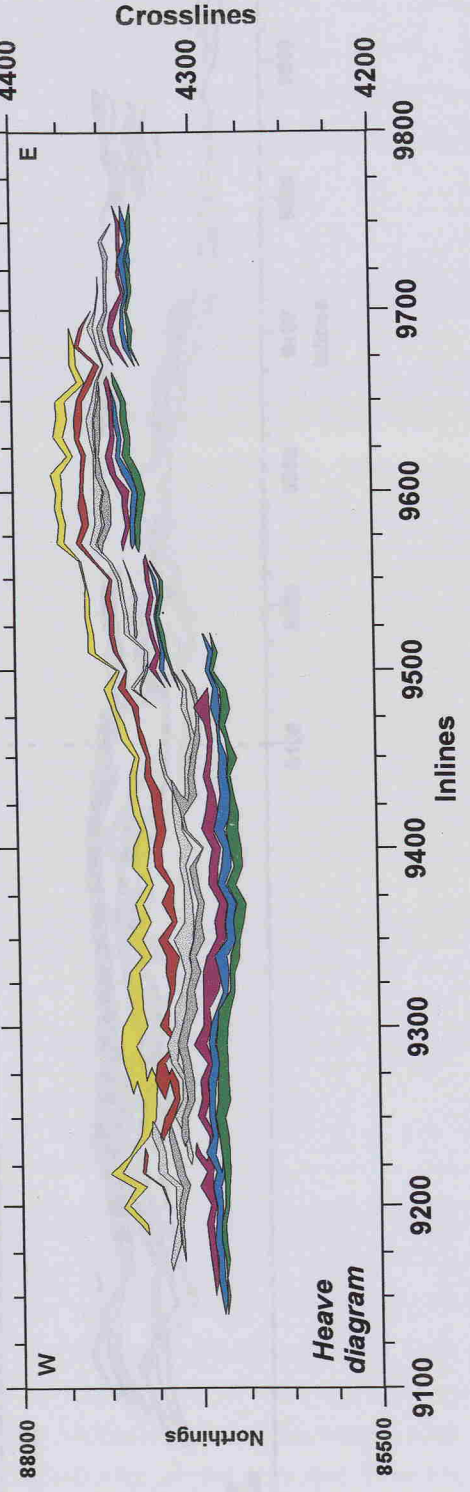
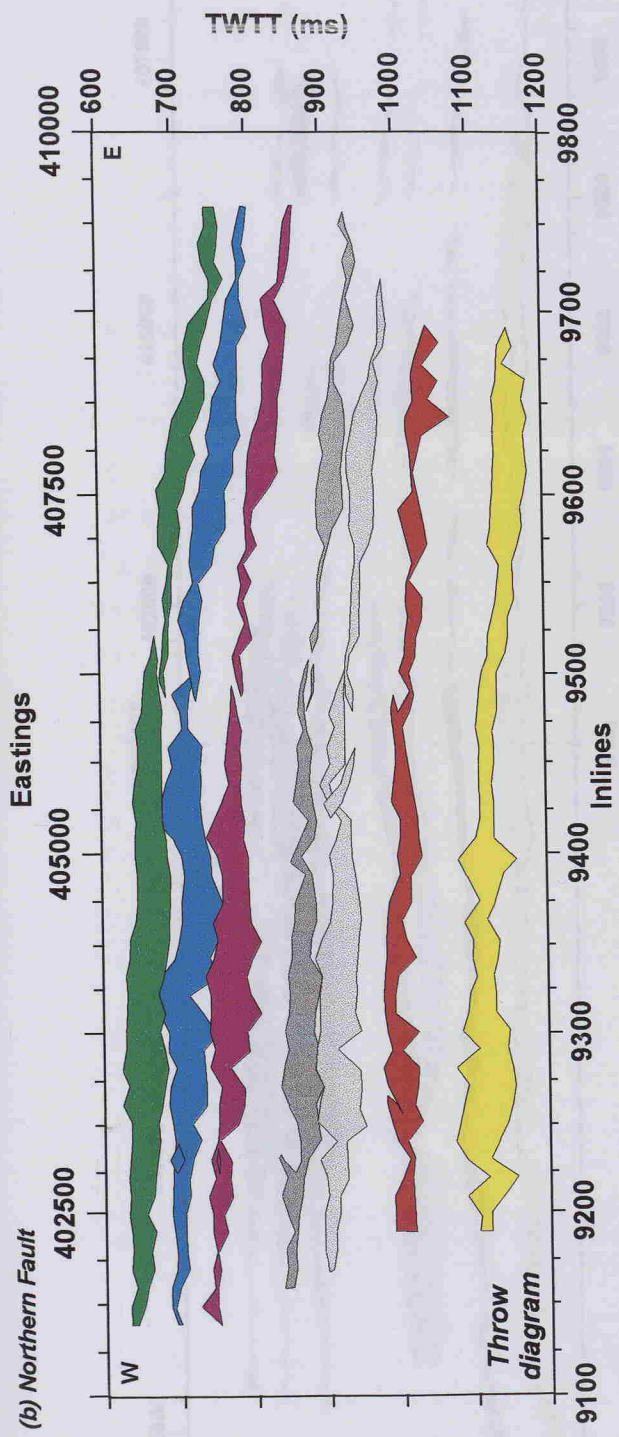
4.4.2 Fault interpretations

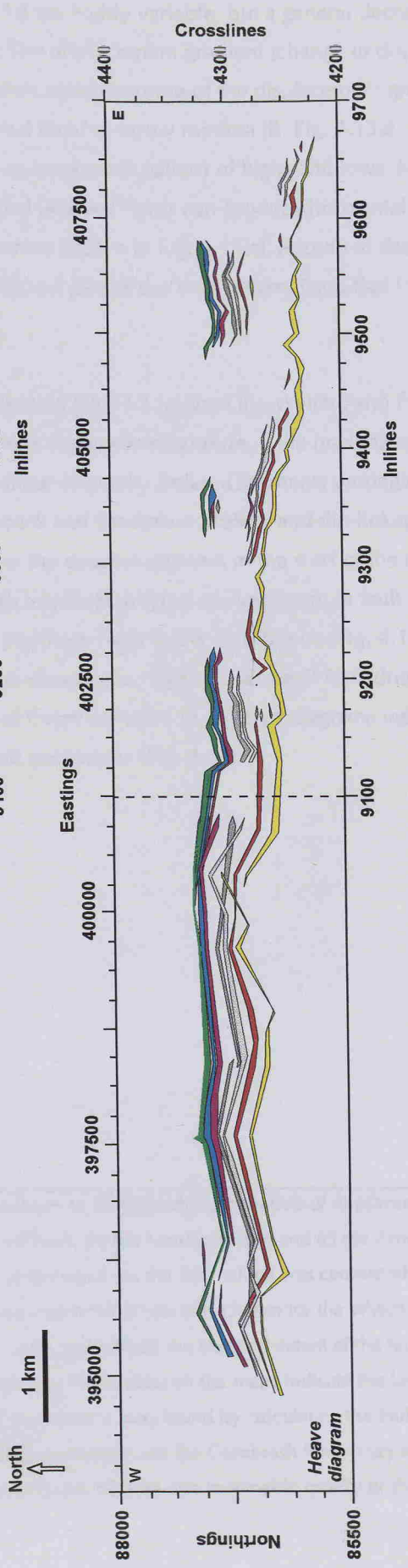
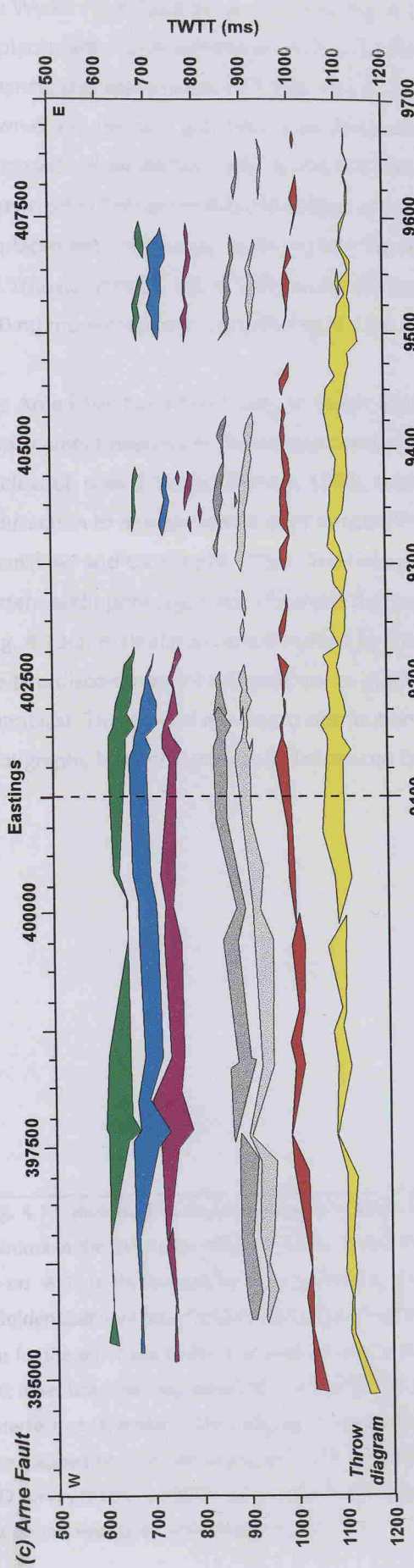
The displacement characteristics of three principal faults (Wytch Farm, Northern and Arne Faults) have been analysed in detail, with fault throw diagrams to illustrate footwall and hanging-wall intersections with the fault surface (Allan, 1989). The Wytch Farm and Northern Faults were chosen because they are the main reservoir boundary faults; the Arne Fault has reservoir rocks in both its hanging-wall and footwall. The fault throw maps are shown with fault heave diagrams (*i.e.* fault/horizon intersections) to compare vertical and horizontal fault geometries (Fig. 4.12), and throw distribution contour maps (Fig. 4.13). A simple elliptical fault trace with a central throw maximum (which approximates to the nucleation site, Ellis and Dunlap, 1988), as described by Barnett *et al.* (1987) for a single, isolated normal fault, is not evident on any of the maps (Fig. 4.13). That model is not realistic for the faults at Wytch Farm, as the multiple throw maxima and minima suggest that the faults formed through the segment amalgamation (Fig. 4.13).

Fig. 4.12. (following three pages) Heave and throw diagrams for (a) the Wytch Farm Fault, (b) the Northern Fault and (c) the Arne Fault. The hanging-wall and footwall cut-offs are shown for each of the horizons illustrated in the cross-sections (Fig. 4.8 and 4.9), with the exception of the Corallian, due to insufficient data, and the Chalk, which is mostly unfaulted.



(b) Northern Fault





The Wytch Farm Fault throw contours (Fig. 4.13a) are highly variable, but a general decrease in displacement occurs westwards (A, Fig. 4.13a). The displacement gradient (change in displacement over distance) decreases westwards (Fig. 4.13a). A more rapid decrease of the displacement gradient occurs down-dip in the east, and there is a sub-horizontal band of throw minima (B, Fig. 4.13a). The throw is increased below the horizontal band, but with an incoherent pattern of highs and lows. Mansfield and Cartwright (1996) show that dip linkage of normal fault segments can produce horizontal bands of low displacement, which may partly explain the contour pattern in Fig. 4.13(a). A zone of decreased throw in the Triassic units (C, Fig. 4.13a) can be attributed to a part of the Wytch Farm Fault that forms a short (c. 500 m) more-southerly segment (Fig. 4.12a).

The Arne Fault has a much simpler throw distribution (Fig. 4.13c) than the Wytch Farm Fault, with two displacement maxima in the deepest units and one shallower maximum. If the maxima represent nucleation sites (Ellis and Dunlap, 1988), then three originally isolated segments propagated towards intersection to amalgamate at relay ramps (Peacock and Sanderson, 1991), and dip-linkage sites (Mansfield and Cartwright, 1996). The linkage of the deepest segment in the west of the map, to the eastern and upper segments, illustrates that both intersection types are important to fault development (Fig. 4.13c). A similar pattern is formed by the Northern Fault throw distribution (Fig. 4.13b), but there are two discontinuous horizontal zones of lower throws at c. 1000 ms (Zone D Anhydrite) and c. 850 ms (IntraLias). The general non-linear distribution of throw contours in all three diagrams indicates that the stratigraphy has not significantly influenced fault geometries (Fig. 4.13).

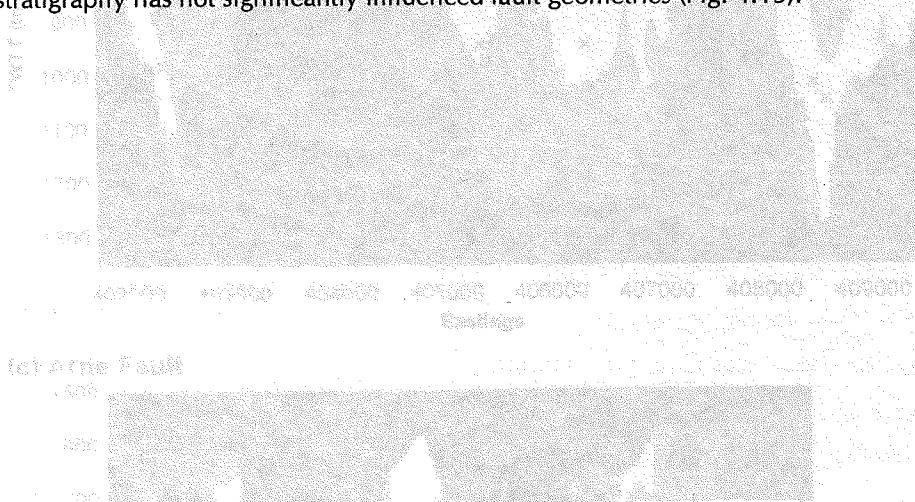
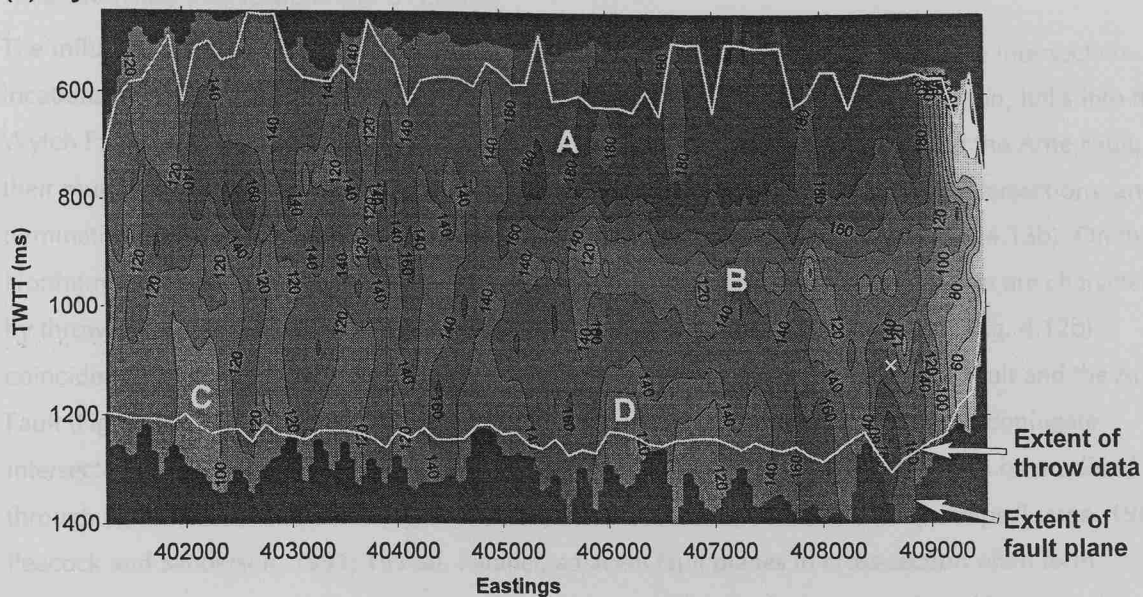
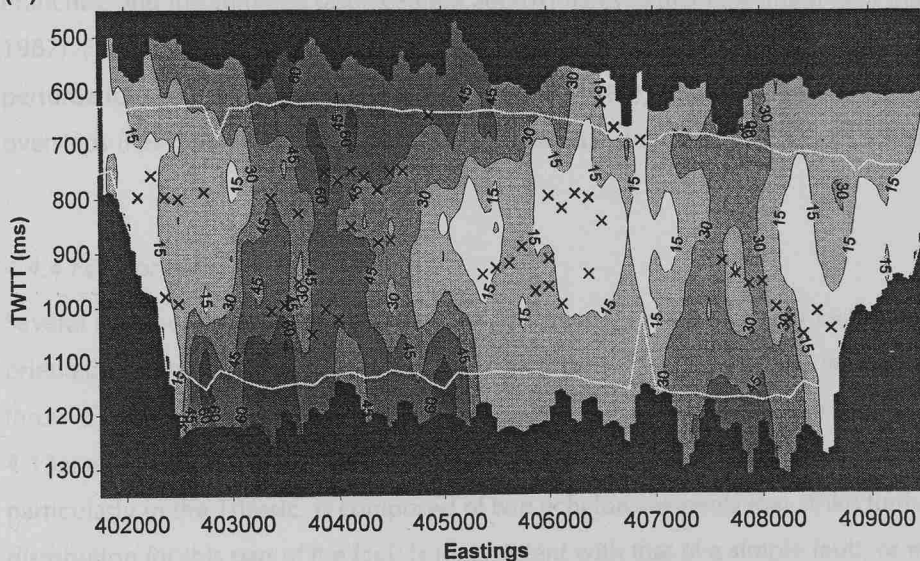


Fig. 4.13. (overleaf) Fault plane maps with throw contours to illustrate the distribution of displacement maxima and minima in the 3D survey area, for (a) the Wytch Farm Fault, (b) the Northern Fault and (c) the Arne Fault. Fault throw in ms. A 50 m (horizontal) by 5 ms (vertical) grid was derived from the data which was contoured using *Surfer32* (Golden Software Inc., Golden, Colorado). A contour interval of 20 ms was chosen for the Wytch Farm Fault, and 10 ms for the other two faults. The outer boundary for each map reflects the mapped extent of the fault plane itself, and the inner boundary represents the limit of the throw data. The crosses on the maps indicate the location of an intersecting fault plane. The data used in the maps' construction was found by calculating the fault throw (in ms) for the mapped horizons between, and including, the Top Sherwood and the Cornbrash from every tenth inline in the 3D survey (9100 to 9800). The contour maps cover only the 3D area due to variable quality of the 2D seismic data, its poorer resolution and greater spacing.

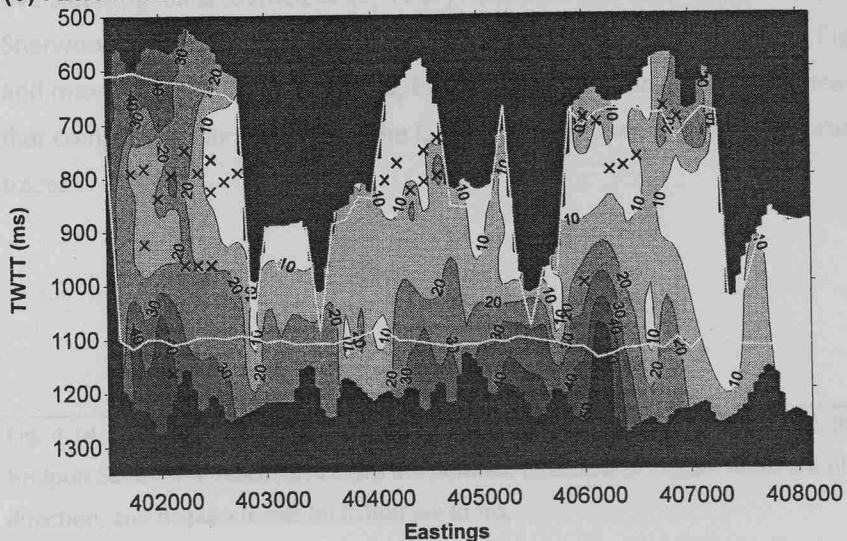
(a) Wyitch Farm Fault



(b) Northern Fault



(c) Arne Fault



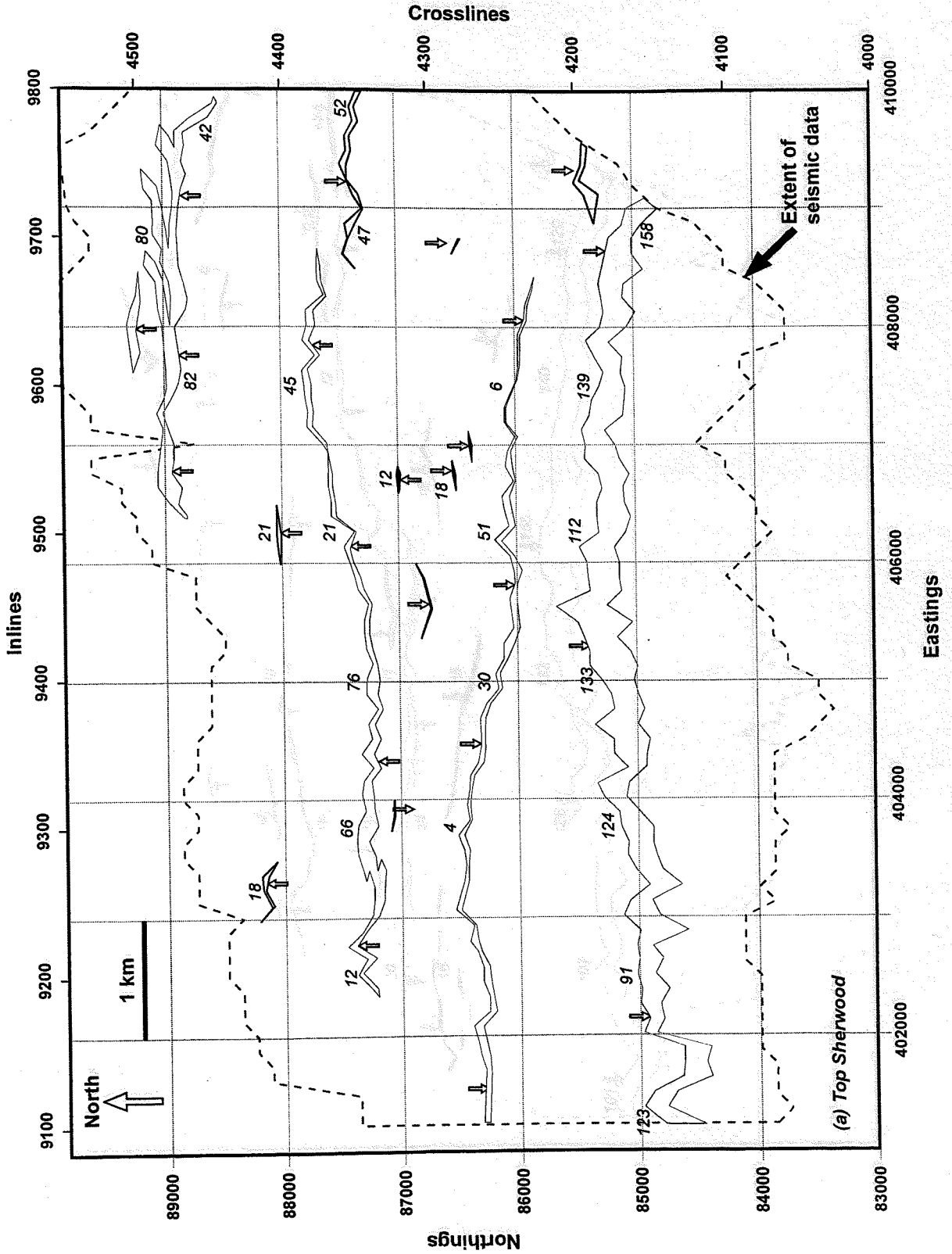
4.4.3 Branches, intersections and oversteps

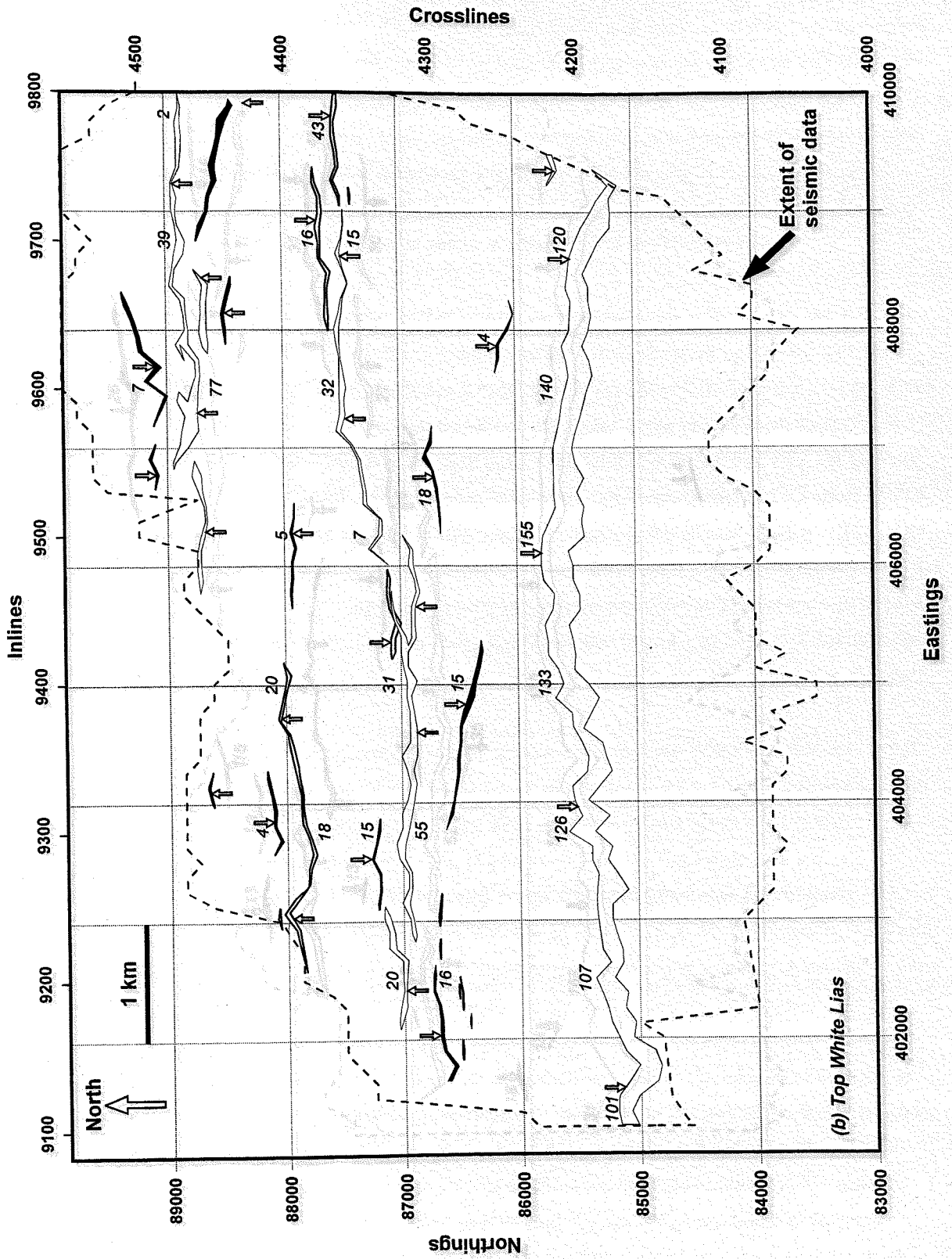
The influence of intersections with antithetic faults has been determined by plotting the intersection locations onto the contour maps (Fig. 4.13). Only one fault, above the seismic resolution, links into the Wytch Farm Fault, but the intersection of antithetic faults with the Northern Fault and the Arne Fault, and their mutual intersection, occurs regularly throughout the survey (*c.f.* Fig. 4.9). Fault intersections (and terminations at other faults) influence the throw distribution of the Northern Fault (Fig. 4.13b). On the Northern Fault, zones of maximum throw are sited either side of intersection points that are characterised by throw minima (Fig. 4.13b). The decreased throw between inlines 9400 and 9550 (Fig. 4.12b) coincides with an increase in complexity of the conjugate geometry of the Northern Fault and the Arne Fault (Fig. 4.9). The Wytch Farm Fault throw increases immediately to the south of the conjugate intersection zone at the Top White Lias and Bridport Sands levels. Fault geometries can be modified through the influence of intersecting antithetic faults (Nicol *et al.*, 1995) and relay ramps (Larsen, 1988; Peacock and Sanderson, 1991; 1994a). Parallel, adjacent fault planes in cross-section often form branches that are connected in map view (e.g. Fig. 4.14a). The displacement is shared between the branches, and the summed displacement approximates to that of a single fault plane (Barnett *et al.*, 1987). Fault throws were summed in the cases of fault branches, and should not therefore produce major perturbations in the contour pattern (Barnett *et al.*, 1987), although displacement minima occur at fault oversteps (Peacock and Sanderson, 1991; 1994a; Mansfield and Cartwright, 1996).

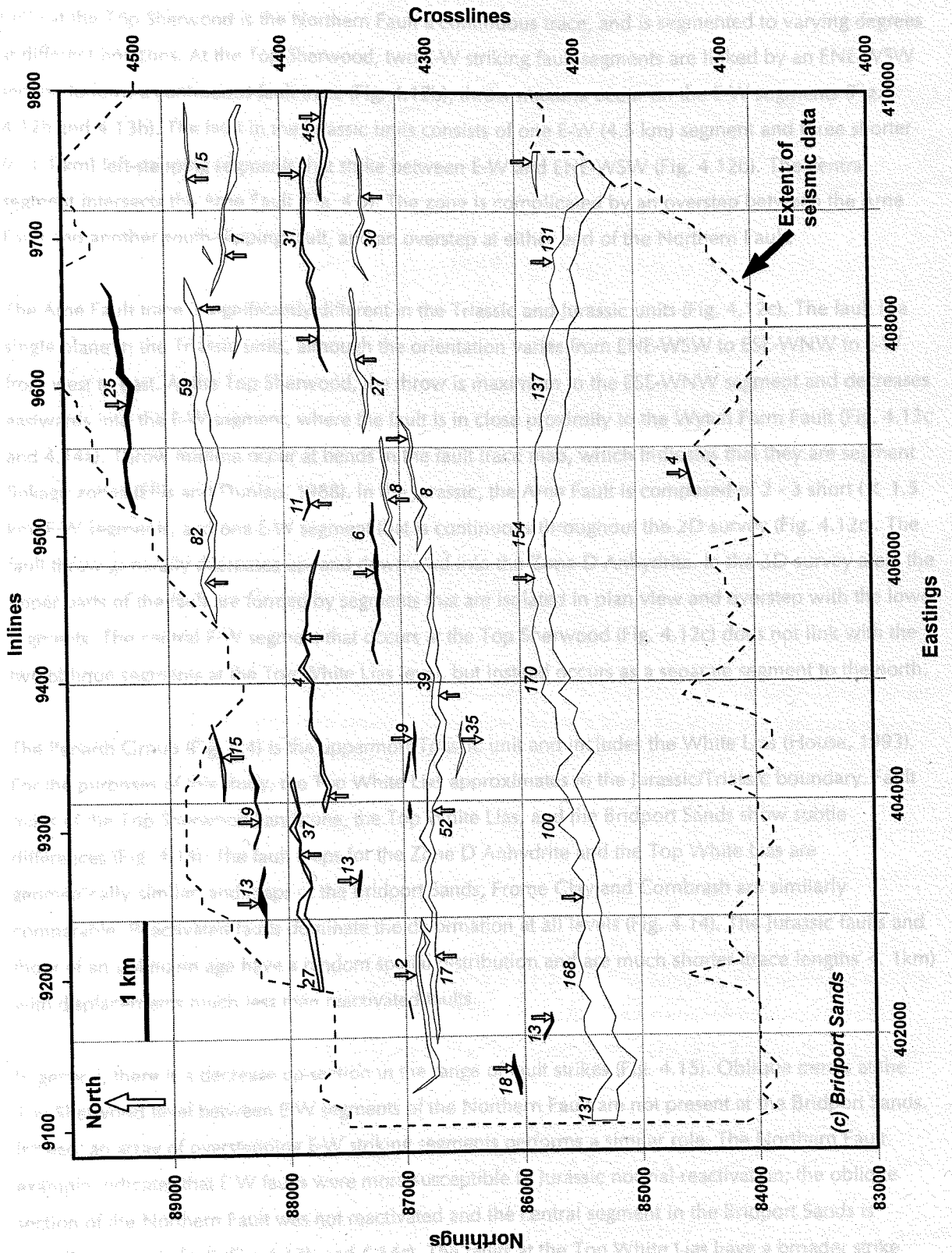
4.4.4 Fault orientations

Several of the undulations in throw can be attributed to orientation. For example, a change in overall orientation from E-W to ENE-WSW of the Wytch Farm Fault (Fig. 4.12a) is accompanied by a decrease in throw (Fig. 4.13a). The largest throws and sub-concentric contours in the Middle Jurassic units (A, Fig. 4.13a) are found at the E-W fault segment. Farther west, the fault has a general ENE-WSW strike and, particularly in the Triassic, is composed of two echelon segments that strike further NE. The throw distribution for this part of the fault is inconsistent with that of a simple fault, or even a set of overstepping faults (Barnett *et al.*, 1987; Mansfield and Cartwright, 1996). Throw minima at the Top Sherwood are associated with ENE-WSW orientated segments (A and B, Fig. 4.12a; C and D, Fig. 4.13a), and maxima with E-W segments (C, Fig. 4.12a). The Wytch Farm Fault heave diagram (Fig. 4.12a) shows that complexities in the strike of the fault at the Top Sherwood are less pronounced in the Jurassic fault traces.

Fig. 4.14. (following three pages) Structural interpretations for (a) Top Sherwood, (b) the Top White Lias, and (c) the Bridport Sands. The reactivated faults are unfilled; Jurassic and Triassic faults are filled. The arrows indicate fault dip direction, and displacements (in italics) are in ms.







Only at the Top Sherwood is the Northern Fault a continuous trace, and is segmented to varying degrees at different horizons. At the Top Sherwood, two E-W striking fault segments are linked by an ENE-WSW section to form a continuous fault trace (Fig. 4.12b); throw maxima occur on the E-W segments (Fig. 4.12b and 4.13b). The fault in the Jurassic units consists of one E-W (4.5 km) segment and three shorter (c. 1.1 km) left-stepping segments that strike between E-W and ENE-WSW (Fig. 4.12b). The central segment intersects the Arne Fault (Fig. 4.9). The zone is complicated by an overstep between the Arne Fault and another south-dipping fault, and an overstep at either end of the Northern Fault.

The Arne Fault trace is significantly different in the Triassic and Jurassic units (Fig. 4.12c). The fault is a single plane in the Triassic units, although the orientation varies from ENE-WSW to ESE-WNW to E-W from west to east. At the Top Sherwood, the throw is maximum in the ESE-WNW segment and decreases eastwards into the E-W segment, where the fault is in close proximity to the Wytch Farm Fault (Fig. 4.13c and 4.14a). Throw minima occur at bends in the fault trace map, which indicates that they are segment linkage zones (Ellis and Dunlap, 1988). In the Jurassic, the Arne Fault is composed of 2 - 3 short (< 1.5 km) E-W segments, and one E-W segment that is continuous throughout the 2D survey (Fig. 4.12c). The fault throw generally decreases up- and downward into the Zone D Anhydrite. In the 3D survey area, the upper parts of the fault are formed by segments that are isolated in plan view and overstep with the lower segments. The central E-W segment that occurs at the Top Sherwood (Fig. 4.12c) does not link with the two oblique segments at the Top White Lias level, but instead occurs as a separate segment to the north.

The Penarth Group (Fig. 4.4) is the uppermost Triassic unit and includes the White Lias (House, 1993). For the purposes of this study, the Top White Lias approximates to the Jurassic/Triassic boundary. Fault maps of the Top Sherwood Sandstone, the Top White Lias, and the Bridport Sands show subtle differences (Fig. 4.14). The fault maps for the Zone D Anhydrite and the Top White Lias are geometrically similar, and maps of the Bridport Sands, Frome Clay and Cornbrash are similarly comparable. Reactivated faults dominate the deformation at all levels (Fig. 4.14). The Jurassic faults and those of an unknown age have a random spatial distribution and are much shorter (trace lengths < 1km) with displacements much less than reactivated faults.

In general, there is a decrease up-section in the range of fault strikes (Fig. 4.15). Oblique trends at the Top Sherwood level between E-W segments of the Northern Fault are not present at the Bridport Sands. Instead, an array of overstepping E-W striking segments performs a similar role. The Northern Fault example indicates that E-W faults were more susceptible to Jurassic normal-reactivation; the oblique section of the Northern Fault was not reactivated and the central segment in the Bridport Sands is actually a Jurassic fault (Fig. 4.13b and 4.14c). The faults at the Top White Lias have a broader strike range than the Bridport Sands, but less than the Top Sherwood (Fig. 4.15). There is an increase in fault density from the Top Sherwood (Fig. 4.14a), through the Top White Lias (Fig. 4.14b) to the Bridport Sands (Fig. 4.14c), although this may be an artefact of a depth-dependent seismic resolution decrease.

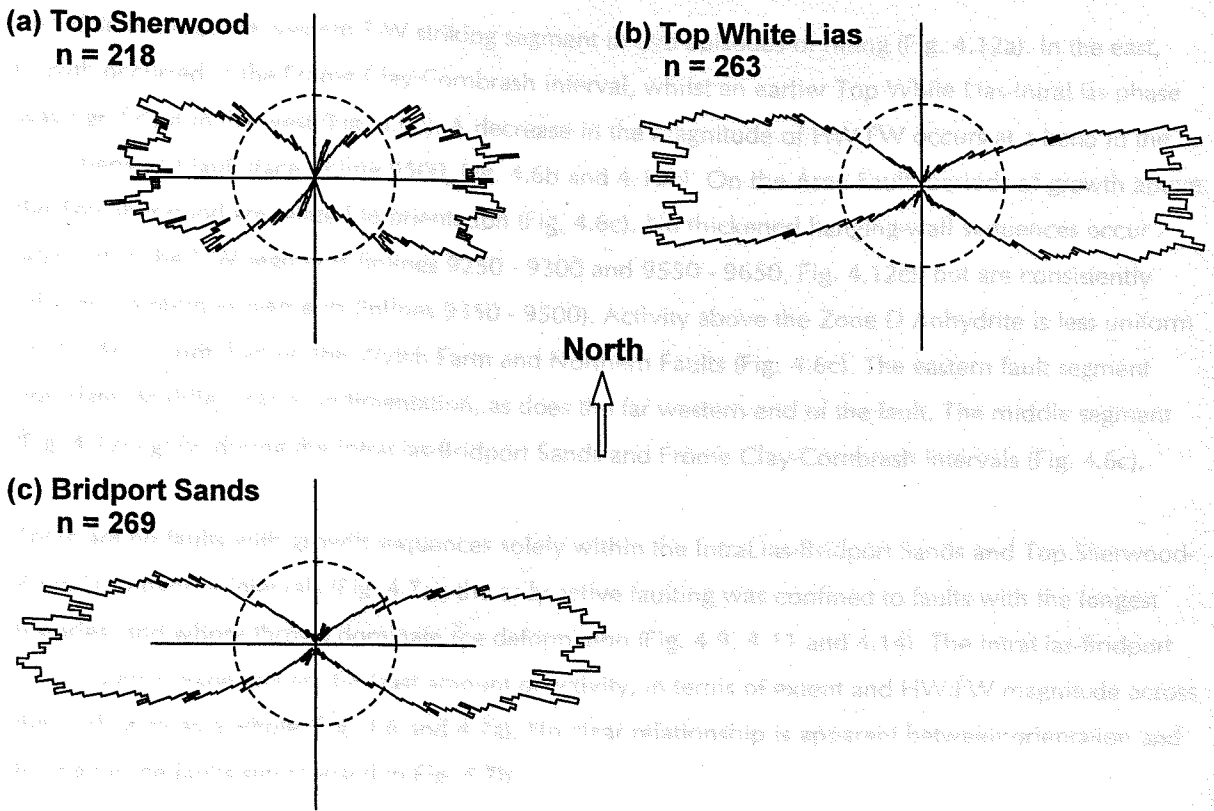


Fig. 4.15. Rose diagrams of fault strike for the (a) Top Sherwood, (b) Top White Lias and (c) Bridport Sands. The fault strike was measured in the interval between every tenth inline. The faults in the Top Sherwood have the greatest range of strikes, and those in the Bridport Sands have a tighter distribution centred on E-W.

4.4.5 Timing of movement

The present day forms of the faults are the result of displacement on several segments at various ages, and there was faulting in both the Triassic and the Jurassic (Fig. 4.6 and 4.7a). The Wytch Farm Fault plane has the a complex throw contour geometry (Fig. 4.13a), and a complicated history (Fig. 4.6a). The concentration of growth faulting between inlines 9400 and 9650, that crosses the Jurassic-Triassic boundary, coincides with the central E-W segment of the Wytch Farm Fault (Fig. 4.12a). The horizontal zone of minimum throw (B, Fig. 4.13a) occurs at the top of the growth sequence and, by definition, maximum displacements occur at the base of thickened hanging-wall sequences with minimum displacements at the top. There is a contrast between the timing of faulting from east to west. In the west (inlines 9400 - 9750) there are two separate periods of growth; the main period occurred in the upper zones of the Mercia Mudstone and the Lower Lias (Fig. 4.6a). In the east (inlines 9150 - 9350), the age of 2 - 3 periods of growth faulting are less consistent. The decrease eastwards of the HW:FW coincides with lower throws (Fig. 4.13a and 4.6a), and with the ENE-WSW strike of the Wytch Farm Fault (Fig. 4.12a).

Three phases of growth faulting are evident on the Northern Fault, with a constant occurrence in the Top Sherwood-Zone D Anhydrite interval (Fig. 4.6b). In the Middle Jurassic, the latest movements in the east

post-date those of the western E-W striking segment in two episodes of rifting (Fig. 4.12a). In the east, growth occurred in the Frome Clay-Cornbrash interval, whilst an earlier Top White Lias-IntraLias phase was significant in the west (Fig. 4.6b). A decrease in the magnitude of HW:FW occurs at a bend in the Top Sherwood fault trace (inline 9500, Fig. 4.6b and 4.12b). On the Arne Fault, periods of growth above the Top Sherwood are related to orientation (Fig. 4.6c). No thickened hanging-wall sequences occur adjacent to the E-W segments (inlines 9250 - 9300 and 9550 - 9650, Fig. 4.12c), but are consistently adjacent to oblique segments (inlines 9350 - 9500). Activity above the Zone D Anhydrite is less uniform on the Arne Fault than on the Wytch Farm and Northern Faults (Fig. 4.6c). The eastern fault segment post-dates Middle Jurassic sedimentation, as does the far western end of the fault. The middle segment (Fig. 4.12c) grew during the IntraLias-Bridport Sands and Frome Clay-Cornbrash intervals (Fig. 4.6c).

There are no faults with growth sequences solely within the IntraLias-Bridport Sands and Top Sherwood-Zone D Anhydrite intervals (Fig. 4.7a); the only active faulting was confined to faults with the longest histories, and whose throws dominate the deformation (Fig. 4.9, 4.11 and 4.14). The IntraLias-Bridport Sands interval experienced the least amount of activity, in terms of extent and HW:FW magnitude across the study area as a whole (Fig. 4.6 and 4.7a). No clear relationship is apparent between orientation and timing for the faults summarised in Fig. 4.7b.

4.5 NORMAL REACTIVATION

The normal faults in the Wytch Farm Oilfield developed during episodic extension (Fig. 4.6, 4.7a and 4.13a). The faults that occur throughout the entire sequence (*i.e.* the Wytch Farm, Northern, Arne Faults, Faults A, E, F and G) dominate the total displacement (Fig. 4.11), with polyphase movement implied by multiple growth sequences (Fig. 4.6 and 4.7a). The greatest strains in the Sherwood Sandstone (Table 4.2) suggest normal fault reactivation in the Triassic units, if uniform extension occurred throughout the sequence. The extension values for the Sherwood Sandstone represent the strains accumulated from both the initial rifting and the subsequent reactivation of the Triassic faults. The Bridport Sands extended the most in the Jurassic, and there is an overall decrease in strain either side of the Bridport Sands. However, fault timing (Fig. 4.6 and 4.7a) and throw distribution data (Fig. 4.13) support neither a system of contemporaneous segment interaction, nor uncomplicated growth of normally-reactivated Triassic faults into the Jurassic units (Fig. 4.16a).

For instance, an oblique overlap was interpreted on Line 50-51 (Fig. 4.16a) as a single plane of offset (e.g. line SP33 04; Fig. 4.6). Throw measurements from two sections are approximately constant from one section to the other, but only if a single plane is assumed. However, if the fault consists of two overlapping segments, the throw histories depart as depicted from the constant value. In addition, there is considerable overlap between the two fault segments, but probably initially overlapped with a substantial overlap zone. The displacement of the overlapping faults is also displaced towards the overlapping zone. The demonstration that the style of interaction was important to the growth of the overlapping faults is consistent with the diploids of the deeper sequence were

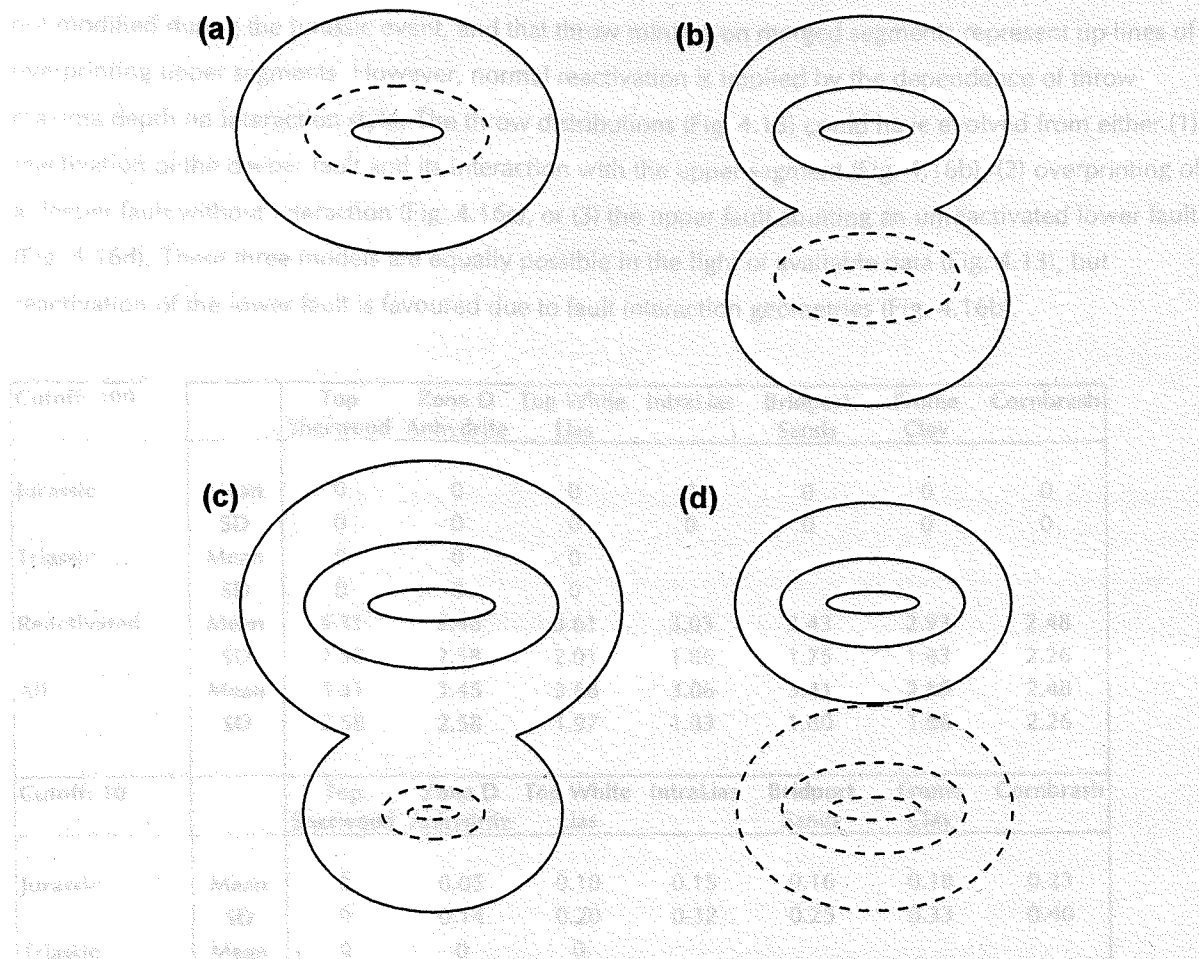


Fig. 4.16. Idealised throw contours on a fault plane for four scenarios (dashed lines represent former tip-lines): (a) Normal reactivation of an existing single, isolated fault. (b) Normal reactivation of the lower segment and interaction with the upper segment. (c) Overprinting of the lower fault by a larger upper fault. (d) Upper and lower faults abut, with or without reactivation of the lower fault. The elliptical contours in each diagram are based on radial propagation of a fault where $D \propto L^2$ (Walsh and Watterson, 1988; D = displacement and L = fault length).

Three distinct interaction geometries occur between lower and upper fault segments: contractional oversteps; extensional oversteps and no overstep (i.e. single planes at the seismic resolution). An example is the Arne Fault. At the western edge of the 3D survey, and into the 2D area, the interaction of its lower and upper segments is varied. For instance, an extensional overstep was interpreted on Line 80-270r (Fig. 4.8), but the fault occurs as a single plane on others (e.g. Line BP85-04, Fig. 4.8). Throw maxima depths on the upper and lower segments are approximately constant from one section to another when the fault is formed of a single plane, and when there is a contractional overstep. However, when the faults overstep with an extensional geometry, the throw maxima depths are displaced from the near-constant depth, and are adjacent to the overstep. In addition, there is considerable overlap between the segments at extensional oversteps, but only minimal overlap at a contractional overstep zone. Willemsen et al. (1996) observed that the maximum slip on overlapping faults is also displaced towards the overlap zone from the fault centre. This demonstrates that the style of interaction was important to the growth of the deeper fault segment. It is conceivable that the tip-lines of the deeper segments were

not modified during the Jurassic event, and that throw minima on merged segments represent tip-lines of overprinting upper segments. However, normal reactivation is implied by the dependence of throw maxima depth on interaction style. The throw distributions (Fig. 4.13) could have evolved from either (1) reactivation of the deeper fault and its interaction with the upper segment (Fig. 4.16b), (2) overprinting of a deeper fault without interaction (Fig. 4.16c), or (3) the upper fault abutting an unreactivated lower fault (Fig. 4.16d). These three models are equally possible in the light of available data (Fig. 4.13), but reactivation of the lower fault is favoured due to fault interaction geometries (Fig. 4.16b).

Cutoff: 100		Top Sherwood	Zone D Anhydrite	Top White Lias	IntraLias	Bridport Sands	Frome Clay	Cornbrash
Jurassic	Mean	0	0	0	0	0	0	0
	SD	0	0	0	0	0	0	0
Triassic	Mean	0	0	0				
	SD	0	0	0				
Reactivated	Mean	5.31	3.46	3.61	3.03	3.43	2.93	2.48
	SD	2.58	2.58	2.01	1.86	1.75	1.83	2.26
All	Mean	5.31	3.45	3.68	3.06	3.41	2.89	2.48
	SD	2.58	2.58	1.97	1.83	1.80	1.86	2.26
Cutoff: 10		Top Sherwood	Zone D Anhydrite	Top White Lias	IntraLias	Bridport Sands	Frome Clay	Cornbrash
Jurassic	Mean	0	0.05	0.10	0.15	0.16	0.18	0.23
	SD	0	0.14	0.20	0.32	0.25	0.33	0.40
Triassic	Mean	0	0	0				
	SD	0	0	0				
Reactivated	Mean	6.91	4.55	4.72	4.32	4.75	4.30	3.83
	SD	2.31	2.53	1.73	1.80	1.38	2.05	2.38
All	Mean	7.07	4.64	4.93	4.53	4.94	4.54	4.14
	SD	2.31	2.56	1.74	1.91	1.44	2.16	2.67
Cutoff: 1		Top Sherwood	Zone D Anhydrite	Top White Lias	IntraLias	Bridport Sands	Frome Clay	Cornbrash
Jurassic	Mean	0.01	0.05	0.11	0.17	0.18	0.20	0.24
	SD	0.04	0.14	0.21	0.31	0.24	0.35	0.40
Triassic	Mean	0	0	0				
	SD	0	0	0				
Reactivated	Mean	6.94	4.58	4.79	4.37	4.83	4.36	3.89
	SD	2.33	2.54	1.72	1.78	1.37	2.05	2.37
All	Mean	7.10	4.68	5.04	4.61	5.06	4.65	4.23
	SD	2.32	2.56	1.75	1.88	1.43	2.17	2.68

Table 4.2. % Extension for the horizons in Table 4.1, with the exception of the Base Chalk, the Corallian and the IntraSherwood (due to a lack of meaningful data). The faults have been analysed at heave cut-offs of 100, 10, and 1 m. The greatest amount of extension occurred in the Top Sherwood, and the lower extensions are related to the Zone D Anhydrite and IntraLias horizons. Triassic faults are defined as those entirely within the Trias; Jurassic faults are with growth in the Jurassic, and may or may not extend into the Trias. The reactivated faults have growth in the Triassic units, but extend upwards into the Jurassic.

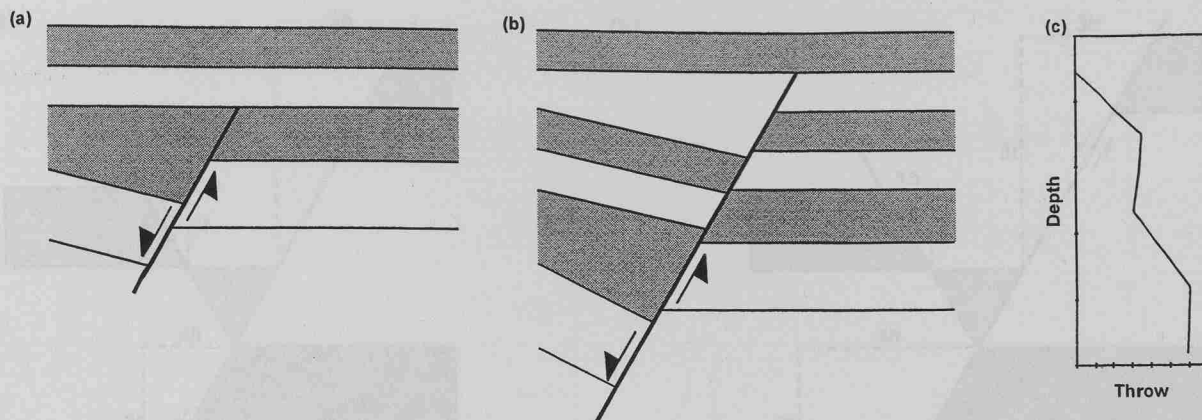


Fig. 4.17. (a) Normal fault with pre-, syn- and post-rift sediments. (b) Reactivation of the fault and upward expansion into newly deposited segments and (c) idealised vertical $d-x$ of the reactivated fault that suggests that a displacement minimum occurs at the top of the original syn-rift unit. The largest displacements are associated with the deepest parts of the fault, under a simple model of reactivation.

4.5.1 Mechanics of individual faults

Reactivation alone does not explain adequately why new faults that apparently initiated in the Jurassic are co-planar to Triassic faults, or why throws on reactivated faults are greatest in the shallower units. Coincidental linkage of all of the largest faults would be highly unlikely without the influence of reactivated Triassic faults. In addition, the deepest parts of the fault should have the largest post-reactivation throws (Fig. 4.17). A mechanism is needed whereby Triassic faults were able to propagate into the Jurassic sediments, and also acquire greater throws at shallow depths (Fig. 4.11). The greater throws in the upper units may be explained by the presence of an antithetic fault (Fig. 4.18a). The downthrow across the entire fault zone is accommodated by two faults on the upper section, and an identical amount of throw is localised onto one fault at depth (Fig. 4.18a). Although the diagram in (Fig. 4.18a) illustrates that an individual fault can acquire a larger throw on its upper section, it does not explain why greater extension would occur at depth (compare Bridport Sands and Top Sherwood, Table 4.2). The heave of the lower section could be increased, however, if the fault dip decreased with depth and a constant throw (Fig. 4.18b). This model may be applicable to the conjugate faults, such as the Arne and Northern Faults, and Faults E and F (Fig. 4.9), but not for the isolated Wytch Farm Fault.

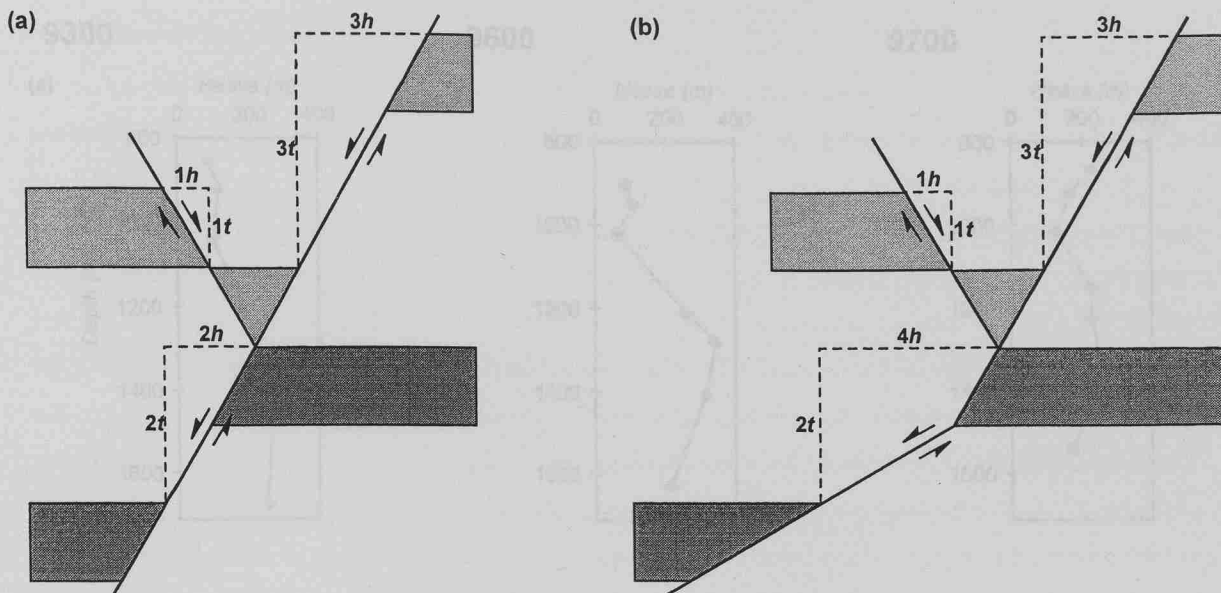


Fig. 4.18. (a) Idealised fault geometry to illustrate that an individual fault can have a smaller throw at depth, and a constant downthrow across the whole fault zone. The heave at depth is half of the combined heave of the upper two faults in this example. (b) Modification of the fault plane geometry so the heave is constant. The throw on the lower section is the same as in (a), but the heave is doubled. Any decrease in the fault dip at depth would lead to an increase in the heave, assuming that the throw remains constant. h = heave, t = throw and the numbers represent the number of units of each.

The Wytch Farm Fault is relatively free from the influence of branches and antithetic faults (Fig. 4.9), and so makes an ideal subject for a study of the mechanics of an individual fault. A comparison of fault heaves and fault throws for the Wytch Farm Fault illustrates that the greater throws in the shallow units are not always associated with greater heaves (Fig. 4.19a and b). The decreasing-upwards heaves are consistent with a reactivation model, *i.e.* the cumulative extension from two events is recorded in the Triassic units (Table 4.2), but space problems are created by increasing-upwards throws on sub-planar faults (Fig. 4.9). Depth-converted fault plane profiles (Fig. 4.19c) illustrate that the fault is steeper in the upper sections, which may explain the lesser heaves (*c.f.* Fig. 4.18b), but not the throw discrepancies (e.g. Fig. 4.13a). Two deformation models (Fig. 4.20) would explain the fault geometries: (1) the lower parts of the faults were subsequently reverse-reactivated during inversion of the Wessex Basin, (2) the upper part of the section became detached from the lower section and deformed independently (*i.e.* thin-skinned extension). Both methods require normal reactivation of the Triassic fault and upward propagation into the overlying Jurassic sequence to form a single fault plane (Fig. 4.16), prior to modification.

9300

9500

9700

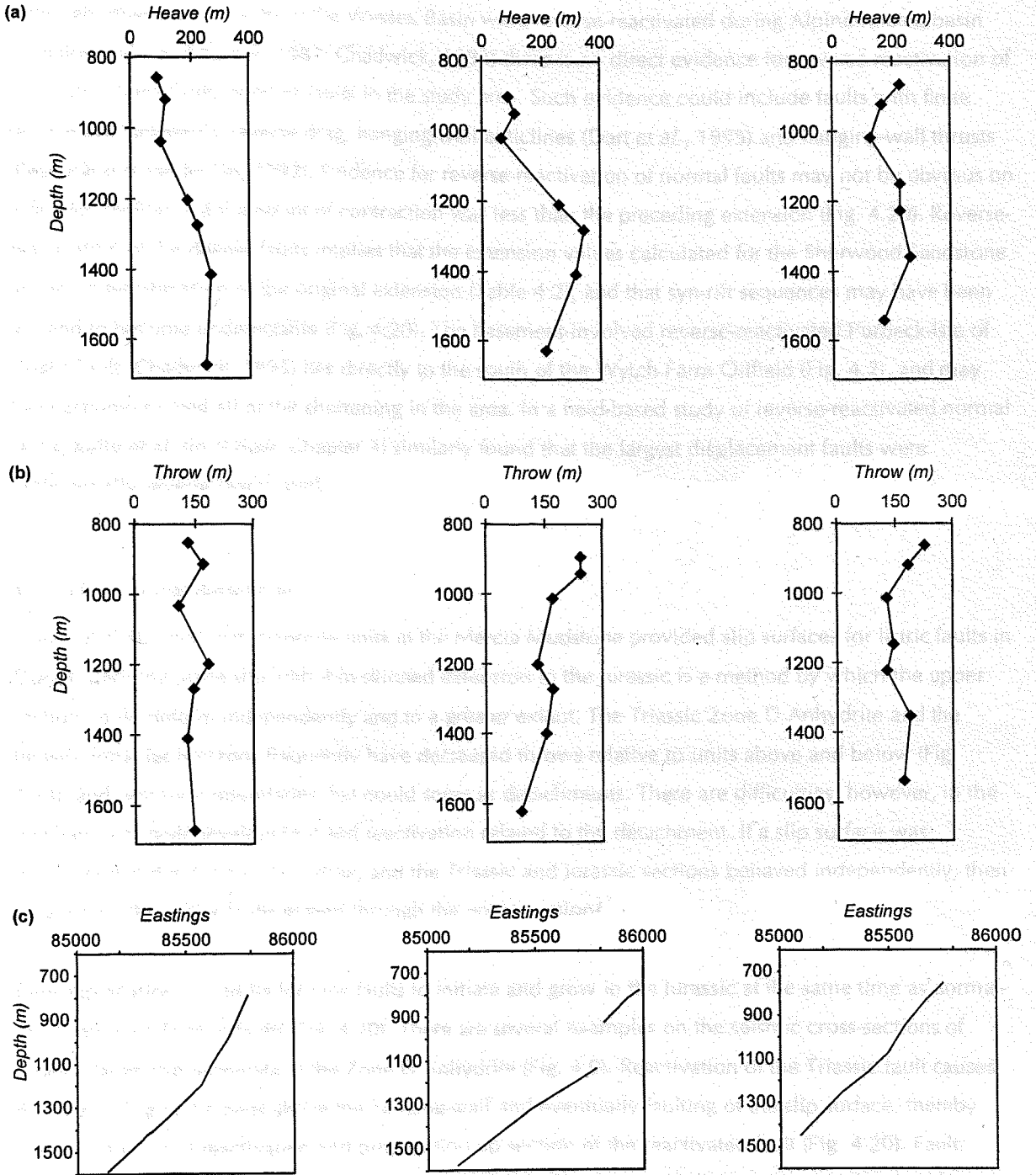


Fig. 4.19. Three synoptic vertical profiles of (a) fault heave and (b) fault throw, and (c) the fault plane of the Wytch Farm Fault. The data have been converted to depths from TWTT, with interval velocities calculated from mapped horizons depths in an exploration well (98/6-7) and the 3D seismic data. The fault has a shallower dip at depth in all three examples.

4.5.1a Reverse reactivation

Although other normal faults in the Wessex Basin were reverse-reactivated during Alpine-related basin inversion (Lake and Karner, 1987; Chadwick, 1993) there is no direct evidence for reverse-reactivation of the Wytch Farm Fault, or other faults in the study area. Such evidence could include faults with finite reverse displacements, reverse drag, hanging-wall anticlines (Dart *et al.*, 1995) and hanging-wall thrusts (Peacock and Sanderson, 1992). Evidence for reverse-reactivation of normal faults may not be obvious on a seismic section, if the amount of contraction was less than the preceding extension (Fig. 4.20). Reverse-reactivation of the deeper faults implies that the extension values calculated for the Sherwood Sandstone are an underestimation of the original extension (Table 4.2), and that syn-rift sequences may have been thinned to become undetectable (Fig. 4.20). The basement-involved reverse-reactivated Purbeck-Isle of Wight Fault (Chadwick, 1993) lies directly to the south of the Wytch Farm Oilfield (Fig. 4.2), and may have accommodated all of the shortening in the area. In a field-based study of reverse-reactivated normal faults, Kelly *et al.* (in review; Chapter 3) similarly found that the largest displacement faults were preferentially reverse-reactivated.

4.5.1b Extensional detachment

House (1993) noted that evaporite units in the Mercia Mudstone provided slip surfaces for listric faults in Dorset. Bedding-plane slip with thin-skinned extension in the Jurassic is a method by which the upper section could deform independently and to a greater extent. The Triassic Zone D Anhydrite and the Jurassic IntraLias horizons frequently have decreased throws relative to units above and below (Fig. 4.13), and represent boundaries that could serve as detachments. There are difficulties, however, in the mechanics of fault development and reactivation related to the detachment. If a slip surface was established at the Zone D Anhydrite, and the Triassic and Jurassic sections behaved independently, then why would the major faults extend through the entire section?

One explanation would be for new faults to initiate and grow in the Jurassic at the same time as normal-reactivation of Triassic faults (Fig. 4.20). There are several examples on the seismic cross-sections of Jurassic faults that terminate at the Zone D Anhydrite (Fig. 4.9). Reactivation of the Triassic fault causes down-warping of the beds above the hanging-wall and eventually faulting of the slip surface, thereby allowing sustained reactivation and propagation up-section of the reactivated fault (Fig. 4.20). Fault segments above the detachment are able to attain larger throws than those below by further bedding-parallel slip. These processes provide the means for fault reactivation and upward propagation, and explain the greater displacements at shallow depths.

In the absence of evidence for reverse-reactivation of any of the normal faults in the study area, the modified detachment model provides the most rigorous explanation for the fault geometries in an extensional regime. A consideration, however, is that the cross-sections do not balance as the excess bed-lengths in the upper units are beyond the section boundaries.

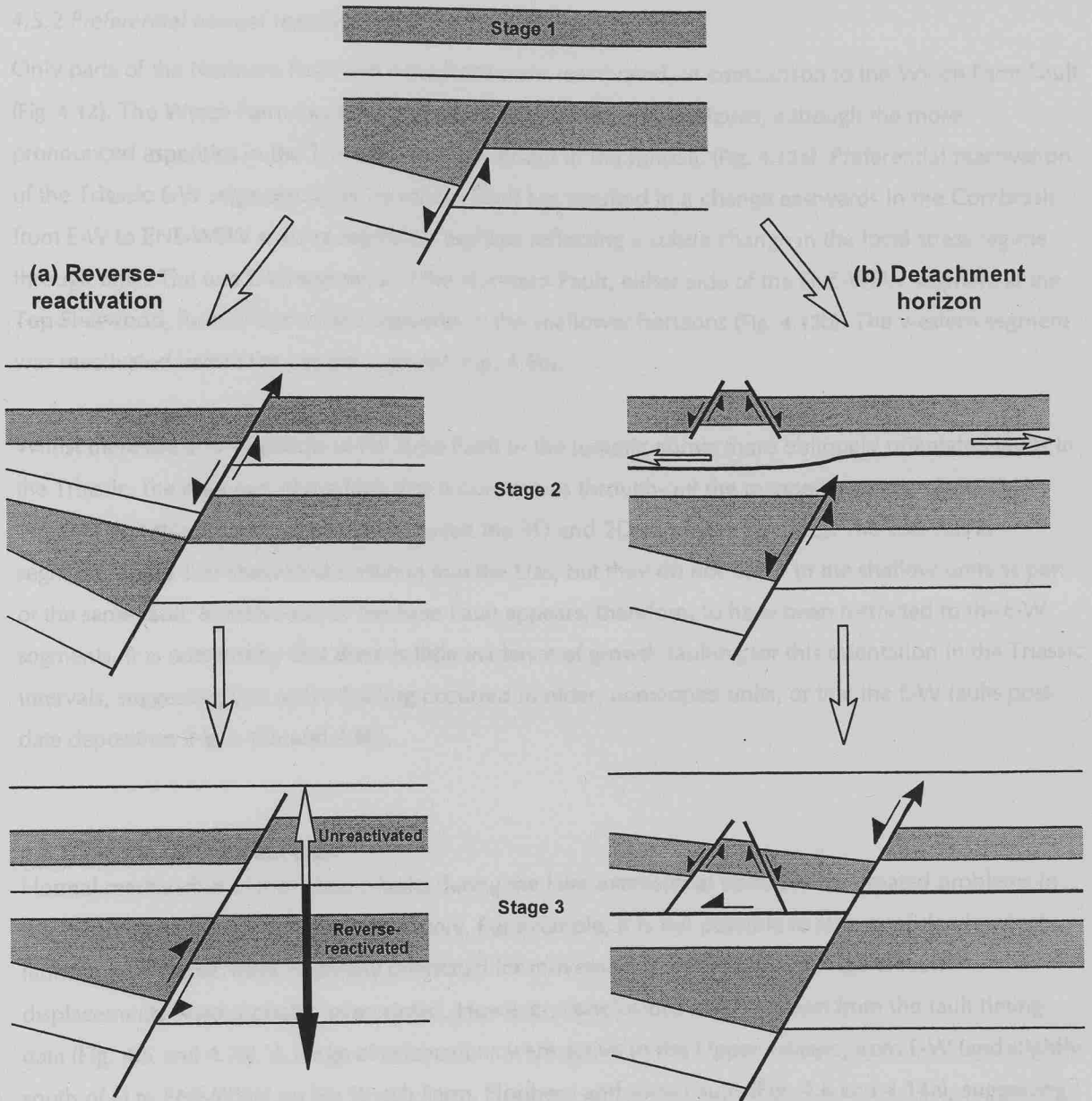


Fig. 4.20. Two methods to explain the fault geometries: (a) modification of the normally-reactivated fault plane by reverse-reactivation of the deeper parts of the fault, and (b) fault development with the presence of a detachment horizon. Stage 1 is identical for both models, and simply illustrates the presence of an early fault (c.f. Fig. 4.17a). In the reverse-reactivation model, the Triassic fault is initially normally-reactivated and propagates up-section (Stage 2). The lower parts of the fault are reverse-reactivated, and the upper parts remain unaffected (Stage 3). Shortening in-between is accommodated by ductile compaction of the Mercia Mudstone. In the detachment model, the Triassic fault reactivation and Jurassic fault initiation above a detachment horizon (Zone D Anhydrite) are contemporaneous (Stage 2). Continued expansion of the deeper fault into the upper sections occurs after faulting of the detachment layer. The upper fault acquires a larger displacement through thin-skinned extension above the detachment.

4.5.2 Preferential normal reactivation

Only parts of the Northern Fault and Arne Fault were reactivated, in comparison to the Wytch Farm Fault (Fig. 4.12). The Wytch Farm Fault has a similar geometry at every horizons, although the more pronounced asperities in the Triassic traces are absent in the Jurassic (Fig. 4.12a). Preferential reactivation of the Triassic E-W segments of the Northern Fault has resulted in a change eastwards in the Cornbrash from E-W to ENE-WSW striking segments, perhaps reflecting a subtle change in the local stress regime through time. The two E-W segments of the Northern Fault, either side of the ENE-WSW segment at the Top Sherwood, form unconnected segments in the shallower horizons (Fig. 4.12b). The western segment was reactivated before the eastern segment (Fig. 4.6b).

Whilst there are E-W segments of the Arne Fault in the Jurassic above more obliquely orientated faults in the Triassic, the only part of the fault that is continuous through-out the mapped sequence is the E-W segment that straddles the boundary between the 3D and 2D surveys (Fig. 4.12c). The ESE-WNW segments at the Top Sherwood continue into the Lias, but they do not occur in the shallow units as part of the same fault. Reactivation of the Arne Fault appears, therefore, to have been restricted to the E-W segments. It is noteworthy that there is little evidence of growth faulting for this orientation in the Triassic intervals, suggesting that active faulting occurred in older, unmapped units, or that the E-W faults post-date deposition (Fig. 4.12b and 4.6b).

4.6 DEFORMATION HISTORY

Normal reactivation of the Triassic faults during the later extensional episodes has created problems in the interpretation of the deformation history. For example, it is not possible to state confidently which faults in the Triassic were optimally orientated for movement at each stage, as original fault displacements were probably overprinted. However, conclusions can be drawn from the fault timing data (Fig. 4.6 and 4.7a). A range of orientations were active in the Upper Triassic, from E-W (and slightly south of E) to ENE-WSW on the Wytch Farm, Northern and Arne Faults (Fig. 4.6 and 4.14a), suggesting either alteration of the stress regime, or the influence of deeper features (Chadwick, 1986). The exception is the ESE-WNW segment of the Arne Fault (Fig. 4.14), but this is actually an amalgamation of E-W striking segments. The thickest growth sequences of the Northern Fault are adjacent to the E-W segments (Fig. 4.6b and 4.12b). In the Lias, the growth faulting is confined to the E-W and ESE-WNW segments on the Wytch Farm Fault and to E-W segments on the Northern Fault. Faulting during the Middle Jurassic was restricted to the E-W segments of the three principal faults, although there is variation on minor faults (Fig. 4.7a).

4.6.1 Comparison with the regional structure of the Wessex Basin

The tectonic history of the Wessex Basin began in the Late Permian which continued to the Early Jurassic (e.g. Atkinson, 1966; Lake and Kerner, 1967; Hibach et al., 1993) and was succeeded by a compressional phase during the Tertiary (Morter et al., 1987; Lake and Kerner, 1967; Chadwick, 1993). The tectonic history can be divided into two major stages: (i) Late Permian to Early Tertiary and (ii) mid-Late

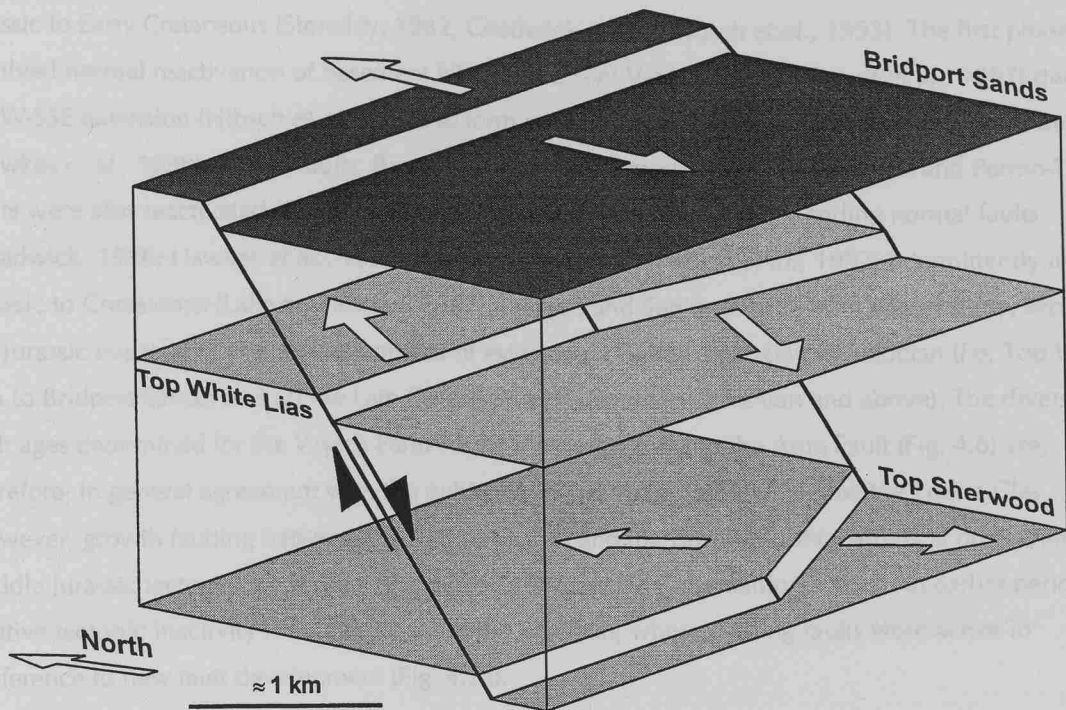


Fig. 4.21. Block diagram to illustrate the changes in active fault orientation and the alteration in the principal stress axes orientation through time.

The active fault orientations evolved temporally from a Triassic system where E-W to ENE-WSW orientations were active, through a Lower Jurassic regime of E-W and ESE-WNW faults, to a Middle Jurassic system of predominantly E-W fault activity. The largest throws on all faults at all horizons are generally associated with the E-W striking segments, suggesting that the E-W faults had the most favourable orientations for normal reactivation, and Triassic throws were overprinted by later deformation events (Fig. 4.13 and 4.14). The active faults imply a change of extension orientation with time, if pure dip-slip deformation is assumed. In the Middle Jurassic, extension perpendicular to the fault strikes indicates that the contractional axis was vertical, with N-S extension. The stress axes during the earlier events are more difficult to assign due to a wider range of active fault orientations. If it is assumed that the E-W orientated faults reflect the deeper fault geometries (Chadwick, 1986; Karner *et al.*, 1987; Lake and Karner, 1987; Hawkes *et al.*, 1998), and the other orientations reflect contemporary stress axes orientations, then the Triassic rocks were deformed under NNW-SSE to NW-SE orientated effective tension, and the Lower Jurassic units extended in a NNE-SSW direction (Fig. 4.21).

4.6.1 Comparison with the regional structure of the Wessex Basin

The development of the Wessex Basin began in the Late Permian which continued to the Early Cretaceous (Chadwick, 1986; Lake and Karner, 1987; Hibschi *et al.*, 1993) and was succeeded by a contractional phase during the Tertiary (Karner *et al.*, 1987; Lake and Karner, 1987; Chadwick, 1993). Fault related subsidence occurred in two major stages: (1) Late Permian to Early Triassic and (2) mid-Late

Jurassic to Early Cretaceous (Stoneley, 1982; Chadwick, 1986; Hibschi *et al.*, 1993). The first phase involved normal reactivation of basement NW-SE and E-W Variscan faults (Karner *et al.*, 1987) during NNW-SSE extension (Hibschi *et al.*, 1993) to form mainly south-dipping (Chadwick, 1986) E-W trending (Hawkes *et al.*, 1998) normal faults. Basement faults (some previously unreactivated) and Permo-Triassic faults were also reactivated (Chadwick, 1986), with the formation of E-W trending normal faults (Chadwick, 1986; Hawkes *et al.*, 1998) under N-S extension (Hibschi *et al.*, 1993) intermittently in the Jurassic to Cretaceous (Lake and Karner, 1987). Jenkyns and Senior (1991), from a field study, separated the Jurassic events into two discrete phases of extension: (1) the Hettangian to Bajocian (*i.e.* Top White Lias to Bridport Sands) and (2) the Late Oxfordian to Portlandian (Corallian and above). The diversity of fault ages determined for the Wytch Farm Fault, Northern Fault and the Arne Fault (Fig. 4.6) are, therefore, in general agreement with the published accounts for the units below the Frome Clay. However, growth faulting between the Bridport Sands and the Cornbrash (Fig. 4.6) is at odds with Middle Jurassic tectonic quiescence (Chadwick, 1986; Jenkyns and Senior, 1991). An earlier period of relative tectonic inactivity is evident, prior to the Bajocian, where existing faults were active in preference to new fault development (Fig. 4.7a).

The overall E-W trend mapped from the seismic data (Fig. 4.12 and 4.14) conforms to the regional E-W structure (Stoneley, 1982; Chadwick, 1986; Lake and Karner, 1987). In detail, the ENE-WSW to ESE-WNW orientations of faults in the Wytch Farm Oilfield are also apparent in the regional faults (Fig. 4.2). For example, the strike range from ESE-WNW to ENE-WSW of the Arne Fault at the Top Sherwood (Fig. 4.14) is recognisable in the orientations of the Cranbourne Fault and the basement-involved, reverse-reactivated Purbeck - Isle of Wight Fault (Fig. 4.2b).

4.7 CONCLUSIONS

1. Faults orientations in the Triassic units range from ENE-WSW to WNW-ESE. Jurassic faults have a more general E-W strike.
2. Normal faults in the Wytch Farm Oilfield have a movement history which, at a minimum, extends from the Sherwood Sandstone to the Corallian.
3. Active faulting occurred during two major phases, one in the Upper Triassic and the other in the Lower - Middle Jurassic. The IntraLias-Bridport Sands and the Top Sherwood-Zone D Anhydrite intervals were periods of relative tectonic quiescence; thickened hanging-wall sequences indicate that only the faults that cut through the entire section were active.
4. Normal reactivation of the Triassic faults occurred during the Jurassic, and dominates the deformation at all levels. The E-W faults were most optimally orientated for normal reactivation, as they have the largest displacements in all units.
5. Although throws are generally greater in the shallower units, the strain is less due to steeper fault geometries.
6. A thin-skinned extension model is appropriate to explain how sub-planar faults have larger throws in the uppermost units. Triassic faults were normally-reactivated during the Jurassic and propagated

through a detachment horizon. The Jurassic units were able to deform independently above the slip surface.

7. Faults in the Triassic formed during NNW-SSE to NW-SE extension. The stress regime was modified during the subsequent rifting events, such that the effective tension axis was orientated NNE-SSW in the Middle Jurassic, and N-S in the Lower Jurassic. The deformation history in the Wytch Farm Oilfield conforms to published accounts of the Wessex Basin history.

The main reservoir occurs in a horst between the north-dipping Wytch Farm Fault and the north-dipping Northern Fault, and is truncated by the Arne Fault. A re-interpretation of the Arne Fault has been carried out, and four new maps have been prepared on the basis of uncertainties inherent in the 2D seismic interpretation. The new maps are all calibrated to the sparse well data that is available for Arne Fault/Top through-out directions, and indicate considerable variation in reserves estimation and disruption to planned target iterations.

A new exploration target is found in a horst that occurs in the EEC 3D data. A previous interpretation of the top reservoir horizon does not match completely either the well data or correlate with the existing interpretation of the BF 3D seismic data. A re-interpretation of the horizons and structures within the EEC data set has yielded an interpretation that provides a tighter correlation to all the available data. A new north-dipping fault has been identified that is located such that the Wytch Farm Fault may continue seawards in overlap or join with the new fault.

5. New interpretations of the structure of the Sherwood Reservoir, Wytch Farm Oilfield, Dorset, UK

5.1 SUMMARY

The understanding of the structure of the Wytch Farm Oilfield is based on the interpretation and calibration of well data and three seismic data sets (BP 2D, BP 3D, EEC 3D). Uncertainty with the interpretation occurs due to the quality of data within the 2D seismic data, and because of a gap between the two 3D seismic data sets.

The main reservoir occurs in a horst between the south-dipping Wytch Farm Fault and the north-dipping Northern Fault, and is traversed by the Arne Fault. A re-interpretation of the Arne Fault has been carried out, and four new maps have been prepared on the basis of uncertainties inherent in the 2D seismic interpretation. The new maps are all calibrated to the sparse well data that is available for Arne Fault/Top Sherwood intersections, and indicate considerable variation in reserves estimation and disruption to planned target locations.

A new exploration target is found in a horst that occurs in the EEC 3D data. A previous interpretation of the top reservoir horizon does not match completely either the well data or correlate with the existing interpretation of the BP 3D seismic data. A re-interpretation of the horizons and structures within the EEC data set has yielded an interpretation that provides a tighter correlation to all the available data. A new south-dipping fault has been identified that is located such that the Wytch Farm Fault may continue eastwards to overstep or join with the new fault.

The main problem at Wytch Farm is provided by a gap between the two 3D seismic surveys. The objective of this study is to reassess problematic areas in the structural interpretation of the main reservoir unit in the Wytch Farm Oilfield, that are important to exploration development, using fault plane analysis techniques. An introductory to the basin geology is followed by a description of the problem, the methods used, and a discussion of new interpretations of the data.

1.1 Geological setting

The Wytch Farm Oilfield (Fig. 1.1) is situated on the Dorset Coast, well in the Wessex Basin (Mollat, 1967). It is in the footwall of the south-dipping Purbeck Tye of Wytch Fault (Coxon and Hayward, 1961; Lake and Farmer, 1967), and in ongrave blocks PL289 and PL290, and offshore block PL314 (Hogg, et al., 1997).

The geosyncline of the Wessex Basin comprises Carboniferous-Carboniferous sediments that were deformed during the Variscan orogeny (Chadwick, 1964) by N to NW directed thrusts and accompanying NW-SE lateral compression (Lake and Farmer, 1967).

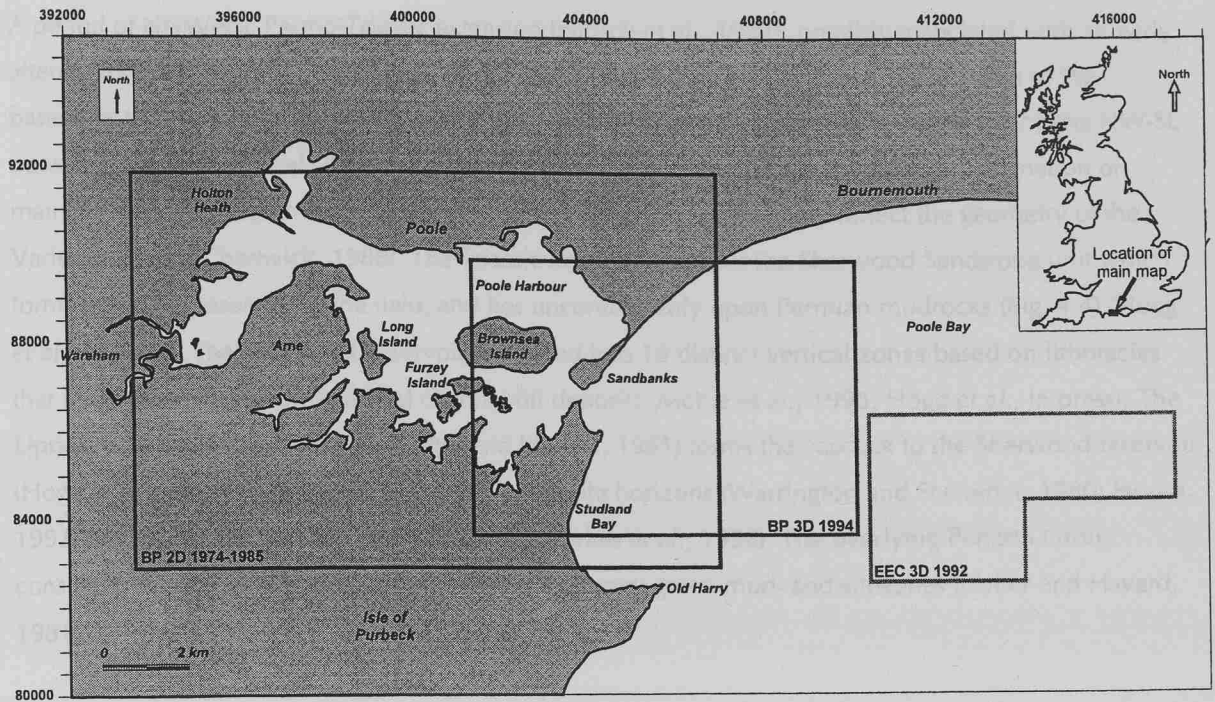


Fig. 5.1. Map of part of the south Dorset Coast to show the extent of the seismic data. The inlines run N-S, and the crosslines E-W in both 3D surveys.

5.2 INTRODUCTION

The analysis of a 2D seismic data with a line spacing of up to 2 km is potentially open to many interpretations, as faults cannot always be confidently interpolated between adjacent lines. An additional complication at Wytch Farm is provided by a gap between the two 3D seismic surveys. The objective of this study is to reassess problematic areas in the structural interpretation of the main reservoir unit in the Wytch Farm Oilfield, that are important to exploration development, using fault plane analysis methods. An introduction to the basin geology is followed by a description of the problem, the methods used, and a discussion of new interpretations of the data.

5.2.1 Geological setting

The Wytch Farm Oilfield (Fig. 5.1) is situated on the Dorset Coast, within the Wessex Basin (Kent, 1949). It is in the footwall of the south-dipping Purbeck-Isle of Wight Fault (Colter and Havard, 1981; Lake and Karner, 1987), within onshore licence blocks PL089 and PL259, and offshore block P534 (Hogg, *et al.*, in press).

The basement to the Wessex Basin comprises Cambrian-Carboniferous sediments that were deformed during the Variscan Orogeny (Chadwick, 1986) by N to NW directed thrusts and accompanying NW-SE lateral ramps (Lake and Karner, 1987).

A period of NNW-SSE Permo-Triassic extension (Hibsch *et al.*, 1993), possibly associated with an early attempt to form the North Atlantic (Stoneley, 1982), may have caused normal reactivation of the basement thrusts (Chadwick, 1986; Lake and Karner, 1987), and strike-slip movement along the NW-SE transfer faults (Karner *et al.*, 1987). The reactivation of the basement thrusts led to the formation of mainly down-to-the-south half-graben with a spatial distribution that may reflect the geometry of the Variscan thrusts (Chadwick, 1986). The Triassic basin fill includes the Sherwood Sandstone unit which forms the major reservoir in the field, and lies unconformably upon Permian mudrocks (Fig. 4.4) (Hogg *et al.*, in press). The Sherwood Reservoir is divided into 10 distinct vertical zones based on lithofacies that range from floodplain to fluvial channel-fill deposits (McKie *et al.*, 1998; Hogg *et al.*, in press). The Upper Triassic Mercia Mudstone (Colter and Havard, 1981) forms the caprock to the Sherwood reservoir (Hogg *et al.*, in press), and contains several evaporite horizons (Warrington and Scrivener, 1980; House, 1993) that were deposited in the central area (Hawkes *et al.*, 1998). The overlying Penarth Group consists of the White Lias Limestone and anhydritic grey-green mud- and siltstones (Colter and Havard, 1981).

Pulsed growth faulting during Jurassic-Early Cretaceous extension above reactivated basement thrusts (Stoneley, 1982; Chadwick *et al.*, 1983; Karner, *et al.*, 1987; Lake and Karner, 1987) took place between two periods of tectonic quiescence in the Late Triassic and mid-Late Cretaceous (Chadwick, 1986). Permo-Triassic normal faults and Variscan basement thrusts were reactivated, including the Portland-Wight Fault (Chadwick, 1986), during the Jurassic rifting events. The thickest sedimentary sequences are related to the normal reactivation of the basement thrusts (Chadwick *et al.*, 1983; Karner *et al.*, 1987). The Jurassic-Cretaceous basin fill consists of a sequence of mudstones, sandstones and limestones, and includes the more minor reservoirs at Wytch Farm (Hogg *et al.*, in press): the Bridport Sands and the limestone member of the Frome Clay. The Bridport Sands are composed of coarse siltstones to fine sandstones that are bioturbated and moderately well-sorted (Colter and Havard, 1981). The limestone member in the Frome Clay formed from a shell accumulation (Hogg *et al.*, in press) within a Middle Jurassic shallowing upward sequence that post-dates clays deposited during a mild deepening event (House, 1993).

Reverse-reactivation of some of the normal faults and dextral reactivation of NW-SE faults occurred during Late Cretaceous-Tertiary basin inversion (Stoneley, 1982; Lake and Karner, 1987; Chadwick, 1993; Hibsch *et al.*, 1993) that was related to the Alpine Orogeny (Chadwick, 1993). The Variscan basement faults may have reactivated once again as reverse faults (Lake and Karner, 1987; Chadwick, 1993), an example of which is the Purbeck Fault Zone, expressed at the surface as the Purbeck Disturbance (Colter and Havard, 1981). The Portland-Wight Fault experienced the greatest amount of reverse-reactivation (Chadwick, 1993), and basin inversion may have resulted in re-mobilisation and loss of hydrocarbons adjacent to the larger reverse-reactivated faults (Lake and Karner, 1987).

The overall present-day structural configuration is a horst that contains the Sherwood Sandstone reservoir, bounded to the south by the south-dipping Wytch Farm Fault and the north-dipping Northern Fault to the north. Beds dip off to the east and west to form a shallow anticline (Fig. 5.2) (Hogg *et al.*, in press). The Arne Fault divides the horst into a north and a south block.

5.2.2 Structural uncertainties

The structural interpretation of the Triassic Sherwood Sandstone Reservoir in the Wytch Farm Oilfield (Fig. 5.2) is based on well data and the interpretation of three seismic data sets (Fig. 5.1):

1. 2D seismic data, acquired between 1974 and 1985, form a grid that provides an east-west line spacing of 0.2 - 1km, and a north-south spacing of up to 2km.
2. BP 3D data (1994) that overlaps partially with the 2D data in the immediate vicinity of Poole Harbour, and extends offshore into Poole Bay (seismic grid: 12.5 x 12.5 m).
3. EEC 3D data (1992). There is no overlap between this and the two BP surveys (seismic grid: 12.5 x 12.5 m).

Uncertainty with the structural interpretation exists for two main reasons. Firstly, the Top Sherwood Sandstone reflector is not clearly identifiable on the earlier 2D seismic data, so any interpretation is based on identification of the Top White Lias (*c.f.* Fig. 4.4), that forms a more prominent reflector. A better image of the top reservoir reflector was, however, obtained by the most recent (1985) 2D data. As a consequence of the 2D data quality, there is low confidence in the structural map of the Top Sherwood beyond the boundaries of the 3D data set. The second source of uncertainty occurs as a result of poor horizon correlation across a gap between the two 3D surveys. The problematic correlation is exacerbated by poor imaging of the Top Sherwood and Top White Lias in the EEC data. A good correlation is found between the two surveys to the north of the Wytch Farm Fault, but this deteriorates southwards with the increasing width of the gap (Ellis, 1998). The continuation of structures from the BP survey into the EEC survey was not fully resolved by the previous interpretation (Ellis, 1998). For example, the Wytch Farm Fault does not appear to continue into the EEC area, and as a consequence the Top Sherwood interpretation is too shallow, based on recent well data.

It is important to resolve the discrepancies, as a horst in the north of the EEC data area forms a potential exploration target, and Extended Reach Development (ERD) wells drilled from the onshore area would traverse the gap. Reduction of the uncertainty regarding the location and geometry of the Arne Fault (Fig. 5.2) is vital to the continued development of the oilfield as it divides the reservoir. Production data suggests that the fault acts as a permeability barrier in some parts of the field, but allows fluid flow in others (Channon, 1996). A recent study of the Arne Fault in the BP 3D area (Ellis, 1997) has revealed that it is formed of several segments.

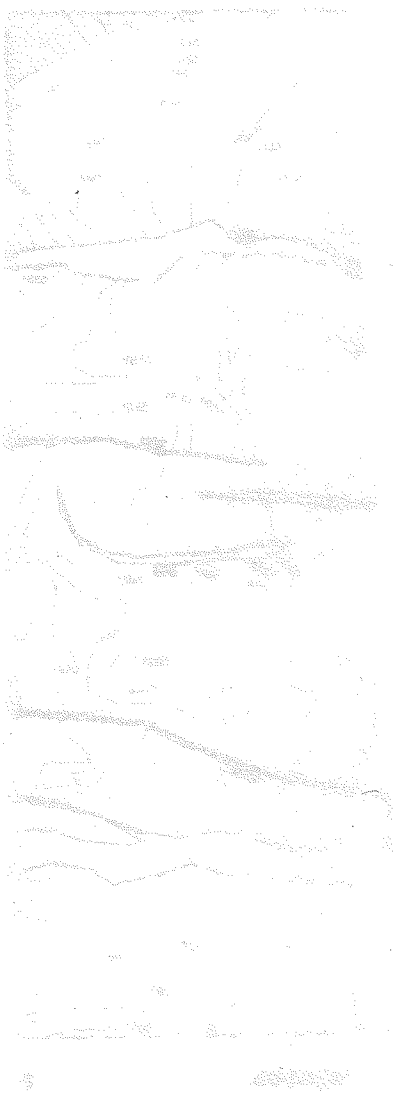


Fig. 5.2 (overleaf) Existing structural interpretation of the Sherwood Sandstone reservoir (mapped by Giles Watts, BP Exploration and Production, Wytch Farm), and location of the Arne Fault picks used in this study on the 2D seismic lines (black diamonds) within Poole Harbour. The map is based on the interpretation of 2D and 3D seismic data, and the horizon depths are calibrated to available well data.

90000
89000
88000
87000
86000
85000
84000

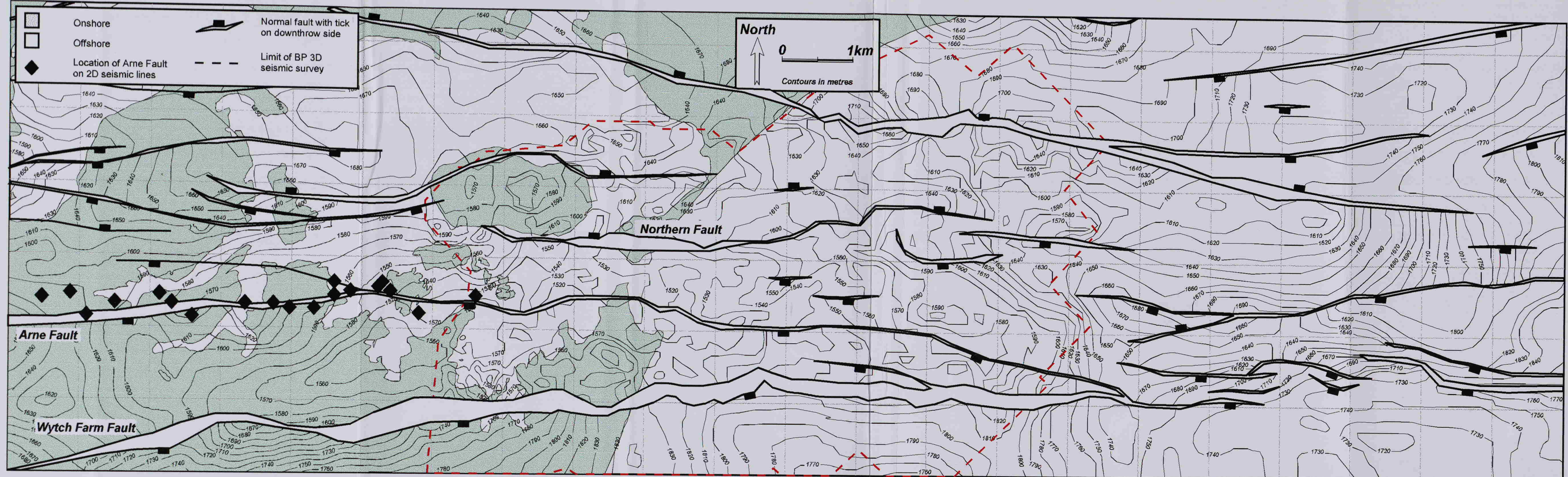
	Onshore		Normal fault with tick on downthrow side
	Offshore		Limit of BP 3D seismic survey
	Location of Arne Fault on 2D seismic lines		

North



0 1km

Contours in metres



395000 397000 399000 401000 403000 405000 407000 409000 411000 413000 415000 417000

5.3 METHODS

The approach used to address the uncertainties involved: (1) re-interpretation of the Arne Fault on the 2D data, and a re-interpretation of the Triassic horizons and faults in the EEC 3D seismic data; (2) calibration of seismic and well data; (3) assessment of timing of movement; (4) application of displacement-distance and displacement-length models to the faults (e.g. Peacock and Sanderson, 1991; Dawers *et al.*, 1993; Cartwright *et al.*, 1995), and (5) understanding of the pre-Sherwood Sandstone structural configuration of the area (e.g. Chadwick, 1986; Lake and Karner, 1987; Hibschi *et al.*, 1993).

5.3.1 Horizon interpretation

A re-interpretation of the 1974-1985 2D and EEC 3D seismic surveys, using *Schlumberger GeoQuest IESX* Unix-based software, was undertaken to re-evaluate the structure of the Top Sherwood. The interpretation of the Arne Fault was concentrated in the area to the west of the previous study of the BP 3D area (Fig. 5.1) (Ellis, 1997), and was identified on the sections from comparison with the existing Top Sherwood depth map (Fig. 5.2). Table 5.1 is a list of the horizons used for the re-interpretation. In the interpretation of both the 2D and the EEC 3D data, the Top White Lias was identified from comparisons with well data (and existing seismic interpretations), and the Top Sherwood horizon was located c. 1.6 ms deeper. The interpretation of the EEC 3D data began with interpretation of the E-W cross-lines, and the cross-referenced points were used to position the horizons on the N-S inlines.

5.3.2 Calibration of the seismic data

Sixteen wells intersect the Arne Fault (Table 5.2), but elsewhere there is no check on the seismic data and there are uncertainties in both the throw and position of the fault (Fig. 5.3) (Martin *et al.*, 1993). The depth to the Top Sherwood uncertainty used in this study is ± 15 ms. Martin *et al.* (1993) found a maximum depth uncertainty of ± 30 ms over the whole of the region, but generally less than ± 15 ms. A similar error (± 15 ms) is applied to the fault throw, as this is calculated from the differential depth between the hanging-wall and the footwall (Fig. 5.3). Martin *et al.* (1993) state that the positional uncertainty is related to the fault throw, but a standard value of ± 200 m was chosen for this project to allow maximum flexibility within the limits of the errors applied to the throw (Fig. 5.3). Fault positions are accurate to ± 200 m on the pre-1985 2D seismic lines (Martin *et al.*, 1993), and ± 50 m on the 3D survey (Hogg *et al.*, in press).

Horizon Name	Description
Top Sherwood	Occasionally consistent reflector, c. 150 ms from P&AWL
Top White Lias	Next consistent strong reflector, c. 20 ms down from P&AWL

Table 5.1 List of the horizons used for this study (cf. Fig. 5.4). Existing BP picks within the 3D survey area (indicated by Charles Watts and Peter EOH, BP Exploration and Production) were extrapolated west to the 2D survey lines and east to the EEC survey area. In the 2D data, all horizons below the Top White Lias are the confidence picks due to poor data quality.

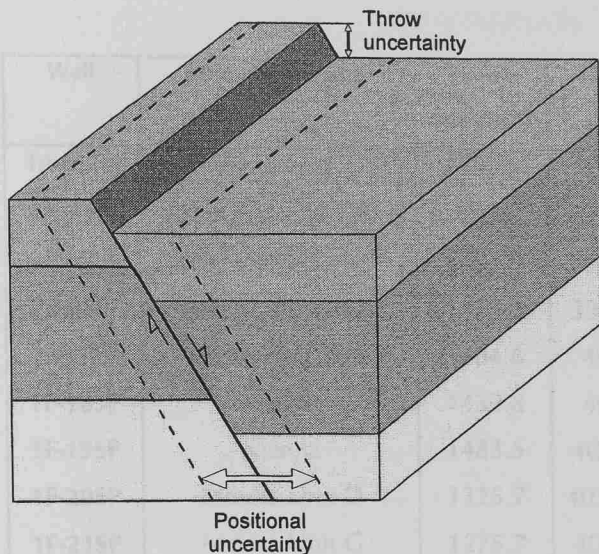


Fig. 5.3. Illustration of the extent of fault throw and position uncertainties (after Martin *et al.* 1993). The throw uncertainty was set at ± 15 ms, and the fault positions are accurate to ± 200 m to reflect the 2D seismic data resolution.

Horizon	Colour	Description
Base Chalk	Orange	Shallowest, most consistent reflector, mainly unfaulted and horizontal, above tilted beds in HW of Wytch Farm and Northern Faults
Cornbrash	Green	Immediately above first strong reflector below Base Chalk, only in the HW of Wytch Farm and Northern Faults
Frome Clay	Blue	Two cycles down from Cornbrash pick
Bridport Sands	Magenta	Two cycles down from Frome Clay pick
IntraLias	Black	First strong event below (c.120 ms) Bridport Sands, top of a set of three equidistant continuous reflectors
Top White Lias	Grey	Bottom reflector of the set of three, strongest and most consistent reflector
Zone D Anhydrite	Red	Next continuous strong reflector, c.80 ms down from PABWL
Top Sherwood	Yellow	Occasionally consistent reflector, c.160 ms from PABWL

Table 5.1. List of the horizons used for this study (c.f. Fig. 5.6). Existing BP picks within the 3D survey area (mapped by Giles Watts and Peter Ellis, BP Exploration and Production) were extrapolated west to the 2D survey lines and east to the EEC study area. In the 2D data, all horizons below the Base White Lias are low-confidence picks, due to poor data quality.

Well	Stratigraphic unit	Depth (mTVDSS)	Geographical location		Fault throw	
			Easting	Northing	mTVD	TWT ms
1A-06SP	Mercia Unit F	1482.1	398577	86471	40	21.0
1A-11SI	Sherwood 80-100	1654	399104	86244	35	18.4
2B-07SI	Sherwood 80-100	1707.9	397940.4	86183.6	60-65	31.5
2B-08SI	Sherwood 80-100	1712.3	398320.2	86123.9	60-65	31.5
1F-17SP	Sherwood 100	1704.6	402484	86262.6	22-25	10.8
1F-18SP	Mercia	1439.8	403792	86541	22.5	11.8
1F-19SP	Mercia	1483.5	404521.9	86368.6	37.2	19.5
1F-20SP	Mercia Unit D	1325.7	403319.67	86596.08	13.2	7.8
1F-21SP	Mercia Unit C	1275.7	403583.7	86586.45	17.3	10.2
1K-06SP	Liassic Group	1144.6	400775.33	86806.93	40	17.1
1K-07SP	Mercia Unit F	1435	399730.1	86739.08	21	9.4
1K-07SP	Lower White Lias	1209.7	400066	86809.8	22	11.0
1L-07SP	Frome/Forest Marble	831.3	401927.3	86726.6	?	?
1M-01SP	Mercia Unit F/G	1254.3	402647.8	86760.82	17.8	10.5
1M-03SP	Mercia Unit F	1409.1	405136.9	86252.4	37	19.4
1M-05SP	Down Cliff Clay	1010.9	403385.17	86657.85	40	23.6
1M-08SP	Mercia Unit B&C	1298.3	402184.3	86423.69	15	8.9

Table 5.2. Details of the wells that are reported as having intersected the Arne Fault (from BP Well Completion Reports, and Knight, 1994).

The well data for the Arne Fault intersections, and the EEC survey area (Fig. 5.4) show how the unit thicknesses and the horizon depths vary in each well. A repeated (*i.e.* thickened) sequence occurs when a gently inclined well trajectory crosses a fault with a similar azimuth, and a cut-out (thinned) unit is found when either a vertical well or a well with an opposing azimuth intersects a fault. The new interpretations of both sets of seismic data all honour the well data.

A line spacing of up to 2 km is provided by the 2D seismic lines (Fig. 5.5), compared to the 12.5 x 12.5m grid of the 3D surveys. Any extrapolation of fault traces between picks from one 2D line to the next is therefore potentially open to many different interpretations.

The well data for the Arne Fault intersections, and the EEC survey area (Fig. 5.4) show how the unit thicknesses and the horizon depths vary in each well. A repeated (*i.e.* thickened) sequence occurs when a gently inclined well trajectory crosses a fault with a similar azimuth, and a cut-out (thinned) unit is found when either a vertical well or a well with an opposing azimuth intersects a fault. The new interpretations of both sets of seismic data all honour the well data.

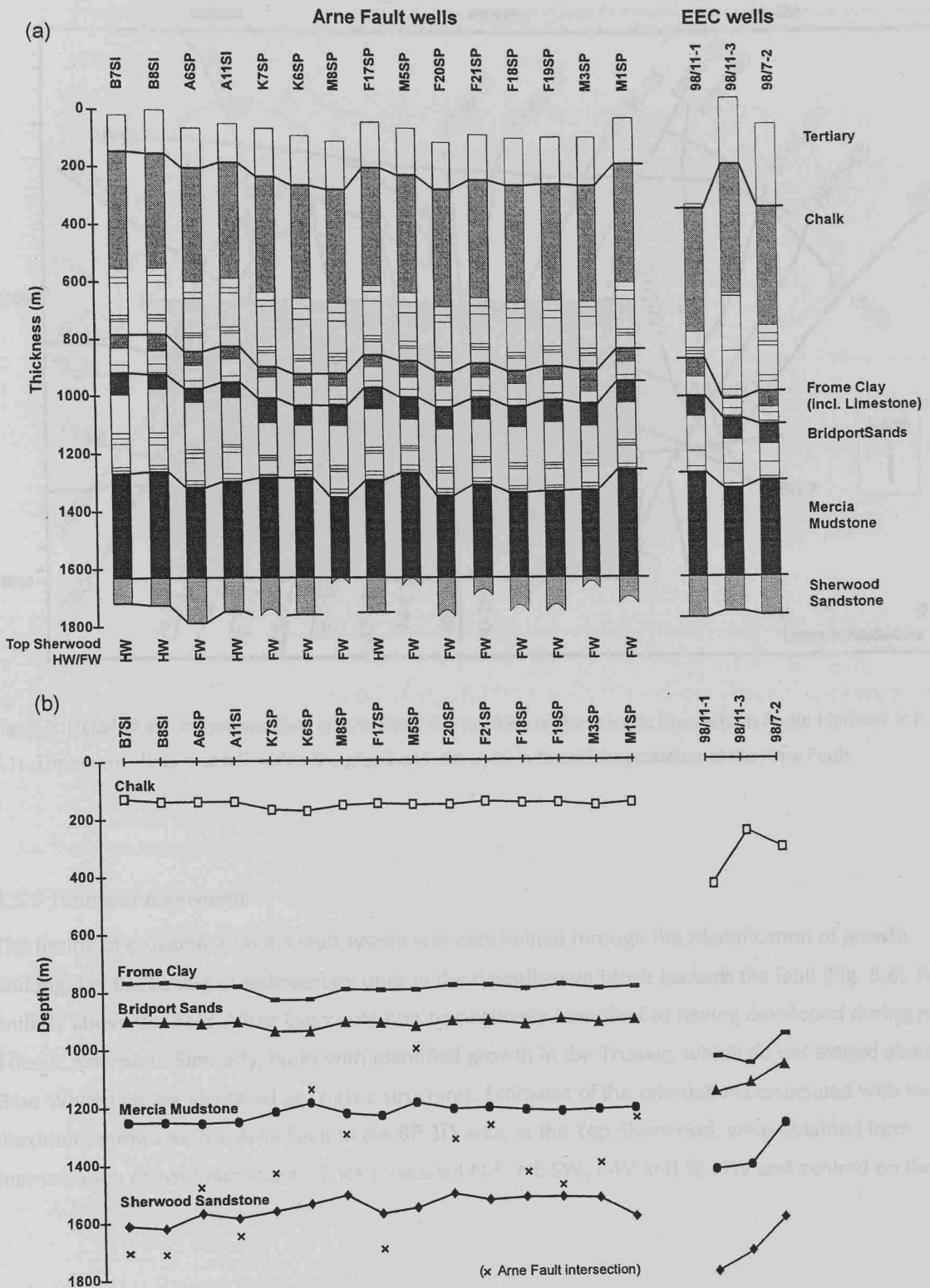


Fig. 5.4. Graphs of (a) unit thickness and (b) depth to the units taken from the wells that intersect the Arne Fault and the exploration wells in the EEC area, arranged in geographical order from west to east. The unit thickness graph is centred on the Mercia Mudstone/Sherwood Sandstone boundary to illustrate the thickness change in the Sherwood Sandstone. A curved line at the column bases indicates those wells which terminated above the base of the Sherwood Sandstone. A hanging-wall (HW) or footwall (FW) position for the well in the Sherwood Sandstone is indicated in (a), and the intersection of the Arne Fault with the well is represented by a cross on (b).

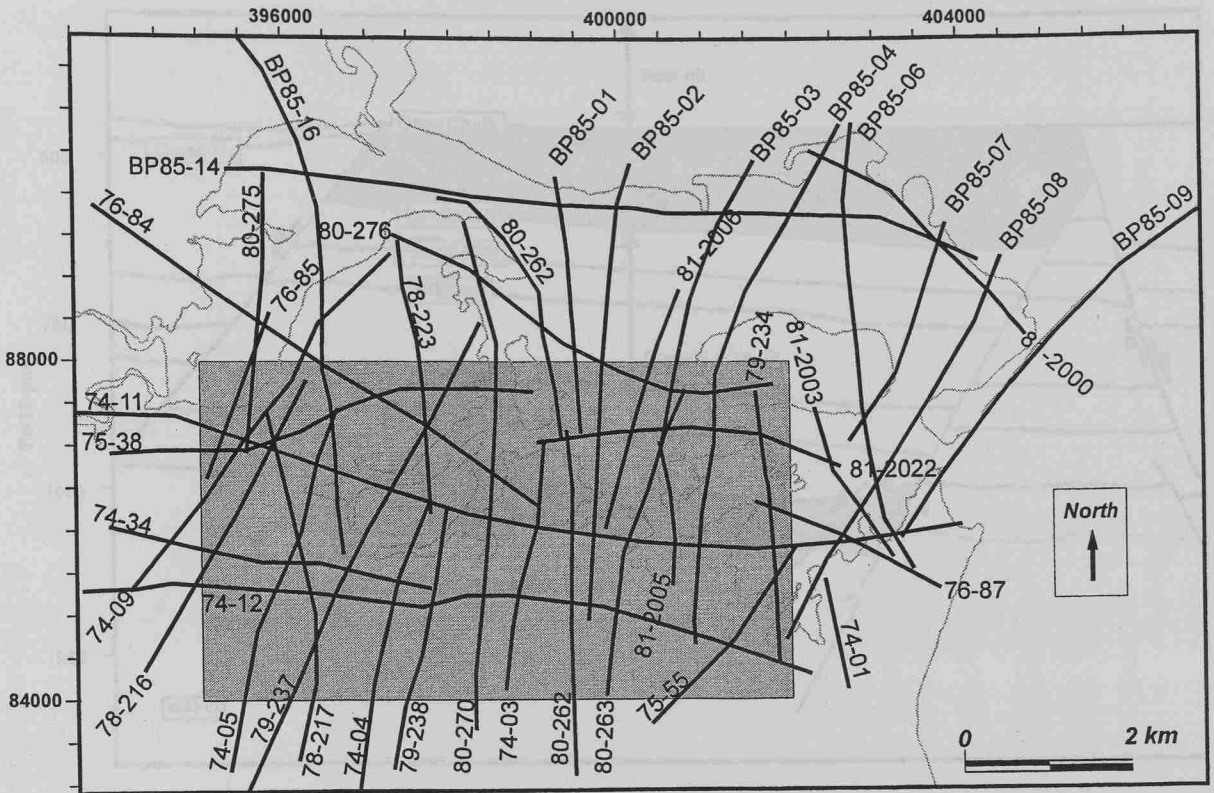


Fig. 5.5. Detail of the 2D seismic data area to show the position of the seismic lines within Poole Harbour (c.f. Fig. 5.1). The seismic lines that fall within the grey box were used in the reinterpretation of the Arne Fault.

5.3.3 Timing of movement

The timing of movement on the fault system was constrained through the identification of growth faulting, *i.e.* thickening of sedimentary units in the downthrown block towards the fault (Fig. 5.6). Faults entirely above the Base White Lias could also be positively identified as having developed during post-Triassic extension. Similarly, faults with identified growth in the Triassic, which do not extend above the Base White Lias are identified as Triassic structures. Estimates of the orientations associated with the maximum throws for the Arne Fault in the BP 3D area, at the Top Sherwood, were obtained from interpretation of synthetic seismic lines orientated N-S, NE-SW, E-W and SE-NW and centred on the fault.

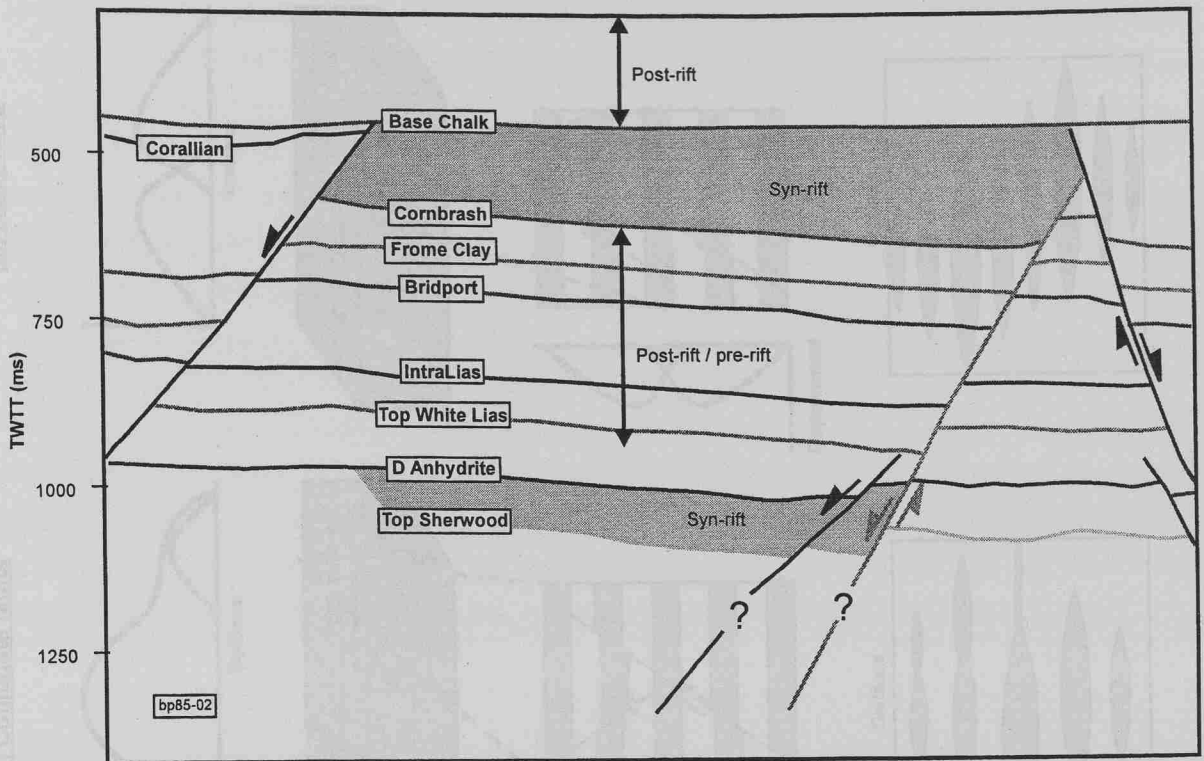


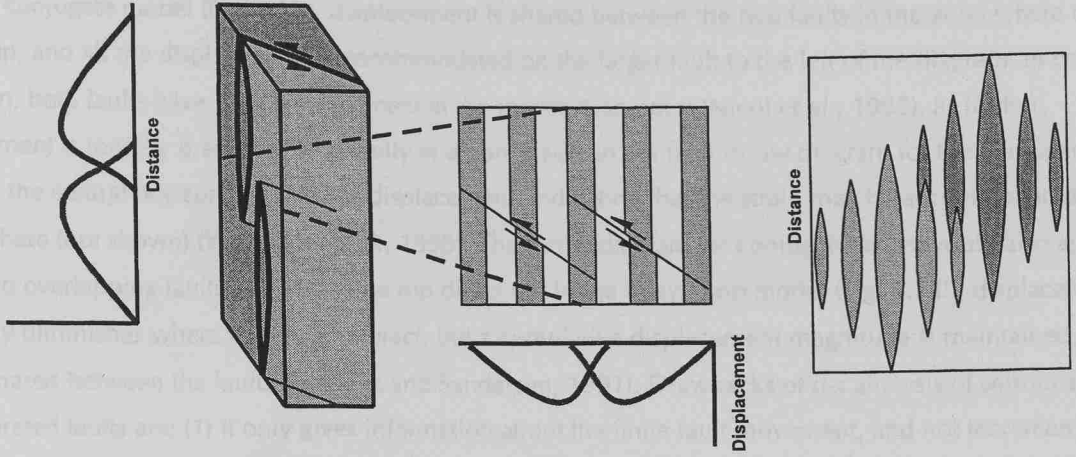
Fig. 5.6. Line drawing of the interpretation of seismic line BP85-02 (Fig. 5.5) with two phases of identified growth faulting: (1) above the Cornbrash pick and (2) in the Mercia Mudstone, below the Zone D Anhydrite.

5.3.4 Displacement-distance and displacement-length analysis

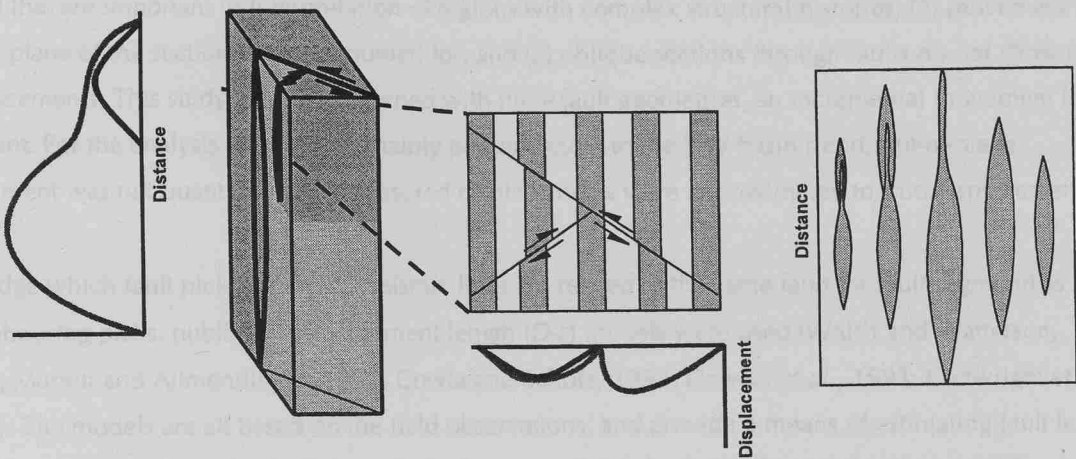
The initial examination of fault geometries was carried out from plots of fault displacement (throw) against distance along the faults (d - x profiles) for each picked horizon. The data were actually plotted as hanging-wall and footwall intersections with the fault planes plotted onto a fault plane map (Allan, 1989) to visualise the fault plane shape. Displacement-distance methods are used to interpret the structural history of fault zones (Muraoka and Kamata, 1983; Williams and Chapman, 1983; Peacock and Sanderson, 1991). For example, displacement minima occur at relay ramps (Peacock and Sanderson, 1991), fault bends and linkage points (Ellis and Dunlap, 1988) (Fig. 5.7), and displacement maxima approximate fault nucleation points (Barnett *et al.*, 1987; Ellis and Dunlap, 1988). The recognition of displacement lows may be important to reservoir juxtapositions and communication analyses. A single, isolated planar fault (Fig. 5.7i) has a smooth, symmetrical displacement-distance profile with a maximum displacement in the centre and zero at each end, both in cross-section and map view (Muraoka and Kamata, 1983; Peacock and Sanderson, 1991).

Fig. 5.7. (overleaf) Relationships between (a) horizontal displacement-distance graphs, (b) fault plane geometry in map view and (c) cross-section, (d) vertical displacement-distance graphs and (e) fault throw diagrams, for (i) simple planar faults, (ii) conjugate faults and (iii) relay ramps.

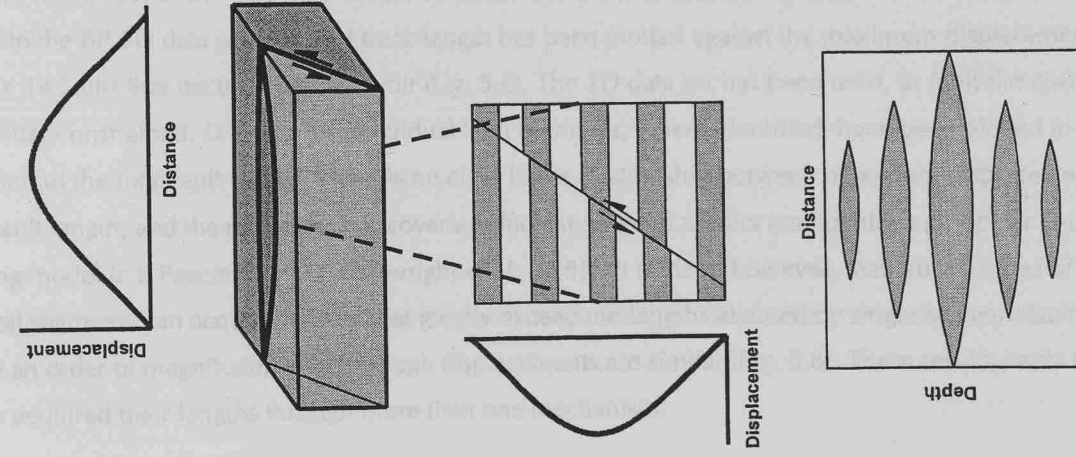
(iii) Relay ramp



(ii) Conjugate faults



(i) Single fault plane



(a) Horizontal displacement-distance graphs

(b) Block diagram of fault

(c) Cross-sectional geometry of fault and (d) displacement-depth graphs

(e) Fault plane solution diagrams

In the conjugate model (Fig. 5.7ii), displacement is shared between the two faults in the zone where they overlap, and all the displacement is accommodated on the larger fault to the left of the diagram. In cross-section, both faults have zero displacement at the intersection point (Nicol *et al.*, 1995), as further movement is initially prevented (e.g. Kelly *et al.*, in press). In the fault throw diagram for the conjugate faults, the central horizon has a lower displacement, indicating that the strain may be accommodated elsewhere (not shown) (Watterson *et al.*, 1998). The throw diagram for conjugate faults would also apply for two overlapping faults with the same dip direction. In the relay ramp model (Fig. 5.7iii), displacement rapidly diminishes where the faults interact, but a cumulative displacement magnitude is maintained, and shared between the faults (Peacock and Sanderson, 1991). Drawbacks of *d-x* analysis of seismically interpreted faults are: (1) it only gives information about the finite fault movement, and not incremental stages that are important in interpretation of regions with complex structural histories; (2) movement out of the plane of the section is not accounted for, and (3) oblique sections through faults do not show true displacements. This study is only concerned with finite fault geometries, so incremental movement is not relevant. For the analysis of 2D lines, mainly perpendicular to the E-W basin trend, out-of-plane movement was not quantifiable, so measured displacements were approximated to true displacements.

To judge which fault picks on the 2D seismic lines are related to the same fault (or fault segment) as neighbouring picks, published displacement-length (*D-L*) models were used (Walsh and Watterson, 1988; Marrett and Allmendinger, 1991; Cowie and Scholz, 1992; Dawers *et al.*, 1993; Cartwright *et al.*, 1995). The models are all based on the field observations, and provide a means of estimating fault length from its maximum throw (and vice versa). To determine the *D-L* relationship for the Sherwood Sandstone faults in the BP 3D data set, the total trace length has been plotted against the maximum displacement for the 14 faults that occur in the reservoir (Fig. 5.8). The 3D data set has been used, as fault dimensions are better constrained. *D-L* data for individual fault segments, where identified, have been plotted in addition to the total fault length. There is no clear linear relationship between maximum displacement and fault length, and the data does not cover a sufficient range to predict confidently a particular *D-L* scaling model (c.f. Peacock, 1991; Cartwright *et al.*, 1995). It is clear, however, that faults formed of several segments can acquire lengths that greatly exceed the lengths attained by single segment faults (by up to an order of magnitude), even though displacements are similar (Fig. 5.8). These results imply that faults acquired their lengths through more than one mechanism.

The *D-L* relationship has been interpreted as linear by Cowie and Scholz (1992) and Dawers *et al.* (1993) (the latter measured average displacement), Walsh and Watterson (1988) found $D \propto L^2$, and Marrett and Allmendinger (1991) argued for $D \propto L^{1.5}$. Significantly, Cartwright *et al.* (1995) observed that variations in the *D-L* relationship of a single fault population are related to the mode of fault growth. An isolated fault that each grew solely through radial propagation would have a greater displacement, relative to length, than a fault that grew through segment linkage (Cartwright *et al.*, 1995). In the formulation of the new interpretations of the reservoir faults the *D-L* scaling laws are applied to the throws at each of the fault picks. If the map distance between two adjacent fault picks was less than the length determined from *D-L* analysis, the two picks were assumed to relate to the same fault (if the orientation was suitable).

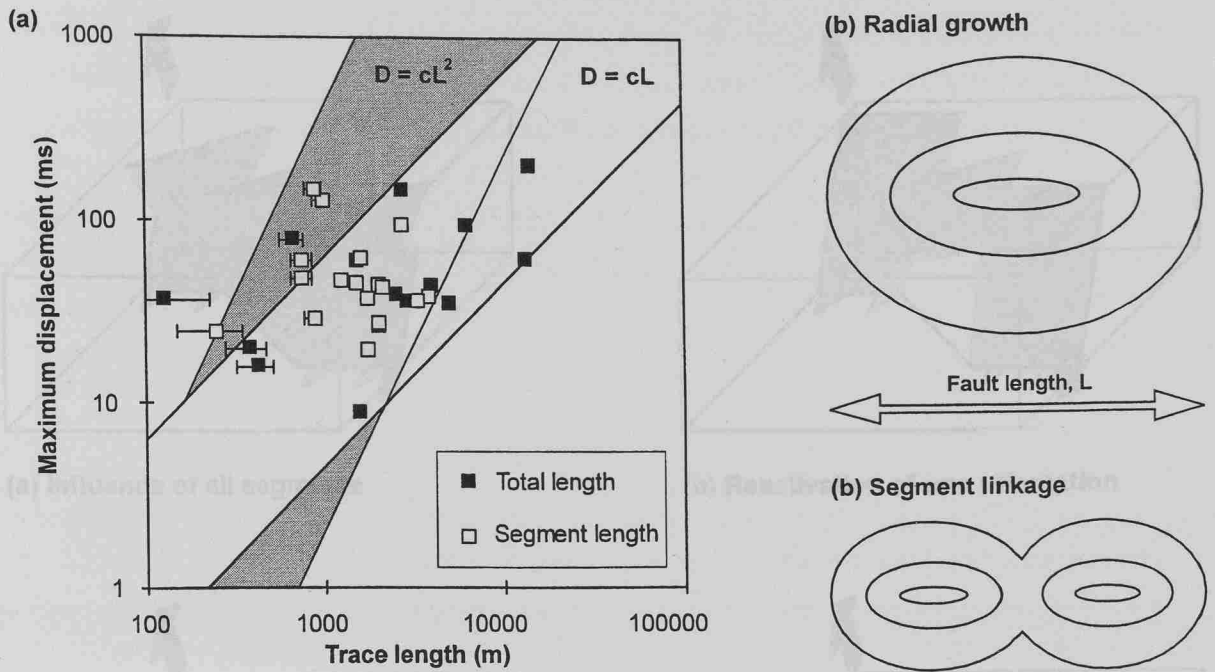
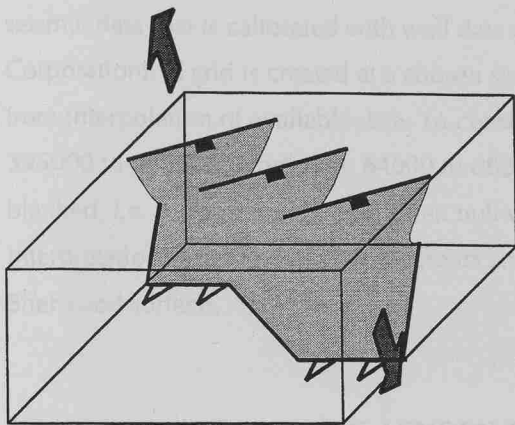


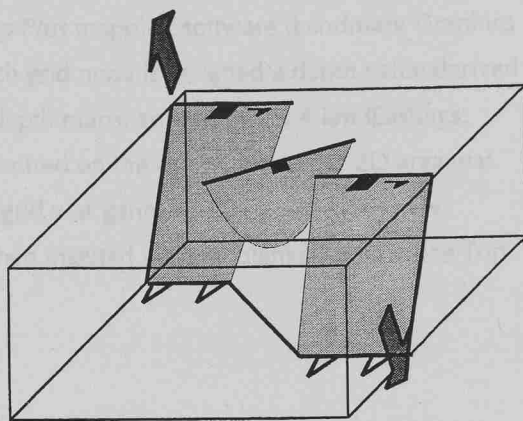
Fig. 5.8. (a) Graph of total trace length against maximum displacement for 14 faults in the Sherwood reservoir (filled squares), and segment trace length against displacement for those faults which have segmented profiles (open squares). Every tenth seismic line was included, equalling a spacing of 125m, so trace length error bars are shown when the symbol width < 250 m. Lines with slopes of 1 and 2 have been drawn on for reference only, as there is no clear linear relationship for this restricted data set. (b) and (c) Throw contours on fault planes of two methods of fault growth, to illustrate how $D-L$ relationships vary with the mode of fault growth (Cartwright *et al.*, 1995).

5.3.5 Pre-Triassic structural geometry

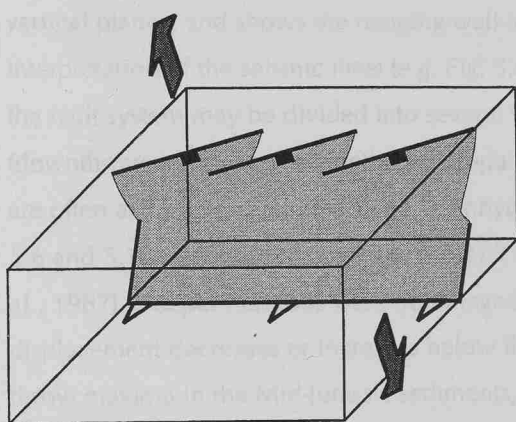
A further consideration in the interpretation of the 2D data is the basement structure and its influence on the orientations of younger faults. Fault orientations within the 3D data areas are more tightly constrained, so the Top Sherwood fault map derived from the 3D data (Fig. 5.2) was used as a guide to the range of possible orientations in the 2D area. Fault trace orientation, and therefore the correlation of fault picks, can be constrained with knowledge of the extension direction associated with the faulting (often perpendicular to fault strike), and the influence of underlying structures (Fig. 5.9). Chadwick (1986) and Lake and Karner (1987) noted that Variscan basement structures were orientated approximately E-W (thrusts) and NW-SE (transfer faults). When there is influence of existing structural trends the faults may not be oriented perpendicular to the extension direction but instead reflect the pre-existing trends. In the case of influence of an inherent structure, a new fault would nucleate within a zone defined by the existing faults (Chadwick, 1986). There is evidence from seismic data that selective normal reactivation of the basement structures may have occurred during the Triassic (Chadwick, 1986; Lake and Karner, 1987) under a NW-SE extension direction (Chadwick, 1986; Lake and Karner, 1987). Hibschi *et al.* (1993) determined a similar extension direction from field analysis of microstructures. A range of structural orientations is therefore possible for the faults in the Sherwood reservoir that reflect the reactivation or influence of the basement faults (Fig. 5.9) (*c.f.* Chadwick, 1986).



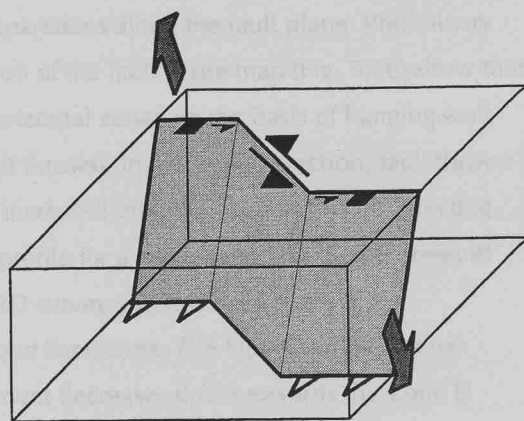
(a) Influence of all segments



(b) Reactivation of one orientation



(d) Influence of one orientation



(c) Reactivation of all segments

Fig. 5.9. Illustration of possible fault orientations associated with NW-SE extension over basement structures oriented E-W and NW-SE, based on Chadwick (1986). (a) The underlying structure influenced the position of the faults but not their orientation. The new faults have an en echelon arrangement that is oriented NW-SE. (b) The E-W orientation was reactivated during extension and continued to grow upwards. Further displacement was accommodated by a relay ramp or a new NE-SW fault segment, that is a reflection of the extension direction. (c) All of the pre-existing faults were reactivated and propagated upward into the Top Sherwood. (d) This example shows how an E-W oriented en echelon zone of NE-SW faults might develop above an E-W fault (Chadwick, 1986).

5.3.6 Arne Fault map construction

The new interpretations of the Arne Fault were drawn by hand onto the previous interpretation of the fault (Fig. 5.2), and the contours were manually adjusted. Contours were deleted if they represented areas that had changed from a hanging-wall to a footwall location, and vice versa, and replaced by continuation of the contour trend in that part of the field. All of the new interpretations agree with well data (Fig. 5.4), so there was no change in the contour pattern in close proximity to the wells. The new fault and contour interpretations were then digitised. The map of the Top Sherwood (Fig. 5.2) is based on

seismic data that is calibrated with well data using the *Zmap Plus* mapping software (Landmark Graphics Corporation). A grid is created at a chosen spacing, and each grid node is assigned a depth value derived from interpolation of available data. To construct the new depth maps, an area of 7 x 4 km (Eastings: 395000 to 402000, Northings: 84000 to 88000, Fig. 5.2) centred on the Arne Fault in the 2D area was blanked, *i.e.* the grid nodes were given null values. A new grid was generated for each of the new interpretations from the digitised contours and faults, and then inserted into the blanked area of the Top Sherwood surface.

5.4 INTERPRETATION OF THE ARNE FAULT

5.4.1 Fault plane map

The fault plane map (Fig. 5.10) is, in effect, a displacement-distance graph in both the horizontal and vertical planes, and shows the hanging-wall and footwall separations along the fault plane. Preliminary interpretation of the seismic lines (e.g. Fig. 5.6) and formation of the fault plane map (Fig. 5.10) show that the fault system may be divided into several vertical and horizontal zones on the basis of hanging-wall (downthrown) and footwall (upthrown) separations (*i.e.* fault throws). In the vertical section, fault throws are often at a minimum in the Zone D Anhydrite level and increased on either side of this horizon (Fig. 5.6 and 5.10), contrary to the expected fault displacement profile for a single fault (Fig. 5.7) (Barnett *et al.*, 1987). Deeper horizons were not imaged at all by the 2D surveys, so it is not known if the displacement decreases or increases below the Top Sherwood Sandstone. The Upper Arne Fault has throw maxima in the Mid-Jurassic sediments, and displacement decreases down towards the Zone D Anhydrite. Throw also decreases upwards into the Cornbrash indicating a vertical fault profile similar to the single fault plane model (Fig. 5.7). The fault system has therefore been subdivided into two vertical segments: the Lower Arne Fault and the Upper Arne Fault. The Lower Arne Fault is defined as the fault segment with maximum throw close to the Top Sherwood (Fig. 5.10). The Lower Arne Fault does not penetrate above the IntraLias at any point within both the 3D and 2D survey areas. In the 2D area the fault is confined mostly to the units below the Zone D Anhydrite, with only a few occurrences above the Top White Lias. The majority of the seismic sections show that the two vertical segments have merged and appear to be a single fault plane, but in some the two segments overstep (e.g. Fig. 5.6).

The horizontal zonation of the fault plane within the 3D area has been described by Ellis (1997), whose results are included (Table 5.3), so the description here concentrates on the 2D survey area (west of 402 000 eastings, Fig. 5.2) for the Lower Arne Fault. It is not clear if the increase in fault plane complexity from the 2D to the 3D survey at the Top Sherwood reflects a more diverse structural history of the onshore area, or due to the difficulties in identifying the fault at greater depths. The fact that the fault also has a complicated profile in the upper, better-imaged horizons suggests a more complicated history.

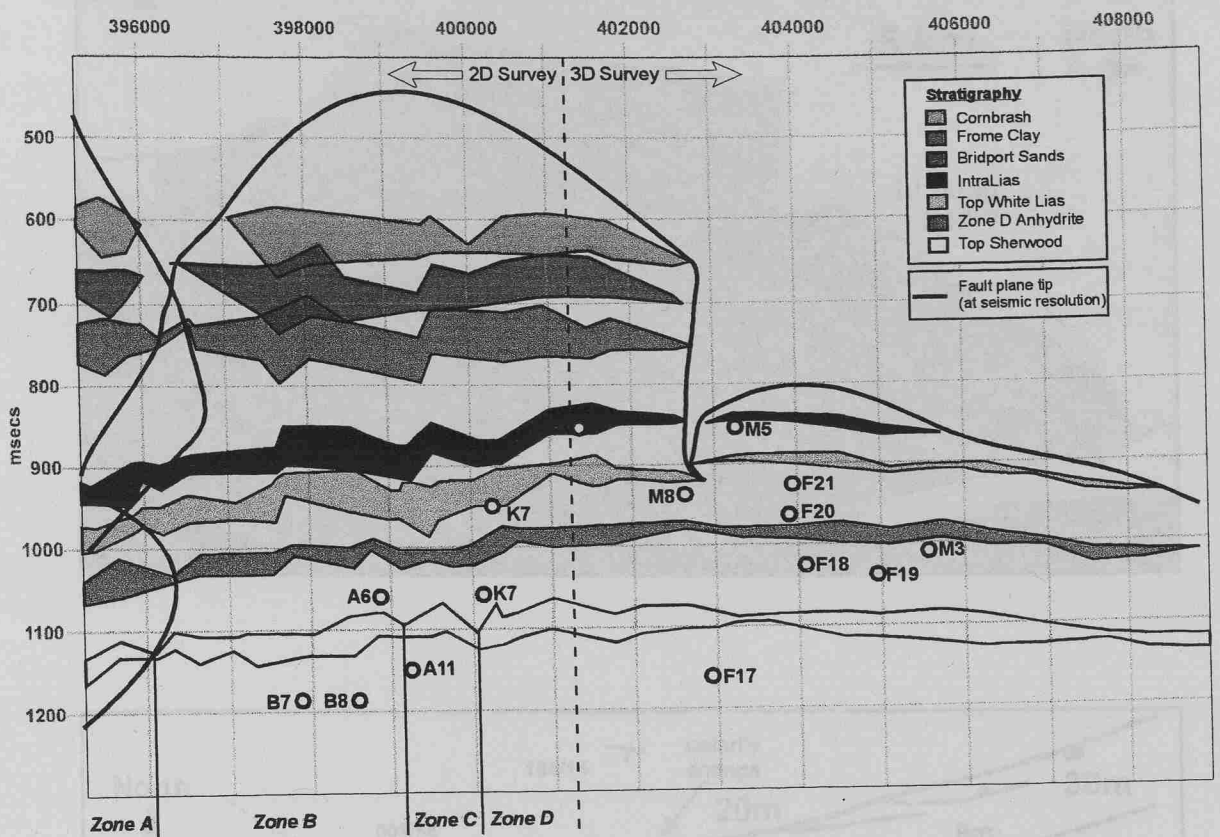


Fig. 5.10. Fault throw diagram incorporating the existing interpretation of the 3D survey area (Ellis 1997), showing the hanging-wall (downthrown) and footwall (upthrown) separations and depths for the Arne Fault system for each of the horizons in Table 5.1. The fault plane has been divided into several vertical and horizontal zones on the basis of fault segmentation (see text for explanation). The Lower Arne Fault has maximum throws close to the Top Sherwood level. The Upper Arne Fault terminates at the unconformity below the Base Chalk, whilst retaining some throw. This indicates that the upper tip-line of the fault propagated further up through the stratigraphy, but was eroded away prior to Chalk deposition. The irregular profiles of the footwalls and hanging-walls within the 2D area may be a function of the lower quality of seismic data on the older surveys.

All of the zone boundaries represent sites of probable segment boundaries and therefore potential relay ramps (Larsen, 1988), where the fault segments may or may not be linked to form a through-going fault plane. The fault zones illustrated in Fig. 5.11 are examples of deformation at fault oversteps, and illustrate two different modes of displacement accommodation and transfer. The relay ramps develop from initially independent fault segments that may eventually link via obliquely oriented faults (Peacock and Sanderson, 1991).

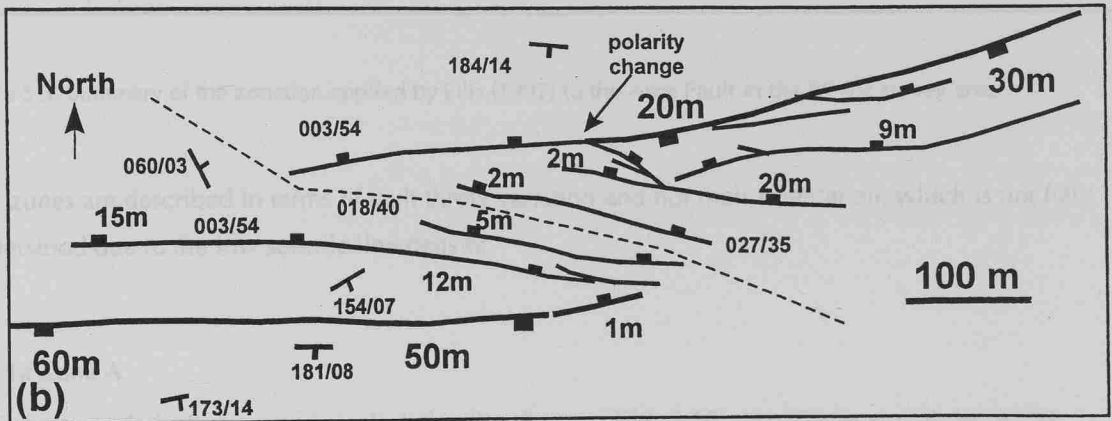
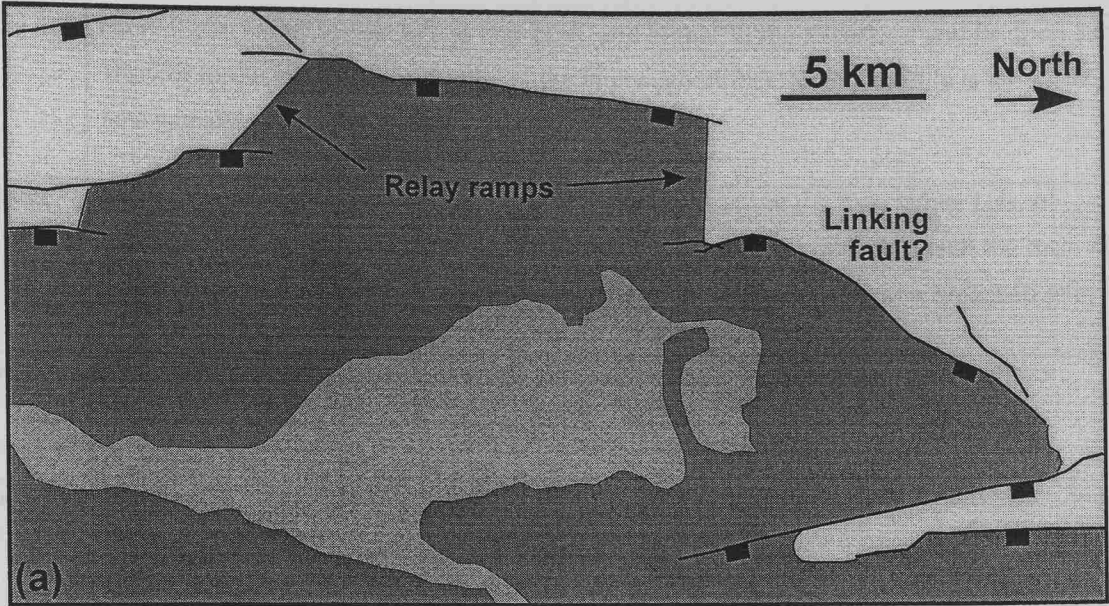


Fig. 5.11. Two maps to illustrate how displacement is transferred from one normal fault to another at an overstep. In both examples it would be possible to follow a route through the relay ramp that does not intersect a fault and, therefore, never encounter a fault-imposed permeability barrier. (a) Map of a relay ramp in the Lower Permian of East Greenland, after Larsen (1988). Displacement is transferred between the fault segments via a zone of rotated bedding. The NW-SE oriented fault in the north of the map may represent a linking fault that has breached a relay ramp. (b) Map of an antithetic relay ramp from Kilve, Somerset (mapped by D.J. Sanderson). Oblique (WNW-ESE) antithetic faults formed to accommodate displacement in the overstep between two E-W trending normal faults. At an antithetic/ synthetic fault intersection point, the dip direction of the bounding fault changes polarity, and the strike of the new fault is similar to that of the original bounding fault. The displacement from the bounding faults is taken up by several en echelon antithetic faults.

Zone 1	Fault displacement lowest in Lias and ZDA, and higher in the Sherwood and Bridport Sands. The low throw values in the middle of the fault suggest that the final profile is an amalgamation of two faults propagating into each other.
Zone 2	Section at a bend in Sherwood fault trace. Either inversion at the Base White Lias, or occurrence of an antithetic fault. Main fault in Bridport is not coincident with the main fault in the Sherwood. This section of the Arne Fault could be interpreted as a breached relay.
Zone 3	Long straight section. Fault cuts at all levels are part of a single fault. The fault throw decreases gradually upwards and tips out in the Lias.
Zone 4	Bend in the Top Sherwood fault trace. Possible inversion with a small (faulted?) anticline at Base White Lias. This section of the fault could be interpreted as a breached relay at Sherwood level.
Zone 5	Fault cuts all structural levels as part of a single fault. The fault throw decreases upwards tipping out at the Top White Lias.

Table 5.3. Summary of the zonation applied by Ellis (1997) to the Arne Fault in the BP 3D survey area.

The zones are described in terms of fault throw variation and not their orientation, which is not fully understood due to the low seismic line density.

5.4.1a Zone A

Only part of this fault segment is included in the diagram (Fig. 5.10), but displacement decreases eastwards from a maximum of 34 ms towards a minimum of 8 ms, that corresponds with the start of Zone B. The maximum displacement for the segment within this zone is actually at the Zone D Anhydrite level with throw decreasing both up- and down-dip. This implies that the fault nucleated above the Top Sherwood, at a shallower depth than the other segments.

5.4.1b Zone B

The fault segment within Zone B continues eastwards for approximately 3 km. In general the fault has a maximum displacement in the centre that decreases both east- and westwards in common with a single fault plane model (c.f. Fig. 5.7), although there are minor deviations. Variations from a smooth fault profile in this zone may represent oversteps between fault segments that were breached during the early stages of deformation.

5.4.1c Zone C

A c.1 km long fault segment has a maximum throw in the centre of the segment that decreases into the zone boundaries either side. The throw at the centre of the faults of 48 ms is actually part of the Upper Arne Fault that has propagated down to the Top Sherwood level either in a gap between two Lower Arne Fault segments, or has overprinted the displacement of the lower fault.

5.4.1d Zone D

The final segment is the western extension of Zones 1 and 2 of the previous study (Ellis, 1997). The sudden change in displacement at the western segment/zone boundary is indicative of the presence of a relay ramp (c.f. Fig. 5.7) (Larsen, 1988), which is supported further by the evidence from Zone C. To the east, the throw increases smoothly towards the centre of the segment.

5.4.2 Seismic calibration with well data

With the exception of M5SP, the wells listed in Table 5.2 indicate fault throws in good agreement with the seismic data. M5SP intersected the fault in the Liassic beds with a throw equivalent to c.23.6 ms. The seismic data at this point suggests a fault throw of < 5 ms, close to the end of one fault segment. Either the well data provide an over-estimation of the fault throw, or the well intersected several faults with throws below the survey resolution with a combined throw of 18.5 ms. Several small faults commonly accommodate a relatively large amount of displacement at the termination of two fault segments in a relay ramp (Fig. 5.11b).

5.4.3 Timing of movement

In the seismic interpretation shown in Fig. 5.6, growth faulting has been identified below the Zone D Anhydrite within the Mercia Mudstone, indicating that the Lower Arne Fault was active during the mid-Upper Triassic. A summary of the timing of syn-sedimentary faulting shows considerable variation, but is apparently related to orientation as the NW-SE orientations in the 3D area suggest the oldest movements (Table 5.4). A NE-SW oriented segment (BP 3D inline: 9250) shows no evidence of growth faulting and must therefore have formed either before or after synsedimentary faulting (Table 5.4). The direction of maximum displacement on the NE-SW oriented fault segment is NW-SE, whilst the E-W fault segments have N-S maximum throw orientations (Fig. 5.12).

Seismic Line	Segment orientation	Pre-rift	Syn-rift	Post-rift
74-09			?Sherwood	
78-216r				
78-217r			ZDA to BWL	BWL
74-05			Top Sherwood to ZDA	Zone D
85-16			Top Sherwood to ZDA	Zone D
74-11			? ZDA to BWL	BWL
79-237			?Sherwood	
74-04				
78-223			Top Sherwood to ZDA	Zone D
80-270r			Top Sherwood to ZDA	Zone D
76-84r				
74-03				Bridport
78-225r				
85-02			Base Mercia to ZDA	BWL
80-263			Base Mercia to ZDA	Zone D
85-03			Base Mercia to ZDA	Chalk
81-2005r	?NW-SE		Intra-Sherwood to ZDA	Zone D
85-04	?NW-SE		Sherwood	BWL
9150	E-W	below Intra-Sherwood	Base Mercia to ZDA	Intra-Lias
9200	E-W/NE-SW	Sherwood	Base Mercia to ZDA	Zone D
9250	E-W/NE-SW		None	
9300	E-W	below Top Sherwood	Base Mercia to Intra-Lias	Fuller's Earth
9350	NW-SE/E-W	below Top Sherwood	Base Mercia to ZDA	Bridport
9400	NW-SE/E-W	below Top Sherwood	Base Mercia to ZDA	Bridport
9450	E-W	below Top Sherwood	Base Mercia to ZDA	Intra-Lias
9500	E-W	below Top Sherwood	Base Mercia to ZDA	Intra-Lias
9550	E-W	below Top Sherwood	Base Mercia to ZDA	Intra-Lias
9600	E-W	below Top Sherwood	Sherwood	Intra-Lias
9650	NW-SE	below Intra-Sherwood	Intra-Sherwood to ZDA	Intra-Lias
9700	NW-SE	below Top Sherwood	Sherwood	BWL

Table 5.4. Details of the segment orientation, and pre-, syn- and post-rift sequences where identified for the Arne Fault. The post-rift deposits identified here relate to the first parallel reflectors above the syn-rift sediments. In some cases the post-rift is also faulted, and forms the pre-rift to shallower package of syn-rift sediments. The blanks in the table represent unidentifiable sedimentary sequences, but do not imply their presence/absence.

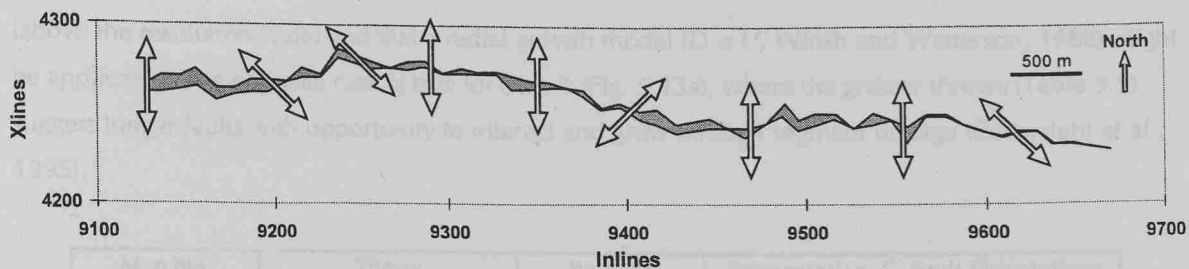


Fig. 5.12. Map of the Arne Fault within the BP 3D area with arrows superimposed to represent the direction of maximum throw for each location.

The growth faulting identified within the Sherwood Sandstone indicates that the first movements on the NW-SE segments occurred prior to deposition of these sediments. The fault continued to grow into the mid-Jurassic, as evidenced in the vertical extent of the fault tip-line. The maximum displacements on the E-W fault segments within the 3D area show that these orientations experienced the final movements, and represent reactivation or continued movement of the Lower Arne Fault during the formation of the upper fault. There are thickened sedimentary sequences adjacent to the Upper Arne Fault in the units above the Cornbrash horizon and below the Cretaceous unconformity (Fig. 5.6). These important observations confirm the hypothesis of at least two separate extensional events (c.f. Stoneley, 1982; Chadwick, 1986; Karner *et al.*, 1987; Lake and Karner, 1987).

5.4.4 New maps

Four new maps of the Lower Arne Fault (Fig. 5.13) have been prepared that honour the well data (Fig. 5.4), but reflect the uncertainties inherent in the interpretation and correlation of sparse seismic data (Fig. 5.3). There are actually 18 possible combinations, if orientation, position and throw are altered (length interpretation is dependent on throw), but four representative maps have been drawn. The four maps were designed primarily to illustrate the range of fault system geometries that could be interpreted from the fault throws (Fig. 5.10), fault locations (Fig. 5.2), orientations of underlying structures (Fig. 5.7) and uncertainty analysis (Fig. 5.3). The secondary aim was to demonstrate how the newly-interpreted fault systems could be located within the scope of the geographical uncertainty (Fig. 5.3).

The maps show combinations of positional, throw, orientation and geometrical variation within the limits imposed by the fault picks (Fig. 5.2) and uncertainties (Fig. 5.3), that together represent highest, medium and lowest cases of probability. The criteria used for each of the models is summarised in Table 5.5. The *D-L* models discussed above have been applied to each fault pick to set the fault length associated with that particular throw, and to assess if adjacent fault picks belong to the same fault. In Map 2 (Fig. 5.13b), for example, the throws have been set at 15 ms below the measured throw (Table 5.5), and all *D-L* relationships predict that the lowest displacement faults are also the shortest (Walsh and Watterson, 1988; Marrett and Allmendinger, 1991; Cowie and Scholz, 1992; Dawers *et al.*, 1993; Cartwright *et al.*, 1995). It is appropriate, therefore, to assume that the shortest faults grew without segment interaction

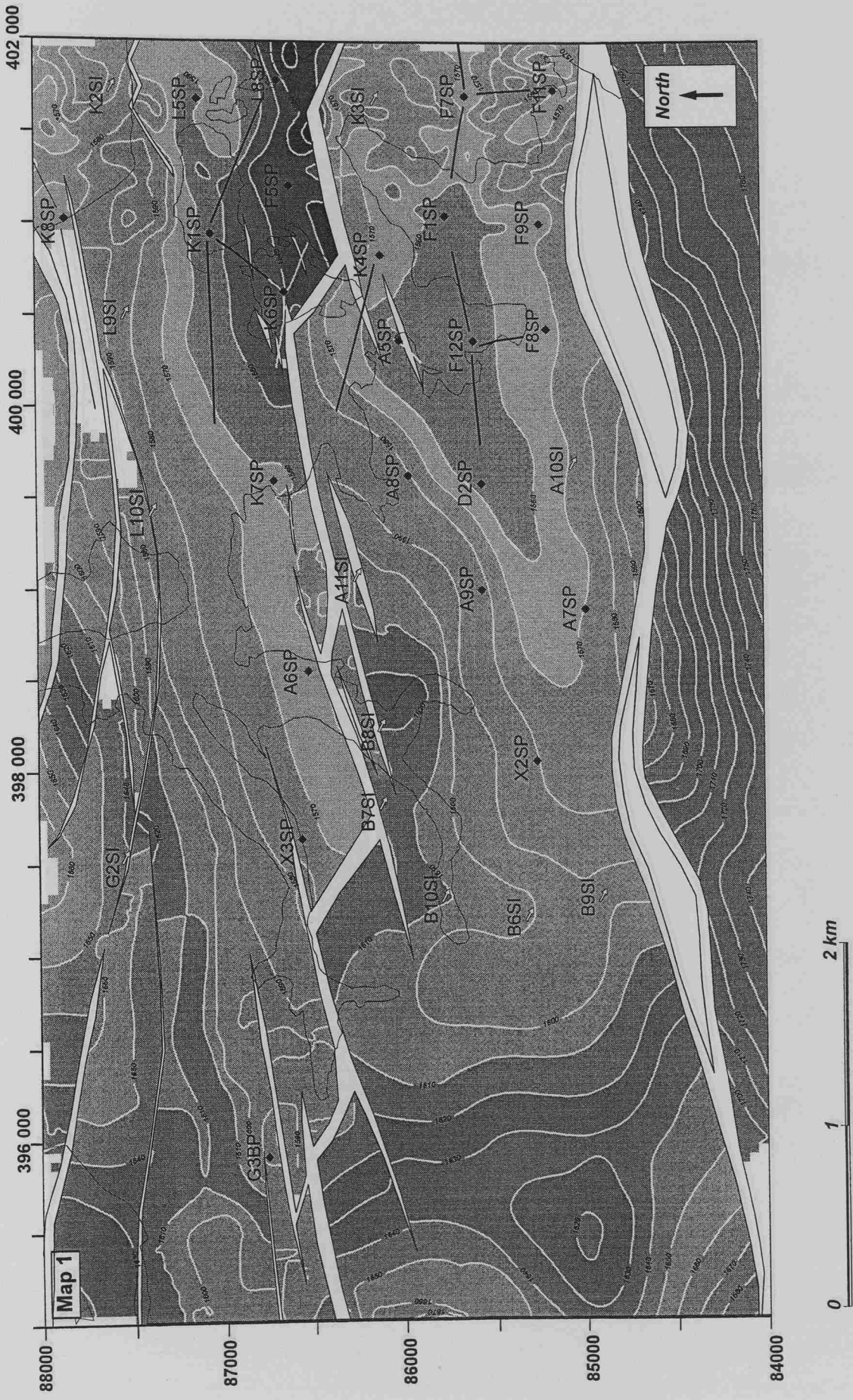


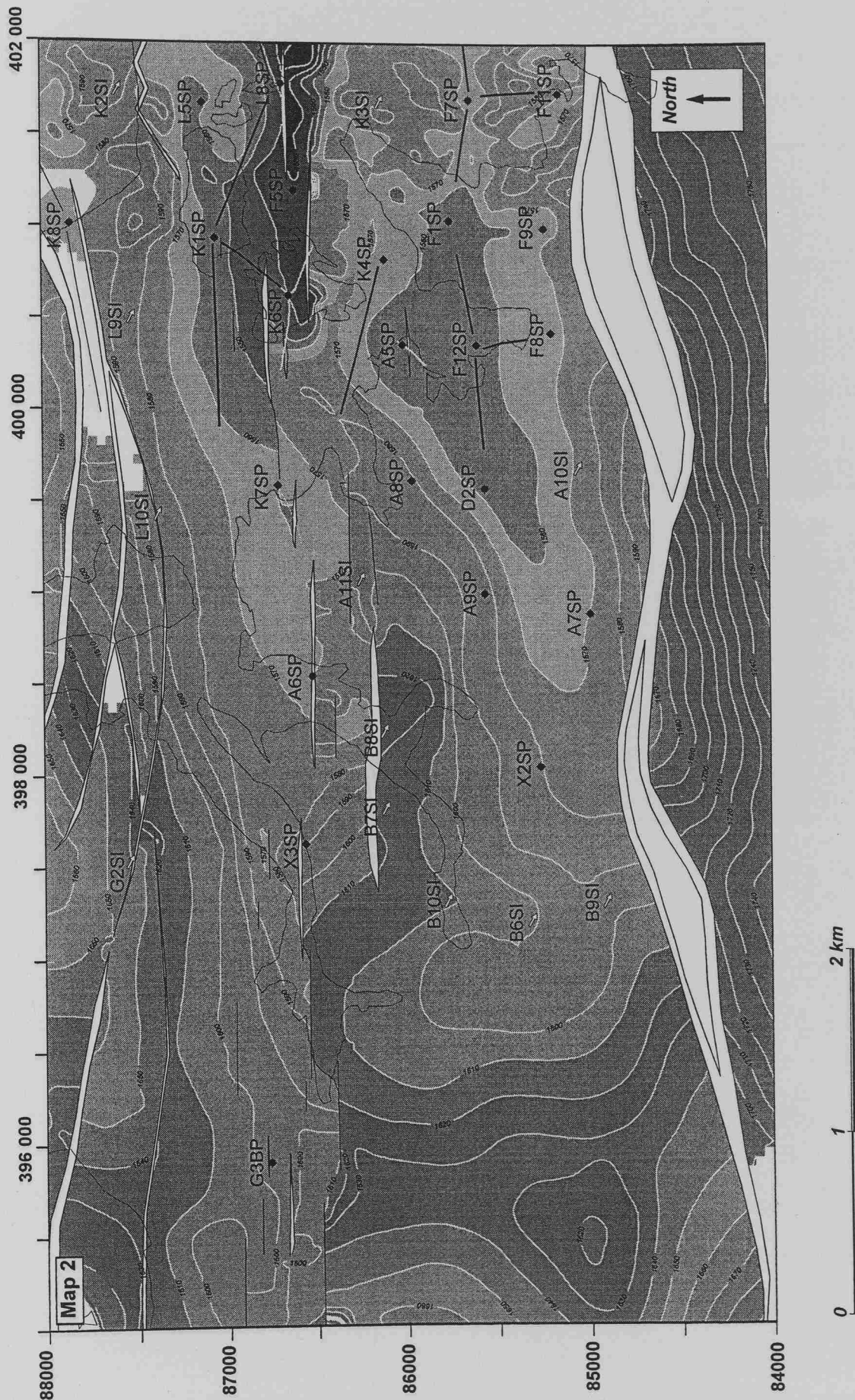
(above the resolution scale) and that a radial growth model ($D \propto L^2$, Walsh and Watterson, 1988) might be applicable. The opposite case is true for Map 1 (Fig. 5.13a), where the greater throws (Table 5.5) suggest longer faults with opportunity to interact and grow through segment linkage (Cartwright et al., 1995).

Map No.	Throw	Position	Segmentation	Fault Orientations
Model 1	Measured + 15ms	Measured	Minimum	ENE-WSW, NW-SE
Model 2	Measured - 15ms	+ 200m North	Maximum	E-W
Model 3	Measured	+ 200m South	Medium	ENE-WSW
Model 4	Measured	Measured	Medium	E-W, NW-SE

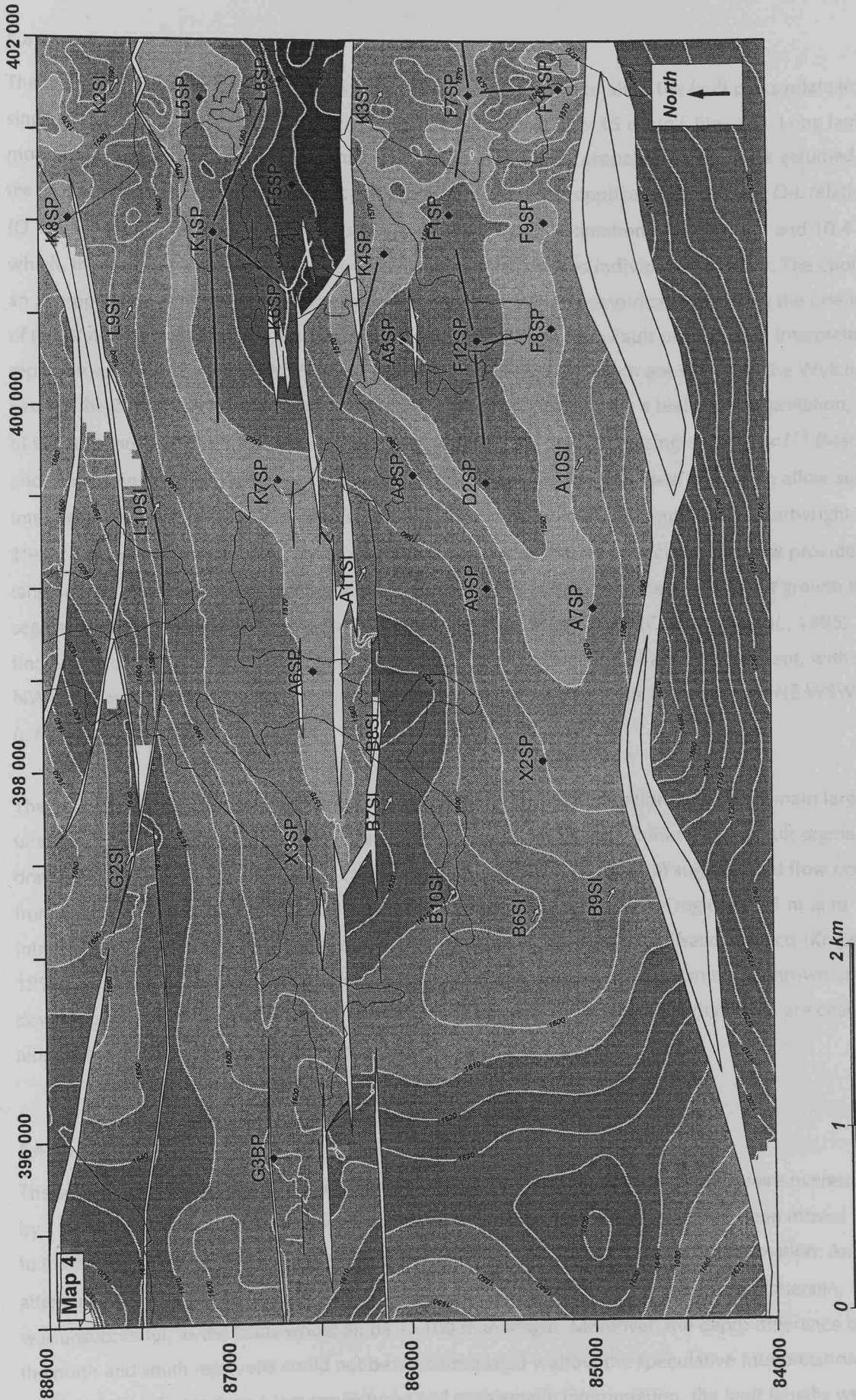
Table 5.5. Criteria for the construction of the four new maps of the Arne Fault within the 2D survey area that reflect position, fault throw, orientation and segmentation uncertainties. The rationale behind the formulation of each map is discussed in the text.

Fig. 5.13. (Following four pages) Four interpretations of the Arne Fault within the 2D area at the Top Sherwood level. The contours represent the depth in TWTT (ms). (a) Map of an interpretation of the Arne Fault system within the 2D seismic studies area with dominant ENE-WSW and NW-SE trends. The two distinct trends are a reflection of the influence of the basement structures suggesting that the heterogeneity of the basement rock influenced the orientation of the NW-SE structures, and the position of the later ENE-WSW faults. (b) Map of an interpretation of the Arne Fault system to include only E-W trending fault segments. The short nature of the many fault segments indicates that there are many places along the fault system where the displacement is at a minimum and would imply that the reservoir is juxtaposed quite irregularly along the fault zone. Linkage between interacting segments, below the resolution of this survey, may indicate that there are several parallel faults on some parts of the system. The existence of linked fault segments would depend on the maturity of the fault system. (c) Interpretation showing an en echelon arrangement of ENE-WSW trending fault segments. This arrangement may reflect an NW-SE extension direction, and the location of an underlying structural trend. The faults are less segmented than in (b), but segment linkage would follow a similar style. (d) Interpretation of the geometry of the Arne Fault that corresponds most closely to the acquired timing data (Table 5.4), the fault orientations and the direction of maximum displacement within the 3D survey area.









5.4.4a Map 1

The map reproduced in Fig. 5.13(a) was constructed by assuming that all of the fault picks relate to a single fault system, and that the fault throws were underestimated by 15 ms (*c.f.* Fig. 5.3). Long faults are more likely than shorter ones to encounter other faults during their propagation, so it was assumed that the faults in this interpretation grew through segment linkage. The application of a linear $D-L$ relationship ($D \propto L$) to the maximum possible throws resulted in fault length estimations between 4.5 and 10.4 km, which, therefore, must relate to the entire fault system rather than to individual segments. The choice of an appropriate $D-L$ model to estimate segment lengths was decided empirically, by using the orientations of the Wytch Farm Fault in the 2D area as a guide (Fig. 5.2). The Arne Fault picks can be interpreted to represent approximately ENE-WSW linear fault segments (Fig. 5.2), which are similar to the Wytch Farm Fault in the 2D area. A fault system dominated by ENE-WSW segments is a realistic interpretation, if all of the faults are part of a single system. However, fault lengths predicted using either $D \propto L^{1.5}$ (Marrett and Allmendinger, 1991) or $D \propto L^2$ (Walsh and Watterson, 1988) are not great enough to allow such an interpretation, and these models are unsuited to faults that grew from segment linkage (Cartwright *et al.*, 1995). The application of a standard $D \propto L^{1.2}$ to the finite fault throws predicts lengths that provide a tangible fit to the geometrical interpretation (Fig. 5.13a), and is based on the premise that growth through segment linkage was followed by radial propagation of the merged faults (Cartwright *et al.*, 1995). The final shape of the fault zone would have evolved during more than one phase of movement, with the NW-SE oriented fault segments reactivated as transfer, or 'short-cut', faults between the ENE-WSW faults (*c.f.* Karner *et al.*, 1987).

The infill well target sizes and locations based on the previous interpretation (Fig. 5.2) remain largely unaffected by Map 1, but the new well trajectory planned from K45P will now cross a fault segment. A drawback of this map is that reservoir communication data (Channon, 1996) suggests that flow occurs from well A11SI to well A6SP (Fig. 5.13a). The Arne Fault has a throw in the region of 35 m at its intersection with A11SI, and juxtaposition analysis indicates only minor sand/sand contacts (Knipe *et al.*, 1994). Similarly, fault seal analysis would suggest poor communication between the upthrown and downthrown side of the fault (Knipe *et al.*, 1994). One possibility, however, is that fluids are channelled along the NW-SE fault between the two wells.

5.4.4b Map 2

The second interpretation (Fig. 5.13b) is based on the presumption that fault throws were overestimated by 15 ms, *i.e.* are assigned to the lower end of the error range. The fault system has been moved 200 m to the north of the interpreted locations (Fig. 5.2), to assess the impact on reserves estimation. An initial attempt to estimate the faults lengths from a radial growth model ($D \propto L^2$, Walsh and Watterson, 1988) was unsuccessful, as the faults would all be < 100 m in length. Moreover, the depth difference between the north and south reservoirs could not be accommodated without the speculative interpretation of multiple faults. To produce a less conjectured and problematic interpretation, the fault lengths were

calculated by using the same $D-L$ relationship for the individual segment lengths in Map 1 ($D \propto L^{1.2}$). The shorter fault lengths reflect the minimum throws used in this model (Fig. 5.13b). The model assumes that the faults grew through segment linkage below the seismic resolution, to acquire lengths and throws above the resolution. The depth difference between the two parts of the reservoir is still accommodated by several isolated (in plan) faults, but there is overlap between them (Fig. 5.13b). Relay ramps, are found between overstepping fault segments. A possible explanation for the geometry of this fault zone is that the low displacement E-W fault segments are part of a deeper fault, close to its tipline.

The size of the northern part of the reservoir is greatly reduced, but the extent of the southern, deeper part is increased. Well A6SP is located to the north of a fault that separates it from A11SI, but adjacent to a low displacement zone where reservoir communication may be largely unaffected. The necessity of drilling an infill well from K4SP may have to be re-assessed, as both the proposed well and the wells already drilled from K6SP are on the same side of the fault zone. In this model there is not a fault that fully compartmentalises the infill well target drilled from K7SP.

On the basis of the approach taken to determine the $D-L$ relationships for the interpretations discussed above, and to maintain consistency, $D \propto L^{1.2}$ has also been applied to formulate the final two models.

5.4.4c Map 3

The map illustrated in Fig. 5.13(c) was produced to show a similar style of fault segmentation to Map 2 (Fig. 5.13b), but with an orientation more in common with Map 1 (Fig. 5.13a). The major geometrical difference between Map 3 (Fig. 5.13c) and Map 1 (Fig. 5.13a) is the lack of a through-going structure. The fault locations in between the ENE-WSW faults that were interpreted as NW-SE short-cut faults on Map 1, have been assigned to ENE-WSW faults on Map 3. All of the faults in this model have a common ENE-WSW orientation with significant overlap between the faults. The measured throws were used in this interpretation, but the faults were moved south by 200 m to investigate the effect on the estimated hydrocarbon volumes. The effect was to increase greatly the northern part of the reservoir at the eastern end of the map, but not affect significantly the western end.

For the most part, there are no through-going faults that interfere with the communication of the two sides of the reservoir, particularly at the eastern end of the map. An advantage of this model is that it provides a simple one-event mechanism of fault development that has a similar orientation to the Wytch Farm Fault. However, if the Lower Arne Fault and the E-W striking Upper Arne Fault form a single fault zone, there ought to be more overstepping fault segments, and more complex geometries, in the vertical section than currently detected.

There is some disruption to the planned infill well trajectories, as the eastern target from K1SP is greatly reduced, and the new well from K4SP now terminates in between two faults. The sizes of the target from K7SP and the western target from K1SP is enlarged and not affected by any major faults.

5.4.4d Map 4

The final interpretation of the Arne Fault (Fig. 5.13d) was produced to combine the linkage style of Map 1 (Fig. 5.13a) within an interpretation dominated by E-W oriented faults. The fault throws and lengths are based on the measured values, and so the faults in this model have similar dimensions to those in Map 3 (Fig. 5.13c). Map 4 was formulated to correspond closely with both the timing data and fault orientations within the 3D area (Fig. 5.2), and also the measured fault locations. A model for the formation of the faults is similar to the evolution of Map 1 (Fig. 5.13a) with the initial development of NW-SE fault segments with a sinistral strike-slip component, following one of the basement trends. The E-W faults opened during a later extensional phase, with the NW-SE faults reactivated as predominantly dip-slip linking faults. The fault orientations illustrated in Fig. 5.13(d) do not, however, conform to the orientations of other faults in the 2D area, which suggests that this interpretation is the least probable.

A6SP and A11SI occupy similar positions relative to faults in this model as in Map 1 (Fig. 5.13a), and so a similar argument concerning their communication may be applied. In this model, however, there is an alternative fault-free route that involves flow up the dip of a proposed relay ramp between two of the E-W fault segments (Fig. 5.13d). The proposed new well trajectory from K4SP will also cross a part of the Arne Fault in this model.

5.4.5 Volumetrics

The new maps (Fig. 5.13) show that there is considerable variation in the possible shape of the Top Sherwood depth contours, indicating changes in reserves distribution: Alteration of the position or geometry of the Arne Fault may impact on the estimated hydrocarbon volumes in both its hanging-wall and footwall. Calculations of the STOOIP (Stock Tank Oil Originally In Place) were carried out for each of the four new interpretations (Fig. 5.13a-d), and the equivalent 7 x 4 km area on the existing map (Fig. 5.2), using a macro in *Zmap Plus*. The STOOIP is derived from the product of the area (bounded north by the Northern Fault and south by the Wytch Farm Fault), oil column height, porosity, hydrocarbon saturation and the recovery factor, divided by a formation volume factor. The STOOIP was estimated individually for the 10 vertical zones that form the Sherwood Reservoir (McKie et al., 1998; Hogg et al., in press). The graphs in Fig. 5.14 show changes in the amount of STOOIP for each of the four models; most of the changes are concentrated in Zones 70 and 80 of the Sherwood Reservoir.

The results indicate that the geometry of the fault does not significantly affect the hydrocarbons volumes (Fig. 5.14), as similar values are indicated by the two fault systems that occupy the measured fault locations (Map1, Fig. 5.13a and Map 4, Fig. 5.13d). The greatest reduction in reserves is predicted for Map 2, which has increased the size of the southern reservoir at the expense of the northern part (Fig. 5.13b), although there is only minimal linkage between the faults. There is a predicted difference of c. 27 mb between the two models where the fault system has been placed at the extremes of the positional uncertainty (Map2, Fig. 5.13b, and Map 3, Fig. 5.13c).

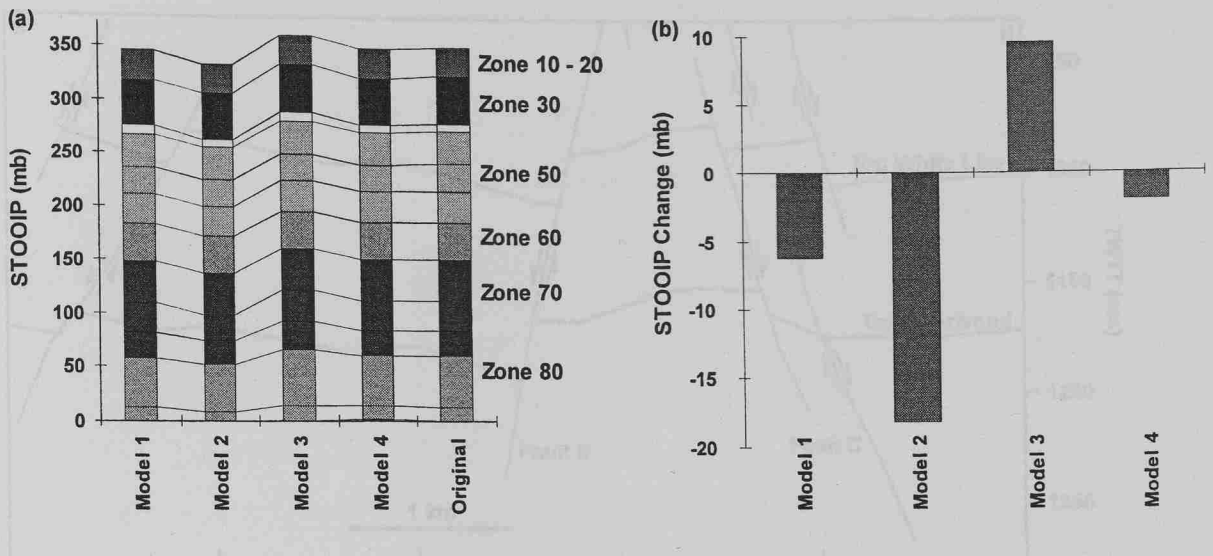


Fig. 5.14. (a) Graph to illustrate the STOPIP (Stock Tank Oil Originally In Place) for each of the four new fault geometries (Fig. 5.13). Most of the changes are confined to the lower zones. The difference between the two extremes is approximately 27 mb. (b) Graph to show the amount of change from the original interpretation (Fig. 5.2) in total volume for each of the models.

5.5 EEC 3D SURVEY AREA RESULTS

The aim of this part of the study is to provide a new interpretation that ties in with available well data and provides a good correlation with the well-constrained BP survey area.

5.5.1 Interpretation based on TWL pick

An initial interpretation based on the depth to the persistent Top White Lias reflector on the cross-lines and in well 98/7-2 (Fig. 5.15) provided a successful correlation north of the Wytch Farm Fault, but proved unsatisfactory in the vicinity of well 98-11/1. The Top Sherwood horizon was too shallow to match both the depths recorded in the well log and those for the BP seismic data to the west (Fig. 5.16). Additionally, this interpretation accounts for neither the thicker Mercia Mudstone sequence, nor the deeper Top Sherwood in well 98/11-1 compared to well 98/11-3 (Fig. 5.4).

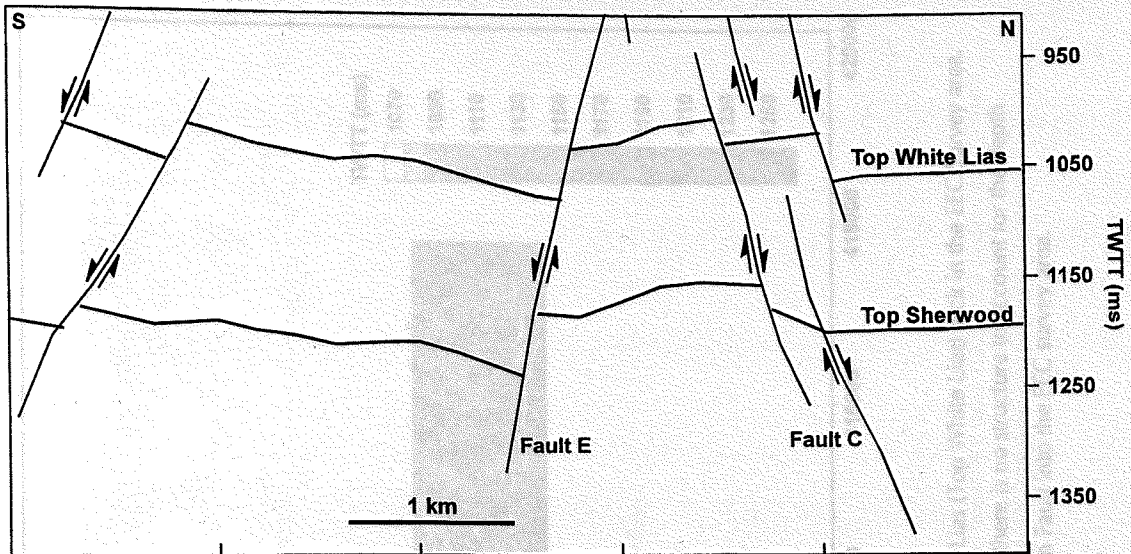


Fig. 5.15. Interpretation of seismic line 300 to which illustrates the depth to the Top Sherwood when based on the assumption that the prominent reflector represents the Top White Lias across the entire survey. The Top Sherwood is too shallow in the extreme south of the section to tie in with the BP survey, and the well data.

5.5.2 Alternative interpretation

A re-interpretation of the southern part of the survey area was carried out (Fig. 5.17), calibrated to the horizon depths recorded in well 98-11/1 (Fig. 5.4). An implication of this interpretation is that the strong, consistent reflector is not exclusively related to the Top White Lias through-out the survey, but to a shallower event, such as the Blue Lias (Fig. 4.4 and Fig. 5.18). Well 98/11-1 is now in the hanging-wall of a previously unidentified south-dipping fault (Fault D) which traverses the survey with a throw of c. 100ms (). A hanging-wall location is an ideal explanation for the deeper horizons in the well, and also may account for the thicker Mercia Mudstone sequence as a result of growth faulting; thickening of the Zone D Anhydrite - Top Sherwood interval occurs adjacent to other faults in the area. The Top Sherwood pick to the north of the fault is calibrated to wells 98/7-2 and 98/11-3 (Fig. 5.4 and 5.17) and is also consistent with the pick of Ellis (1998) and the BP 3D survey area. The depths to the Top Sherwood horizon south of Fault D are similar to the reservoir depths picked in the BP 3D survey across the gap to the west (Fig. 5.17), and thereby provides a more realistic interpretation than one based on the consistent reflector thought to represent the Top White Lias.

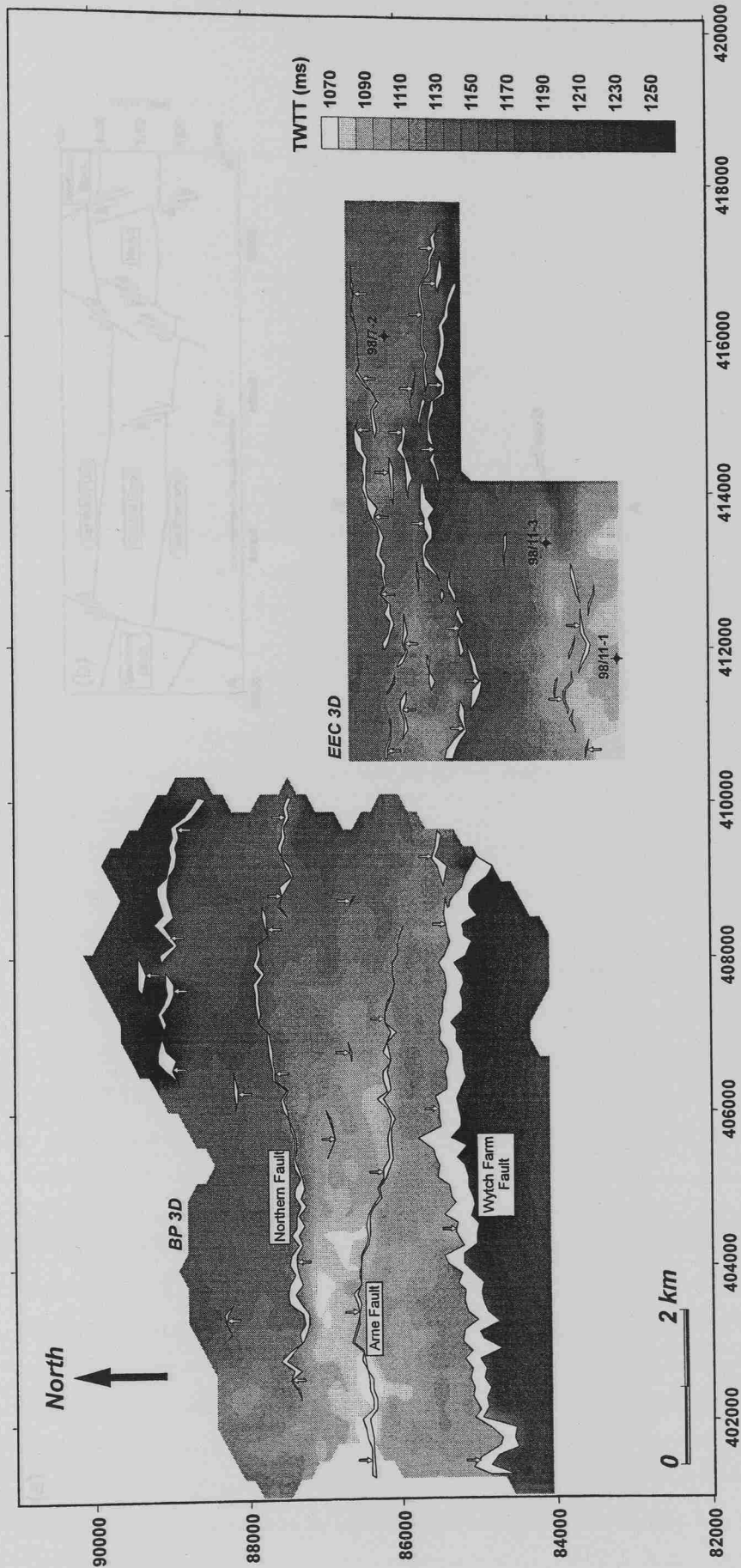


Fig. 5.16. Map of the Top Sherwood horizon pick based on the consistent Top White Lias (Top White Lias) pick in the EEC Survey area. The reservoir horizon is too shallow when compared with well data south of the Wytch Farm Fault, but that there is no structure to account for the depth difference between the two surveys. In this interpretation there is no obvious continuation of the Wytch Farm Fault into the EEC survey area.

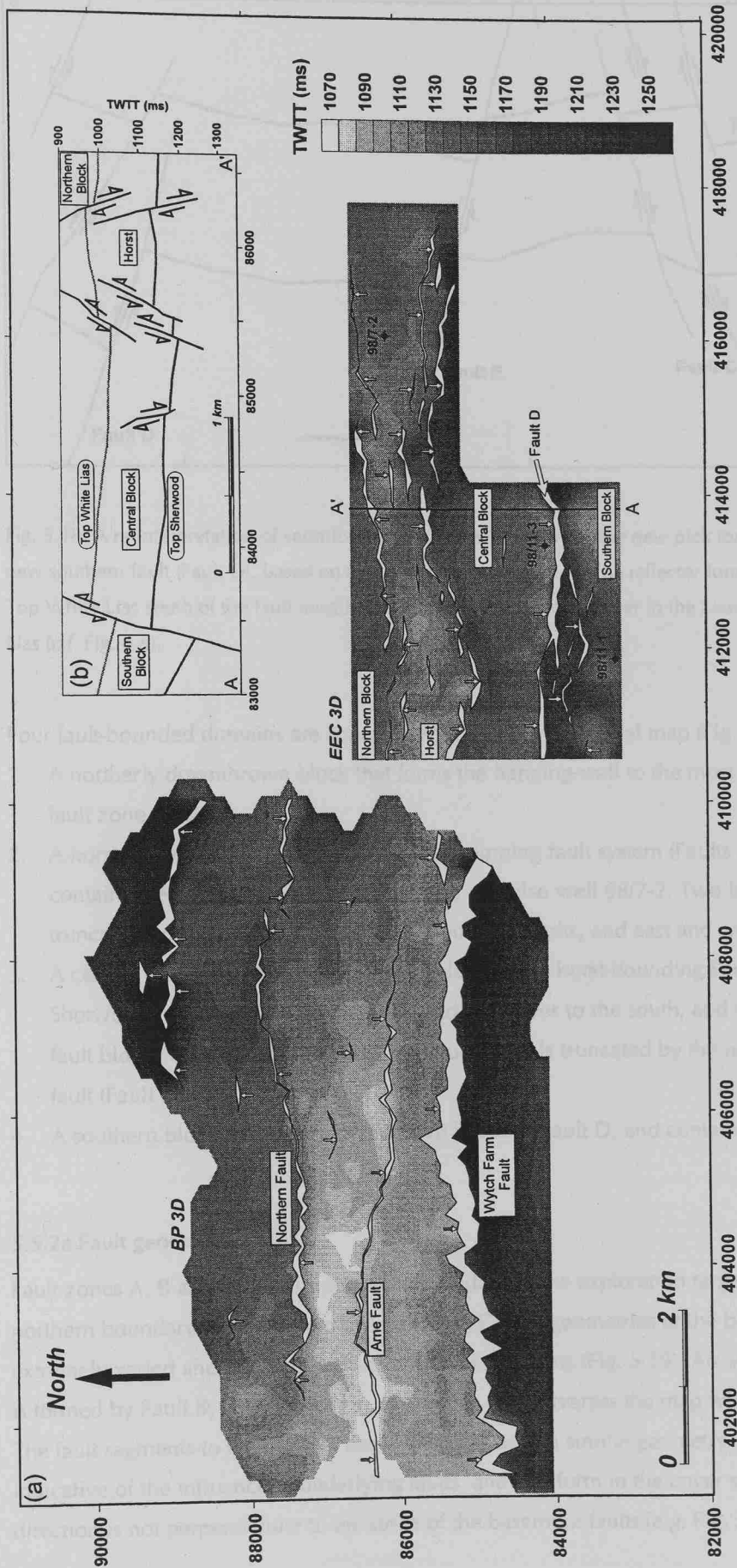


Fig. 5.17. (a) A new interpretation of the Top Sherwood horizon based on the new horizon pick (Fig. 5.18). The horizon is now calibrated to the 98/11-1 well data, and there is also a much tighter correlation with the depth to the Top Sherwood picked on the BP 3D data. (b) Synoptic cross-section through the EEC 3D survey to illustrate the division of the area into four distinct fault-bounded zones.

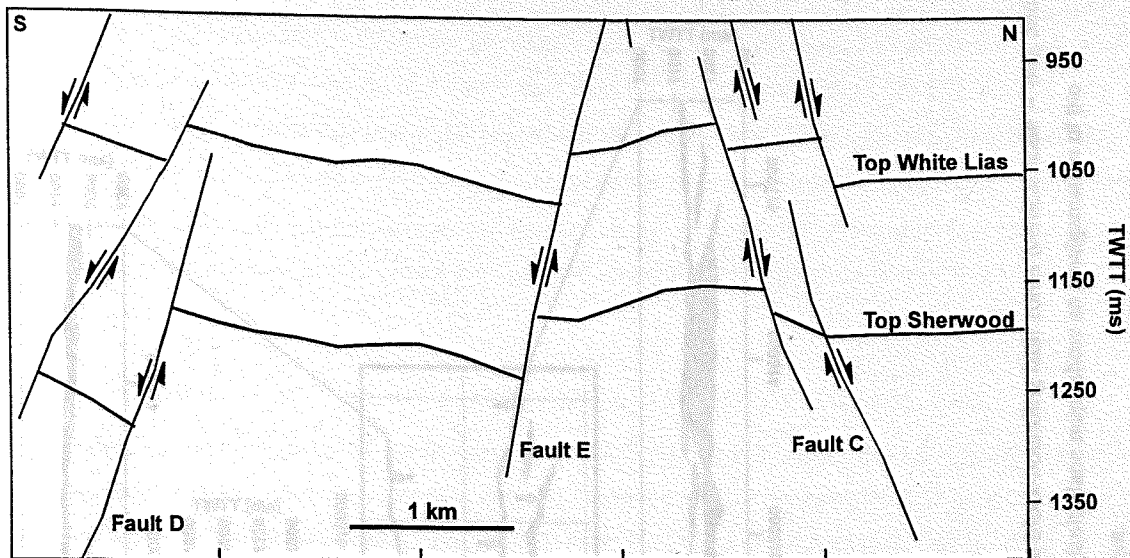


Fig. 5.18. A re-interpretation of seismic line 300 (Fig. 5.15) to show the new pick for the Top Sherwood, south of the new southern fault (Fault D), based on the data from well 98/11-1. The reflector formally considered to represent the Top White Lias south of the fault must in fact relate to a boundary higher in the Liassic stratigraphy, such as the Blue Lias (c.f. Fig. 4.4).

Four fault-bounded domains are apparent from the new structural map (Fig. 5.19). From north to south:

1. A northerly downthrown block that forms the hanging-wall to the most northerly, and north-dipping, fault zone (Fault C).
2. A horst block between Fault C and a south-dipping fault system (Faults A, B and E). The horst block contains the exploration target in this area, and also well 98/7-2. Two individual structural crests are truncated north and south by the horst-bounding faults, and east and west by dip closures.
3. A central block that is the downthrown block of the horst-bounding Faults A, B and E. The Top Sherwood pick is deeper to the north, and shallower to the south, and resembles a rotated domino fault block. The southern extent of this fault block is truncated by the newly identified south-dipping fault (Fault D).
4. A southern block that is the downthrown block to Fault D, and contains well 98/11-1.

5.5.2a Fault geometries

Fault zones A, B and E form the southern boundary of the exploration target in the horst, and the northern boundary is constrained by Fault zone C. The geometries of the block-bounding fault zones are extremely varied and often composed of several segments (Fig. 5.19). An array of normal fault segments is formed by Fault B, and parts of Faults C and E, and traverses the map with an ENE-WSW orientation. The fault segments to the north of the B-C-E array have a similar geometry. Echelon patterns are often indicative of the influence of underlying faults, and can form in the cover sequence when the extension direction is not perpendicular to the strike of the basement faults (e.g. Fig. 5.9) (Chadwick, 1986).

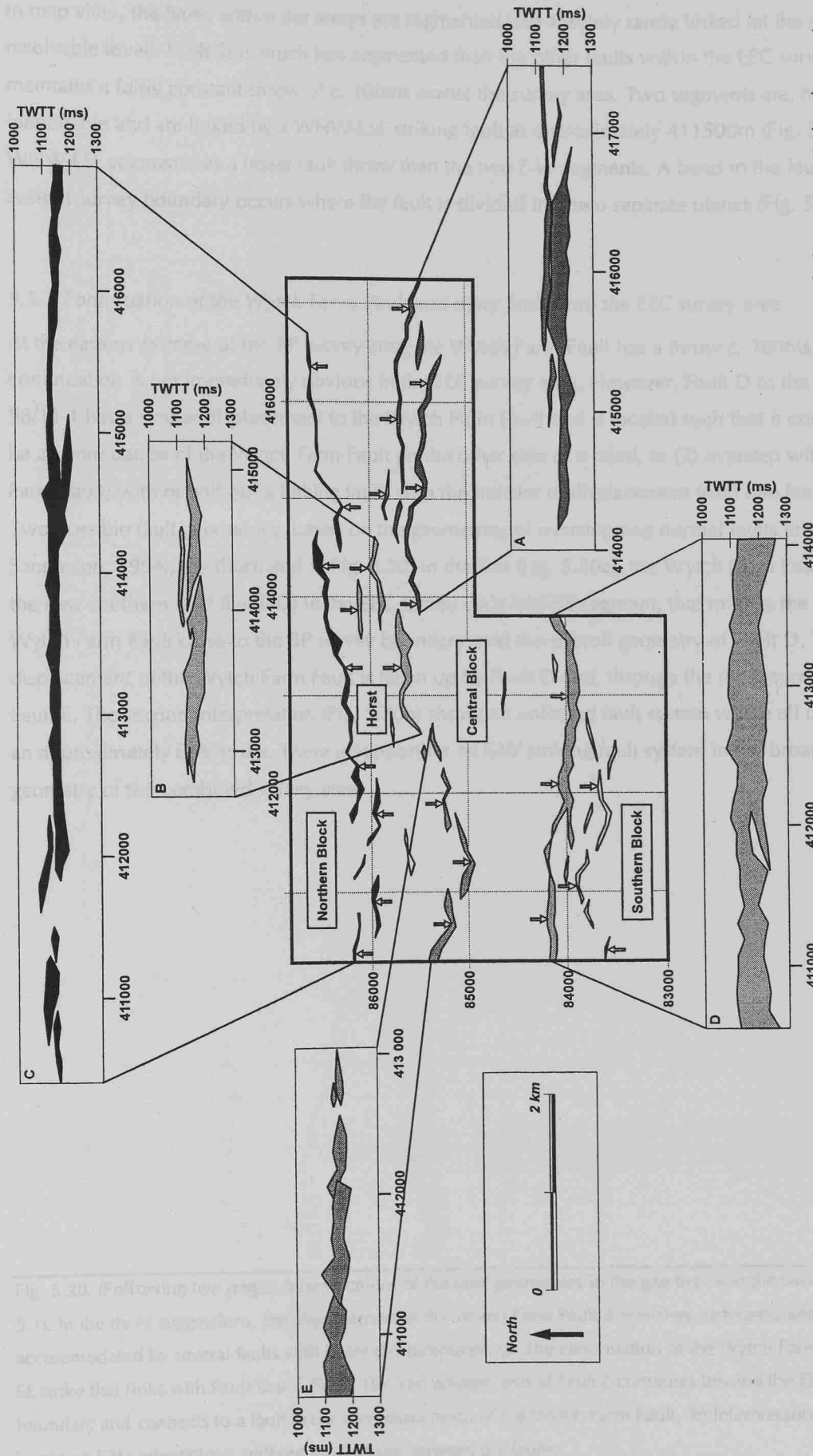


Fig. 5.19. Fault plane maps showing the vertical hanging-wall/footwall separations at the Top Sherwood level for the block-bounding fault zones (vertical scale = ms), and their location on a map of the interpreted faults in the EEC survey area (the arrows indicate fault dip direction). The fault plane maps show an amalgamation of the displacement at sites of segment overlap where it was not possible to determine accurately the throw of each segment.

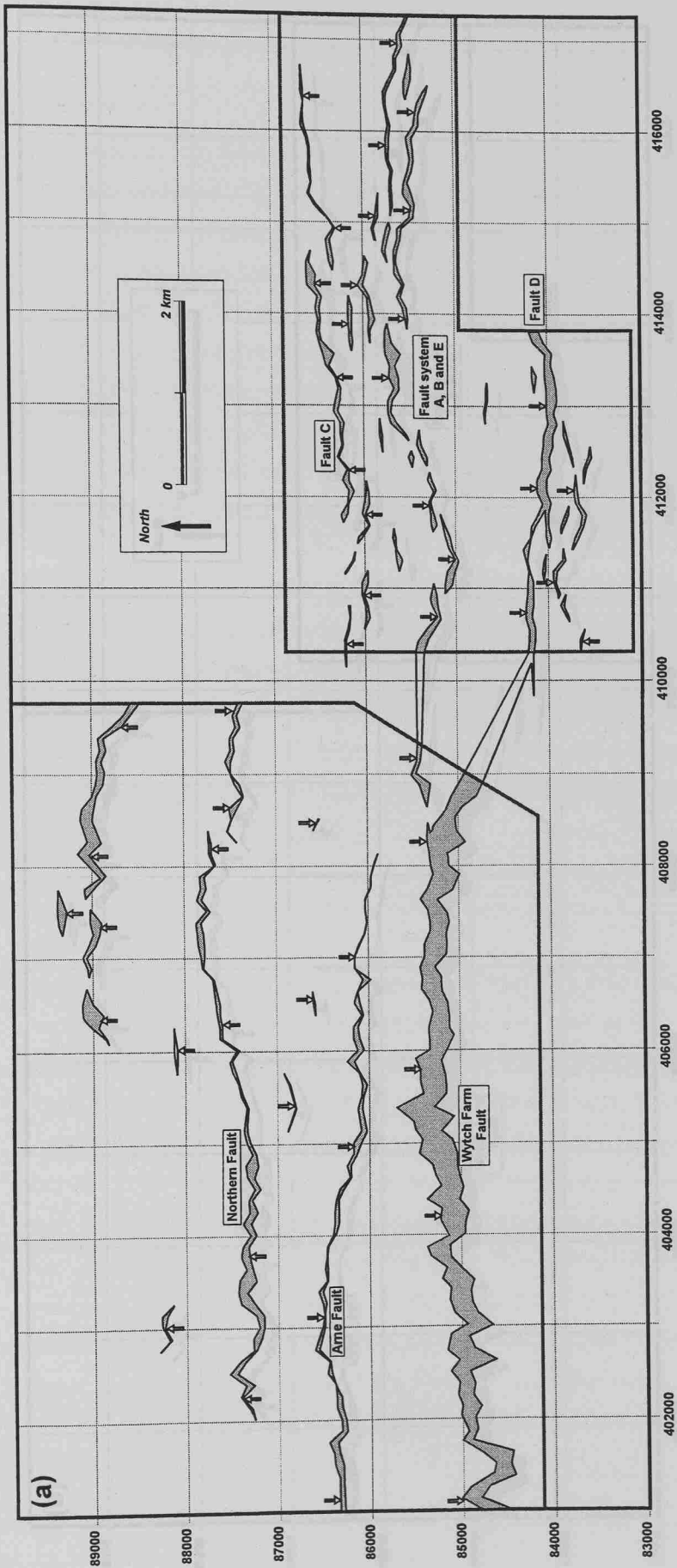
In map view, the faults within the arrays are segmented and are only rarely linked (at the seismically resolvable level). Fault D is much less segmented than the other faults within the EEC survey area, and maintains a fairly constant throw of c. 100ms across the survey area. Two segments are, however, identifiable and are linked by a WNW-ESE striking fault at approximately 411500m (Fig. 5.19). The WNW-ESE segment has a lesser fault throw than the two E-W segments. A bend in the fault close to the eastern survey boundary occurs where the fault is divided into two separate planes (Fig. 5.19).

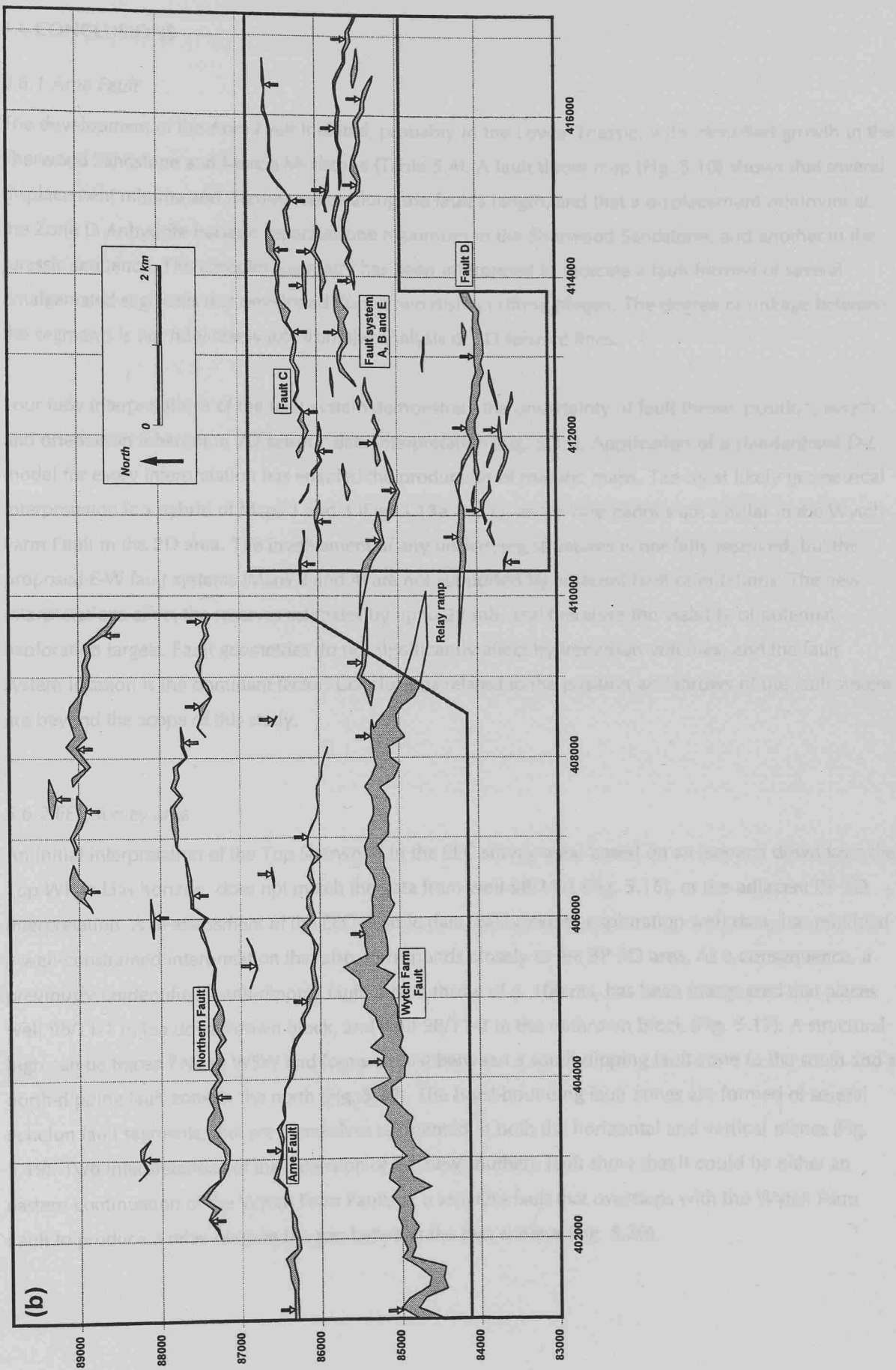
5.5.3 Continuation of the Wytch Farm Fault and other faults into the EEC survey area

At the eastern extreme of the BP survey area, the Wytch Farm Fault has a throw c. 100ms, but its continuation is not immediately obvious in the EEC survey area. However, Fault D to the north of well 98/11-1 has a similar displacement to the Wytch Farm Fault and is located such that it could either: (1) be a continuation of the Wytch Farm Fault on the other side of a bend, or (2) overstep with the Wytch Farm Fault, with or without a linking fault, with the transfer of displacement from one fault to the other. Two possible fault geometries, based on the geometries of overstepping normal faults (e.g. Peacock and Sanderson, 1994), are illustrated in Fig. 5.20. In the first (Fig. 5.20a), the Wytch Farm Fault connects to the new southern fault (Fault D) in the EEC survey via a NW-SE segment, that mimics the strike of the Wytch Farm Fault close to the BP survey boundary, and the overall geometry of Fault D. The displacement of the Wytch Farm Fault is taken up by Fault D and, through the development of a branch, Fault E. The second interpretation (Fig. 5.20b) shows an unlinked fault system where all of the faults have an approximately E-W strike. There is support for an E-W striking fault system in the broad structural geometry of the combined survey areas.



Fig. 5.20. (Following two pages) Interpretations of the fault geometries in the gap between the two 3D surveys (Fig. 5.1). In the three suggestions, the displacement of the Wytch Farm Fault diminishes eastwards, and the throw is accommodated by several faults with lesser displacements. (a) The continuation of the Wytch Farm Fault with a NW-SE strike that links with Fault D (c.f. Fig. 5.19). The western end of Fault E continues beyond the EEC survey boundary and connects to a fault to the immediate north of the Wytch Farm Fault. (b) Interpretation of the faults based on E-W orientations, without any linkage between the faults.





5.6 CONCLUSIONS

5.6.1 Arne Fault

The development of the Arne Fault initiated, probably in the Lower Triassic, with identified growth in the Sherwood Sandstone and Mercia Mudstone (Table 5.4). A fault throw map (Fig. 5.10) shows that several displacement minima and maxima occur along the fault's length, and that a displacement minimum at the Zone D Anhydrite horizon separates one maximum in the Sherwood Sandstone, and another in the Jurassic sequence. The complex geometry has been interpreted to indicate a fault formed of several amalgamated segments that developed during two distinct rifting phases. The degree of linkage between the segments is not fully resolvable from the analysis of 2D seismic lines.

Four new interpretations of the fault system demonstrate the uncertainty of fault throw, position, length and orientation inherent in 2D seismic data interpretation (Fig. 5.13). Application of a standardised *D-L* model for every interpretation has enabled the production of realistic maps. The most likely geometrical interpretation is a hybrid of Maps 1 and 3 (Fig. 5.13a and c), as the orientations are similar to the Wytch Farm Fault in the 2D area. The involvement of any underlying structures is not fully resolved, but the proposed E-W fault systems (Maps 2 and 4) are not supported by adjacent fault orientations. The new interpretations affect the reserves estimates by up to 27 mb, and therefore the viability of potential exploration targets. Fault geometries do not significantly affect hydrocarbon volumes, and the fault system location is the dominant factor. Conclusions related to the position and throws of the fault system are beyond the scope of this study.

5.6.2 EEC survey area

An initial interpretation of the Top Sherwood in the EEC survey area, based on an isopach down from the Top White Lias horizon, does not match the data from well 98/11-1 (Fig. 5.16), or the adjacent BP 3D interpretation. A re-assessment of the EEC seismic data, calibrated to exploration well data, has provided a well-constrained interpretation that also corresponds closely to the BP 3D area. As a consequence, a previously unidentified south-dipping fault, with a throw of c. 100 ms, has been interpreted that places well 98/11-1 in the downthrown block, and well 98/11-2 in the upthrown block (Fig. 5.17). A structural high can be traced ENE to WSW and forms a horst between a south-dipping fault zone to the south and a north-dipping fault zone to the north (Fig. 5.19). The horst-bounding fault zones are formed of several echelon fault segments, that are themselves segmented in both the horizontal and vertical planes (Fig. 5.19). Two interpretations of the extension of the new southern fault show that it could be either an eastern continuation of the Wytch Farm Fault, or a separate fault that oversteps with the Wytch Farm Fault to produce a relay ramp in the gap between the two surveys (Fig. 5.20).

6. A comparison of the structure of Kilve, Somerset, and the Wytch Farm Oilfield, Dorset

6.1 SUMMARY

Kilve, Somerset, and Wytch Farm, Dorset, are both within sub-basins of the Wessex Basin, and were filled by similar Triassic and Jurassic sediments. The geometry of the structures mapped from the exposures at Kilve are compared to those interpreted from the Wytch Farm seismic data sets. The comparison is based on maps and cross-sections of the Triassic and Jurassic rocks. Normal faults have similar geometries in both cross-section and map view. They overstep at relay ramps in map view, and with either extensional or contractional geometries in cross-section. Conjugate normal faults are also common to both sub-basins. There is no evidence for reverse-reactivated normal faults, or conjugate strike-slip faults in Wytch Farm, although such contractional faults occur at Kilve.

The value of the structures at Kilve as a field-based analogue is demonstrated by examples from the Wytch Farm interpretation. In addition, a model for conjugate normal fault zone development derived from the seismic interpretation is similar to the development model for conjugate strike-slip faults at Kilve.

6.2 INTRODUCTION

The objectives of this study are to provide a comparative study of the structures in two localities in southern Britain (Fig. 6.1). The study of two areas has provided the opportunity to compare fault geometries in the field and on seismic sections, and also to consider how the deformation in the two areas is related.

The onshore Wessex Basin (Fig. 6.1) extends from west Dorset to the Dorset coast (Kent, 1945), and includes the Wytch Farm Oilfield. The exposures at Kilve, north Somerset, are related to the Bristol Channel Basin development (e.g. Peacock and Sanderson, 1983), and is on the north-western flank of the Wessex Basin in a trough between the Mendips and Exmoor. The south-west of England is traversed by several NW-SE strike-slip faults (Fig. 6.1), that have a protracted history (Karnier et al., 1987) which extends back to the Permian, and culminated in digital reactivation during the Late Cretaceous - Tertiary Alpine Orogeny (Laba and Karnier, 1987). The Wytch Farm Oilfield and the exposures at Kilve are both to the immediate west of major NW-SE strike-slip faults (Fig. 6.1). Movement of the NW-SE suite of SW England is responsible for offset of the E-W basins in the Wessex Basin (Laba and Karnier, 1987), and also for the opening and closing of pull-apart basins at oversteeps between strike-slip fault segments, such as the Brixey Basin (Dobson and Hughes, 1971).

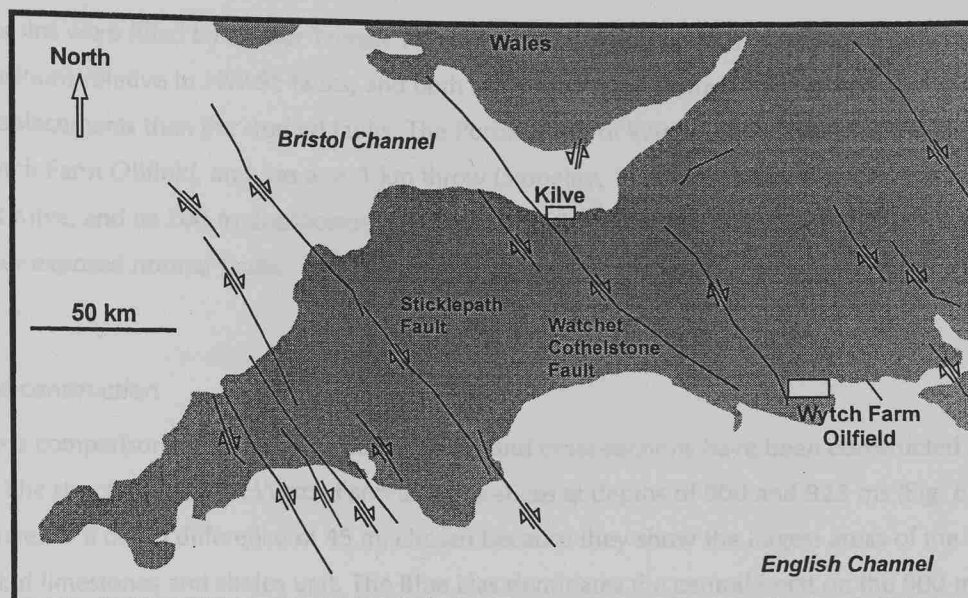


Fig. 6.1. Map of SW Great Britain (after Lake and Karner, 1987) to show the location of the Wytch Farm Oilfield, Dorset, and Kilve, Somerset, in the Wessex Basin. The Wytch Farm Oilfield lies to the immediate north of the Channel Basin (Karner *et al.*, 1987), and the Lower Lias at Kilve is the onshore exposure of the Bristol Channel Basin, both sub-basins of the Wessex Basin. Both the Wytch Farm Oilfield and Kilve are adjacent to the eastern side of dextral NW-SE strike-slip faults that traverse SW England.

6.2 INTRODUCTION

The objectives of this study are to provide a comparative study of the structures in two localities in southern Britain (Fig. 6.1). The study of two areas has provided the opportunity to compare fault geometries in the field and on seismic sections, and also to consider how the deformation in the two areas is related.

The onshore Wessex Basin (Fig. 6.1) extends from west Kent to the Dorset coast (Kent, 1949), and includes the Wytch Farm Oilfield. The exposures at Kilve, north Somerset, are related to the Bristol Channel Basin development (e.g. Peacock and Sanderson, 1991), and is on the north-western flank of the Wessex Basin in a trough between the Mendips and Exmoor. The south-west of England is traversed by several NW-SE strike-slip faults (Fig. 6.1), that have a protracted history (Karner *et al.*, 1987) which extends back to the Permian and culminated in dextral movements during the Late Cretaceous - Tertiary Alpine Orogeny (Lake and Karner, 1987). The Wytch Farm Oilfield and the exposure at Kilve are both to the immediate west of major NW-SE strike-slip faults (Fig. 6.1). Movement of the NW-SE faults of SW England is responsible for offsets of the E-W basins in the Wessex Basin (Lake and Karner, 1987), and also for the opening and closing of pull-apart basins at oversteps between strike-slip fault segments, such as the Bovey Basin (Bristow and Hughes, 1971).

The sub-basins were filled by similar Triassic to Jurassic sediments (Fig. 6.2), in addition to occupying similar positions relative to NW-SE faults, and both are bounded by normal faults with significantly greater displacements than the studied faults. The Purbeck-Isle of Wight Fault lies to the immediate south of the Wytch Farm Oilfield, and has a > 1 km throw (Stoneley, 1982). The Blue Ben Fault is exposed in the cliff at Kilve, and its 200 m displacement (Whittaker and Green, 1983) is considerably larger than any of the other exposed normal faults.

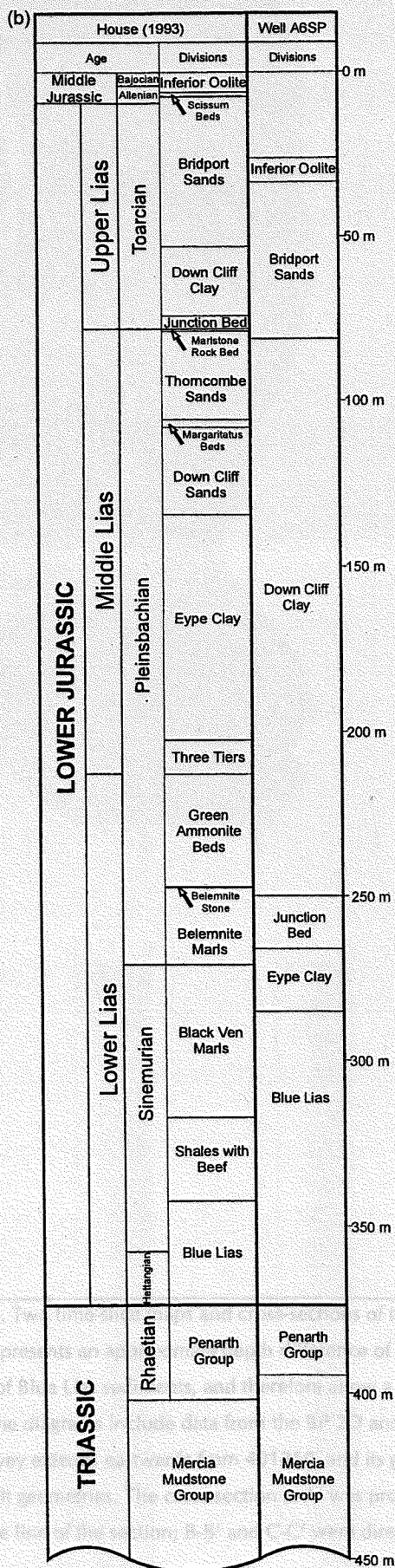
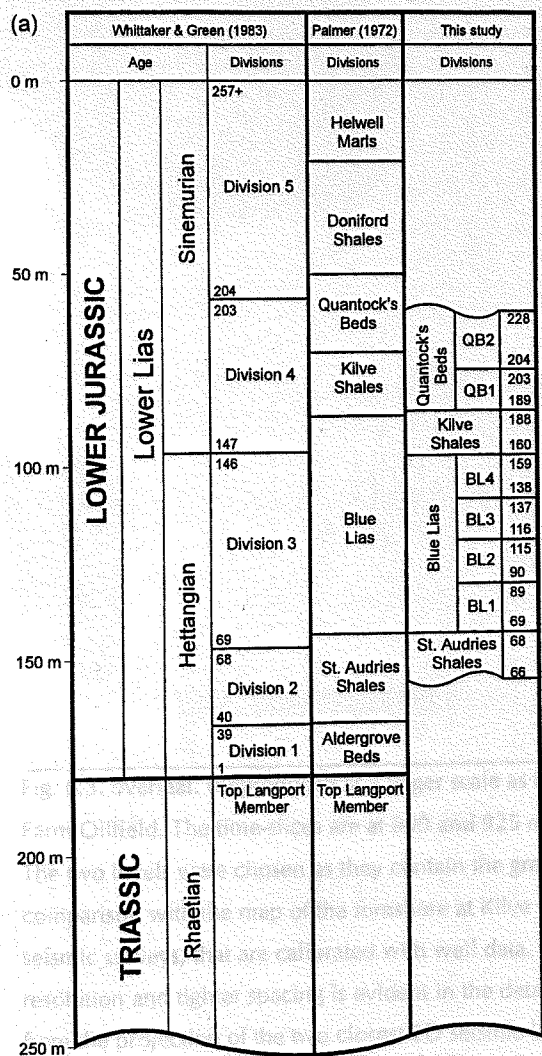
6.2.1 Map construction

To enable a comparison of the two sub-basins, maps and cross-sections have been constructed (Fig. 6.3 and 6.4). The structure maps of Wytch Farm are time-slices at depths of 900 and 925 ms (Fig. 6.3), which approximates to a depth difference of 45 m, chosen because they show the largest areas of the Blue Lias interbedded limestones and shales unit. The Blue Lias dominates the central horst on the 900 ms time-slice, the area surrounding the horst on the 925 ms map (Fig. 6.3), and the Kilve foreshore (Fig. 6.4). The map data was extracted from fault and horizon seismic interpretation data. The faults were detected by locating the X and Y co-ordinates of fault intersections with each time-slice. The fault planes were then mapped from the intersection data. The stratigraphy at 50 m intervals on each seismic line was found by calculating the depth difference between the closest mapped horizon above and below the time line. The lithological unit was resolved from a comparison of the differential depths with well data of unmapped units between those horizons. Fault dips could be measured, as the data has effectively been depth-converted, although the method is based on the assumption that the velocity is constant between each pair of mapped horizons. Cross-section A-A' was based on the mapped fault positions, and the fault geometries were resolved from the projection of two adjacent 2D seismic lines. The other two sections are direct interpretations of 3D seismic lines.

The Kilve foreshore (Fig. 6.4) was mapped onto a series of c. 1:500 aerial photographs. Stratigraphic boundaries were determined from a log of every bed on the foreshore, which were then compared with an extremely detailed account of the Lower Liassic stratigraphy (Whittaker and Green, 1983). The resolution of the photographs was sufficient to image the majority of the gently-dipping beds, which allowed accurate placement of the stratigraphic boundaries.

The rationale for producing a composite cross-section of Kilve Beach was to attempt to obtain a representative section from the most southerly to the most northerly fault (Fig. 6.4). A single traverse was not possible owing to the general E-W strike of the normal faults and width of the oblique coastline, so five individual sections were drawn. The section lines were positioned to emulate as closely as possible a continuous section. This was achieved by drawing the first section (in the west), and then tracking eastwards along the most northerly fault, until it was the most southerly fault on the foreshore. The next section was drawn, and the process was repeated. The three sections taken from the eastern end of the map are not as dispersed, and there is closer agreement between unit depths at section boundaries (Fig. 6.4).

Fig. 6.2. Stratigraphic logs of (a) the Lower Liassic exposure at Kilve, compared to published accounts, and (b) the Jurassic and Triassic of the Dorset coast (after House, 1993) with a log from Well A6SP, Wytch Farm (from BP Well Completion Report). The logs are shown side-by-side, and centred on the Triassic/Jurassic boundary, for comparison. All thicknesses are in metres to allow a direct comparison.



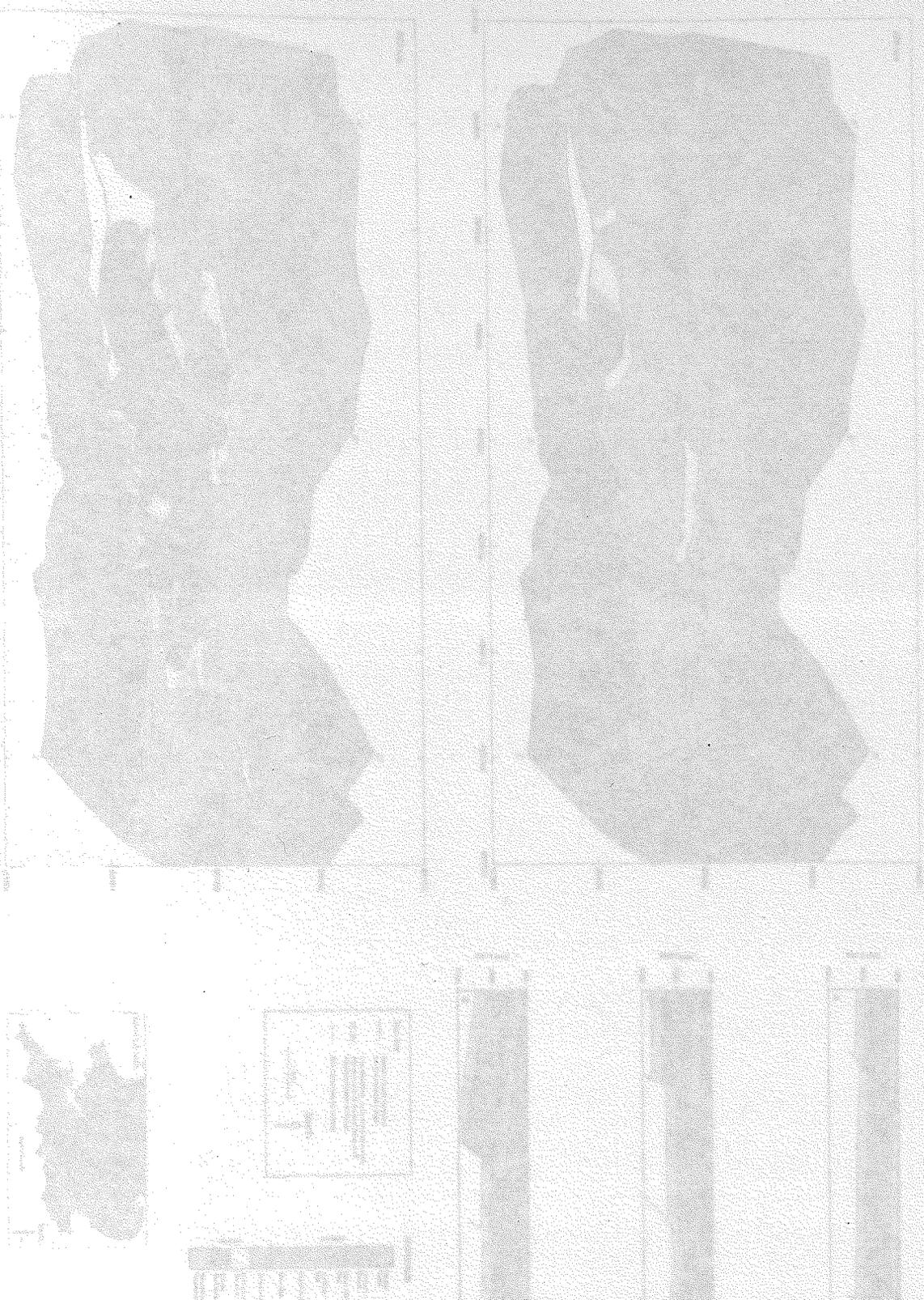


Fig. 6.3. overleaf. (Reproduced at a larger scale as Enclosure 1). Two time-slice maps and cross-sections of the Wytch Farm Oilfield. The time-slices are at 900 and 925 ms, which represents an approximate depth difference of 45 m. The two levels were chosen as they contain the greatest areas of Blue Lias sediments, and therefore allow a direct comparison with the map of the foreshore at Kilve (Fig. 6.4). The diagrams include data from the BP 2D and 3D seismic surveys, that are calibrated with well data. The 3D survey extends eastwards from 401250, and its greater resolution and tighter spacing is evident in the detail of the fault geometries. The cross-section A-A' was produced from the projection of the two closest 2D seismic lines onto the line of the section; B-B' and C-C' were directly constructed from 3D lines.

Fig. 6.4. overleaf. (Reproduced at a larger scale as Enclosure 2). Map of the exposure at Kilve (mapped by P.G. Kelly and D.J. Sanderson, drawn by D.C.P. Peacock and P.G. Kelly), and a composite cross-section. The stratigraphic divisions of Palmer (1972) are preferred for descriptive reasons. Normal and reverse-reactivated normal faults have approximately E-W strikes, dextral strike-slip faults strike NNW-SSE and sinistral strike-slip faults have NE-SW strikes. The cross-section construction is discussed in the text.

Enclosure 2. Map of the exposure at Kite, mapped by P.C. Kelly and D.J. Sanderson, drawn by D.C.P. Peacock and P.C. Kelly, and a composite cross-section. Normal and reverse-scarped normal faults have approximately E-W strikes, several strike-slip faults strike NNW-SSE and initial strike-slip faults have NE-SW strikes.



Map Key

- Reverse-scarped normal fault: Symbol on downthrown side.
- Reverse fault: Symbol on downthrown side.
- Strike-slip fault: Arrows on downthrown side.
- Dip direction: Indicated by dip amount in normal fault, and dip amount in normal fault, and dip amount in strike-slip fault.
- Stratigraphic boundary: Dashed line.

North ↑
100 m

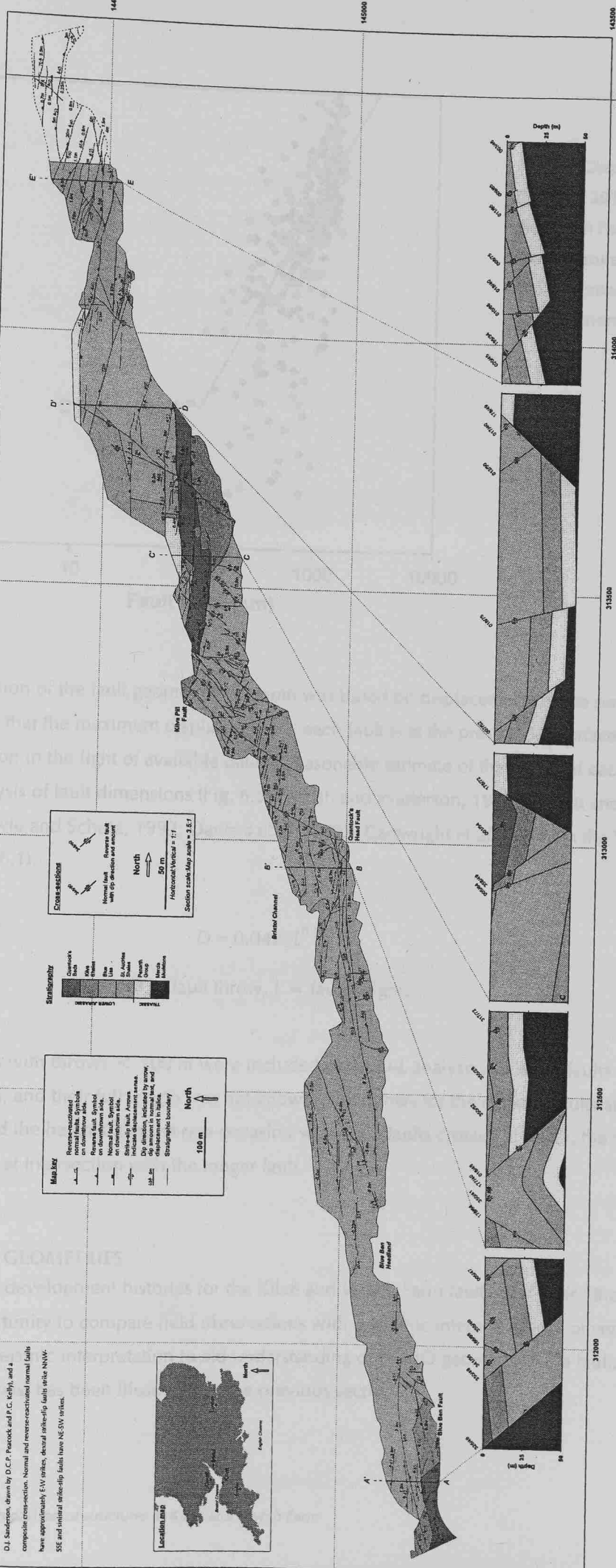


Cross-sections

- Normal fault with dip direction and amount: Symbol with arrow and angle.
- Reverse fault with dip direction and amount: Symbol with arrow and angle.

North ↑
50 m

Horizontal/Vertical = 1:1
Section scale: Map scale = 3.5:1



144500 145000 145500
317000 317500 318000 318500 319000 319500 320000 320500 321000 321500 322000 322500 323000 323500 324000 324500 325000 325500 326000 326500 327000 327500 328000 328500 329000 329500 330000 330500 331000 331500 332000 332500 333000 333500 334000 334500 335000 335500 336000 336500 337000 337500 338000 338500 339000 339500 340000 340500 341000 341500 342000 342500 343000 343500 344000 344500 345000 345500 346000 346500 347000 347500 348000 348500 349000 349500 350000 350500 351000 351500 352000 352500 353000 353500 354000 354500 355000 355500 356000 356500 357000 357500 358000 358500 359000 359500 360000 360500 361000 361500 362000 362500 363000 363500 364000 364500 365000 365500 366000 366500 367000 367500 368000 368500 369000 369500 370000 370500 371000 371500 372000 372500 373000 373500 374000 374500 375000 375500 376000 376500 377000 377500 378000 378500 379000 379500 380000 380500 381000 381500 382000 382500 383000 383500 384000 384500 385000 385500 386000 386500 387000 387500 388000 388500 389000 389500 390000 390500 391000 391500 392000 392500 393000 393500 394000 394500 395000 395500 396000 396500 397000 397500 398000 398500 399000 399500 400000 400500 401000 401500 402000 402500 403000 403500 404000 404500 405000 405500 406000 406500 407000 407500 408000 408500 409000 409500 410000 410500 411000 411500 412000 412500 413000 413500 414000 414500 415000 415500 416000 416500 417000 417500 418000 418500 419000 419500 420000 420500 421000 421500 422000 422500 423000 423500 424000 424500 425000 425500 426000 426500 427000 427500 428000 428500 429000 429500 430000 430500 431000 431500 432000 432500 433000 433500 434000 434500 435000 435500 436000 436500 437000 437500 438000 438500 439000 439500 440000 440500 441000 441500 442000 442500 443000 443500 444000 444500 445000 445500 446000 446500 447000 447500 448000 448500 449000 449500 450000 450500 451000 451500 452000 452500 453000 453500 454000 454500 455000 455500 456000 456500 457000 457500 458000 458500 459000 459500 460000 460500 461000 461500 462000 462500 463000 463500 464000 464500 465000 465500 466000 466500 467000 467500 468000 468500 469000 469500 470000 470500 471000 471500 472000 472500 473000 473500 474000 474500 475000 475500 476000 476500 477000 477500 478000 478500 479000 479500 480000 480500 481000 481500 482000 482500 483000 483500 484000 484500 485000 485500 486000 486500 487000 487500 488000 488500 489000 489500 490000 490500 491000 491500 492000 492500 493000 493500 494000 494500 495000 495500 496000 496500 497000 497500 498000 498500 499000 499500 500000 500500 501000 501500 502000 502500 503000 503500 504000 504500 505000 505500 506000 506500 507000 507500 508000 508500 509000 509500 510000 510500 511000 511500 512000 512500 513000 513500 514000 514500 515000 515500 516000 516500 517000 517500 518000 518500 519000 519500 520000 520500 521000 521500 522000 522500 523000 523500 524000 524500 525000 525500 526000 526500 527000 527500 528000 528500 529000 529500 530000 530500 531000 531500 532000 532500 533000 533500 534000 534500 535000 535500 536000 536500 537000 537500 538000 538500 539000 539500 540000 540500 541000 541500 542000 542500 543000 543500 544000 544500 545000 545500 546000 546500 547000 547500 548000 548500 549000 549500 550000 550500 551000 551500 552000 552500 553000 553500 554000 554500 555000 555500 556000 556500 557000 557500 558000 558500 559000 559500 560000 560500 561000 561500 562000 562500 563000 563500 564000 564500 565000 565500 566000 566500 567000 567500 568000 568500 569000 569500 570000 570500 571000 571500 572000 572500 573000 573500 574000 574500 575000 575500 576000 576500 577000 577500 578000 578500 579000 579500 580000 580500 581000 581500 582000 582500 583000 583500 584000 584500 585000 585500 586000 586500 587000 587500 588000 588500 589000 589500 590000 590500 591000 591500 592000 592500 593000 593500 594000 594500 595000 595500 596000 596500 597000 597500 598000 598500 599000 599500 600000 600500 601000 601500 602000 602500 603000 603500 604000 604500 605000 605500 606000 606500 607000 607500 608000 608500 609000 609500 610000 610500 611000 611500 612000 612500 613000 613500 614000 614500 615000 615500 616000 616500 617000 617500 618000 618500 619000 619500 620000 620500 621000 621500 622000 622500 623000 623500 624000 624500 625000 625500 626000 626500 627000 627500 628000 628500 629000 629500 630000 630500 631000 631500 632000 632500 633000 633500 634000 634500 635000 635500 636000 636500 637000 637500 638000 638500 639000 639500 640000 640500 641000 641500 642000 642500 643000 643500 644000 644500 645000 645500 646000 646500 647000 647500 648000 648500 649000 649500 650000 650500 651000 651500 652000 652500 653000 653500 654000 654500 655000 655500 656000 656500 657000 657500 658000 658500 659000 659500 660000 660500 661000 661500 662000 662500 663000 663500 664000 664500 665000 665500 666000 666500 667000 667500 668000 668500 669000 669500 670000 670500 671000 671500 672000 672500 673000 673500 674000 674500 675000 675500 676000 676500 677000 677500 678000 678500 679000 679500 680000 680500 681000 681500 682000 682500 683000 683500 684000 684500 685000 685500 686000 686500 687000 687500 688000 688500 689000 689500 690000 690500 691000 691500 692000 692500 693000 693500 694000 694500 695000 695500 696000 696500 697000 697500 698000 698500 699000 699500 700000 700500 701000 701500 702000 702500 703000 703500 704000 704500 705000 705500 706000 706500 707000 707500 708000 708500 709000 709500 710000 710500 711000 711500 712000 712500 713000 713500 714000 714500 715000 715500 716000 716500 717000 717500 718000 718500 719000 719500 720000 720500 721000 721500 722000 722500 723000 723500 724000 724500 725000 725500 726000 726500 727000 727500 728000 728500 729000 729500 730000 730500 731000 731500 732000 732500 733000 733500 734000 734500 735000 735500 736000 736500 737000 737500 738000 738500 739000 739500 740000 740500 741000 741500 742000 742500 743000 743500 744000 744500 745000 745500 746000 746500 747000 747500 748000 748500 749000 749500 750000 750500 751000 751500 752000 752500 753000 753500 754000 754500 755000 755500 756000 756500 757000 757500 758000 758500 759000 759500 760000 760500 761000 761500 762000 762500 763000 763500 764000 764500 765000 765500 766000 766500 767000 767500 768000 768500 769000 769500 770000 770500 771000 771500 772000 772500 773000 773500 774000 774500 775000 775500 776000 776500 777000 777500 778000 778500 779000 779500 780000 780500 781000 781500 782000 782500 783000 783500 784000 784500 785000 785500 786000 786500 787000 787500 788000 788500 789000 789500 790000 790500 791000 791500 792000 792500 793000 793500 794000 794500 795000 795500 796000 796500 797000 797500 798000 798500 799000 799500 800000 800500 801000 801500 802000 802500 803000 803500 804000 804500 805000 805500 806000 806500 807000 807500 808000 808500 809000 809500 810000 810500 811000 811500 812000 812500 813000 813500 814000 814500 815000 815500 816000 816500 817000 817500 818000 818500 819000 819500 820000 820500 821000 821500 822000 822500 823000 823500 824000 824500 825000 825500 826000 826500 827000 827500 828000 828500 829000 829500 830000 830500 831000 831500 832000 832500 833000 833500 834000 834500 835000 835500 836000 836500 837000 837500 838000 838500 839000 839500 840000 840500 841000 841500 842000 842500 843000 843500 844000 844500 845000 845500 846000 846500 847000 847500 848000 848500 849000 849500 850000 850500 851000 851500 852000 852500 853000 853500 854000 854500 855000 855500 856000 856500 857000 857500 858000 858500 859000 859500 860000 860500 861000 861500 862000 862500 863000 863500 864000 864500 865000 865500 866000 866500 867000 867500 868000 868500 869000 869500 870000 870500 871000 871500 872000 872500 873000 873500 874000 874500 875000 875500 876000 876500 877000 877500 878000 878500 879000 879500 880000 880500 881000 881500 882000 882500 883000 883500 884000 884500 885000 885500 886000 886500 887000 887500 888000 888500 889000 889500 890000 890500 891000 891500 892000 892500 893000 893500 894000 894500 895000 895500 896000 896500 897000 897500 898000 898500 899000 899500 900000 900500 901000 901500 902000 902500 903000 903500 904000 904500 905000 905500 906000 906500 907000 907500 908000 908500 909000 909500 910000 910500 911000 911500 912000 912500 913000 913500 914000 914500 915000 915500 916000 916500 917000 917500 918000 918500 919000 919500 920000 920500 921000 921500 922000 922500 923000 923500 924000 924500 925000 925500 926000 926500 927000 927500 928000 928500 929000 929500 930000 930500 931000 931500 932000 932500 933000 933500 934000 934500 935000 935500 936000 936500 937000 937500 938000 938500 939000 939500 940000 940500 941000 941500 942000 942500 943000 943500 944000 944500 945000 945500 946000 946500 947000 947500 948000 948500 949000 949500 950000 950500 951000 951500 952000 952500 953000 953500 954000 954500 955000 955500 956000 956500 957000 957500 958000 958500 959000 959500 960000 960500 961000 961500 962000 962500 963000 963500 964000 964500 965000 965500 966000 966500 967000 967500 968000 968500 969000 969500 970000 970500 971000 971500 972000 972500 973000 973500 974000 974500 975000 975500 976000 976500 977000 977500 978000 978500 979000 979500 980000 980500 981000 981500 982000 982500 983000 983500 984000 984500 985000 985500 986000 986500 987000 987500 988000 988500 989000 989500 990000 990500 991000 991500 992000 992500 993000 993500 994000 994500 995000 995500 996000 996500 997000 997500 998000 998500 999000 999500 1000000

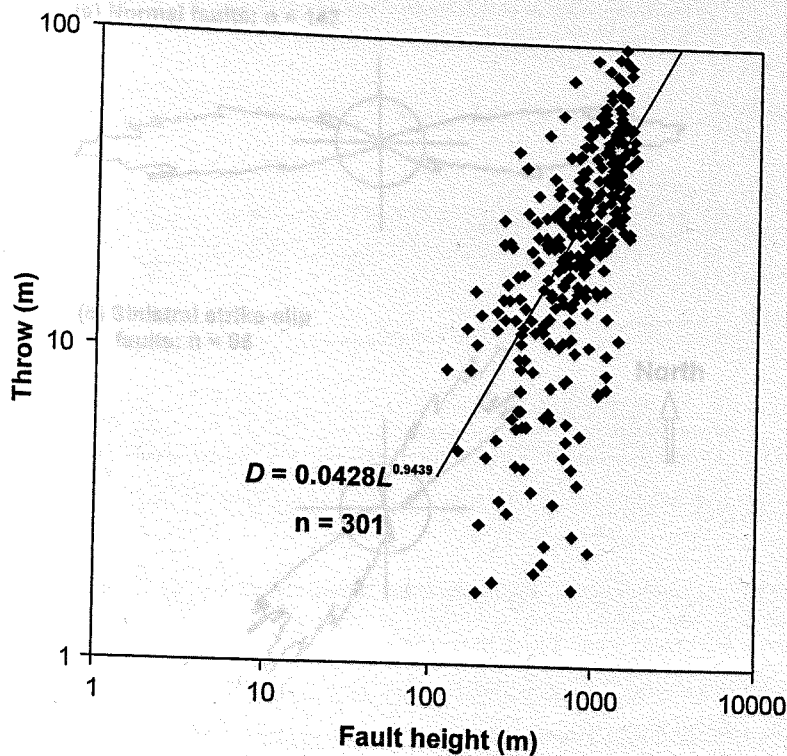


Fig. 6.5. Graph of fault height and throw for 301 fault measurements in the Wyitch Farm data set. The faults were measured from seismic sections, and the throws and heights were depth converted.

Interpretation of the fault geometries at depth was based on displacements at the surface. It is unrealistic to assume that the maximum displacement of each fault is at the present day surface, but there was no other option in the light of available data. A reasonable estimate of the height of each fault was obtained from analysis of fault dimensions (Fig. 6.5) (Walsh and Watterson, 1988; Marrett and Allmendinger, 1991; Cowie and Scholz, 1992; Dawers *et al.*, 1993; Cartwright *et al.*, 1995) in the Wyitch Farm data (Equation 6.1).

$$D = 0.0428L^{0.9439} \quad \text{Equation 6.1}$$

D = fault throw, L = fault height.

Only faults with throws < 100 m were included in the D - L analysis, as larger faults intersect the boundaries, and their full length was not known. The throws for the mapped faults at Kilve were then used to find the heights. On the rare occasion when two faults crossed at depth, the shorter fault was terminated at intersection with the longer fault.

6.3 FAULT GEOMETRIES

The similar development histories for the Kilve and Wyitch Farm faults, and their lithologies provide an ideal opportunity to compare field observations with a seismic interpretation. Conversely, the advantage of using a seismic interpretation to aid understanding of the 3D geometry of the faults on the north Somerset coast has been illustrated in the previous section.

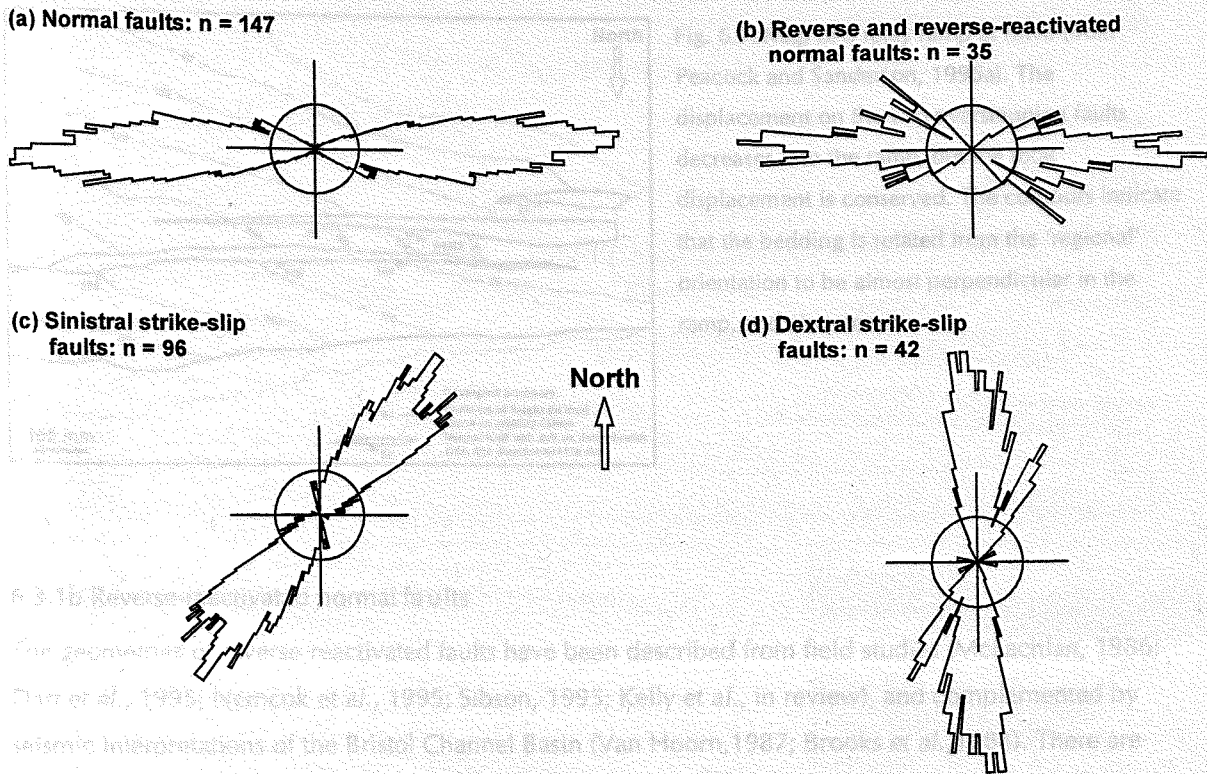


Fig. 6.6. Rose diagrams of fault orientations at Kilve. (a) Normal faults have approximately E-W strikes, whilst (b) the reverse-reactivated fault strikes have a greater range. (c) Sinistral faults strike NE-SW, and (d) dextral faults have strikes between NNE-SSW and NNW-SSE.

6.3.1 Overview of the structures on the north Somerset coast

6.3.1a Normal faults

The exposure of E-W striking normal faults (Fig. 6.6a) in the cliff sections and on the wave-cut platform has enabled insights into the 3D geometry of normal faults. The faults dip either towards the north or south, with an average dip of 54° , although the south-dipping faults are often steeper. Normal fault densities (number of faults per unit distance) are greatest in the hanging-walls of the faults > 40 m throw, e.g. the Blue Ben and Quantock's Head Faults (Fig. 6.4); vein densities are also higher adjacent to faults. The overall structure from north to south is a series of horst and graben; the south-dipping graben-bounding faults dominate the displacement (Fig. 6.4). Peacock and Sanderson (1991) described the displacement characteristics of normal faults in map view (Fig. 6.7), and illustrated how the displacement decreases on each fault into the relay ramps. The m-scale relay ramps at Kilve provide useful analogues for relay ramps between km-scale normal faults in the hydrocarbon basins of the North Sea, which may have been important to fluid migration or entrapment (Peacock and Sanderson, 1994a). Normal faults, often segmented, occur in cliff sections either as single planes (Fig. 6.8a), in conjugate sets (Fig. 6.8b) or as master faults with smaller antithetic faults (Fig. 6.8c).

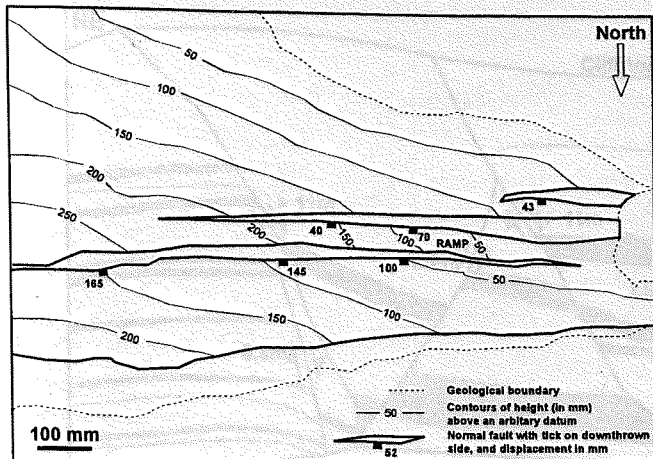


Fig. 6.7. Map of a relay ramp at Kilve (from Peacock and Sanderson, 1995a). The displacement on the two overstepping faults decreases into the ramp, but the total displacement is conserved. The contours indicate that the bedding is rotated from the 'regional' orientation to be almost perpendicular in the ramp, and also steeper.

6.3.1b Reverse-reactivated normal faults

The geometries of reverse-reactivated faults have been described from field studies (McLachlan, 1986; Dart *et al.*, 1995; Nemcok *et al.*, 1995; Sibson, 1995; Kelly *et al.*, in review), and complemented by seismic interpretations of the Bristol Channel Basin (Van Hoorn, 1987; Brooks *et al.*, 1988). There are three categories of reverse-reactivated faults exposed in the cliffs: faults with finite normal displacements (Fig. 6.9a), finite reverse displacements (Fig. 6.9b) and, most commonly, complex fault zones composed of sub-parallel reverse and normal faults (Fig. 6.9c). It is more difficult to identify reverse-reactivated normal faults on the wave-cut platform without 3D control, but their occurrence is suggested by adjacent zones of folded, and occasionally sub-vertical, bedding and multiple sets of slickenside lineations (Kelly *et al.*, in review; Chapter 3). The reverse-reactivated normal faults have a greater range of strikes than the normal faults (Fig. 6.6), but there is no distinction between the strike range for reactivated faults with finite normal and finite reverse displacements. These data indicate that the more oblique normal faults were preferentially reverse-reactivated and that, prior to the contraction, the normal faults had a greater range of strikes (Fig. 6.6). There are no normal faults at Kilve with finite normal throws > 22 m that were not reverse-reactivated, but normal faults with smaller displacements were reversed (Fig. 6.10). The amount of reverse movement on the normal faults is not quantifiable, so conclusions cannot be drawn regarding the true nature of the relationship between throw magnitude and reactivation. Displacement transfer between reverse-reactivated normal faults occurs between both under- and overlapping faults (Kelly *et al.*, in review). The displacement is accommodated by an array of obliquely orientated reverse faults in an underlapping fault zone, and across a network of conjugate strike-slip faults between a pair overlapping faults (Fig. 6.4) (Kelly *et al.*, in review; Chapter 3). Relics of relay ramps (Peacock and Sanderson, 1991; 1994a) occur adjacent to reverse-reactivated faults.

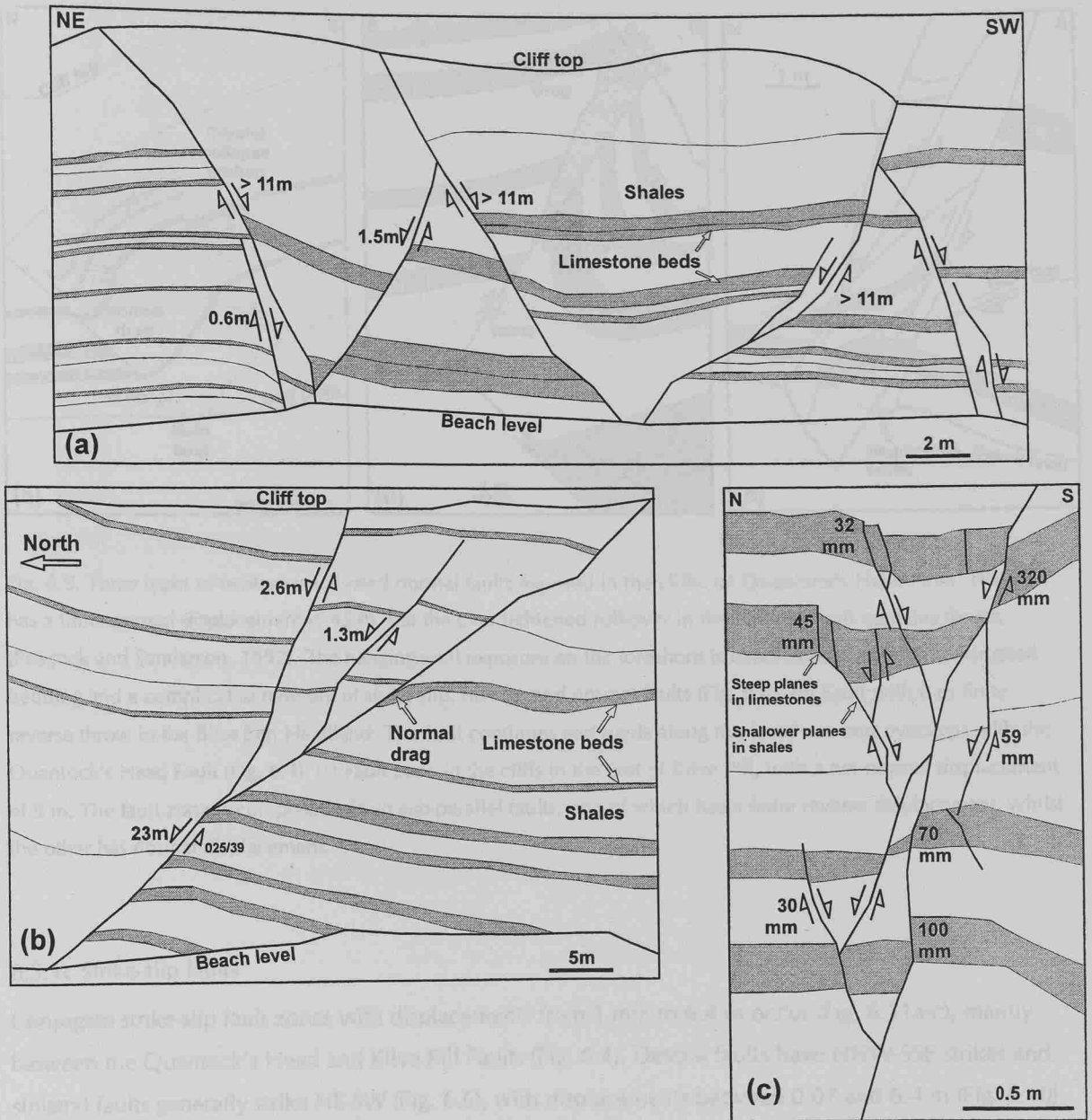


Fig. 6.8. Line drawings, from photographs, of normal faults at Kilve. (a) Conjugate normal faults in the cliff to the immediate west of the steps at East Quantock's Head. The displacement is marked as > 11 m when it was not possible to match the beds on either side of the fault planes (i.e. the displacement $>$ cliff height). (b) Fault with synthetic branches in the cliffs to the east of Kilve Pill. (c) Line-drawing of a network of antithetic and synthetic normal faults in the cliffs, 25 m east of (b). The faults are steeper in the limestone units, and shallower in the interbedded shales.

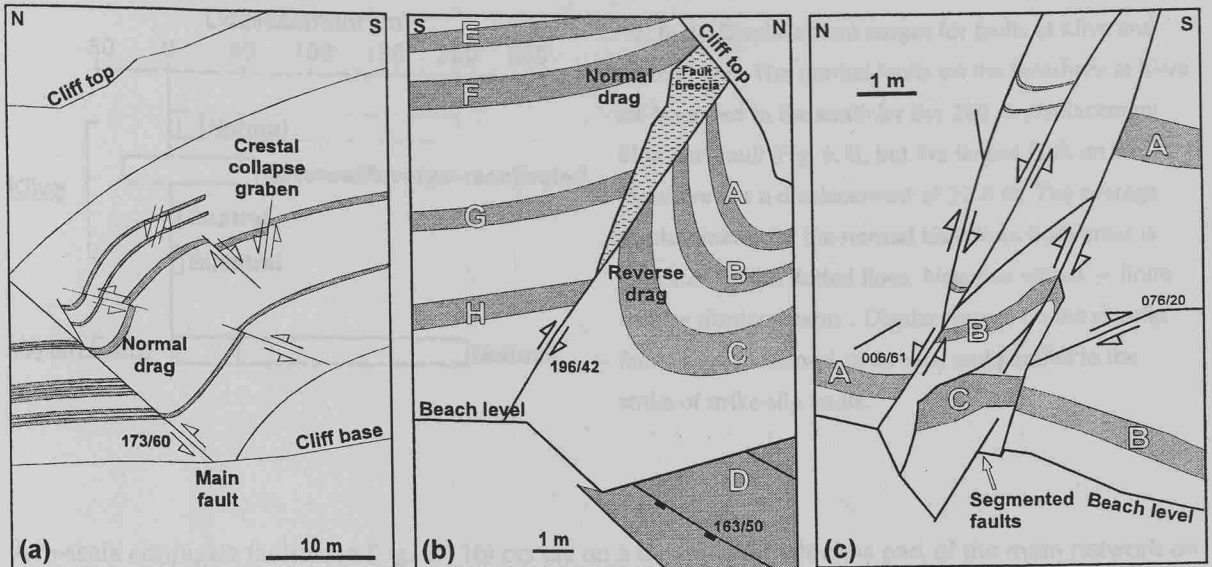


Fig. 6.9. Three types of reverse-reactivated normal faults exposed in the cliffs. (a) Quantock's Head Fault. The fault has a finite normal displacement c. 45 m, but the over-tightened roll-over in the hanging-wall contains thrusts (Peacock and Sanderson, 1992). The hanging-wall exposure on the foreshore is characterised by highly disrupted bedding and a complicated network of strike-slip, reverse and normal faults (Fig. 6.4). (b) Fault with 8 m finite reverse throw in the Blue Ben Headland. The fault continues eastwards along the foreshore and oversteps with the Quantock's Head Fault (Fig. 6.4). (c) Fault zone in the cliffs to the east of Kilve Pill, with a net normal displacement of 5 m. The fault zone is composed of two sub-parallel faults, one of which has a finite reverse displacement, whilst the other has normal displacement.

6.3.1c Strike-slip faults

Conjugate strike-slip fault zones with displacements from 1 mm to 6.4 m occur (Fig. 6.11a-c), mainly between the Quantock's Head and Kilve Pill Faults (Fig. 6.4). Dextral faults have NNW-SSE strikes and sinistral faults generally strike NE-SW (Fig. 6.6), with displacements between 0.07 and 6.4 m (Fig. 6.10). Deformation on the mm-scale (Fig. 6.11a) consists of an E-W pressure-solution cleavage, a dominant dextral fault that intersects several sinistral faults, and rotated blocks. A deformation sequence is implied by the fault zone geometry, in which the pressure solution was instrumental to the fault zone evolution (*c.f.* Willemsse *et al.*, 1997). An E-W pressure solution cleavage developed adjacent to a stuck intersection between conjugate faults. Volume loss through pressure-solution also occurs at the intersection of conjugate normal faults (Odonne and Massonnat, 1992b). Individual blocks, bounded by the pressure-solution cleavage, rotated anticlockwise during sinistral movement of the master fault (at A, Fig. 6.11a). An irregular fault plane is developed from the coalescence of triangle-shaped openings at the corners of rotating blocks (at B, Fig. 6.11a). The blocks furthest away from the conjugate intersection experienced the greatest amounts of rotation.

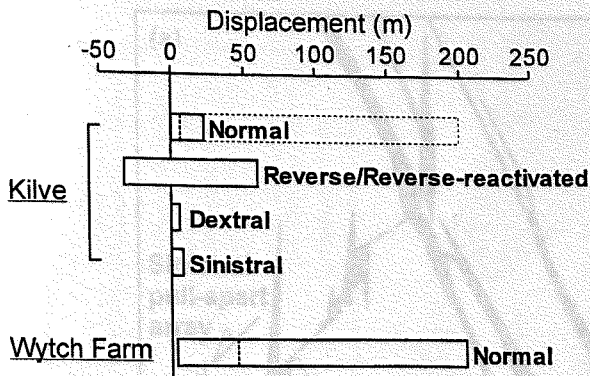


Fig. 6.10. Displacement ranges for faults at Kilve and Wytch Farm. The normal faults on the foreshore at Kilve are bounded to the south by the 200 m displacement Blue Ben Fault (Fig. 6.4), but the largest fault on the foreshore has a displacement of 33.8 m. The average displacements for the normal fault from both areas is indicated by the dotted lines. Negative values = finite reverse displacements. Displacements on the dip-slip faults were measured as throws, and parallel to the strike of strike-slip faults.

A m-scale conjugate fault zone (Fig. 6.11b) occurs on a dextral fault which is part of the main network on the wave-cut platform (Fig. 6.11c). The network is mainly confined to a horst (Fig. 6.4), and is interpreted as a displacement transfer zone between two reverse-reactivated normal faults (Kelly *et al.*, in review). Displacement is transferred between overstepping strike-slip faults at strike-slip relay ramps (Fig. 6.11d) (Peacock and Sanderson, 1995a). An initial stage of antithetic fault development between the overstepping faults is succeeded by a renewed phase of synthetic faulting (Peacock and Sanderson, 1995a). The deformation sequence is similar to that explicit in cross-cutting relationships of the sinistral and dextral faults in the entire network (Kelly *et al.*, in press; Chapter 2). Strike-slip faults, with minor dip-slip components, exposed in the cliff have similar geometries to normal faults; sub-vertical faults in the limestone units are linked by shallower faults through the interbedded shales (Fig. 6.11e).

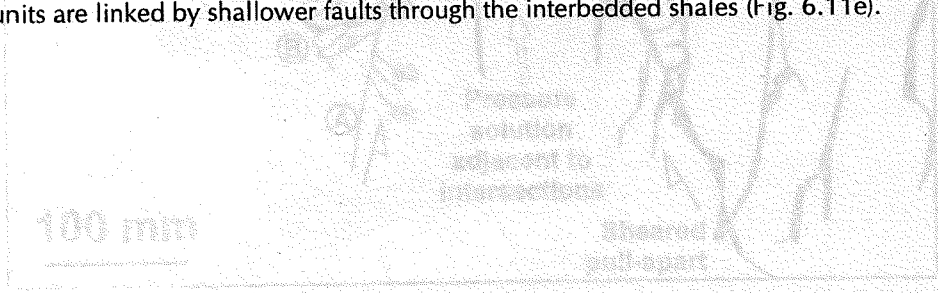


Fig. 6.11. (a) Map of a network of conjugate strike-slip faults. (b) Map of a m-scale conjugate fault zone at East Quantoxhead. (c) Map of a m-scale conjugate fault zone at East Quantoxhead showing strike-slip relay ramps. (d) Map of a strike-slip relay ramp. (e) Map of a strike-slip fault zone exposed in the cliff at East Quantoxhead. The strike-slip fault has a minor dip-slip component of normal displacement, and resembles a normal fault in cross-section. Fault plane dip and dip direction are shown in all diagrams given in brackets.

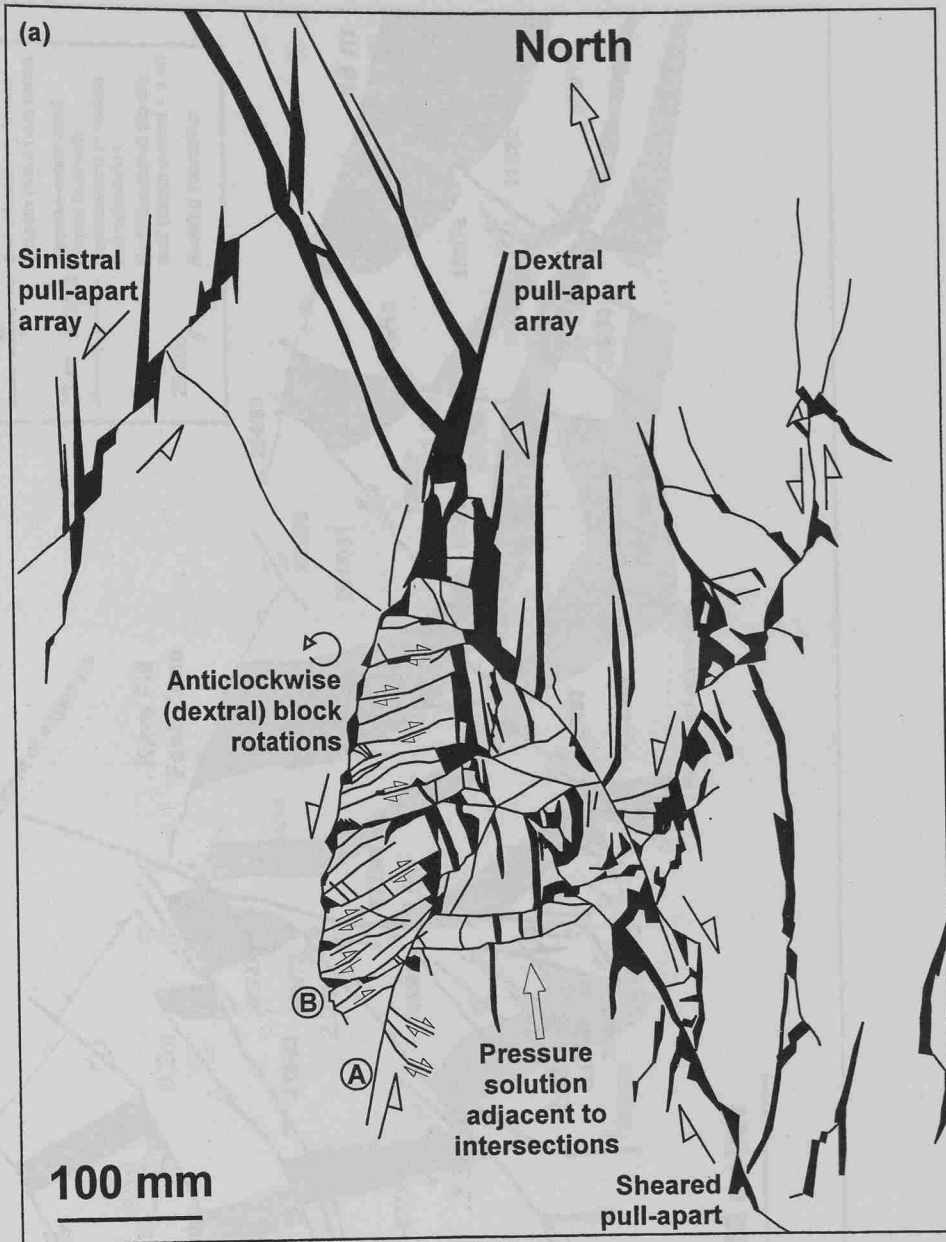
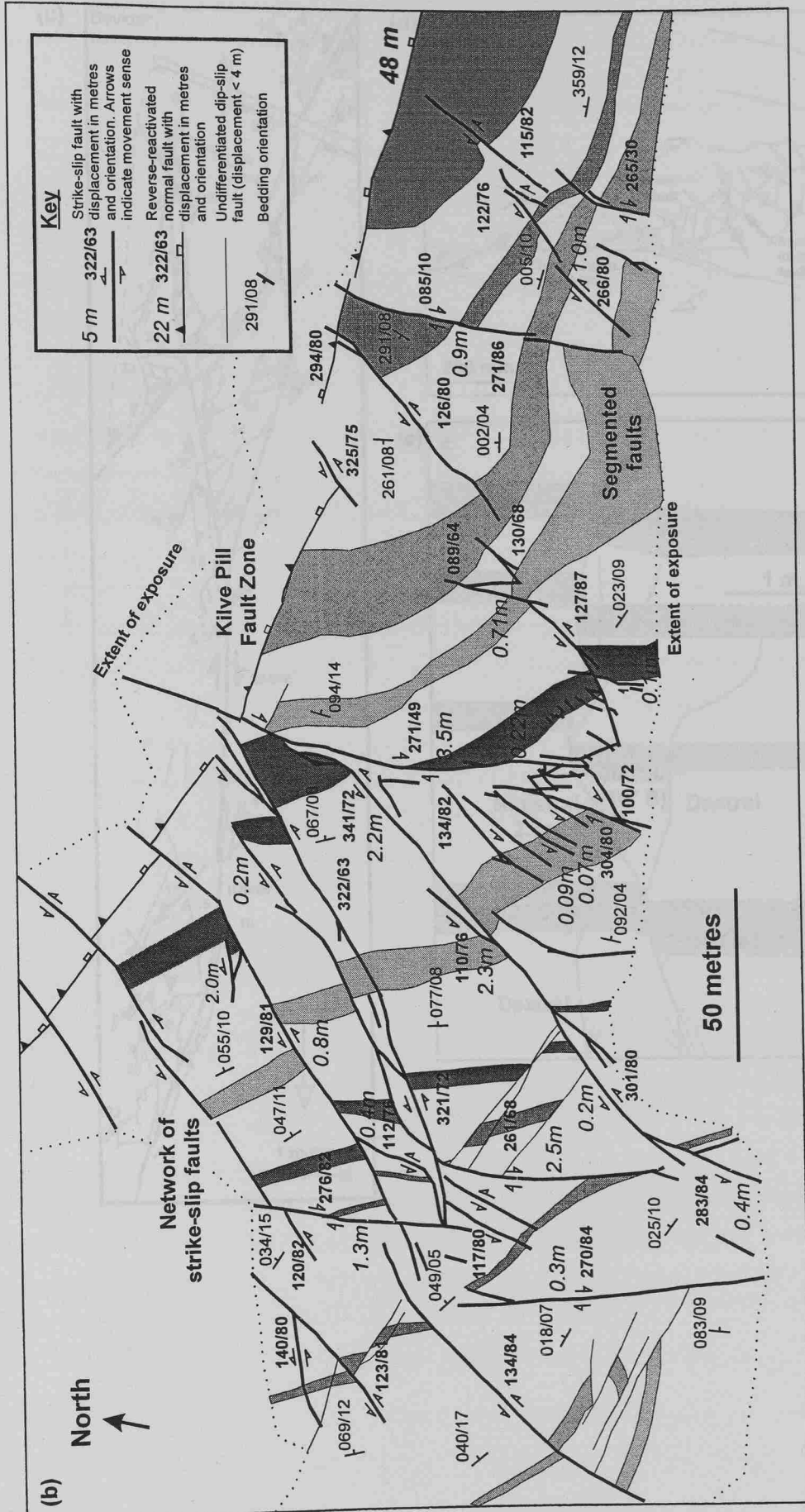
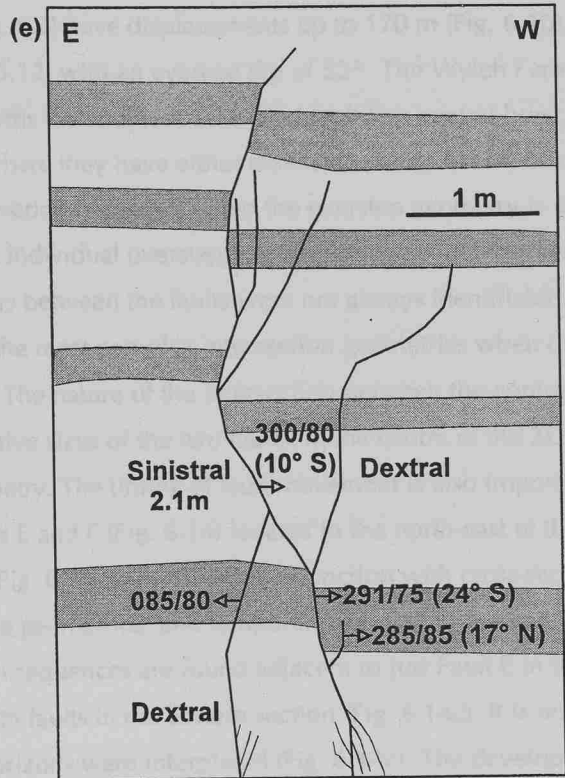
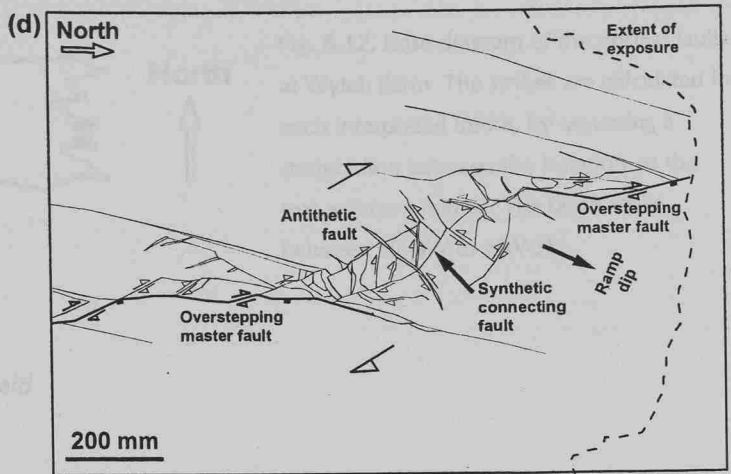
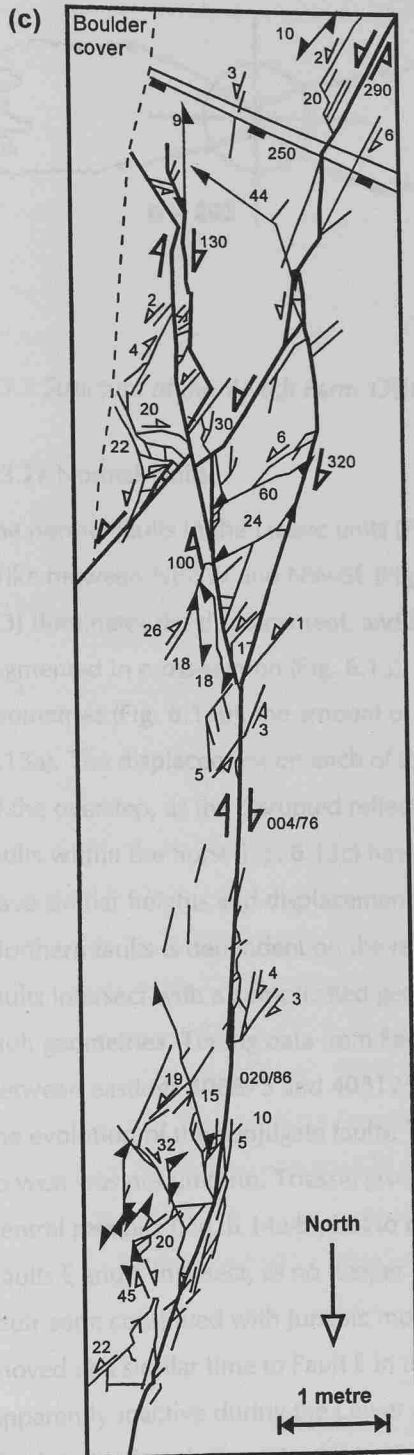


Fig. 6.11. (Above and next two pages) The geometry of strike-slip faults. (a) Map of a mm-scale fault zone to the immediate west of the Blue Ben Headland (Fig. 6.4). The faults have highly irregular planes, and through-going faults are not fully developed from pull-apart arrays (Kelly *et al.*, in press). The acute conjugate angles are dominated by an E-W pressure-solution cleavage adjacent to the intersections. Anti-clockwise rotated blocks are delimited by the pressure-solution cleavage between two sub-parallel sinistral faults. (b) Map of a network of conjugate strike-slip faults between two overlapping reverse-reactivated normal faults (Kelly *et al.*, in press; in review). (c) Map of a m-scale conjugate fault zone at East Quantoxhead (Kelly *et al.*, in press). There are rare occurrences of pull-apart arrays between master faults, and sheared pull-aparts adjacent to the master faults. The strike-slip faults often overstep and displacement is transferred from one fault to another at (d) a strike-slip relay ramp (after Peacock and Sanderson, 1995a). (e) Strike-slip fault zone exposed in the cliff at East Quantoxhead. The strike-slip fault has a minor component of normal displacement, and resembles a normal fault in cross-section. Fault plane dip and dip direction are shown with lineation pitches in brackets.





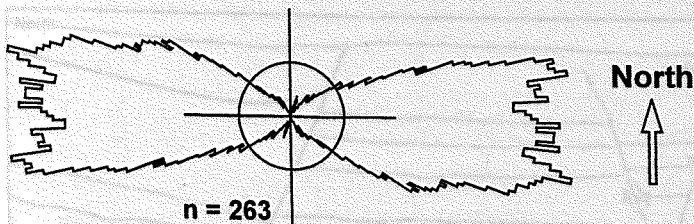


Fig. 6.12. Rose diagram of the normal faults at Wytch Farm. The strikes are calculated for each interpreted inline, by assuming a straight line between the location on the two adjacent inlines. The faults strike between NE-SW to NW-SE.

6.3.2 Structure of the Wytch Farm Oilfield

6.3.2a Normal faults

The normal faults in the Liassic units (Fig. 6.3) have displacements up to 170 m (Fig. 6.10), and have a strike between NE-SW and NW-SE (Fig. 6.12) with an average dip of 52° . The Wytch Farm Fault (Fig. 6.3) dominates the displacement, and forms the southern bounding fault to a central horst. The faults are segmented in cross-section (Fig. 6.13), where they have either extensional (Fig. 6.13a) or contractional geometries (Fig. 6.13b); the amount of overlap is greatest when the overstep geometry is extensional (Fig. 6.13a). The displacement on each of the individual overstepping faults was not determined in the region of the overstep, as the disrupted reflectors between the faults were not always identifiable. The conjugate faults within the horst (Fig. 6.13c) have the most complex intersection geometries when the two faults have similar heights and displacements. The nature of the intersection between the conjugate Arne and Northern faults is dependent on the relative sizes of the two faults. In the centre of the 3D survey the two faults intersect with a complicated geometry. The timing of fault movement is also important to conjugate fault geometries. Timing data from Faults E and F (Fig. 6.14) located in the north-east of the survey, between eastings 406875 and 408125 (Fig. 6.3), were used in conjunction with cross-sections to analyse the evolution of the conjugate faults. The geometrical and temporal evolution of the fault zone from east to west was not uniform. Triassic growth sequences are found adjacent to just Fault E in the western and central sections (Fig. 6.14a-b), but to both faults in the eastern section (Fig. 6.14c). It is not known if Faults E and F intersect, as no deeper horizons were interpreted (Fig. 6.14c). The development of the fault zone continued with Jurassic movements. All parts of Fault F were active at the same time, and moved at a similar time to Fault E in the eastern and western sections (Fig. 6.14a and c). Fault E was apparently inactive during the Lower Jurassic movements (Fig. 6.14b). Only Fault E was active during the third stage of evolution (Fig. 6.14a-c). The three development stages can be summarised as: (1) isolated fault development, through (2) propagation of both faults towards their mutual intersection, to (3) propagation of one fault that breaches the intersection. The intersection geometries also indicate that younger faults usually terminate at the older fault (Fig. 6.14b-c).

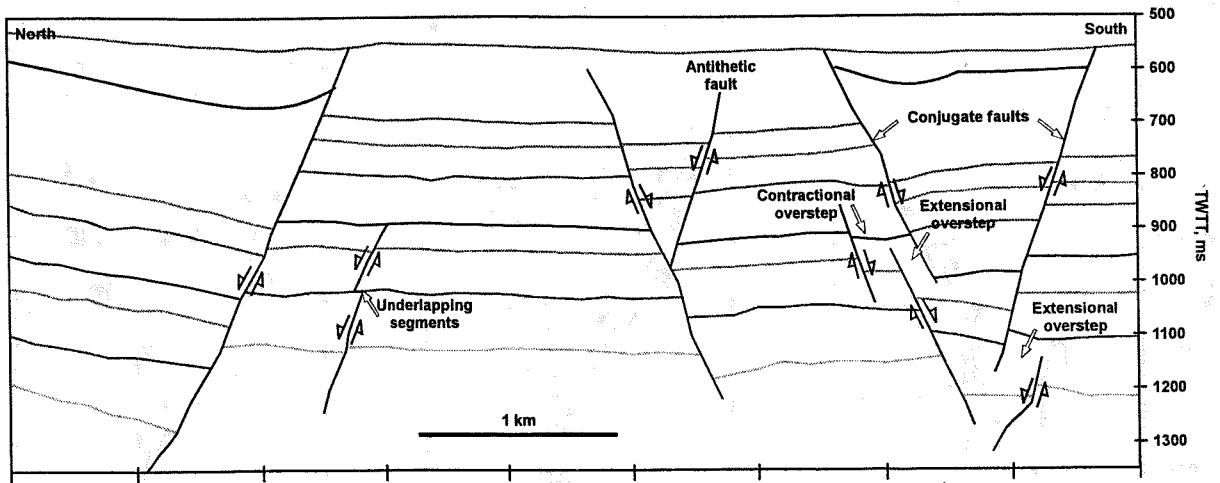


Fig. 6.13. Normal fault geometries in the Wytch Farm Oilfield. The faults are segmented in cross-section, and overlap at either extensional or contractional oversteps. The reflectors are often chaotic in oversteps, so it is not always possible to interpret the displacements on the individual segments. The deformation style across the seismic survey is dominated by conjugate normal faults.

The normal faults are also segmented in map view (Fig. 6.3). It is not possible to draw any rigorous conclusions about the fault segmentation in the 2D survey area, due to the low data coverage. However, relay ramps were observed in the 3D survey area. They are recognisable from steeper bed dips between overlapping faults, and localised change of the bed dip direction to be perpendicular to the fault strikes (Peacock and Sanderson, 1991) (Fig. 6.3). A second type of displacement transfer zone occurs between the Arne and Northern Faults. At the Top Sherwood level, the Northern Fault forms a continuous trace. In the Liassic units the fault is composed of three individual segments. In map view, the displacement between the two eastern segments is transferred via a south-dipping fault (Fig. 6.3). Many of the faults, such as the Wytch Farm Fault, have irregular planes (Fig. 6.3). Points of minimum and maximum throw along their lengths suggest that the faults were individual segments that subsequently merged (Ellis and Dunlap, 1988; Peacock and Sanderson, 1991; 1994a).

6.3.2b Strike-slip and reverse-reactivated normal faults

No evidence for strike-slip faults, or reverse-reactivation of the normal faults was found during the extensive examination of the Wytch Farm seismic data sets. Strike-slip faults are more difficult to detect on individual seismic sections, unless they also have a dip-slip component, as faults were interpreted at reflector offsets and terminations. Strike-slip faults might be interpreted from abnormal juxtaposition of lithologies on time-slice maps constructed from the combined sections. Although the distribution of lithologies on the two time-slice maps is wholly consistent with normal faults and a gentle dip to the east and west (Fig. 6.3), the faults would need strike-slip displacements > 50 m to be visible on the maps (the largest strike-slip fault displacement at Kilve is 6.4 m).

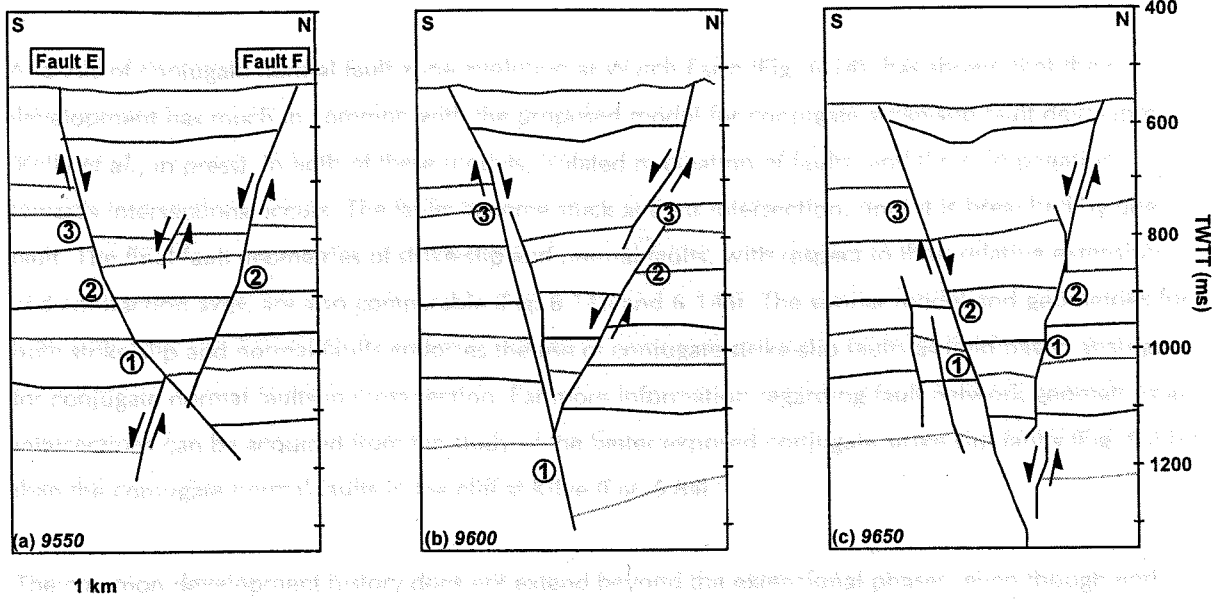


Fig. 6.14. Three cross-sections through the conjugate Faults E and F. The sections are truncated seismic inline interpretations, whose numbers are indicated in the bottom left corners, and arranged from west to east (left to right). The circled numbers represent the relative timing of the faults on each section (1 = oldest movements, 3 = most recent). Growth sequences in the hanging-walls were used to identify fault activity. Fault E experienced the most recent movements, in all three cases. A breakdown of fault zone evolution is detailed in the text.

The occurrence of reverse-reactivated normal faults cannot be discounted by the data interpretation, although structures such as hanging-wall anticlines and thrusts were not apparent. Several of the examples from Kilve are fault zones that retained finite normal displacements (Fig. 6.9a), or reactivated and unreactivated faults in the same fault zone with a net normal displacement (Fig. 6.9c). The reverse-reactivated fault in the latter case would not be detected if the reverse displacement was below seismic resolution, or if the faults were not separated sufficiently to be interpreted as individual fault zones. Any reversal of the normal faults was not sufficient to displace the Base Chalk horizon on any of the sections.

6.4 APPLICABILITY OF FIELD STUDY TO SEISMIC INTERPRETATION

The preceding descriptions have demonstrated the similarities between normal fault geometries at both locations (Fig. 6.3, 6.4, 6.8 and 6.13). The similar geometries of the normal faults in both cross-section (Fig. 6.8 and 6.13) and map view (Fig. 6.3 and 6.4) in the two sub-basins of the Wessex Basin, and the common development history, confirm the suitability of the Kilve exposure as a field-based analogue. An ideal illustration occurred when a well intersected an ESE-WNW section of the Arne Fault between two E-W segments. The estimated throw from the seismic interpretation was 23.6 ms, but the well intersected the fault with a throw < 5 ms equivalent. A bend in a fault trace would be mapped if faults that overstep at a relay ramp were incorrectly interpreted as a single fault. Field examples (e.g. Fig. 6.7) show that throw minima occur at breached relay ramps, and it is possible to pass from the footwall to the hanging-wall of an unbreached relay ramp, and not encounter a fault (Peacock and Sanderson, 1991).

6.3 CONCLUSIONS

Analysis of conjugate normal fault zone evolution at Wytch Farm (Fig. 6.14), has shown that their development has much in common with the proposed model for conjugate strike-slip fault development (Kelly *et al.*, in press). In both of these models, isolated nucleation of faults, and their propagation towards intersections occurs. The faults become stuck at their intersection, until it is breached by one fault. The final fault geometries of strike-slip and normal faults, with respect to their relative extension and contraction axes, are also comparable (Fig. 6.11b and 6.14a). The similar model and geometries for both strike-slip and normal faults endorses the use of conjugate strike-slip faults as field-based analogues for conjugate normal faults in cross-section. Far more information regarding fault network geometries and intersections can be acquired from the study of the better-exposed conjugate strike-slip faults (Fig. 6.11c), than the conjugate normal faults in the cliff at Kilve (Fig. 6.8a).

The common development history does not extend beyond the extensional phases, even though both areas form part of the Wessex Basin. This observation is particularly important to the assessment of hydrocarbon traps, in the light of the faults that formed during the contractional phase at Kilve. The Wytch Farm reservoirs are contained within the central horst (Fig. 6.3), and are thought to have been charged during the reverse-reactivation of the Purbeck-Isle of Wight Fault (Colter and Havard, 1981). The strike-slip faults at Kilve are interpreted to be associated with reverse-reactivation (Kelly *et al.*, in review), and are concentrated in a horst (Fig. 6.4). Escape of hydrocarbons may have occurred if either of the horst-bounding faults were reverse-reactivated, or if a linked network of strike-slip faults developed in the horst. All of the strike-slip offsets at Kilve are below the seismic resolution, even though the network covers a significant area (Fig. 6.8c). Selley and Stoneley (1982) postulated that significant hydrocarbon accumulations elsewhere in the Wessex Basin may have been lost during basin inversion.

The lack of reverse-reactivation of the normal faults at Wytch Farm implies that not all aspects of the model proposed for the contraction at Kilve (Kelly *et al.*, in review; Chapter 3) can be universally applied. There are, however, similarities between the two sub-basins, when the faults beyond the seismic data set are considered. The south-dipping Purbeck-Isle of Wight fault lies to the immediate south of the oilfield, and was reverse-reactivated during Late Cretaceous – Tertiary basin inversion (Stoneley, 1982; Lake and Karner, 1987; Chadwick, 1993). Interpretation of a cross-section through the Purbeck-Isle of Wight fault (Stoneley, 1982) shows a finite normal displacement > 1 km, even though the fault experienced the greatest amount of reverse-reactivation in the basin (Lake and Karner, 1987; Chadwick, 1993). Karner *et al.* (1987) concluded that only the basement-involved faults were reversed during basin inversion. The reversal of the largest faults in the region is similar to the selective reverse-reactivation of the Quantock's Head and Kilve Pill Faults.

6.5 CONCLUSIONS

Normal faults have similar geometries at both locations. This takes the form of segmentation in cross-section where the faults overstep with either extensional or contractional geometries. Conjugate normal faults were observed in the cliffs at Kilve and on the seismic sections from the Wytch Farm Oilfield. The normal faults at Kilve often overstep at relay ramps, and relics of relay ramps are common adjacent to the largest faults in the field. Relay ramps are also recognised from steeper beds between overstepping faults on the time-slice maps of the Triassic – Jurassic succession at Wytch Farm. Bends in fault traces have lower displacements than estimated from seismic interpretation, and therefore are likely to be relay ramps. The normal faults at Kilve therefore provide a useful analogue for the deformation at Wytch Farm. Formation of a development model for the conjugate normal faults at Wytch Farm has revealed that they evolved in a similar way to conjugate strike-slip faults. The strike-slip fault network at Kilve is more accessible to study than the limited examples of cross-sections of conjugate normal faults.

There is no evidence for contraction at Wytch Farm, which caused reversal of normal faults and strike-slip fault formation at Kilve. However, reverse-reactivation affected the largest faults (the Quantock's Head and Kilve Pill Faults), whilst many lesser displacement faults were unaffected. Reverse-reactivation of the Purbeck – Isle of Wight Fault to the south of the oilfield may have performed a similar role to the largest displacement faults at Kilve.

7. Conclusions

There were two objectives for the study in the preceding chapters. Firstly, to propose models that describe the development of segmented faults in both extensional and compressional settings and, secondly, to apply fault analysis methods to problematic areas in the seismic interpretation of normal faults in the Wessex Basin. Segmented normal faults have been described from the Wessex Basin in Chapter 4, and the interaction between faults that developed during polyphase extension has been discussed. The conclusions drawn from the study of the normal faults have been applied to the interpretation of seismic data elsewhere in the basin. Conjugate strike-slip fault development, and subsequent network development, has been addressed in Chapter 2. The degree of fault interaction, in contractional settings, of strike-slip faults and reverse-reactivated normal faults was analysed in Chapter 3, which also included descriptions of the geometries of displacement transfer zones between selectively reverse-reactivated normal faults. The field study in Somerset, and the seismic study in Dorset provided the opportunity to compare fault geometries from two sub-basins of the Wessex Basin (Chapter 6). The following sections summarise the conclusions from each chapter.

7.1 EXTENSIONAL DEFORMATION

The geometries of normal faults that formed during the development of the Wessex Basin have been described in Chapters 4 and 5. The dynamics of basin formation has been well-documented (e.g. Stoneley, 1982; Chadwick *et al.*, 1983; Chadwick, 1986; Karner *et al.*, 1987), but the kinematics of individual normal faults has not been addressed prior to this study.

Recent studies of normal fault geometries elsewhere have shown that faults are often highly segmented, and overstep at relay ramps in map view (Larsen, 1988; Peacock and Sanderson, 1991; 1994a), and also overlap in cross-section (Peacock and Sanderson, 1994b; Mansfield and Cartwright, 1995). The normal faults in the Wessex Basin are similarly segmented in map view and cross-section, and their displacement profiles have been used to further understanding of the deformation style in the basin. The largest faults, such as the Arne Fault, are composed of several segments, both vertically and horizontally.

Previous studies of overstepping faults (Peacock and Sanderson, 1991; Peacock and Zhang, 1994; Mansfield and Cartwright, 1995) have concentrated on fault segments that developed during a single extensional or contractional phase. Polyphase extension has been identified from growth sequences in the hanging-walls of the largest faults in the Wessex Basin, and linkage between faults of different ages has been identified. Willemse *et al.* (1996) identified a shift from the centre, towards an overlap zone, of the maximum displacements on individual segments. Similarly, the depths to maximum displacement of both fault segments at vertical oversteps suggest that both segments were active, and hence the lower segment was reactivated during the later extension phase.

The resolution of the 3D seismic data sets was sufficient to analyse in detail the distribution of extension, which reveals that the normal reactivation of the normal faults was the dominant process. The

identification of growth sequences also showed that contemporaneous fault reactivation and new fault development occurred. However, only reactivated faults were active during two periods of relative tectonic quiescence, which suggests that the existing faults were easier to displace. Strain localisation is apparent from the reactivated faults, as they dominate the displacement at all levels, and is most pronounced in the Triassic units. There is a more homogenous spatial distribution, and higher density, of faults in the Jurassic, although finite strains are less than in the Trias. Multiple growth sequences indicate reactivation, but the faults often have a displacement minimum at the Triassic/Jurassic boundary. Such displacement profiles indicate that the reactivated faults could not have simply propagated upwards from the Triassic. To explain the geometries, thin-skinned extension above a detachment has been proposed. Either an anhydrite unit in the Mercia Mudstone (House, 1993), or a Liassic clay unit may have provided a slip surface during the younger phases of extension.

The fault orientations and dates of activity conform to published accounts of the Wessex Basin structures (e.g. Stoneley, 1982; Chadwick *et al.*, 1983; Chadwick, 1986; Karner *et al.*, 1987; Lake and Karner, 1987).

7.2 CONTRACTIONAL DEFORMATION

A deformation model for the strike-slip faults on the north Somerset coast, and at Beadnell, Northumbria, has been discussed (Chapter 2). Through-going faults develop from initiation, dilation and interaction of veins and vein arrays. The faults meet at conjugate intersection points, which are breached by the dominant fault of the pair. A combination of the model in Chapter 2, and the strike-slip relay ramp model (Peacock and Sanderson, 1995a) can be used to describe the formation of strike-slip fault networks from isolated fault development to interacting faults at relay ramps and conjugate intersections. The role of the strike-slip faults in north Somerset has been put into the context of the contractional phase of basin development (Chapter 3). The strike-slip faults have been previously dated as post reverse-reactivation (Dart *et al.*, 1995), but the interaction geometries of the strike-slip and normal faults indicate that the strike-slip faults formed at a similar time to the reverse-reactivation (Chapter 3).

Selective reverse-reactivation of normal faults has been identified from the onshore exposure of structures related to the Bristol Channel Basin (Chapter 3). Fault dip and fault size are both important to their reverse-reactivation. Although the geometries of overstepping normal faults (Larsen, 1988; Peacock and Sanderson, 1991; 1994a; Mansfield and Cartwright, 1995), thrusts (Dahlstrom, 1969; Boyer and Elliot, 1982) and strike-slip faults (Peacock and Sanderson, 1995a; Willemse *et al.*, 1997) have been previously described, overstep zones between reverse-reactivated faults have remained largely unstudied. The nature of under- and overlapping zones is of economic importance, as reverse-reactivation is a common feature of normal faults in the hydrocarbon basins around the UK (e.g. Southern North Sea, Badley *et al.*, 1989; East Shetland Basin, Thomas and Coward, 1995; Wessex Basin, Stoneley, 1982; Lake and Karner, 1987; Chadwick, 1993). Two distinct styles have been described from the north Somerset exposures (Chapter 3): (1) obliquely-oriented reverse faults in an underlap zone, and (2) a network of conjugate

strike-slip faults (*c.f.* Chapter 2). Both examples occur between faults with opposing dip directions, and indicate that new fault development accompanied reactivation of existing structures. Regional analysis of reverse-reactivated faults through-out the Wessex Basin was beyond the scope of this study, but none of the normal faults at Wytch Farm show evidence of reverse-reactivation. However, the Purbeck-Isle of Wight Fault lies to the south of Wytch Farm and was reverse-reactivated (Stoneley, 1982), which therefore conforms to a selective reverse-reactivation model.

7.3 STRAIN DISTRIBUTION

The common feature of the described normal, reverse-reactivated and strike-slip fault networks is the localisation of strain onto a set of master faults. In the strike-slip fault zones, the master faults develop from coalescence of several segments, which are able to accommodate greater strains than unlinked faults. In an extensional setting, the deformation is dominated by the repeated reactivation of a series of faults, and reverse-reactivation similarly affected only selected faults. Although the reactivated faults dominate the deformation, the formation of new faults is contemporaneous in both extensional and contractional settings. The analysis of the strike-slip fault zones has shown that the rock deforms at different rates, where continued propagation of one fault occurs at the same time as the development of new faults and veins (Chapter 2). The geometries of the under- and overlapping zones between reverse-reactivated faults indicate that new faults (both reverse and strike-slip) developed, at a similar time to the reactivation, to accommodate the contraction (Chapter 3). Existing normal faults at Wytch Farm were reactivated, and propagated upwards from the Triassic, at the same time as new normal faults were formed in the Jurassic (Chapter 4).

7.4 RECOMMENDATIONS FOR FURTHER WORK

1. A study of strike-slip faults in different lithologies to the limestones is needed to test the generality of the deformation model.
2. The study of reverse-reactivated fault data from inverted basins around the UK is necessary to identify the style of displacement transfer between over- and underlapping reverse-reactivated faults zones. A wider analysis of the normal faults in the Wessex Basin, and other basins, should be undertaken to test the applicability of the models for their selective reactivation. Seismic studies would provide 3D control of the geometries, which could then be compared with the north Somerset faults.
3. Interpretation of several reflectors between the chosen horizons in the Wytch Farm data sets is needed to constrain more tightly the vertical displacement-distance profiles. Analysis of the remaining inlines in the 3D data will also be helpful to the study.
4. The understanding of the Arne Fault system, and other faults in the 2D data area, would be improved from the acquisition and interpretation of 3D seismic data.

References

- Allan, U.S. (1989) Model for hydrocarbon migration and entrapment within faulted structures. *Bulletin of the American Association of Petroleum Geologists* **73**, 803-811.
- Anders, M.H. and Schlische, R.W. (1994) Overlapping faults, intrabasin highs, and the growth of normal faults. *Journal of Geology* **102**, 165-180.
- Anderton, R., Bridges, P.H., Leeder, M.R. and Sellwood, B.W. (1979) *A Dynamic Stratigraphy of the British Isles: A Study in Crustal Evolution*. Chapman and Hall, London. 301 pp.
- Angelier, J. (1984) Tectonic analysis of fault slip data sets. *Journal of Geophysical Research* **89**, 5835-5848.
- Aydin, A. and Nur, A. (1982) Evolution of pull-apart basins and their scale independence. *Tectonics* **1**, 91-105.
- Badley, M.E., Price, J.D. and Backshall, L.C. (1989) Inversion, reactivated faults and related structures: seismic examples from the southern North Sea. In Cooper, M.A. and Williams, G.D. (eds) *Inversion Tectonics*. Geological Society of London Special Publication **44**, 201-222.
- Barnett, J.A.M., Mortimer, J., Rippon, J.H., Walsh, J.J. and Watterson, J. (1987) Displacement geometry in the volume containing a single normal fault. *Bulletin of the American Association of Petroleum Geologists* **71**, 925-937.
- Beach, A. (1975) The geometry of en-echelon vein arrays. *Tectonophysics* **28**, 245-263.
- Beeler, N.M., Tullis, T.E., Blanpied, M.L. and Weeks, J.D. (1996) Frictional behaviour of large-displacement experimental faults. *Journal of Geophysical Research* **101**, 8697-8715.
- Benard, F., Mascle, A., Le Gall, B., Doglizez, B. and Rossi, T. (1990) Palaeo-stress fields in the Variscan foreland during the Carboniferous from microstructural analysis in the British Isles. *Tectonophysics* **177**, 1-13.
- Bosworth, W. (1992) Mesozoic and early Tertiary rift tectonics in East Africa. *Tectonophysics* **209**, 115-137.
- Bowyer, M.O'N. and Kelly, P.G. (1995) Strain and scaling relationships of faults and veins at Kilve, Somerset, UK. *Proceedings of the Ussher Society* **8**, 411-415.

- Boyer, S.E. and Elliott, D. (1982) Thrust systems. *Bulletin of the American Association of Petroleum Geologists* **66**, 1196-1230.
- Brewer, J.A and Smithe, D.K. (1984) MOIST and the continuity of crustal reflectors along the Caledonian-Appalachian orogen. *Journal of the Geological Society of London* **141**, 104-120.
- Bristow, C.M. and Hughes, D.E. (1971) A Tertiary thrust on the southern margin of the Bovey Basin. *Geological Magazine* **108**, 61-68.
- Brooks, M., Traynor, P. M. and Trimble, T. J. (1988) Mesozoic reactivation of Variscan thrusting in the Bristol Channel area, UK. *Journal of the Geological Society of London* **145**, 439-444.
- Cartwright, J.A., Trudgill, B.D. and Mansfield, C.S. (1995) Fault growth by segment linkage: an explanation for scatter in maximum displacement and trace length data from the Canyonlands Grabens of SE Utah. *Journal of Structural Geology* **17**, 1319-1326.
- Chadwick, R.A. (1986) Extension tectonics in the Wessex Basin, southern England. *Journal of the Geological Society of London* **143**, 465-488.
- Chadwick, R.A. (1993) Aspects of basin inversion in southern Britain. *Journal of the Geological Society of London* **150**, 311-322.
- Chadwick, R.A., Kenolty, N. and Whittaker, A. (1983) Crustal structure beneath southern England from deep seismic reflection profiles. *Journal of the Geological Society of London* **140**, 893-912.
- Channon, S. (1996) An analysis of Chloride data. *Unpublished BP Draft report (Wytech Farm Library)*.
- Chester, F.M. and Logan, J.M. (1986) Implications for mechanical properties of brittle faults from observations of the Punchbowl Fault Zone, California. *Pure and Applied Geophysics* **124**, 79-106.
- Childs, C., Nicol, A., Walsh, J.J. and Watterson, J. (1996) Growth of vertically segmented normal faults. *Journal of Structural Geology* **18**, 1389-1397.
- Childs, C., Watterson, J. and Walsh, J.J. (1995) Fault overlap zones within developing normal fault systems. *Journal of the Geological Society of London* **152**, 535-550.
- Cloke, I.R., Moss, S.J. and Craig, J. (1997) The influence of basement reactivation on the extensional and inversional history of the Kutai Basin, East Kalimantan, SE Asia. *Journal of the Geological Society of London* **154**, 157-162.

- Collier, R.E. LL. (1989) Tectonic evolution of the Northumberland Basin; the effects of renewed extension upon an inverted extensional basin. *Journal of Geological Society of London* **146**, 981-989.
- Colter, V.S. and Havard, D.J. (1981) The Wytch Farm Oilfield. In Illing, L.V. and Hobson, G.D. (eds) *Petroleum Geology of the Continental Shelf of North-West Europe*. Heyden, London, 494-503.
- Cooper, M.A. and Williams, G.D. (eds.) (1989) *Inversion tectonics*. Geological Society of London Special Publication **44**, 375 pp.
- Cowie, P.A. and Scholz, C.H. (1992) Physical explanation for the displacement-length relationship of faults using a post-yield fracture mechanics model. *Journal of Structural Geology* **14**, 1133-1148.
- Cruikshank, K.M., Zhao, G. and Johnson, A.M. (1991) Analysis of minor fractures associated with joints and faulted joints. *Journal of Structural Geology* **13**, 865-886.
- Dahlstrom, C.D.A. (1969) Balanced cross-sections. *Canadian Journal of Earth Sciences* **6**, 743-757.
- Dart, C.J., McClay, K. and Hollings, P.N. (1995) 3D analysis of inverted extensional fault systems, southern Bristol Channel basin, UK. In Buchanan, J.G. and Buchanan, P.G. (eds). *Basin Inversion*, Geological Society of London Special Publication **88**, 393-413.
- Davison, I. (1987) Normal fault geometry related to sediment compaction and burial. *Journal of Structural Geology* **9**, 393-401.
- Davison, I. (1994) Linked fault systems; extensional, strike-slip and contractional. In Hancock, P.L. (ed) *Continental Deformation*, 121-142.
- Dawers, N.H., Anders, M.H. and Scholz C.H. (1993) Growth of normal faults: displacement-length scaling. *Geology* **21**, 1107-1110.
- Dragoni, M. and Piombo, A. (1993) Propagation of an aseismic dislocation through asperities with smooth borders. *Physics of the Earth and Planetary Interiors* **80**, 1-11.
- Dyer, R. (1988) Using joint interactions to estimate palaeostress magnitudes. *Journal of Structural Geology* **10**, 685-699.
- Ellis, M.A. and Dunlap, W.J. (1988) Displacement variation along thrust faults: implications for the development of large faults. *Journal of Structural Geology* **10**, 183-192.

- Ellis, P. (1997) Review of the Structure of the Arne Fault, Wytch Farm, Dorset. *Unpublished BP Report No. SDT/015/97.*
- Ellis, P. (1998) A note on the continuity of Wytch Farm structures into the Elf 98-12 survey area. *Subsurface Description Team, BPX Shared Petrotechnical Resource, Sunbury. Unpublished BP Report SDT/0/98.*
- Enfield, M. and Coward, M. (1987) The structure of the West Orkney Basin, northern Scotland. *Journal of the Geological Society of London* **144**, 871-884.
- Evans, J., Jenkins, D. and Gluyas, J. (in press) The Kimmeridge Bay Oilfield: an enigma demystified. In Underhill, J.R. (ed) *Development, Evolution and Petroleum Geology of the Wessex Basin*, Geological Society of London Special Publication **133**, 407-413.
- Færseth, R.B. (1996) Interaction of Permo-Triassic and Jurassic extensional fault-blocks during the development of the northern North Sea. *Journal of the Geological Society* **153**, 931-944.
- Freund, R. (1974) Kinematics of transform and transcurrent faults. *Tectonophysics* **21**, 93-134.
- Gamond, J.F. (1983) Displacement features associated with fault zones: a comparison between observed examples and experimental models. *Journal of Structural Geology* **5**, 33-45.
- Gawthorpe, R.L. and Hurst, J.M. (1993) Transfer zones in extensional basins: their structural style and influence on drainage development and stratigraphy. *Journal of the Geological Society of London* **150**, 1137-1152.
- Gibbs, A. (1987) Development of extension and mixed-mode sedimentary basins. In Coward, M.P., Dewey, J.F. and Hancock, P.L. (eds) *Continental Extensional Tectonics*, Geological Society of London Special Publication **28**, 19-34.
- Gillespie, P.A., Walsh, J.J and Watterson, J. (1992) Limitations of dimension and displacement data from single faults and the consequences for data analysis and interpretation. *Journal of Structural Geology* **14**, 1157-1172.
- Hancock, P.L. (1985) Brittle microtectonics: principles and practices. *Journal of Structural Geology* **7**, 437-457.

- Hawkes, P.W., Fraser, A.J. and Einchcomb, C.C.G. in press. The tectono-stratigraphic development and exploration history of the Weald and Wessex Basins, southern England. In Underhill, J.R. (ed) *Development, Evolution and Petroleum Geology of the Wessex Basin*, Geological Society of London Special Publication **133**, 39-66.
- Hayward, A.B. and Graham, R.H. (1989) Some geometrical characteristics of inversion. In Cooper, M.A. and Williams, G.D. (eds) *Inversion Tectonics*, Geological Society of London Special Publication **55**, 17-39.
- Hempton, M.R. and Dunne, L.A. (1984) Sedimentation in pull-apart basins: active examples in eastern Turkey. *Journal of Geology* **92**, 513-530.
- Hibsch, C., Cushing, E.M., Cabrera, J., Mercier, J., Prasil, P. and Jarrige, J-J. (1993) Palaeostress evolution in Great Britain from Permian to Cenozoic: A microtectonic approach to the geodynamic evolution of the southern UK basins. *Bulletin des Centres des Recherches Exploration-Production elf Aquitaine* **17**, 303 - 330.
- Hogg, A.J.C., Evans, I.J., Harrison, P.F., Meling, T., Smith, G.S., Thompson, S.D. and Watts, G.F.T. (in press) Reservoir management of the Wytch Farm Oilfield, Dorset, UK: Providing options for growth into later field life. *Petroleum Geology of Northwest Europe - Proceedings of the Barbican Conference, 26 - 29 October, 1997*.
- Horsfield, W.T. (1980) Contemporaneous movement along crossing conjugate normal faults. *Journal of Structural Geology* **2**, 305-310.
- House, M.R. (1993) *Geology of the Dorset Coast. Second Edition*. Geologists' Association Guide No. 22. The Holywell Press, Oxford. 164 pp.
- House, W.M. and Gray, D.R. (1982) Displacement transfer at thrust terminations in Southern Appalachians - Saltville Thrust as example. *Bulletin of the American Association of Petroleum Geologists* **66**, 830-842.
- Huyghe, P. and Mugnier, J-L. (1992) Short-cut geometry during structural inversions: competition between faulting and reactivation. *Bulletin de la Societe Geologique de France* **163**, 691-700.
- Jamison, W.R. (1989) Fault-fracture strain in Wingate Sandstone. *Journal of Structural Geology*, **11**, 959-974.
- Jenkyns, H.C. and Senior, J.R. (1991) Geological evidence for intra-Jurassic faulting in the Wessex Basin and its margins. *Journal of the Geological Society* **148**, 245-260.

- Karner, G.D., Lake, S.D. and Dewey, J.F. (1987) The thermal and mechanical development of the Wessex Basin, southern England. In Coward, M.P., Dewey, K.J. and Hancock, P.L. (eds) *Continental Extensional Tectonics*, Geological Society of London Special Publication **28**, 517-536.
- Kelly, P.G. (1996) Strike-slip faulting and block rotations at Kilve, Somerset. *Geoscientist* **6**, 14-16.
- Kelly, P.G., Peacock, D.C.P., Sanderson, D.J., and McGurk, A.C. (in review) Selective reverse-reactivation of normal faults and hanging-wall indentation in north Somerset. *Journal of Structural Geology*.
- Kelly, P.G., Sanderson, D.J. and Peacock, D.C.P. (in press) Linkage and evolution of conjugate strike-slip fault zones in limestones of Somerset and Northumbria. *Journal of Structural Geology*.
- Kent, P.E. (1949) A structure-contour map of the surface of buried pre-Permian rocks in England and Wales. *Proceedings of the Geologists' Association, London* **60**, 80-104.
- Kimbell, G.S., Chadwick, R.A., Holliday, D.W. and Werngren, O.C. (1989) The structure and evolution of the Northumberland Trough from new seismic reflection data and its bearing on modes of continental extension. *Journal of the Geological Society of London* **146**, 775-787.
- Kirby, G.A. and Swallow, P.W. (1987) Tectonism and sedimentation in the Flamborough Head region of north-east England. *Proceedings of the Yorkshire Geological Society* **46**, 301-309.
- Knight, F. (1994) A study into the sub-seismic faulting in the Mercia Mudstone. *Unpublished BP Report No. 2130 (Wytch Farm Library)*.
- Knipe, R.J., Baxter, K., Clennell, M.B., Farmer, A.B., Fisher, Q.J., Jones, G., Bolton, A.J., Kidd, B.E., Porter, J.R. and White, E.A. (1994) Faulting and fault sealing in the Wytch Farm Field, Blocks 97/10 and 98/6, U.K.C.S.: A Pilot Study. Rock Deformation Research Group, University of Leeds. *Unpublished report*.
- Knott, S.D., Beach, A., Brockbank, P.J., Brown, J.L., McCallum, J.E. and Welbon, A.I. (1996) Spatial and mechanical controls on normal fault populations. *Journal of Structural Geology* **18**, 359-372.
- Koestler, A.G. and Ehrmann, W.U. (1991) Description of brittle extensional features in chalk on the crest of a salt ridge (NW Germany). In Roberts, A.M., Yielding, G. and Freeman, B. (eds). *The Geometry of Normal Faults*, Geological Society of London Special Publication **56**, 113-123.

- Lake, S.D. and Karner, G.D. (1987) The structure and evolution of the Wessex Basin, southern England: an example of inversion tectonics. *Tectonophysics* **137**, 347-378.
- Larsen, P.-H. (1988) Relay structures in a Lower Permian basement-involved extension system, East Greenland. *Journal of Structural Geology* **10**, 3-8.
- Lebel, D. and Mountjoy, E.W. (1995) Numerical modelling of propagation and overlap of thrust faults, with application to the thrust-fold belt of central Alberta. *Journal of Structural Geology* **17**, 631-646.
- Mandal, N. and Chattopadhyay, A. (1995) Modes of reverse-reactivation of domino-type normal faults: experimental and theoretical approach. *Journal of Structural Geology* **17**, 1151-1163.
- Mann, P., Hempton, M.R., Bradley, D.C. and Burke, K. (1983) Development of pull-apart basins. *Journal of Geology* **91**, 529-554.
- Mansfield, C.S. and Cartwright, J.A. (1996) High resolution fault displacement mapping from three-dimensional seismic data: evidence for dip linkage during fault growth. *Journal of Structural Geology* **18**, 249-263.
- Marone, C. (1995) Fault zone strength and failure criteria. *Geophysical Research Letters* **22**, 723-726.
- Marrett, R. and Allmendinger, R.W. (1991) Estimates of strain due to the brittle faulting: sampling of fault populations. *Journal of Structural Geology* **13**, 735-738.
- Marshak, S., Wilkerson, M.S. and Hsui, A.T. (1992) Generation of curved fold-thrust belts: insights from simple physical and analytical models. In McClay, K.R. (ed) *Thrust Tectonics*. Chapman and Hall, 83-92.
- Martin, B., Dickens, J., Burrow-Newton, P. and Smith, M. (1993) Wytch Farm Field: Sherwood Reservoir Depth Uncertainty Study. *Unpublished BP Report No. EXB/105/93*.
- McClay, K.R. and White, M.J. (1995) Analogue modelling of orthogonal and oblique rifting. *Marine and Petroleum Geology* **12**, 137-151.
- McCoss, A. (1986) Simple constructions for deformation in transpression/transension zones. *Journal of Structural Geology* **8**, 715-718.
- McGrath, A.G. and Davison, I. (1995) Damage zone geometry around fault tips. *Journal of Structural Geology* **17**, 1011-1023.

- McKie, T., Aggett, J. and Hogg, A.J.C. (1998) Reservoir architecture of the Upper Sherwood Sandstone, Wytch Farm Field, southern England. *In* Underhill, J.R. (ed) *Development, Evolution and Petroleum Geology of the Wessex Basin*, Geological Society of London Special Publication **133**, 399-406.
- McLachlan, A.C. (1986) *A Revised Interpretation of the Structures Within the Mesozoic of North-West Somerset*. Unpublished MSc thesis, Imperial College, London.
- Morley, C.K., Nelson, R.A., Patton, T.L. and Munn, S.G. (1990) Transfer zones in the East African Rift System and their relevance to hydrocarbon exploration in rifts. *Bulletin of the American Association of Petroleum Geologists* **74**, 1234-1253.
- Muraoka, H. and Kamata, H. (1983) Displacement distribution along minor fault traces. *Journal of Structural Geology* **5**, 483-495.
- Nemcok, M., Gayer R. and Miliorizos, M. (1995) Structural analysis of the inverted Bristol Channel Basin: implications of the geometry and timing of fracture porosity. *In*: Buchanan, J.G. and Buchanan, P.G. (eds) *Basin Inversion*. Geological Society of London Special Publication **88**, 355-392.
- Nicholson, C., Seeber, L., Williams, P. and Sykes, L.R. (1986) Seismicity and fault kinematics through the Eastern Transverse Ranges, California: Block rotation, strike-slip faulting and low-angle thrusts. *Journal of Geophysical Research* **91**, 4891-4908.
- Nicol, A., Walsh, J.J., Watterson, J. and Bretan, P.G. (1995) Three-dimensional geometry and growth of conjugate normal faults. *Journal of Structural Geology* **17**, 847-862.
- Odonne, F. and Massonnat, G. (1992a) Compatibility of strain and displacement around simple and conjugate faults, analog models of natural structures. *Bulletin de la Societe Geologique de France* **163**, 701-712.
- Odonne, F. and Massonnat, G. (1992b) Volume loss and deformation around conjugate fractures - comparison between a natural example and analog experiments. *Journal of Structural Geology* **14**, 963-972.
- Olson, J.E. and Pollard, D.D. (1991) The initiation and growth of en echelon veins. *Journal of Structural Geology* **13**, 595-608.
- Palmer, C.P. (1972) The Lower Lias (Lower Jurassic) between Watchet and Lillstock in north Somerset (UK). *Newsletters on Stratigraphy* **2**, 1-30.

- Peacock, D.C.P. (1991) Displacement and segment linkage in strike-slip fault zones. *Journal of Structural Geology* **13**, 1025-1035.
- Peacock, D.C.P. (1996) Field examples of variations in fault patterns at different scales. *Terra Nova* **8**, 361-371.
- Peacock, D.C.P. and Sanderson, D.J. (1991) Displacements, segment linkage and relay ramps in normal fault zones. *Journal of Structural Geology* **13**, 721-733.
- Peacock, D.C.P. and Sanderson, D.J. (1992) Effects of layering and anisotropy on fault geometry. *Journal of the Geological Society of London* **149**, 793-802.
- Peacock, D.C.P. and Sanderson, D.J. (1993) Estimating strain from fault slip using a line sample. *Journal of Structural Geology* **15**, 1513-1516.
- Peacock, D.C.P. and Sanderson, D.J. (1994a) Geometry and development of relay ramps in normal fault systems. *Bulletin of the American Association of Petroleum Geologists* **78**, 146-165.
- Peacock, D.C.P. and Sanderson, D.J. (1994b) Strain and scaling of faults in the chalk at Flamborough Head, U.K. *Journal of Structural Geology* **16**, 97-107.
- Peacock, D.C.P. and Sanderson, D.J. (1995a) Strike-slip relay ramps. *Journal of Structural Geology* **17**, 1351-1360.
- Peacock, D.C.P. and Sanderson, D.J. (1995b) Pull-aparts, shear fractures and pressure solution. *Tectonophysics* **241**, 1-13.
- Peacock, D.C.P. and Zhang, X. (1994) Field examples and numerical modelling of oversteps and bends along normal faults in cross-section. *Tectonophysics* **234**, 147-167.
- Pollard, D.D., Segall, P. and Delaney, P.T. (1982) Formation and interpretation of dilatant echelon cracks. *Geological Society of America Bulletin* **93**, 1291-1303.
- Rawson, P.F. and Wright, J.K. (1992) *The Yorkshire Coast*. Geologists' Association Guide No. 34, London.
- Reches, Z. and Lockner, D.A. (1994) Nucleation and growth of faults in brittle rocks. *Journal of Geophysical Research* **99**, 18159-18173.

Roberts, A.M., Price, J.D. and Olsen, T.S. (1990) Late Jurassic half-graben control on the siting and structure of hydrocarbon accumulations: UK/Norwegian Central Graben. *In* Hardman, R.F.P. and Brooks, J, (eds) *Tectonic Events Responsible for Britain's Oil and Gas Reserves*, Geological Society of London Special Publication **55**, 229-257.

Roberts, D.G. (1989) Basin inversion in and around the British Isles. *In* Cooper, M.A. and Williams, G.D. (eds) *Inversion Tectonics*. Geological Society of London Special Publication **44**, 131-152.

Robson, D.A. (1977) The structural history of the Cheviot and adjacent regions. *Scottish Journal of Geology* **13**, 255-262.

Rothery, E. (1988) En-echelon vein array development in extension and shear. *Journal of Structural Geology* **10**, 63-71.

Sahimi, M. & Arbabi, S. (1996) Scaling laws for fracture of heterogeneous materials and rock. *Physical Review Letters* **77**, 3689-3692.

Sanderson, D.J. and Marchini, W.R.D. (1984) Transpression. *Journal of Structural Geology* **6**, 449-458.

Schlische, R.W. (1993) Anatomy and evolution of the Triassic-Jurassic continental rift system, eastern North America. *Tectonics* **12**, 1026-1042.

Scholz, C.H., Dawers, N.H., Yu, J.-Z. and Anders, M.H. (1993) Fault growth and fault scaling laws: preliminary results. *Journal of Geophysical Research* **98**, 21 951-21 961.

Scott, D.R., Marone, C.J. and Sammis, C.G. (1994) The apparent friction of granular fault gouge in sheared layers. *Journal of Geophysical Research* **99**, 7231-7246.

Segall, P. and Pollard, D.D. (1980) Mechanics of discontinuous faults. *Journal of Geophysical Research* **85**, 4337-4350.

Selley, R.C. and Stoneley, R. (1986) Petroleum habitat in south Dorset, England. *In* Brooks, J. and Glennie, K.W. (eds) *Petroleum Geology of north west Europe*. Proceedings of the 3rd Conference, London Vol. 1. Graham and Trotman. 139-148.

Shiells, K.A.G. (1964) The geological structure of north-east Northumberland. *Transactions of the Royal Society of Edinburgh*, **65**, 449-481.

Sibson, R.H. (1985) A note on fault reactivation. *Journal of Structural Geology* **7**, 751-754.

Sibson, R.H. (1989) Earthquake faulting as a structural process. *Journal of Structural Geology* **11**, 1-14.

Sibson, R.H. (1995) Selective fault reactivation during basin inversion: potential for fluid redistribution through fault-valve action. In Buchanan, J.G. and Buchanan, P.G. (eds). *Basin Inversion*, Geological Society of London Special Publication **88**, 3-19.

Stark, C.P. and Stark, J.A. (1991) Seismic fluids and percolation theory. *Journal of Geophysical Research* **96**, 8417-8426.

Stauffer, D. and Aharony, A. (1992) *Introduction to Percolation Theory*- (Second Edition). Taylor and Francis, London.

Stoneley, R. (1982) The structural development of the Wessex Basin. *Journal of the Geological Society of London* **139**, 543-554.

Tapponnier, P., Peltzer, G., Le Dain, A. Y., Armijo, R. & Cobbold, P. (1982) Propagating extrusion tectonics in Asia: New insights from simple experiments with plasticine. *Geology* **10**, 611-616.

Thomas, D.W. and Coward, M.P. (1995) Late Jurassic-Early Cretaceous inversion of the northern East Shetland Basin, northern North Sea. In Buchanan, J.G. and Buchanan, P.G. (eds). *Basin Inversion*, Geological Society of London Special Publication **88**, 275-306.

Thomas, D.W. and Coward, M.P. (1996) Mesozoic regional tectonics and South Viking Graben formation: evidence for localised thin-skinned detachments during rift development and inversion. *Marine and Petroleum Geology* **13**, 149-177.

Trudgill, B. and Cartwright, J. (1994) Relay-ramp forms and normal-fault linkages, Canyonlands National Park, Utah. *Geological Society of America Bulletin* **106**, 1143-1157.

Turcotte, D.L. (1995) Chaos, fractals and nonlinear phenomena in Earth Sciences. *Reviews of Geophysics* **33**, 341-3.

Van Hoorn, B. (1987) The South Celtic Sea/Bristol Channel Basin: origin, deformation and inversion history. *Tectonophysics* **137**, 309-334.

Walsh, J.J. and Watterson, J. (1987) Distribution of cumulative displacement and seismic slip on a single normal fault surface. *Journal of Structural Geology* **9**, 1039-1046.

- Walsh, J.J. and Watterson, J. (1988) Analysis of the relationship between displacements and dimensions of faults. *Journal of Structural Geology* **10**, 239-247.
- Wang, X.A. (1995) Estimation of the variation in apparent displacement along normal fault traces refracted by differential compaction. *Journal of Structural Geology* **17**, 1789-1792.
- Warrington, G. and Scrivener, R.C. (1980) The Lyme Regis (1901) Borehole succession and its relationship to the Triassic sequence of the east Devon coast. *Proceedings of the Ussher Society* **5**, 24-32.
- Watterson, J., Nicol, A. and Walsh, J.J. (1998) Strains at the intersections of synchronous conjugate normal fault. *Journal of Structural Geology* **20**, 363-370.
- Whittaker, A. and Green, G.W. (1983) *Geology of the county around Weston-super-Mare*. Geological Survey of Great Britain.
- Willemse, E.J.M. (1997) Segmented normal faults: Correspondence between three-dimensional mechanical models and field data. *Journal of Geophysical Research* **102**, 675-692.
- Willemse, E.J.M., Peacock, D.C.P. and Aydin, A. (1997) Nucleation and growth of strike-slip faults in limestone. *Journal of Structural Geology* **19**, 1461-1477.
- Willemse, E.J.M., Pollard, D.D. and Aydin, A. (1996) Three-dimensional analysis of slip distributions on normal fault arrays with consequences for fault scaling. *Journal of Structural Geology* **18**, 295-309.
- Williams, G.D. and Chapman, T. (1983) Strains developed in the hangingwalls of thrusts due to their slip/propagation rate: a dislocation model. *Journal of Structural Geology* **9**, 563-571.
- Williams, G.D., Powell, C.M. and Cooper, M.A. (1989) Geometry and kinematics of inversion tectonics. In Cooper, M.A. and Williams, G.D. (eds) *Inversion Tectonics*. Geological Society of London Special Publication **44**, 3-16.
- Wojtal, S. (1989) Measuring displacement gradients and strains in faulted rocks. *Journal of Structural Geology* **11**, 669-678.

Appendix 1 – Field Photographs

A1. 1. Photograph of the intersection between the conjugate strike-slip faults illustrated in Fig. 2.6.

A1. 2. Photographs of examples of strike-slip faults exposed in the cliff to the east of Quantock's Head (Fig. 2.9).

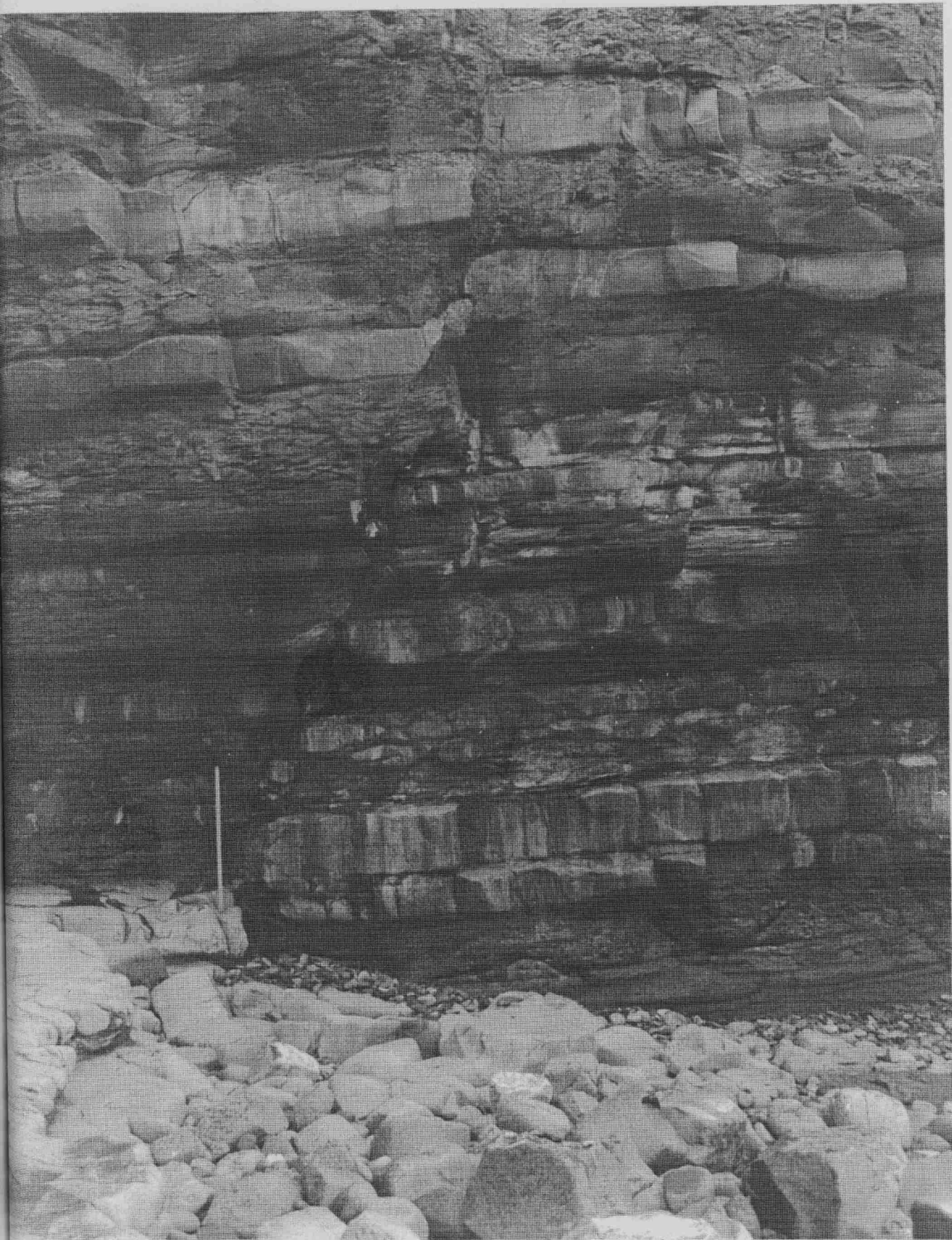
A1. 3. Photograph of a conjugate strike-slip fault zone with associated pull-apart arrays (Fig. 2.3 and Fig. 6.11).

A1. 4. Photograph of reverse-reactivated normal faults exposed in the cliffs at Kilve (Fig. 6.9).

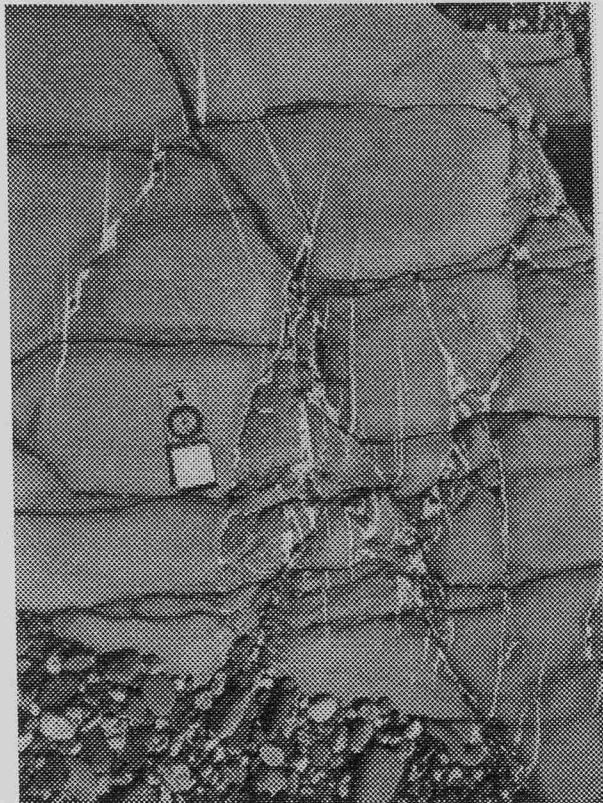
A1. 5. Photograph of an intersection zone between strike-slip faults and the reverse-reactivated Kilve Pill Fault Zone (Fig. 3.10).



A1.1. Intersection between conjugate strike-slip faults illustrated in Fig. 2.6



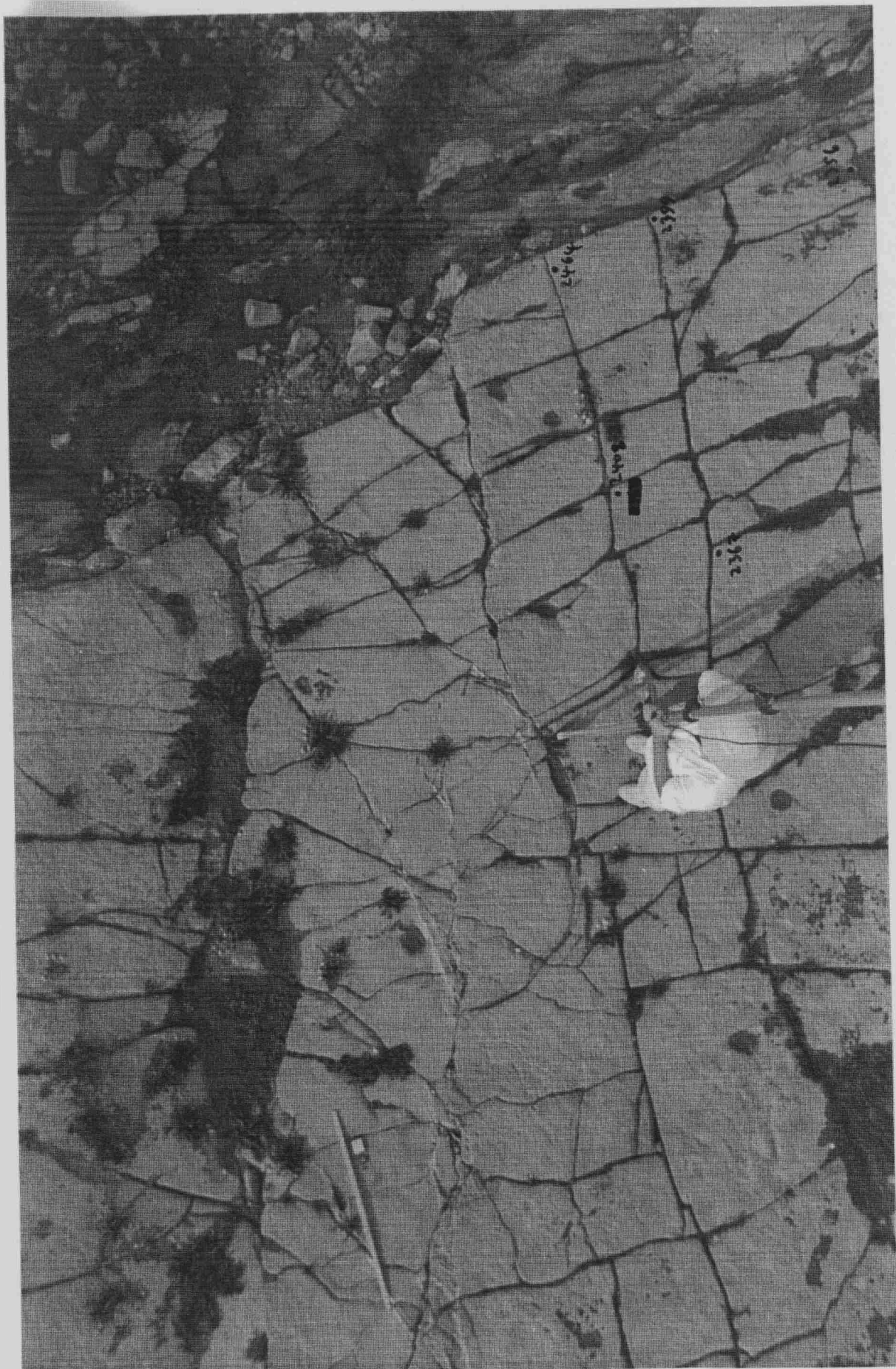
A1.2. Strike-slip faults exposed in the cliff to the east of Quantock's Head (Fig. 2.9).



A1.3. Conjugate strike-slip fault zone, with associated pull-apart arrays (Fig. 2.3 and Fig. 6,11).



A1.4. Reverse-reactivated normal fault zone exposed in the cliffs east of Kilve Pill (Fig. 6.9)



A1.5. Intersection zone between strike-slip faults and the reverse-reactivated Kilve Pill Fault Zone (Fig. 3.10)

Appendix 2 – Field maps

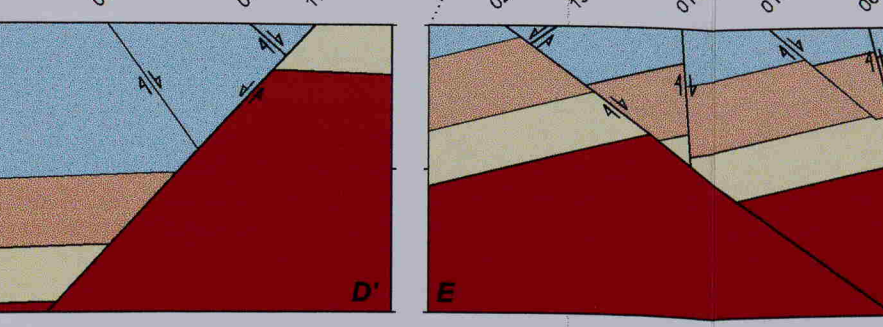
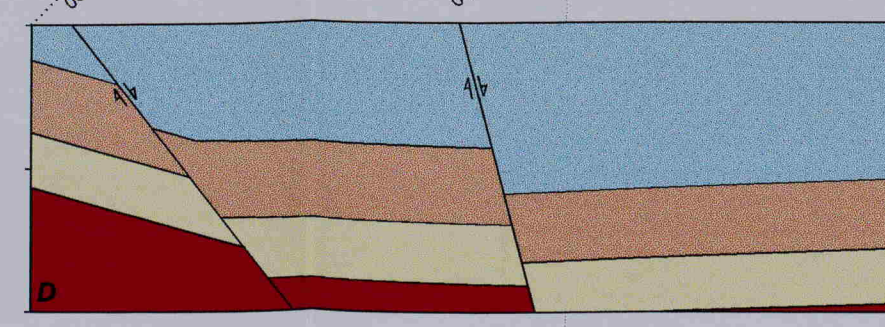
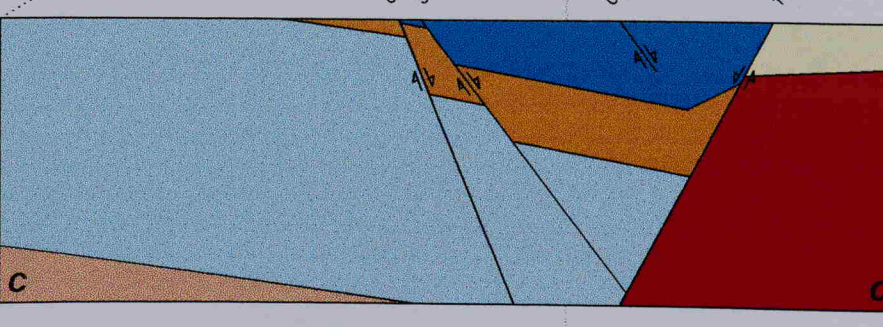
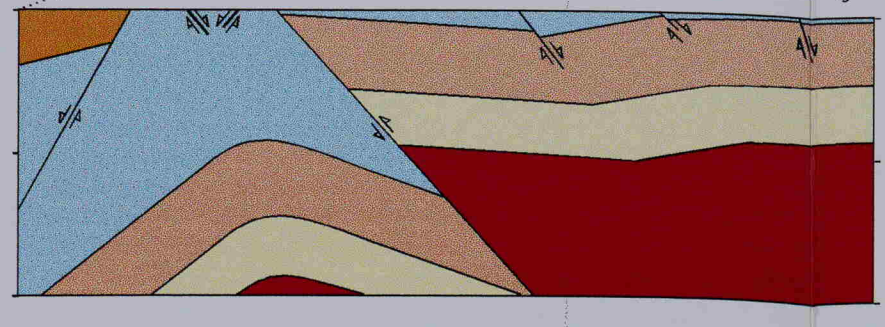
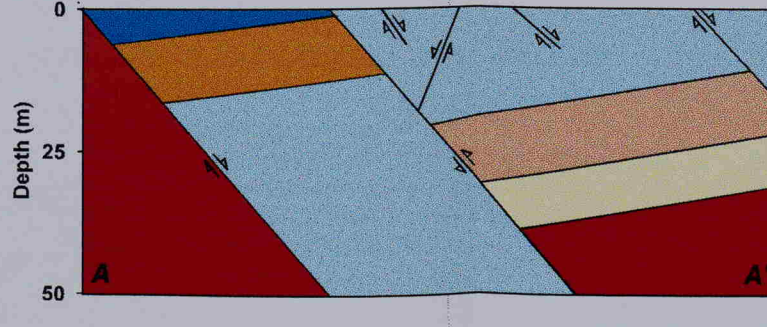
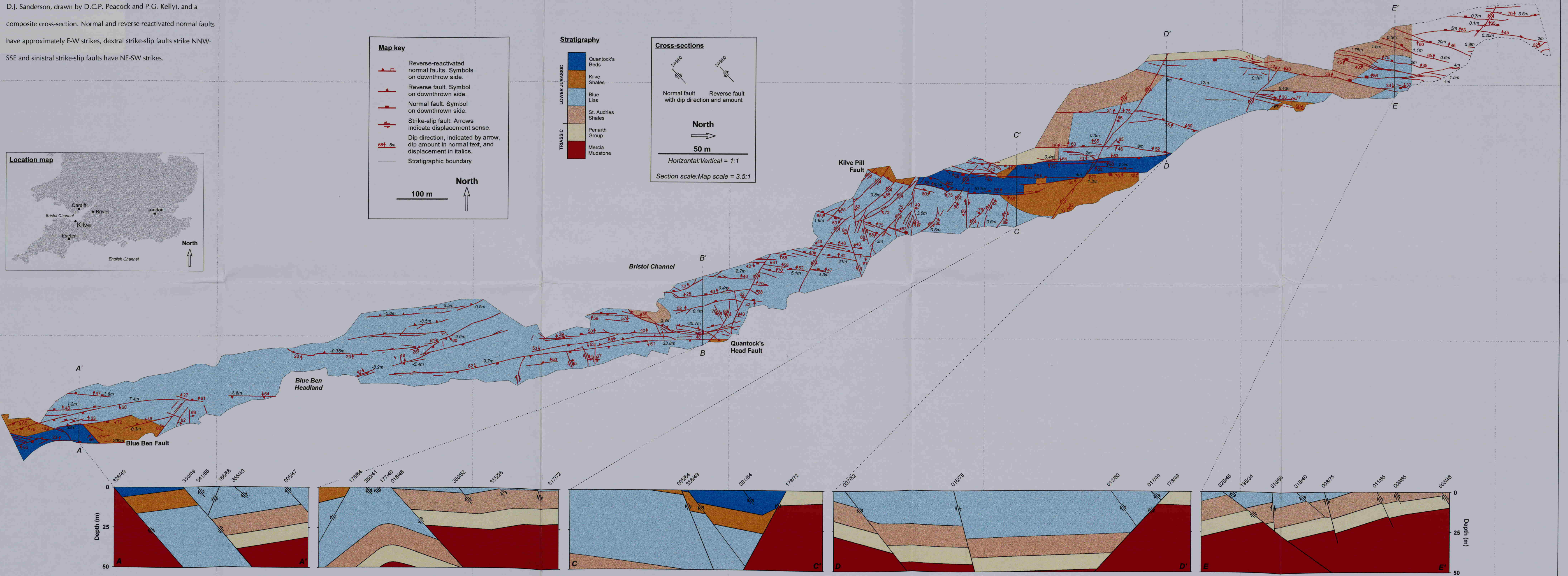
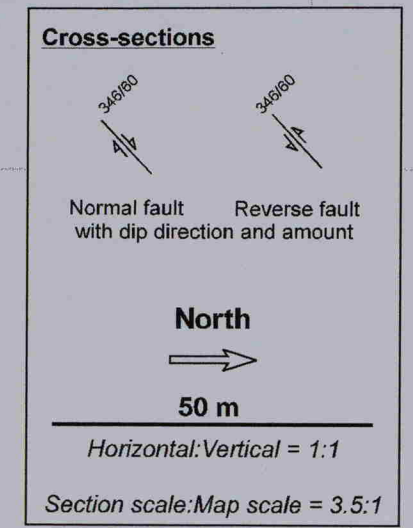
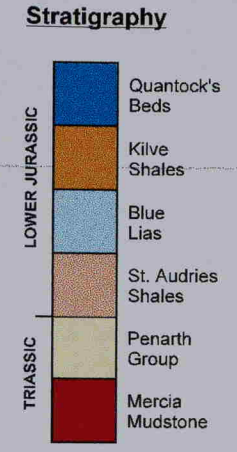
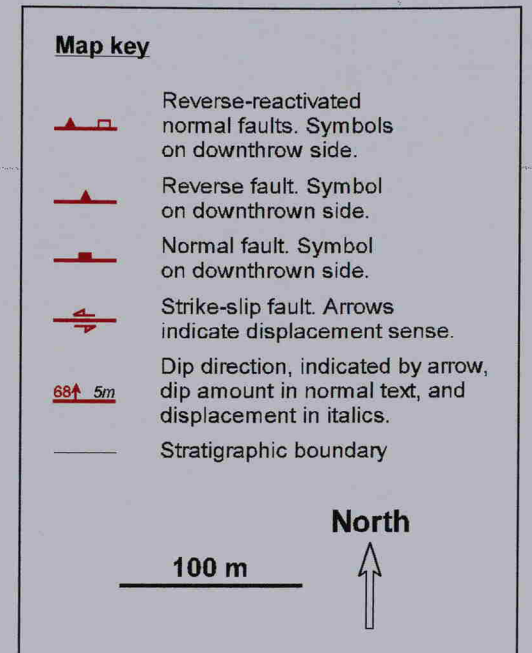
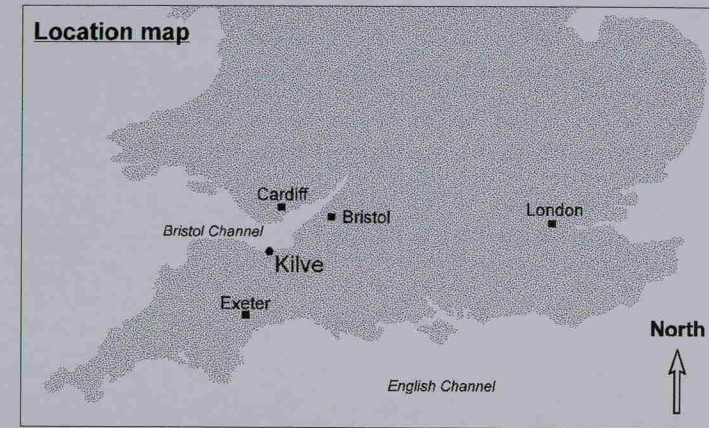
A2. 1. Map of the strike-slip fault zone in Fig. 2.6(a)

A2. 2. Map of the strike-slip fault zone in Fig. 2.6(b)

A2. 3. Map of the strike-slip fault zone in Fig. 2.11(b)

A2. 4. Map with colour-coded fault traces to show the variation in fault dip for the normal and reverse-reactivated normal faults on the Kilve foreshore. There is no unambiguous relationship between dip direction and dip amount.

Enclosure 2. Map of the exposure at Kilve (mapped by P.G. Kelly and D.J. Sanderson, drawn by D.C.P. Peacock and P.G. Kelly), and a composite cross-section. Normal and reverse-reactivated normal faults have approximately E-W strikes, dextral strike-slip faults strike NNW-SSE and sinistral strike-slip faults have NE-SW strikes.



312000

312500

313000

313500

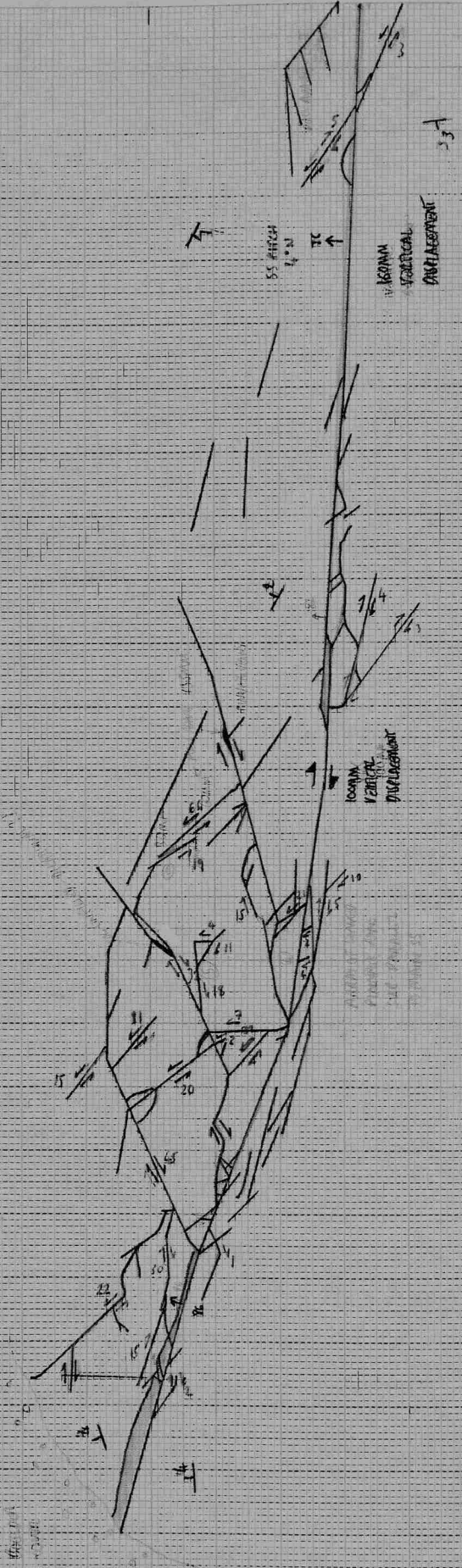
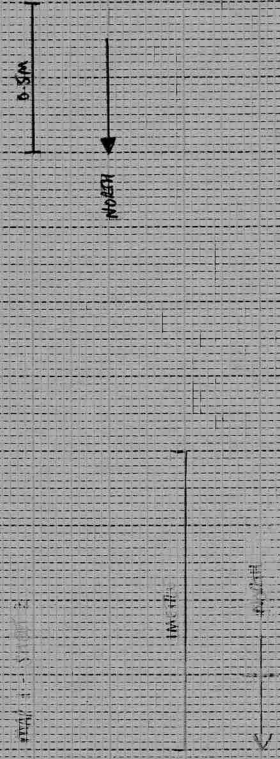
314000

314500

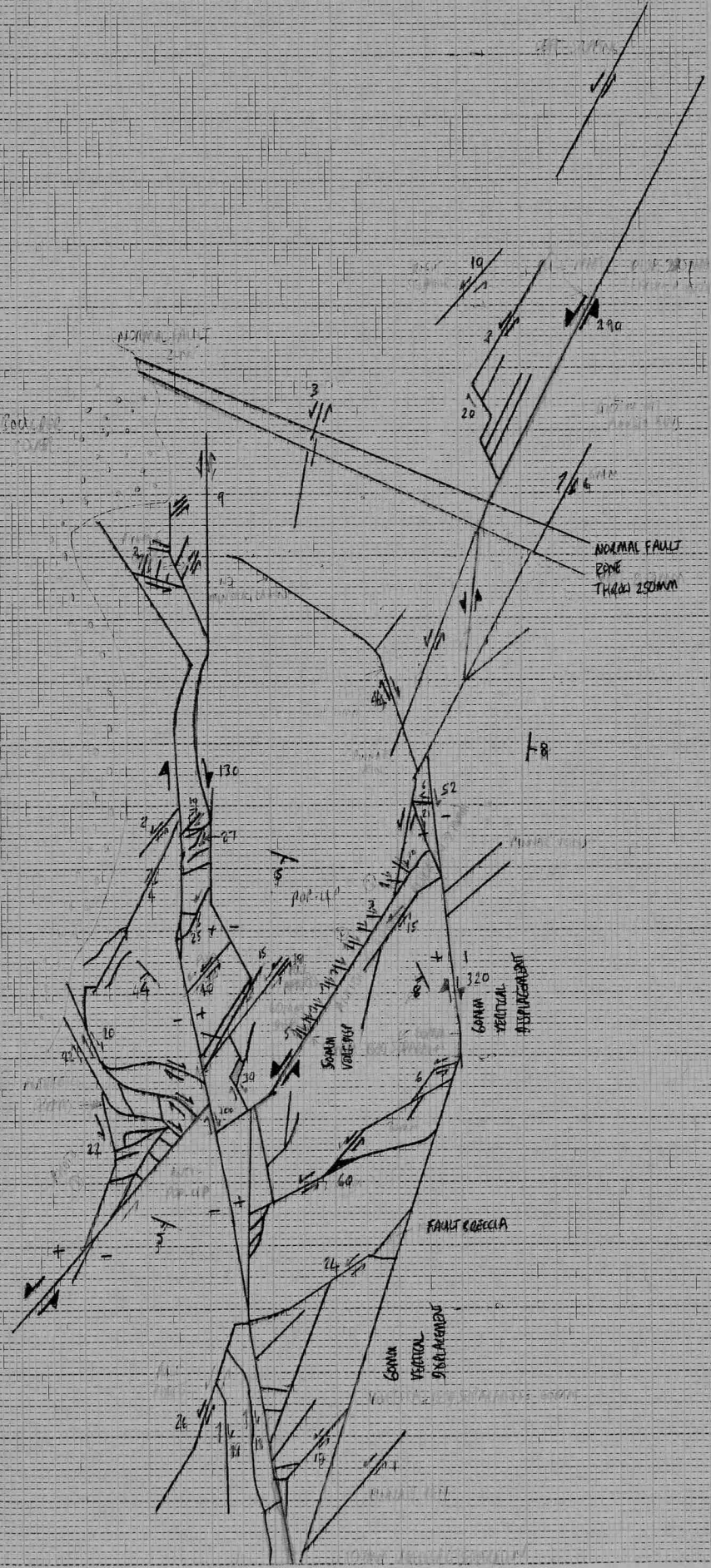
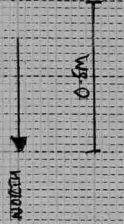
143500

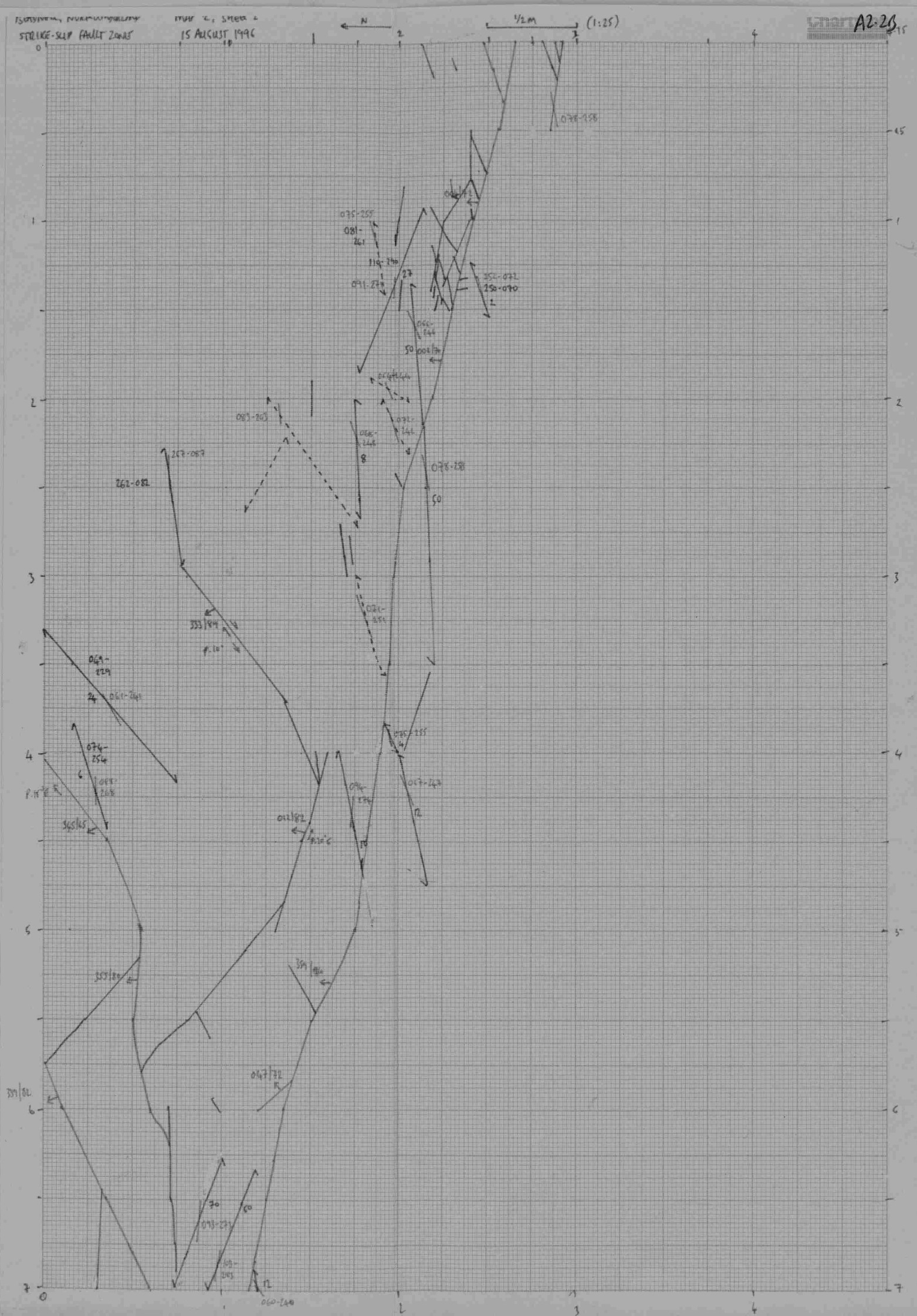
144500

145000



KILIG, SAMBEBET - MAP 1, SHEET 1
 24-25 APRIL 1996
 VEIN NETWORK AROUND N-S STRIKING, DEXTERAL STRIKE SLIP FAULT
 LOCATION: 200M WEST HANE (KUNJ STEN), 100M NORTHERN OF CLIFF





Map key

- Reverse-reactivated normal faults. Symbols on downthrown side.
- Reverse fault. Symbol on downthrown side.
- Normal fault. Symbol on downthrown side.
- Dip direction, indicated by arrow, dip amount in normal text, and displacement in italics.

100 m

North

Fault plane coloured for fault dip amount

- < 30°
- 30-39°
- 40-49°
- 50-59°
- 60-69°
- 70-79°
- 80-89°

